

**Journal of
Mechanics of
Materials and Structures**

Volume 11, No. 5

December 2016



JOURNAL OF MECHANICS OF MATERIALS AND STRUCTURES

msp.org/jomms

Founded by Charles R. Steele and Marie-Louise Steele

EDITORIAL BOARD

ADAIR R. AGUIAR	University of São Paulo at São Carlos, Brazil
KATIA BERTOLDI	Harvard University, USA
DAVIDE BIGONI	University of Trento, Italy
YIBIN FU	Keele University, UK
IWONA JASIUK	University of Illinois at Urbana-Champaign, USA
C. W. LIM	City University of Hong Kong
THOMAS J. PENCE	Michigan State University, USA
GIANNI ROYER-CARFAGNI	Università degli studi di Parma, Italy
DAVID STEIGMANN	University of California at Berkeley, USA
PAUL STEINMANN	Friedrich-Alexander-Universität Erlangen-Nürnberg, Germany

ADVISORY BOARD

J. P. CARTER	University of Sydney, Australia
D. H. HODGES	Georgia Institute of Technology, USA
J. HUTCHINSON	Harvard University, USA
D. PAMPLONA	Universidade Católica do Rio de Janeiro, Brazil
M. B. RUBIN	Technion, Haifa, Israel

PRODUCTION production@msp.org

SILVIO LEVY Scientific Editor


Cover photo: Wikimedia Commons

See msp.org/jomms for submission guidelines.

JoMMS (ISSN 1559-3959) at Mathematical Sciences Publishers, 798 Evans Hall #6840, c/o University of California, Berkeley, CA 94720-3840, is published in 10 issues a year. The subscription price for 2016 is US \$575/year for the electronic version, and \$735/year (+\$60, if shipping outside the US) for print and electronic. Subscriptions, requests for back issues, and changes of address should be sent to MSP.

JoMMS peer-review and production is managed by EditFLOW® from Mathematical Sciences Publishers.

PUBLISHED BY

 **mathematical sciences publishers**
nonprofit scientific publishing

<http://msp.org/>

© 2016 Mathematical Sciences Publishers

INTERFACE STRESS OF ORTHOTROPIC MATERIALS WITH A NANODEFECT UNDER ANTIPLANE SHEAR LOADING

JUNHUA XIAO, CHUANFU SHI, YAOLING XU AND FUCHENG ZHANG

A theoretical study is conducted on an orthotropic solid with a nanodefekt (e.g., inclusion, hole, or crack) under far-field antiplane shear loading. A rigorous analytical solution of the stress fields is presented using the Gurtin–Murdoch surface/interface model and a conformal mapping technique. Several new and existing solutions are considered for the special and degenerated cases. The major results of the study are as follows:

- (1) Interface stresses are greatly dependent on size when the size of a defect is at the nanometer scale, and the interface stresses approach the classical elasticity results when a defect has large characteristic dimensions.
- (2) The interface effect of a nanodefekt decreases with an increase in defect section aspect ratio.
- (3) When the modulus of the defect (inclusion) increases, the interface effect decreases, i.e., the interface effect can be neglected when the inclusion is sufficiently hard.

1. Introduction

Several composite materials can be regarded as orthotropic solids in engineering applications. The general properties, as well as the fracture and damage properties, of orthotropic solids have received considerable attention with respect to elastic-plastic and fracture damage theories. When the size of defects (e.g., inclusion, hole, or crack) in an orthotropic solid is at the nanometer scale, the interface effect of nanodefekts plays an important role in micromechanical properties because of the high surface-to-volume ratios of this solid material [Nan and Wang 2013; Grekov and Yazovskaya 2014].

In recent years, significant progress has been made in addressing the fracture characteristics of orthotropic solids with holes or cracks from a fundamental perspective by applying classical elastoplastic theory. Tang and Hwang [1991] discussed the near-tip field solution for a plane stress mode I stationary crack in an elastic-perfectly orthotropic plastic material based on phenomenological plasticity theory. Gao and Tong [1995] used the Cauchy integral method to study the fundamental solutions for the complex stress functions and the stress intensity factors of an equal-parameter orthotropic plate with an elliptical hole or crack. Ozturk and Erdogan [1997] formulated the mode I crack problem for an inhomogeneous orthotropic plane and obtained a solution for various loading conditions and material parameters. Kim, Lee, and Joo [1999] presented a numerical solution by applying the Fourier integral transform method on the problem of a three-layered orthotropic material with a center crack that was subjected to an arbitrary antiplane shear loading. Berbinau and Soutis [2001] presented a new analytical method for solving mixed boundary value problems along holes in orthotropic plates. Kwon and Meguid [2002] proposed a general solution for the field intensity factors and the energy release rate of a Griffith crack normal to

Keywords: orthotropic materials, nanodefekts, interface stresses, antiplane shear, Gurtin–Murdoch surface/interface model.

the interface between a rectangular piezoelectric ceramic and two of the same rectangular orthotropic materials with finite lengths under combined in-plane electrical and antiplane mechanical loadings. Lee, Kwon, Lee, and Kwon [2002] provided the dynamic field intensity factors for the problem of an interfacial crack moving along the interface between a piezoelectric material and two orthotropic materials under electromechanical longitudinal shear loading. Li [2003] analytically determined the stress intensity factors for the problem of an orthotropic strip with two collinear cracks normal to the strip boundaries under remote uniform antiplane shear loading. Faal and Fariborz [2007] derived the stress fields in an orthotropic infinite plane with Volterra-type climb and glide edge dislocations. Chalivendra [2008] developed quasistatic stress fields for a crack oriented along one of the principal axes of an inhomogeneous orthotropic medium by conducting asymptotic analysis coupled with the Westergaard stress function approach. Zhang and Deng [2008] derived elastic stress fields near the cohesive zone of a crack aligned with the principal axes of a degenerated orthotropic material using complex variable and eigenfunction expansion methods. Xiao and Jiang [2009] obtained a closed-form solution for orthotropic materials weakened by a doubly periodic array of cracks under far-field antiplane shear loading by applying elliptical function and analytical function theories on the boundary value problems. Moharrami and Ayatollahi [2011] conducted stress analysis on an orthotropic plane with a Volterra-type dislocation. The distributed dislocation technique was adopted to obtain the integral equations for an orthotropic plane weakened by cracks under time-harmonic antiplane traction. Goldstein and Shifrin [2012] investigated a crack that was initially located on a symmetry axis of an orthotropic plane and subjected to biaxial loading. Liu and Zhou [2014] presented a solution for a plane rectangular crack in a 3D infinite orthotropic elastic material by applying a generalization of Almansi's theorem and the Schmidt method. Liu, Zhou, Wu, and Wu [2015] investigated a nonlocal theory solution for a rectangular crack in a 3D infinite orthotropic elastic medium using a generalization of Almansi's theorem and the Schmidt method. Peng, Li, and Feng [2015] investigated the interaction between a mode I crack and a symmetrical shape inclusion in an orthotropic medium subjected to remote stress by using transformation toughening theory and the Eshelby inclusion method.

Extensive investigations have also been conducted on the effective properties of orthotropic composite solids. Zhao and Yu [2000] presented a model for orthotropic damage on materials by combining the macroscopic mechanical properties with the microstructure parameters of a material based on Eshelby's equivalence principle. Bouyge, Jasiuk, Boccara, and Ostoja-Starzewski [2002] determined the couple-stress moduli and characteristic lengths of a 2D matrix-inclusion composite with the inclusions arranged in a periodic square array and both linear elastic constituents being of Cauchy type. Yang and Becker [2004] studied the effective properties and microscopic deformation of anisotropic plates with periodic holes via direct mathematical homogenization. Ieşan and Scalia [2007] investigated linear theory of inhomogeneous and orthotropic elastic materials with voids. Nie, Chan, Shin, and Roy [2008] presented analytic solutions for elastic fields induced by normal and shear eigenstrains in an elliptical region embedded into orthotropic composite materials by applying conformal transformation and the complex function method. Monchiet, Gruescu, Cazacu, and Kondo [2012] achieved effective compliance of an orthotropic medium with arbitrarily oriented cracks by using newly derived expressions of the Eshelby tensor.

The present work constitutes research on the interface stresses of an orthotropic solid with a nanodefekt. A closed-form solution for the problem of orthotropic materials with a nanosized elliptical defect is presented under antiplane shear loading by applying the Gurtin–Murdoch surface/interface model and a

conformal mapping technique. The influences of defect size, matrix material moduli ratio, defect shape ratio, and defect elastic property on stress fields are discussed.

2. Computational model and basic equations

A schematic diagram of an orthotropic solid with an isotropic nanodefect (i.e., nanoelliptical inclusion) that considers the interface effect is presented in Figure 1. Regions Ω_I and Ω_M denote the elliptical defect and the matrix, respectively. The Gurtin–Murdoch surface/interface model [Gurtin and Murdoch 1975; 1978; Gurtin et al. 1998] indicates that interface L can be regarded as a layer without thickness and with different material properties from the defect and the matrix. The semimajor and semiminor axes of the elliptical defect are denoted as a and b , respectively. I , O , and M denote the defect, interface, and matrix, respectively. G_I denotes the antiplane shear modulus of the defect (inclusion). C_{44} and C_{55} are the principal shear moduli of the orthotropic solid, which are located along the y - and x -axes in Figure 1, respectively. The Oz -axis is perpendicular to the section in the Cartesian coordinate system. The matrix is subjected to far-field antiplane shear stress τ_{yz}^∞ .

The governing equation and the constitutive equation of the matrix can be given as [Li 2003]

$$\frac{\partial \tau_{xz}}{\partial x} + \frac{\partial \tau_{yz}}{\partial y} = 0, \tag{1}$$

$$\begin{Bmatrix} \tau_{xz} \\ \tau_{yz} \end{Bmatrix} = \begin{bmatrix} C_{55} & 0 \\ 0 & C_{44} \end{bmatrix} \begin{Bmatrix} \partial w / \partial x \\ \partial w / \partial y \end{Bmatrix}, \tag{2}$$

where w is the antiplane displacement.

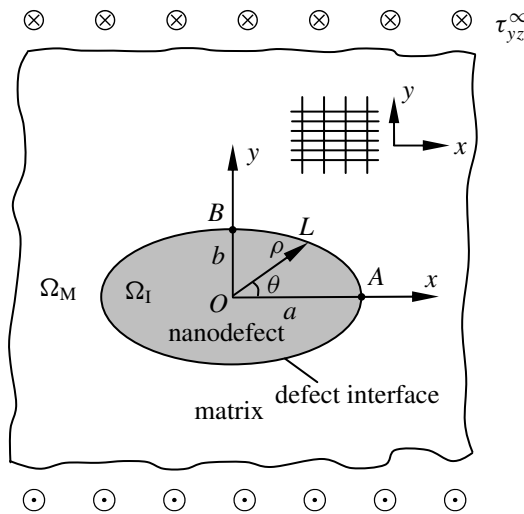


Figure 1. Schematic diagram of an orthotropic solid with a nanodefect (nanoelliptical inclusion) considering interface effect (z -plane, $z = x + iy$).

Nonclassical boundary conditions on nanodefekt interface L can be written as [Luo and Wang 2009; Sharma et al. 2003]

$$w_P(t) = w_M(t) \quad t = \rho e^{i\theta}, \tag{3}$$

$$\tau_{rz}^P(t) - \tau_{rz}^M(t) = \frac{2\mu^S}{\rho} \frac{\partial \epsilon_{\theta z}^0}{\partial \theta} \quad t = \rho e^{i\theta}, \tag{4}$$

where (ρ, θ) denotes the polar coordinates on the interface L ; $\tau_{\theta z}^0$ and $\epsilon_{\theta z}^0$ denote the stress and strain components on the interface, respectively; $\mu^S = C_{44}^S |\sin \theta| + C_{55}^S |\cos \theta|$; and C_{44}^S and C_{55}^S denote the interface elastic constants along the y - and x -axes in Figure 1, respectively. The unit for interface elastic constants C_{44}^S and C_{55}^S is N/m. The expression of μ^S in terms of θ is merely an assumption made by the authors.

The interfacial strain for a coherent interface is equal to the associated tangential strain in the abutting materials, i.e.,

$$\epsilon_{\theta z}^0 = \epsilon_{\theta z}^P = \epsilon_{\theta z}^M. \tag{5}$$

3. Analysis and solution

By substituting (2) into (1), a second-order linear homogeneous partial differential equation with constant coefficients on w is obtained as

$$C_{55} \frac{\partial^2 w}{\partial x^2} + C_{44} \frac{\partial^2 w}{\partial y^2} = 0. \tag{6}$$

The solution for (6) can be expressed as

$$w = \text{Re}F(z_m), \tag{7}$$

where $f(z_m)$ is an analytical function with respect to z_m , $z_m = x + imy$, and $m = \sqrt{C_{55}/C_{44}}$.

By substituting (7) into (2), the expressions obtained are

$$\begin{aligned} \tau_{xz} &= C_{55} \frac{\partial \text{Re}f(z_m)}{\partial x} = C_{55} \text{Re}f'(z_m), \\ \tau_{yz} &= mC_{44} \frac{\partial \text{Re}f(z_m)}{\partial (my)} = -mC_{44} \text{Im}f'(z_m), \end{aligned} \tag{8}$$

where $f'(z_m)$ denotes the derivative with respect to z_m . Then, (8) can be rewritten as

$$\frac{\tau_{xz}}{C_{55}} - i \frac{\tau_{yz}}{\sqrt{C_{44}C_{55}}} = \text{Re}f'(z_m) + i\text{Im}f'(z_m) = f'(z_m). \tag{9}$$

The z_m -plane (Figure 2) is generated by the map of $z_m = x + imy$ from the z -plane (Figure 1), where O_1 and O_2 denote the foci of the elliptical inclusion.

To solve the problem in Figure 2, a new variable ζ is introduced as

$$\zeta = \xi + i\eta = le^{i\phi}, \tag{10}$$

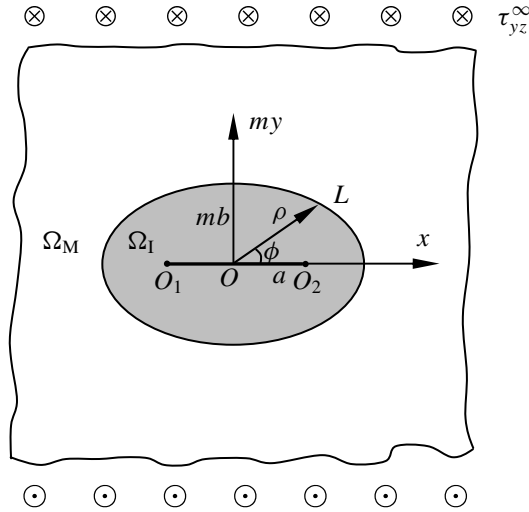


Figure 2. z_m -plane corresponding to the plane z ($z_m = x + imy$).

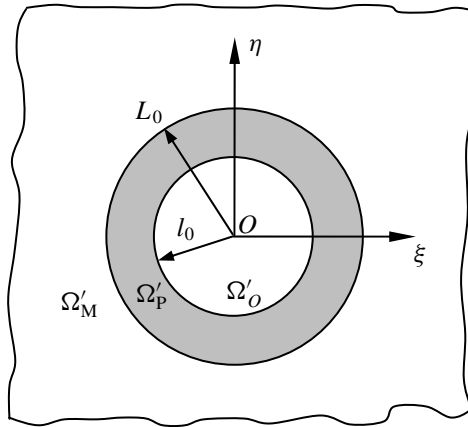


Figure 3. Conformal mapping in the ζ -plane ($\zeta = \xi + i\eta$).

where (l, ϕ) denotes the polar coordinates in the ζ -plane. The z_m -plane is mapped onto the ζ -plane via conformal transformation,

$$z_m = \Omega(\zeta) = \zeta + \frac{n}{\zeta}, \tag{11}$$

where $n = (a^2 - m^2b^2)/4$. Region Ω_I in the z_m -plane is mapped onto circular region Ω'_O , with radius l_0 , and circular region Ω'_P , with radius L_0 , shown in **Figure 3**, respectively.

From the transformation relationship between **Figures 2** and **3**, the equations obtained are

$$x = \xi + \frac{n\xi}{\xi^2 + \eta^2}, \quad my = \eta - \frac{n\eta}{\xi^2 + \eta^2}. \tag{12}$$

From (12), the following expressions are derived:

$$l_0 = \sqrt{n}, \tag{13}$$

$$L_0 = \frac{a+mb}{2}. \tag{14}$$

In an annular region, an analytical function $F(\zeta)$ can be expanded into a Laurent series [Muskhelishvili 1953]:

$$F(\zeta) = a^* \ln \zeta + \sum_{k=-\infty}^{\infty} a_k \zeta^k, \tag{15}$$

where a^* and a_k are complex constants to be determined. The exact solution can be obtained by taking the following finite terms of the series:

$$F_I(\zeta) = A_1 \left(\zeta + n/\zeta \right) = A_1 \left(l e^{i\phi} + \frac{n e^{-i\phi}}{l} \right) \quad \text{in } \Omega'_I, \tag{16}$$

$$F_M(\zeta) = B_1 \zeta + B_{-1} \frac{1}{\zeta} = B_1 l e^{i\phi} + \frac{B_{-1}}{l} e^{-i\phi} \quad \text{in } \Omega'_M, \tag{17}$$

where A_1 , B_1 , and B_{-1} are complex constants.

By applying far-field conditions, coefficient B_1 can be obtained from (9) and (17) as

$$B_1 = -i \frac{\tau_{yz}^\infty}{\sqrt{C_{44} C_{55}}}. \tag{18}$$

The boundary conditions on L_0 in Figure 3 can be summarized as

$$w_I(z) = w_M(z), \tag{19}$$

$$\tau_{rz}^I(z) - \tau_{rz}^M(z) = \frac{2\mu^S}{L_0} \frac{\partial \epsilon_{\theta z}^{L_0}}{\partial \theta}, \tag{20}$$

where $\mu^S = C_{44}^S |\sin \theta| + C_{55}^S |\cos \theta|$, and C_{44}^S and C_{55}^S denote the interface elastic constants along the y - and x -axes in Figure 1, respectively.

From boundary conditions (19) and (20), the expressions obtained are

$$\left(1 + \frac{n}{L_0^2} \right) A_1 = B_1 - \frac{B_{-1}}{L_0^2}, \tag{21}$$

$$\left[G_I \left(1 - \frac{n}{L_0^2} \right) + \frac{\mu^S}{L_0} \left(1 + \frac{n}{L_0^2} \right) \right] A_1 = C_{44} \left(B_1 + \frac{B_{-1}}{L_0^2} \right). \tag{22}$$

By integrating (21) and (22) into (18), the expressions

$$A_1 = S_1 B_1, \quad B_{-1} = S_{-1} B_1, \tag{23}$$

are derived, where

$$\begin{aligned} S_1 &= \frac{2C_{44}}{G_I(1-n/L_0^2) + (\mu^S/L_0)(1+n/L_0^2) + C_{44}(1+n/L_0^2)}, \\ S_{-1} &= \frac{G_I(1-n/L_0^2) + (\mu^S/L_0)(1+n/L_0^2) - C_{44}(1+n/L_0^2)}{G_I(1-n/L_0^2) + (\mu^S/L_0)(1+n/L_0^2) + C_{44}(1+n/L_0^2)} L_0^2. \end{aligned} \quad (24)$$

From (9), (16), (17), (18), and (23), the overall stress fields in the composites can be expressed as

$$\tau_{yz} + i\tau_{xz} = G_I S_1 \frac{\tau_{yz}^\infty}{\sqrt{C_{44}C_{55}}} \quad \text{in the inclusion,} \quad (25)$$

$$\frac{\tau_{yz}}{\sqrt{C_{44}C_{55}}} + i \frac{\tau_{xz}}{C_{55}} = \frac{\zeta^2 - S_{-1}}{\zeta^2 - n} \frac{\tau_{yz}^\infty}{\sqrt{C_{44}C_{55}}} \quad \text{in the matrix,} \quad (26)$$

where $\zeta = \xi + i\eta = (z_m + \sqrt{z_m^2 - 4n})/2$, $z_m = x + imy$.

4. Special cases

(1) *Orthotropic solid with a rigid nanoelliptical inclusion:*

Let $G_I \rightarrow \infty$ in (25) and (26). The stress fields degenerate into

$$\tau_{yz} + i\tau_{xz} = \frac{2C_{44}}{1-n/L_0^2} \frac{\tau_{yz}^\infty}{\sqrt{C_{44}C_{55}}} \quad \text{in the inclusion,} \quad (27)$$

$$\frac{\tau_{yz}}{\sqrt{C_{44}C_{55}}} + i \frac{\tau_{xz}}{C_{55}} = \frac{\zeta^2 - L_0^2}{\zeta^2 - n} \frac{\tau_{yz}^\infty}{\sqrt{C_{44}C_{55}}} \quad \text{in the matrix.} \quad (28)$$

(2) *Orthotropic solid with a nanoelliptical hole:*

Let $G_I = 0$. Equation (26) degenerates into

$$\frac{\tau_{yz}}{\sqrt{C_{44}C_{55}}} + i \frac{\tau_{xz}}{C_{55}} = \frac{\zeta^2 - (\mu^S/L_0 - C_{44})/(\mu^S/L_0 + C_{44})L_0^2}{\zeta^2 - n} \frac{\tau_{yz}^\infty}{\sqrt{C_{44}C_{55}}}. \quad (29)$$

Equation (29) agrees with the existing results [Xiao et al. 2014, Equation (23)].

(3) *Nanocrack in an orthotropic solid:*

Take $b = 0$ in (29). The crack tip stress field can be obtained as

$$\frac{\tau_{yz}}{\sqrt{C_{44}C_{55}}} + i \frac{\tau_{xz}}{C_{55}} = \frac{4\zeta^2 - (2\mu^S/a - C_{44})/(2\mu^S/a + C_{44})a^2}{4\zeta^2 - a^2} \frac{\tau_{yz}^\infty}{\sqrt{C_{44}C_{55}}}. \quad (30)$$

The III-type stress intensity factor at tip A in Figure 1 can be defined as

$$K_{\text{III}}^A = \lim_{\substack{y=0 \\ z \rightarrow a}} \tau_{yz} \sqrt{2\pi(z-a)} = \tau_{yz}^\infty \sqrt{\pi a} \frac{C_{44}}{C_{44} + 2\mu^S/a} = K_A^* \tau_{yz}^\infty \sqrt{\pi a}, \quad (31)$$

where $K_A^* = K_{\text{III}}^A/(\tau_{yz}^\infty \sqrt{\pi a})$ denotes the dimensionless stress intensity factor at tip A. When ignoring the interface effect of inclusion, i.e., $\mu^S = 0$, (31) degenerates into the existing solution presented by Hwu [1991], i.e.,

$$K_{\text{III}}^A = \tau_{yz}^\infty \sqrt{\pi a}. \quad (32)$$

5. Results and discussion

The interface elastic constant can be obtained through atomistic simulations. Studies on orthotropic solids remain lacking; thus, we consider $C_{44}^S/C_{55}^S = C_{44}/C_{55}$ in this work. We assume that the ratio of the elastic constant C_{44}^S of the interface to that of the matrix along the y -axis is a real constant α , i.e., $\alpha = C_{44}^S/C_{44}$, where α varies from $-2 \cdot 10^{-10}$ m to $2 \cdot 10^{-10}$ m [Luo and Wang 2009]. Then, $\mu^S = C_{44}^S|\sin \theta| + C_{55}^S|\cos \theta| = C_{44}^S(|\sin \theta| + C_{55}^S/C_{44}|\cos \theta|)$. We then define the section aspect ratio of the elliptical inclusion as $\gamma = b/a$, $\beta = G_I/C_{44}$.

Example 1. A comparison of the present solution for $\alpha = 0$ (classical elasticity theory) with the finite element results is plotted in Figure 4, where $a = 5$ nm, $\gamma = b/a = 0.5$, $\beta = G_I/C_{44} = 0$, $C_{55} = 12$ GPa, and $C_{44} = 5.7$ GPa. The finite element results agree with the present solution when $\alpha = 0$. With the increase in angle θ from 0° to 90° , the interface stress concentration factors decrease monotonously when $\alpha = 2 \cdot 10^{-10}$ m and $\alpha = 0$, whereas the interface stress concentration factors initially decrease and then increase when $\alpha = -2 \cdot 10^{-10}$ m.

Example 2. The variation in the stress concentration factors at points A and B (Figure 1) with the semimajor axis of the inclusion is plotted in Figure 5, where $\gamma = b/a = 0.2$, $\beta = G_I/C_{44} = 2$, and $C_{55}/C_{44} = 2$. Stress τ_{yz}^A is calculated using (26) when $\rho = a$ and $\theta = 0^\circ$ (Figure 1). Then, stress τ_{yz}^A is the bulk stress, and stress concentration factor $\tau_{yz}^A/\tau_{yz}^\infty$ is dimensionless.

Figure 5 shows that stress concentration factors are dramatically dependent on size when the size of an elliptical inclusion is at the nanometer scale. The present solution approaches classical elasticity theory when the inclusion has large characteristic dimensions.

Example 3. The material moduli ratio C_{55}/C_{44} can be regarded as a parameter in studying the influence of material orthotropy on stress concentration factors. The variation in the stress concentration factors

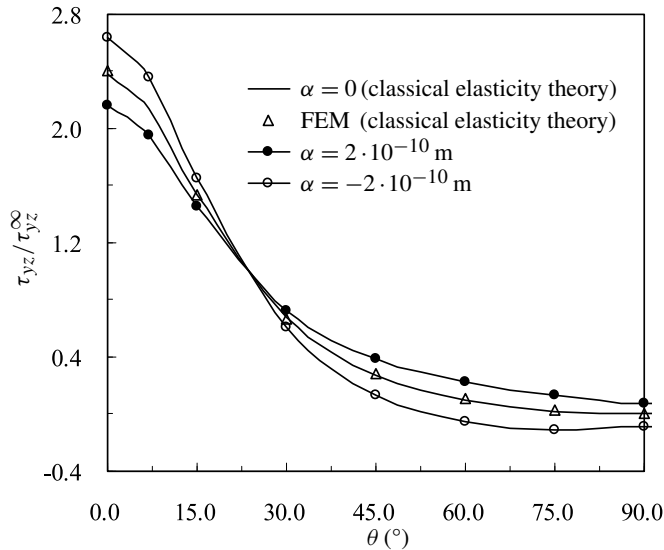


Figure 4. Distribution of the interface stress concentration factors on the interface of the elliptic hole.

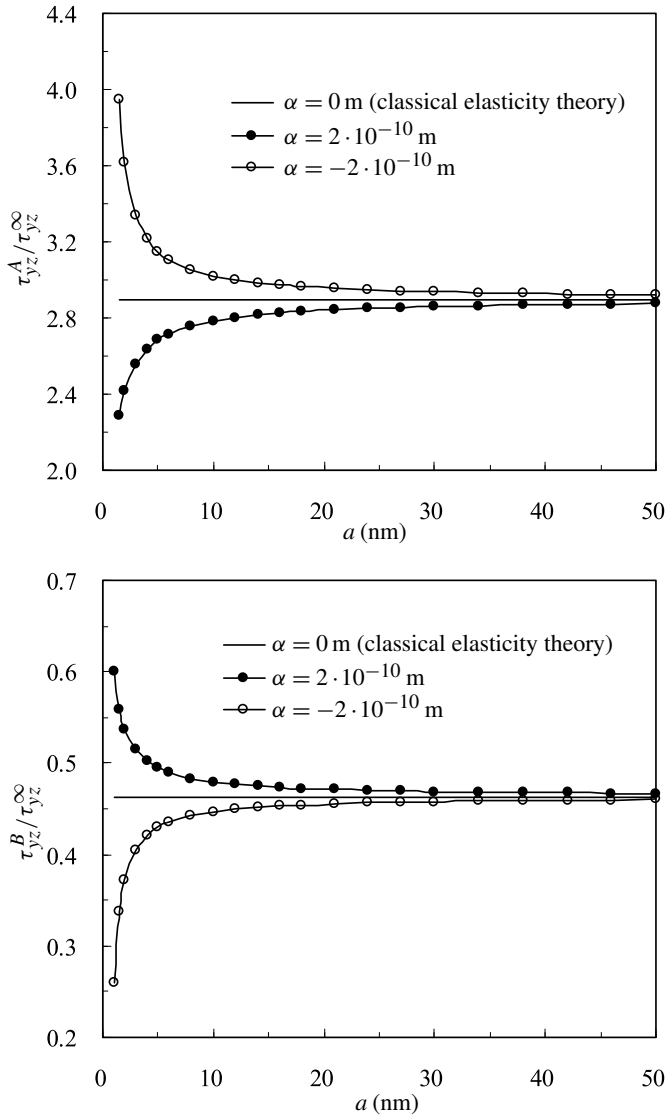


Figure 5. Variation of the stress concentration factors at points A (top) and B (bottom) with the size of the elliptic inclusion.

at points A and B with $\lg(C_{55}/C_{44})$ is plotted in Figure 6, where $a = 5$ nm, $\gamma = b/a = 0.2$, and $\beta = G_1/C_{44} = 2$.

When the ratio of the elastic main direction $\lg(C_{55}/C_{44})$ increases, the increase in C_{55}/C_{44} shields the stress concentration factor at point A but amplifies said factor at point B.

Example 4. Figure 7 shows the variation in the stress concentration factors at points A and B with the inclusion section aspect ratio $\gamma = b/a$, where $a = 5$ nm, $\beta = G_1/C_{44} = 2$, and $C_{55}/C_{44} = 2$.

When the inclusion section aspect ratio γ increases gradually from 0 to 1, the stress concentration factor at point A decreases monotonically, whereas at point B it increases monotonically. The interface

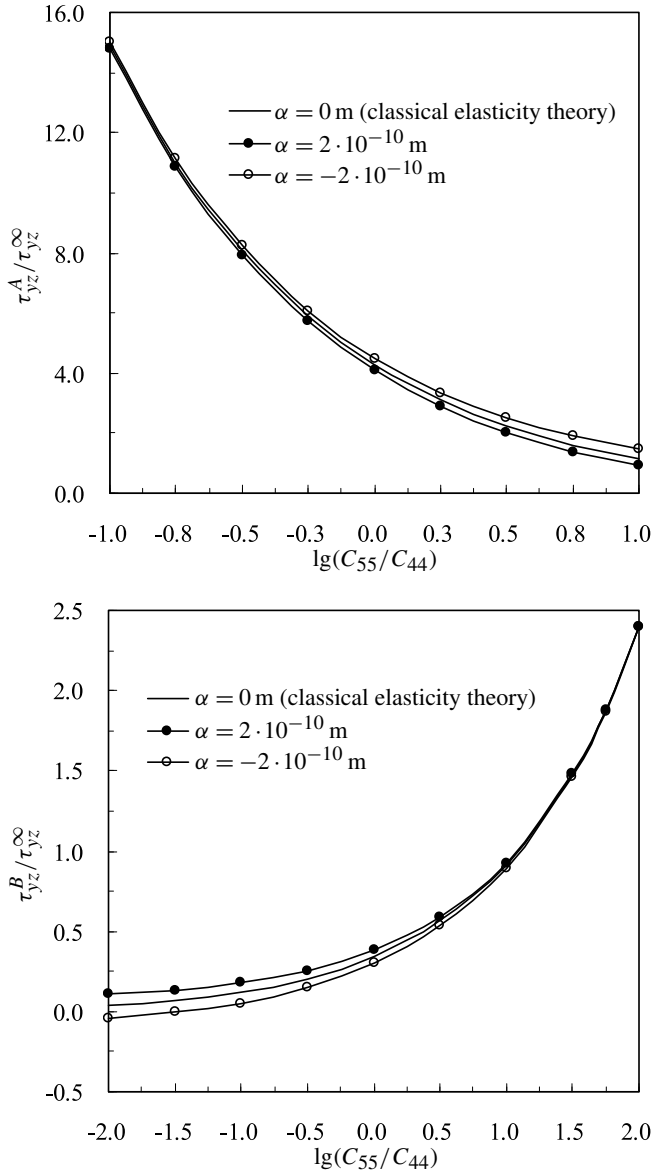


Figure 6. Variation of the stress concentration factors at points *A* (top) and *B* (bottom) with the ratio of the elastic main direction C_{55}/C_{44} .

effect of the nanoinclusion decreases with the increase in the inclusion section aspect ratio γ .

Example 5. The variation in the stress concentration factors at points *A* and *B* with the dimensionless logarithmic inclusion shear modulus $\lg(G_1/G_{44})$ is plotted in Figure 8, where $a = 5$ nm, $\gamma = b/a = 0.2$, and $C_{55}/C_{44} = 2$.

Figure 8 illustrates an interesting phenomenon in which the interface effect can be neglected when

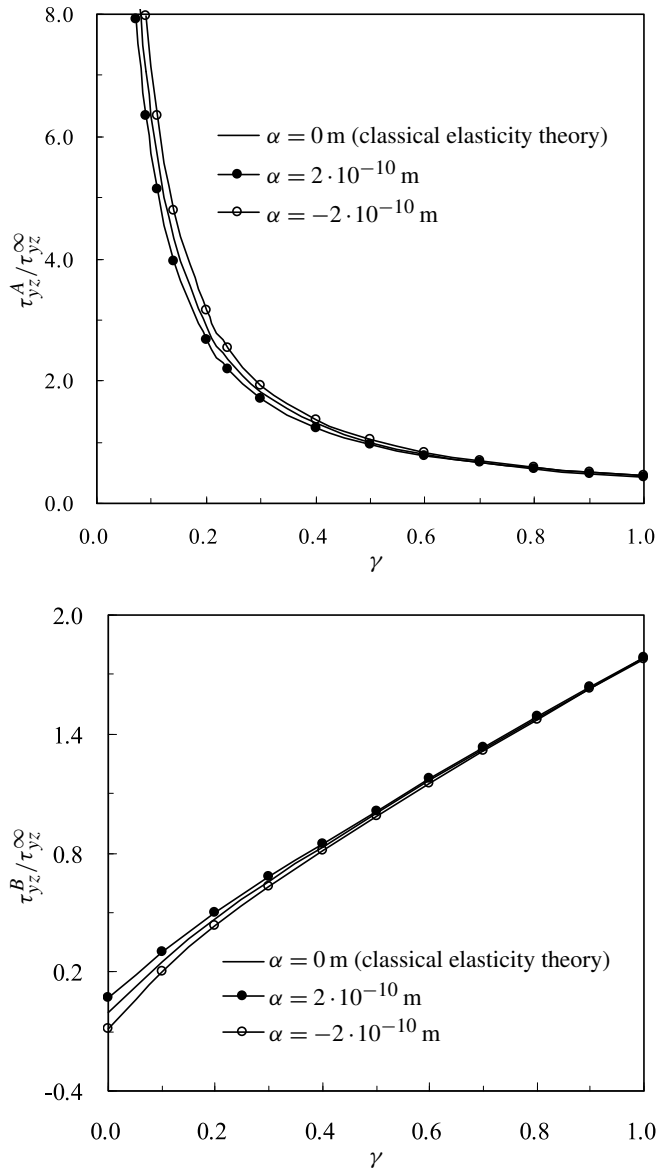


Figure 7. Variation of the stress concentration factors at points *A* (top) and *B* (bottom) with the elliptic inclusion shape ratio $\gamma = b/a$.

the inclusion is sufficiently hard. The influence of the interface effect depends on the modulus of the inclusion, i.e., the interface effect decreases with the increase in the modulus of the inclusion.

6. Conclusions

The problem of an orthotropic solid with a nanodefect under far-field antiplane shear loading was investigated using the Gurtin–Murdoch surface/interface model and a conformal mapping technique. An

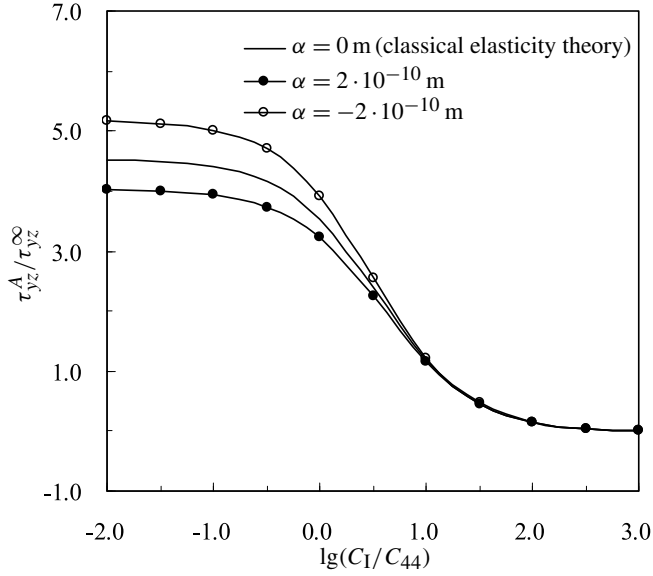
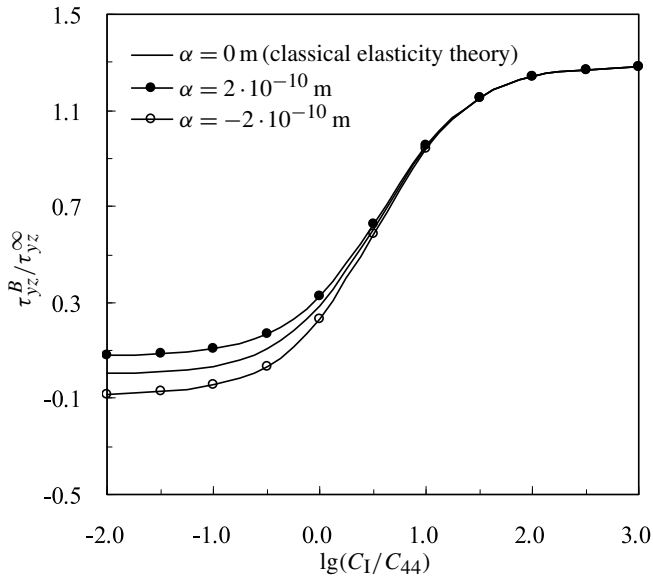
(a) Stress concentration factor at point *A*.(b) Stress concentration factor at point *B*.

Figure 8. Variation of the stress concentration factors at points *A* and *B* with the elliptic cavity shape ratio $\gamma = b/a$.

analytical solution for the overall stress field in the nanoinhomogeneous material was obtained. The proposed solution is generalized, such that several new and existing solutions can be regarded as special or degenerate cases. The effects of defect size, matrix material moduli ratio, defect shape ratio, and inclusion elastic property on the interface stresses were discussed.

Acknowledgments

This work was supported by the National Natural Science Foundation of China (11302186), the National Natural Science Foundation for Distinguished Young Scholars (50925522), the Hebei Province High School Top Young Talent (BJ2014058) and the Natural Science Foundation of Hebei Province (A2013203103, A2013203213).

References

- [Berbinau and Soutis 2001] P. Berbinau and C. Soutis, “A new approach for solving mixed boundary value problems along holes in orthotropic plates”, *Int. J. Solids Struct.* **38**:1 (2001), 143–159.
- [Bouyge et al. 2002] F. Bouyge, I. Jasiuk, S. Boccara, and M. Ostoja-Starzewski, “A micromechanically based couple-stress model of an elastic orthotropic two-phase composite”, *Eur. J. Mech. A Solids* **21**:3 (2002), 465–481.
- [Chalivendra 2008] V. B. Chalivendra, “Mode-I crack-tip stress fields for inhomogeneous orthotropic medium”, *Mech. Mater.* **40**:4–5 (2008), 293–301.
- [Faal and Fariborz 2007] R. T. Faal and S. J. Fariborz, “Stress analysis of orthotropic planes weakened by cracks”, *Appl. Math. Model.* **31**:6 (2007), 1133–1148.
- [Gao and Tong 1995] C. F. Gao and X. H. Tong, “The fundamental solutions for the equal-parameter orthotropic plate containing an elliptical hole or a crack”, *Acta Mech. Sinica* **27**:5 (1995), 609–613. In Chinese.
- [Goldstein and Shifrin 2012] R. V. Goldstein and E. I. Shifrin, “Conditions for Mode I crack deviation in orthotropic plane subjected to biaxial loading”, *Int. J. Eng. Sci.* **61** (2012), 36–47.
- [Grekov and Yazovskaya 2014] M. A. Grekov and A. A. Yazovskaya, “The effect of surface elasticity and residual surface stress in an elastic body with an elliptic nanohole”, *J. Appl. Math. Mech.* **78**:2 (2014), 172–180.
- [Gurtin and Murdoch 1975] M. E. Gurtin and A. I. Murdoch, “A continuum theory of elastic material surfaces”, *Arch. Ration. Mech. Anal.* **57**:4 (1975), 291–323.
- [Gurtin and Murdoch 1978] M. E. Gurtin and A. I. Murdoch, “Surface stress in solids”, *Int. J. Solids Struct.* **14**:6 (1978), 431–440.
- [Gurtin et al. 1998] M. E. Gurtin, J. Weissmüller, and F. Larché, “A general theory of curved deformable interfaces in solids at equilibrium”, *Philos. Mag. A* **78**:5 (1998), 1093–1109.
- [Hwu 1991] C. Hwu, “Collinear cracks in anisotropic bodies”, *Int. J. Fract.* **52**:4 (1991), 239–256.
- [İeşan and Scalia 2007] D. İeşan and A. Scalia, “On the deformation of functionally graded porous elastic cylinders”, *J. Elasticity* **87**:2 (2007), 147–159.
- [Kim et al. 1999] S. H. Kim, K. Y. Lee, and S. C. Joo, “Stress intensity factor for orthotropic three layered material with crack under arbitrary anti-plane shear”, *Theor. Appl. Fract. Mech.* **32**:2 (1999), 101–109.
- [Kwon and Meguid 2002] J. H. Kwon and S. A. Meguid, “Analysis of a central crack normal to a piezoelectric-orthotropic interface”, *Int. J. Solids Struct.* **39**:4 (2002), 841–860.
- [Lee et al. 2002] J. S. Lee, S. M. Kwon, K. Y. Lee, and J. H. Kwon, “Anti-plane interfacial Yoffe-crack between a piezoelectric and two orthotropic layers”, *Eur. J. Mech. A Solids* **21**:3 (2002), 483–492.
- [Li 2003] X.-F. Li, “Closed-form solution for two collinear mode-III cracks in an orthotropic elastic strip of finite width”, *Mech. Res. Commun.* **30**:4 (2003), 365–370.
- [Liu and Zhou 2014] H.-T. Liu and Z.-G. Zhou, “Basic solution of a plane rectangular crack in a 3-D infinite orthotropic elastic material”, *Mech. Res. Commun.* **61** (2014), 7–18.
- [Liu et al. 2015] H.-T. Liu, Z.-G. Zhou, L.-Z. Wu, and W.-J. Wu, “Non-local theory solution to a rectangular crack in a 3D infinite orthotropic elastic medium”, *Int. J. Solids Struct.* **58** (2015), 207–219.
- [Luo and Wang 2009] J. Luo and X. Wang, “On the anti-plane shear of an elliptic nano inhomogeneity”, *Eur. J. Mech. A Solids* **28**:5 (2009), 926–934.

- [Moharrami and Ayatollahi 2011] A. Moharrami and M. Ayatollahi, “Anti-plane elastodynamic analysis of orthotropic planes weakened by several cracks”, *Appl. Math. Model.* **35**:1 (2011), 50–60.
- [Monchiet et al. 2012] V. Monchiet, C. Gruescu, O. Cazacu, and D. Kondo, “A micromechanical approach of crack-induced damage in orthotropic media: Application to a brittle matrix composite”, *Eng. Fract. Mech.* **83** (2012), 40–53.
- [Muskhelishvili 1953] N. I. Muskhelishvili, *Some basic problems of the mathematical theory of elasticity: Fundamental equations, plane theory of elasticity, torsion and bending*, Noordhoff, Groningen, 1953.
- [Nan and Wang 2013] H. S. Nan and B. L. Wang, “Effect of crack face residual surface stress on nanoscale fracture of piezoelectric materials”, *Eng. Fract. Mech.* **110** (2013), 68–80.
- [Nie et al. 2008] G. H. Nie, C. K. Chan, F. G. Shin, and S. Roy, “Elliptical inhomogeneity in orthotropic composite materials due to uniform eigenstrains”, *Compos. B Eng.* **39**:2 (2008), 374–385.
- [Ozturk and Erdogan 1997] M. Ozturk and F. Erdogan, “Mode I crack problem in an inhomogeneous orthotropic medium”, *Int. J. Eng. Sci.* **35**:9 (1997), 869–883.
- [Peng et al. 2015] B. Peng, Z. Li, and M. Feng, “The mode I crack-inclusion interaction in orthotropic medium”, *Eng. Fract. Mech.* **136** (2015), 185–194.
- [Sharma et al. 2003] P. Sharma, S. Ganti, and N. Bhate, “Effect of surfaces on the size-dependent elastic state of nanoinhomogeneities”, *Appl. Phys. Lett.* **82**:4 (2003), 535–537.
- [Tang and Hwang 1991] L. Q. Tang and K. C. Hwang, “The near-tip fields for a plane stress mode I stationary crack in an elastic-perfectly orthotropic plastic material”, *Acta Mech. Sinica* **23**:4 (1991), 448–457. In Chinese.
- [Xiao and Jiang 2009] J. Xiao and C. Jiang, “Exact solution for orthotropic materials weakened by doubly periodic cracks of unequal size under antiplane shear”, *Acta Mech. Solida Sin.* **22**:1 (2009), 53–63.
- [Xiao et al. 2014] J.-h. Xiao, C.-f. Shi, Y.-l. Xu, and F.-c. Zhang, “Study on orthotropic materials containing elliptic cavity under anti-plane shear due to interface stress”, *J. Yanshan Univ.* **38**:3 (2014), 272–276. In Chinese.
- [Yang and Becker 2004] Q.-S. Yang and W. Becker, “Effective stiffness and microscopic deformation of an orthotropic plate containing arbitrary holes”, *Comput. Struct.* **82**:27 (2004), 2301–2307.
- [Zhang and Deng 2008] W. Zhang and X. Deng, “Asymptotic stress field in a degenerate orthotropic material containing a cohesive zone ahead of a crack tip”, *J. Elasticity* **90**:3 (2008), 271–282.
- [Zhao and Yu 2000] A. Zhao and J. Yu, “The overall elastic moduli of orthotropic composite and description of orthotropic damage of materials”, *Int. J. Solids Struct.* **37**:45 (2000), 6755–6771.

Received 6 Jul 2015. Revised 17 Mar 2016. Accepted 22 Mar 2016.

JUNHUA XIAO: xiaojunhua@ysu.edu.cn

Key Laboratory of Mechanical Reliability for Heavy Equipments and Large Structures of Hebei Province, Yanshan University, Qinhuangdao, 066004, China

CHUANFU SHI: 794509661@qq.com

Key Laboratory of Mechanical Reliability for Heavy Equipments and Large Structures of Hebei Province, Yanshan University, Qinhuangdao, 066004, China

YAOLING XU: xylysu@163.com

Key Laboratory of Mechanical Reliability for Heavy Equipments and Large Structures of Hebei Province, Yanshan University, Qinhuangdao, 066004, China

FUCHENG ZHANG: zfc@ysu.edu.cn

State Key Laboratory of Metastable Materials Science and Technology, Yanshan University, Qinhuangdao, 066004, China

PROPAGATION OF WAVES IN MASONRY-LIKE SOLIDS

MARIA GIRARDI, CRISTINA PADOVANI AND DANIELE PELLEGRINI

This paper deals with the propagation of progressive elastic waves in masonry-like solids. The constitutive equation of masonry-like materials models the mechanical behavior of materials (such as masonry, rocks and stones) that do not withstand tensile stresses. The stress function \mathbb{T} delivering the Cauchy stress \mathbf{T} corresponding to an infinitesimal strain tensor \mathbf{E} is nonlinear and differentiable on an open subset W of the set of all strains. We consider the propagation of small amplitude elastic waves in a masonry-like body subjected to a given homogenous strain field \mathbf{E} belonging to W . We obtain the propagation condition, which involves the acoustic tensor $\mathbf{A}(\mathbf{E}, \mathbf{n})$, which depends on both \mathbf{E} and the direction of propagation \mathbf{n} , and prove that, due to the presence of cracks, the wave propagation velocities in masonry are lower than in a linear elastic material.

Introduction

The study of elastic waves finds its main applications in addressing earthquakes and seismological problems [Ewing et al. 1957], in the evaluation of cracks in elastic media [Crampin 1981], as well as in the acoustic determination of third-order elastic constants and residual stresses [Winkler and Liu 1996; Pao et al. 1984; Ogden and Singh 2011]. A further application is in assessing the mechanical behavior of constructions in response to earthquakes by studying the propagation properties of seismic waves. In [Safack 1999] the changes in the propagation characteristics of seismic waves in a building were shown to be more reliable indicators of damage than changes in natural frequencies. In [Ivanovic et al. 2001; Safak et al. 2009] the wave propagation method is used for structural health monitoring purposes.

A detailed treatment of elastic waves is available in [Royer and Dieulesaint 2000], which addresses the different types of waves that propagate in isotropic and anisotropic solids, with particular focus on the propagation and generation of waves in crystals. Progressive waves and the Fresnel–Hadamard condition for their propagation, involving the acoustic tensor, are discussed in [Truesdell and Toupin 1960]. Progressive waves have been studied in [Gurtin 1972; Chadwick 1989] for isotropic and transversely isotropic linear elastic media. Lastly, the acoustic tensor and its eigenvalues and eigenvectors are explicitly calculated in [Chadwick 1989].

This paper deals with the propagation of progressive elastic waves in a masonry-like body subjected to a given homogeneous strain field. Unlike [Gurtin 1972; Chadwick 1989], which deal with linear elasticity, here we consider the constitutive equation of masonry-like materials [Del Piero 1989; Lucchesi et al. 2008], which models the mechanical behavior of materials (such as masonry, rocks and stones) that

This research has been cofunded by the Fondazione Cassa di Risparmio di Lucca within the framework of the MONSTER project (Structural Monitoring of Heritage Buildings by Wireless Technologies and Innovative Computing Tools, 2014-2016). This support is gratefully acknowledged.

Keywords: nonlinear elasticity, masonry-like materials, progressive waves, acoustic tensor.

do not withstand tensile stresses. A masonry-like material is a nonlinear hyperelastic material with zero tensile strength and infinite compressive strength. For the Cauchy stress \mathbf{T} and the infinitesimal strain \mathbf{E} (both belonging to the set Sym of symmetric tensors), the stress-strain relation is determined by the nonlinear relation $\mathbf{T} = \mathbb{C}[\mathbb{P}(\mathbf{E})]$, where \mathbb{C} is the fourth-order elasticity tensor, and \mathbb{P} is the nonlinear projection of the strain tensor onto the image of the set $\mathbb{C}^{-1}\text{Sym}^-$ of negative-semidefinite stresses Sym^- under \mathbb{C}^{-1} with respect to the energetic scalar product on Sym . The tensor $\mathbf{E}^f = \mathbf{E} - \mathbb{P}(\mathbf{E})$, which is positive-semidefinite and orthogonal to \mathbf{T} , is called fracture strain and is different from zero where fractures arise.

The constitutive equation of isotropic masonry-like materials is briefly described in [Section 1](#), which also presents the explicit expression for the stress function $\mathbb{T}(\mathbf{E}) = \mathbb{C}[\mathbb{P}(\mathbf{E})]$ as \mathbf{E} varies in the four regions V_i , $i = 0, 1, 2, 3$. Regions V_i characterize the different types of behavior that a masonry-like material can exhibit. In V_3 the material behaves like a linear elastic material, since the stress is negative-semidefinite. In V_0 the stress tensor is zero and the material can crack in all directions. Regions V_1 and V_2 exhibit mixed behavior: the stress tensor has respectively two and one eigenvectors corresponding to the zero eigenvalue, and the material can fracture orthogonally to these directions. As demonstrated in [\[Lucchesi et al. 2008; Padovani and Šilhavý 2015\]](#), the function \mathbb{T} is differentiable on $W = \bigcup_{i=0}^3 W_i$, with W_i being the interior of set V_i . The derivative $D_{\mathbf{E}}\mathbb{T}(\mathbf{E})$ of \mathbb{T} with respect to \mathbf{E} is a symmetric fourth-order tensor from Sym with values in Sym , whose spectral representation has been calculated in [\[Lucchesi et al. 2008\]](#) and is recalled here.

The boundary-initial-value problem of the dynamics of masonry-like solids has been addressed in [\[Casarosa et al. 1998; Lucchesi et al. 1999; Degl'Innocenti et al. 2006\]](#), which deal with the nonlinearity of the equation of motion. The exact solution to the problem of free longitudinal vibrations of both finite and infinite beams has been calculated in [\[Casarosa et al. 1998; Lucchesi et al. 1999\]](#). The main features of the solution is the development of a shock wave [\[Šilhavý 1997\]](#) at the interface between the cracked and compressed parts of the beam, which determines a loss of mechanical energy and a progressive decay of the solution. As far as the numerical solution of the dynamic problem of masonry structures is concerned, Degl'Innocenti et al. [\[2006\]](#) proposed a method to integrate with respect to time the system of ordinary differential equations obtained by discretizing the structure into finite elements. The method has been implemented in the NOSA-ITACA code [\[Binante et al. 2014\]](#) and was used to study the dynamic behavior of historical masonry buildings [\[Callieri et al. 2010; De Falco et al. 2014\]](#).

The approach followed in this paper is rather different: instead of addressing the boundary-initial-value problem of dynamics, we consider the propagation of progressive elastic waves in a masonry-like body subjected to a given homogeneous strain field \mathbf{E} belonging to W . By using the differentiability of the stress function at \mathbf{E} and considering elastic displacements superimposed on \mathbf{E} , we obtain the linearized equation of the motion involving the constant fourth-order tensor $D_{\mathbf{E}}\mathbb{T}(\mathbf{E})$. We then consider progressive waves and determine the condition they must satisfy in order to propagate in the masonry body. This condition involves the acoustic tensor $\mathbf{A}(\mathbf{E}, \mathbf{n})$, whose eigenvalues and eigenvectors are calculated in [Section 2](#).

Unlike the linear elastic case, in which the acoustic tensor depends only on the direction of propagation \mathbf{n} , here it depends on the strain \mathbf{E} as well. Moreover, even though symmetric, $\mathbf{A}(\mathbf{E}, \mathbf{n})$ is positive-semidefinite, since its eigenvalues are non-negative.

The acoustic tensor and the properties of progressive waves are analyzed as the given homogeneous strain field \mathbf{E} varies in the regions W_i , $i = 0, 1, 2, 3$. For $\mathbf{E} \in W_0$, the material is completely cracked and elastic waves cannot propagate. For $\mathbf{E} \in W_1, W_2$, due to the presence of cracks, the wave propagation velocities in masonry are lower than in a linear elastic material. Moreover, longitudinal waves propagate only for some values of \mathbf{n} , depending on the directions of cracking. For the remaining values of \mathbf{n} the waves are neither longitudinal nor transverse and propagate with different velocities in different directions. Finally, if $\mathbf{E} \in W_3$, masonry behaves like a linear elastic material.

Section 3 provides a detailed description of the two-dimensional case. In order to highlight the difference between a masonry-like and a linear elastic material, pictures illustrating the effects of the presence of cracks on the propagation of elastic waves are presented.

1. The constitutive equation

Let Lin be the set of all second-order tensors with the scalar product

$$\mathbf{A} \cdot \mathbf{B} = \text{tr}(\mathbf{A}^T \mathbf{B})$$

for any $\mathbf{A}, \mathbf{B} \in \text{Lin}$, with \mathbf{A}^T the transpose of \mathbf{A} . For Sym , the subspace of symmetric tensors, Sym^- and Sym^+ are the sets of all negative-semidefinite and positive-semidefinite elements of Sym . Given the symmetric tensors \mathbf{A} and \mathbf{B} , we denote by $\mathbf{A} \otimes \mathbf{B}$ the fourth-order tensor defined by

$$\mathbf{A} \otimes \mathbf{B}[\mathbf{H}] = (\mathbf{B} \cdot \mathbf{H})\mathbf{A}$$

for $\mathbf{H} \in \text{Lin}$, and by $\mathbb{1}_{\text{Sym}}$ the fourth-order identity tensor on Sym . For \mathbf{a} and \mathbf{b} vectors, the dyad $\mathbf{a} \otimes \mathbf{b}$ is defined by $\mathbf{a} \otimes \mathbf{b}\mathbf{h} = (\mathbf{b} \cdot \mathbf{h})\mathbf{a}$, for any vector \mathbf{h} , and \cdot is the scalar product in the space of vectors. We define the subspaces

$$\text{Span}(\mathbf{a}, \mathbf{b}) = \{\mathbf{v} = a\mathbf{a} + b\mathbf{b} : a, b \in \mathbb{R}\},$$

$$\text{Span}(\mathbf{a})^\perp = \{\mathbf{v} : \mathbf{a} \cdot \mathbf{v} = 0\}$$

of the three-dimensional vector space.

Now, let \mathbb{C} be the isotropic fourth-order tensor of the elastic constants

$$\mathbb{C} = 2\mu\mathbb{1}_{\text{Sym}} + \lambda\mathbf{I} \otimes \mathbf{I}, \quad (1-1)$$

where $\mathbf{I} \in \text{Sym}$ is the identity tensor and μ and λ are the Lamé moduli of the material satisfying the conditions

$$\mu > 0, \quad \lambda \geq 0. \quad (1-2)$$

\mathbb{C} is symmetric,

$$\mathbf{A} \cdot \mathbb{C}[\mathbf{B}] = \mathbf{B} \cdot \mathbb{C}[\mathbf{A}] \text{ for all } \mathbf{A}, \mathbf{B} \in \text{Sym}, \quad (1-3)$$

and in view of (1-2) is positive-definite on Sym ,

$$\mathbf{A} \cdot \mathbb{C}[\mathbf{A}] > 0 \text{ for all } \mathbf{A} \in \text{Sym}, \quad \mathbf{A} \neq \mathbf{0}. \quad (1-4)$$

Then \mathbb{C} is invertible, with inverse \mathbb{C}^{-1} . We define the energetic scalar product on Sym by setting $(\mathbf{A}, \mathbf{B}) = \mathbf{A} \cdot \mathbb{C}[\mathbf{B}]$ for any $\mathbf{A}, \mathbf{B} \in \text{Sym}$.

A masonry-like material is a nonlinear elastic material characterized by the fact that, for $\mathbf{E} \in \text{Sym}$, there exists a unique triplet $(\mathbf{T}, \mathbf{E}^e, \mathbf{E}^f)$ of elements of Sym such that [Lucchesi et al. 2008]

$$\mathbf{E} = \mathbf{E}^e + \mathbf{E}^f, \quad (1-5)$$

$$\mathbf{T} = \mathbb{C}[\mathbf{E}^e], \quad (1-6)$$

$$\mathbf{T} \in \text{Sym}^-, \quad \mathbf{E}^f \in \text{Sym}^+, \quad (1-7)$$

$$\mathbf{T} \cdot \mathbf{E}^f = 0. \quad (1-8)$$

\mathbf{T} is the Cauchy stress corresponding to strain \mathbf{E} ; \mathbf{E}^e and \mathbf{E}^f are respectively the elastic and inelastic parts of \mathbf{E} ; \mathbf{E}^f is also called fracture strain. Denoting by $\mathbb{P} : \text{Sym} \rightarrow \text{Sym}$ the metric projection onto the closed convex cone $\mathbb{C}^{-1}\text{Sym}^-$ with respect to the energetic scalar product, it is possible to prove that $\mathbf{E}^e = \mathbb{P}(\mathbf{E})$ and $\mathbf{T} = \mathbb{C}[\mathbb{P}(\mathbf{E})]$ [Padovani and Šilhavý 2015]. The stress function $\mathbb{T} : \text{Sym} \rightarrow \text{Sym}$ is given by

$$\mathbb{T}(\mathbf{E}) = \mathbf{T} = \mathbb{C}[\mathbb{P}(\mathbf{E})] \text{ for any } \mathbf{E} \in \text{Sym}. \quad (1-9)$$

The explicit expression for the stress function \mathbb{T} , calculated in [Lucchesi et al. 2008], is recalled in the following.

For $\mathbf{E} \in \text{Sym}$, let $e_1 \leq e_2 \leq e_3$ be its ordered eigenvalues and $\mathbf{q}_1, \mathbf{q}_2, \mathbf{q}_3$ the corresponding eigenvectors. We introduce the orthonormal basis of Sym (with respect to the scalar product \cdot)

$$\begin{aligned} \mathbf{O}_{11} &= \mathbf{q}_1 \otimes \mathbf{q}_1, & \mathbf{O}_{22} &= \mathbf{q}_2 \otimes \mathbf{q}_2, & \mathbf{O}_{33} &= \mathbf{q}_3 \otimes \mathbf{q}_3, \\ \mathbf{O}_{12} &= 1/\sqrt{2}(\mathbf{q}_1 \otimes \mathbf{q}_2 + \mathbf{q}_2 \otimes \mathbf{q}_1), & \mathbf{O}_{13} &= 1/\sqrt{2}(\mathbf{q}_1 \otimes \mathbf{q}_3 + \mathbf{q}_3 \otimes \mathbf{q}_1), \\ \mathbf{O}_{23} &= 1/\sqrt{2}(\mathbf{q}_2 \otimes \mathbf{q}_3 + \mathbf{q}_3 \otimes \mathbf{q}_2). \end{aligned} \quad (1-10)$$

Given \mathbf{E} , the corresponding stress satisfying the constitutive equation of masonry-like materials is given by

$$\text{if } \mathbf{E} \in V_0, \text{ then } \mathbf{T} = \mathbf{0}, \quad (1-11)$$

$$\text{if } \mathbf{E} \in V_1, \text{ then } \mathbf{T} = E e_1 \mathbf{O}_{11}, \quad (1-12)$$

$$\text{if } \mathbf{E} \in V_2, \text{ then } \mathbf{T} = 2\mu/(2+\alpha)\{[2(1+\alpha)e_1 + \alpha e_2]\mathbf{O}_{11} + [\alpha e_1 + 2(1+\alpha)e_2]\mathbf{O}_{22}\}, \quad (1-13)$$

$$\text{if } \mathbf{E} \in V_3, \text{ then } \mathbf{T} = \mathbb{C}[\mathbf{E}], \quad (1-14)$$

where the sets V_k are

$$V_0 = \{\mathbf{E} \in \text{Sym} : e_1 \geq 0\}, \quad (1-15)$$

$$V_1 = \{\mathbf{E} \in \text{Sym} : e_1 \leq 0, \quad \alpha e_1 + 2(1+\alpha)e_2 \geq 0\}, \quad (1-16)$$

$$V_2 = \{\mathbf{E} \in \text{Sym} : \alpha e_1 + 2(1+\alpha)e_2 \leq 0, \quad 2e_3 + \alpha \text{tr } \mathbf{E} \geq 0\}, \quad (1-17)$$

$$V_3 = \{\mathbf{E} \in \text{Sym} : 2e_3 + \alpha \text{tr } \mathbf{E} \leq 0\}, \quad (1-18)$$

with $\alpha = \lambda/\mu$ and the Young's modulus $E = \mu(2\mu + 3\lambda)/(\mu + \lambda)$. As for the fracture strain, we have

if $\mathbf{E} \in V_0$, then $\mathbf{E}^f = \mathbf{E}$, (1-19)

if $\mathbf{E} \in V_1$, then $\mathbf{E}^f = (e_2 + \alpha/(2(1 + \alpha))e_1)\mathbf{O}_{22} + (e_3 + \alpha/(2(1 + \alpha))e_1)\mathbf{O}_{33}$, (1-20)

if $\mathbf{E} \in V_2$, then $\mathbf{E}^f = [e_3 + \alpha/(2 + \alpha)(e_1 + e_2)]\mathbf{O}_{33}$, (1-21)

if $\mathbf{E} \in V_3$, then $\mathbf{E}^f = \mathbf{0}$. (1-22)

Thus, as \mathbf{E} varies in the four regions $V_i, i = 0, 1, 2, 3$, the corresponding stress tensor \mathbf{T} and fracture strain \mathbf{E}^f have rank $i = 0, 1, 2, 3$ and $r = 3, 2, 1, 0$, respectively.

For W_k , the interior of V_k , function \mathbb{T} turns out to be differentiable on $W = \bigcup_{i=0}^3 W_i$ [Lucchesi et al. 2008; Padovani and Šilhavý 2015]. The derivative $D_E\mathbb{T}(\mathbf{E})$ of $\mathbb{T}(\mathbf{E})$ with respect to \mathbf{E} in the regions W_i has been calculated in [Lucchesi et al. 2008]. $D_E\mathbb{T}(\mathbf{E})$ is a symmetric fourth-order tensor from Sym into itself and has the following expressions:

if $\mathbf{E} \in W_0$, then $D_E\mathbb{T}(\mathbf{E}) = \mathbb{O}$, (1-23)

where \mathbb{O} is the null fourth-order tensor,

if $\mathbf{E} \in W_1$, then $D_E\mathbb{T}(\mathbf{E}) = E \left(\mathbf{O}_{11} \otimes \mathbf{O}_{11} - \frac{e_1}{e_2 - e_1} \mathbf{O}_{12} \otimes \mathbf{O}_{12} - \frac{e_1}{e_3 - e_1} \mathbf{O}_{13} \otimes \mathbf{O}_{13} \right)$, (1-24)

if $\mathbf{E} \in W_2$, then $D_E\mathbb{T}(\mathbf{E}) = 2\mu\mathbf{O}_{12} \otimes \mathbf{O}_{12} - \frac{2\mu}{2 + \alpha} \frac{2(1 + \alpha)e_1 + \alpha e_2}{e_3 - e_1} \mathbf{O}_{13} \otimes \mathbf{O}_{13}$
 $- \frac{2\mu}{2 + \alpha} \frac{\alpha e_1 + 2(1 + \alpha)e_2}{e_3 - e_2} \mathbf{O}_{23} \otimes \mathbf{O}_{23} + \frac{2\mu(2 + 3\alpha)}{2 + \alpha} \frac{\mathbf{O}_{11} + \mathbf{O}_{22}}{\sqrt{2}} \otimes \frac{\mathbf{O}_{11} + \mathbf{O}_{22}}{\sqrt{2}}$
 $+ 2\mu \frac{\mathbf{O}_{11} - \mathbf{O}_{22}}{\sqrt{2}} \otimes \frac{\mathbf{O}_{11} - \mathbf{O}_{22}}{\sqrt{2}}$, (1-25)

if $\mathbf{E} \in W_3$, then $D_E\mathbb{T}(\mathbf{E}) = \mathbb{C}$. (1-26)

From (1-24) and (1-25), bearing in mind that they are the spectral decomposition of $D_E\mathbb{T}(\mathbf{E})$ for $\mathbf{E} \in W_1$ and $\mathbf{E} \in W_2$ [Itskov 2015], by taking (1-16) and (1-17) into account, we conclude that $D_E\mathbb{T}(\mathbf{E})$ has non-negative eigenvalues [Lucchesi et al. 2008] and is positive-semidefinite; hence it satisfies the Legendre–Hadamard condition [Šilhavý 1997]

$$\frac{\mathbf{a} \otimes \mathbf{b} + \mathbf{b} \otimes \mathbf{a}}{2} \cdot D_E\mathbb{T}(\mathbf{E}) \left[\frac{\mathbf{a} \otimes \mathbf{b} + \mathbf{b} \otimes \mathbf{a}}{2} \right] \geq 0 \quad \text{for each vector } \mathbf{a}, \mathbf{b}. \tag{1-27}$$

For $\mathbf{E} \in W_3$, $D_E\mathbb{T}(\mathbf{E})$ coincides with the tensor of elastic constants (1-1); it is positive-definite and then strongly elliptic [Gurtin 1972].

2. Progressive waves

We are interested in studying the propagation of small amplitude elastic waves in an infinite masonry-like solid \mathcal{B} with homogeneous mass density ρ , homogeneous material properties μ , and λ satisfying (1-2), subjected to a uniform stress $\mathbf{T} = \mathbb{T}(\mathbf{E})$, with \mathbf{E} being a given uniform strain belonging to $W = \bigcup_{i=0}^3 W_i$.

From the differentiability of \mathbb{T} at \mathbf{E} in W [Padovani and Šilhavý 2015], it follows that

$$\mathbb{T}(\mathbf{E} + \mathbf{H}) = \mathbf{T} + D_E\mathbb{T}(\mathbf{E})[\mathbf{H}] + o(\mathbf{H}), \quad \mathbf{H} \in \text{Sym}, \quad \mathbf{H} \rightarrow \mathbf{0}. \tag{2-1}$$

We consider small elastic displacements \mathbf{u} , defined on $\mathcal{B} \times (0, \infty)$, such that their gradient $\nabla \mathbf{u}$ is small, and denote by $\partial^2 \mathbf{u} / \partial t^2$ the acceleration and by div the divergence. For such displacements superimposed on strain \mathbf{E} , from (2-1), neglecting terms of order $o(\nabla \mathbf{u})$, we obtain the linearized equation of motion in the absence of body forces

$$\operatorname{div}(D_E \mathbb{T}(\mathbf{E})[(\nabla \mathbf{u} + \nabla \mathbf{u}^T)/2]) = \rho \partial^2 \mathbf{u} / \partial t^2 \text{ on } \mathcal{B}. \quad (2-2)$$

A progressive wave has the form

$$\mathbf{u}(\mathbf{x}, t) = \mathbf{m} \psi(\mathbf{n} \cdot \mathbf{x} - vt), \quad (2-3)$$

where the unit vectors \mathbf{m} and \mathbf{n} are respectively the polarization vector (or direction of motion) and the direction of propagation, v is the wave velocity and ψ an arbitrary function of class C^2 on $(-\infty, \infty)$ such that

$$d^2 \psi / ds^2 \neq 0. \quad (2-4)$$

The wave \mathbf{u} in (2-3) is longitudinal if $\mathbf{m} = \pm \mathbf{n}$, and transverse if $\mathbf{m} \cdot \mathbf{n} = 0$. Moreover, \mathbf{u} is elastic if it satisfies the equation of motion (2-2).

From (2-3) we get [Gurtin 1972]

$$\nabla \mathbf{u} = \psi' \mathbf{m} \otimes \mathbf{n}, \quad (2-5)$$

$$\partial^2 \mathbf{u} / \partial t^2 = \psi'' v^2 \mathbf{m}, \quad (2-6)$$

with

$$\psi' = d\psi / ds|_{s=\mathbf{n} \cdot \mathbf{x} - vt}, \quad (2-7)$$

$$\psi'' = d^2 \psi / ds^2|_{s=\mathbf{n} \cdot \mathbf{x} - vt}. \quad (2-8)$$

From (2-5) it follows that

$$D_E \mathbb{T}(\mathbf{E}) \left[\frac{\nabla \mathbf{u} + \nabla \mathbf{u}^T}{2} \right] = \psi' D_E \mathbb{T}(\mathbf{E}) \left[\frac{\mathbf{m} \otimes \mathbf{n} + \mathbf{n} \otimes \mathbf{m}}{2} \right]. \quad (2-9)$$

Moreover, since $D_E \mathbb{T}(\mathbf{E})$ is independent of \mathbf{x} ,

$$\operatorname{div} \left(D_E \mathbb{T}(\mathbf{E}) \left[\frac{\nabla \mathbf{u} + \nabla \mathbf{u}^T}{2} \right] \right) = \psi'' D_E \mathbb{T}(\mathbf{E}) \left[\frac{\mathbf{m} \otimes \mathbf{n} + \mathbf{n} \otimes \mathbf{m}}{2} \right] \mathbf{n} = \rho \psi'' A(\mathbf{E}, \mathbf{n}) \mathbf{m}, \quad (2-10)$$

where $A(\mathbf{E}, \mathbf{n})$ is the tensor defined by

$$A(\mathbf{E}, \mathbf{n}) \mathbf{a} = \rho^{-1} D_E \mathbb{T}(\mathbf{E}) \left[\frac{\mathbf{a} \otimes \mathbf{n} + \mathbf{n} \otimes \mathbf{a}}{2} \right] \mathbf{n} \text{ for every vector } \mathbf{a}. \quad (2-11)$$

We call $A(\mathbf{E}, \mathbf{n})$ the acoustic tensor for strain \mathbf{E} and direction \mathbf{n} . From (2-2), by taking (2-6), (2-10) and (2-4) into account, we obtain the condition

$$A(\mathbf{E}, \mathbf{n}) \mathbf{m} = v^2 \mathbf{m}, \quad (2-12)$$

which expresses the Fresnel–Hadamard propagation condition [Gurtin 1972]. Thus, for an elastic progressive wave to propagate in a direction \mathbf{n} , its polarization vector must be an eigenvector of the acoustic

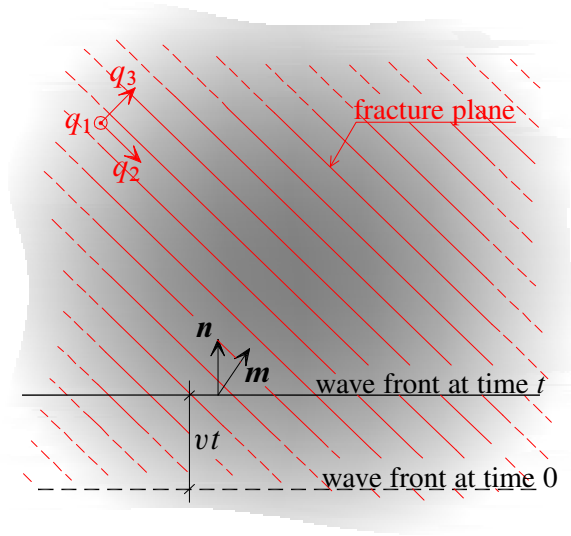


Figure 1. Depiction of a plane wave with direction of propagation \mathbf{n} and polarization vector \mathbf{m} in a cracked body.

tensor $A(\mathbf{E}, \mathbf{n})$ and the square of the velocity of propagation must be the associated eigenvalue. Figure 1 depicts a progressive wave with direction of propagation \mathbf{n} and polarization \mathbf{m} in an infinite body subjected to a homogeneous strain field $\mathbf{E} \in W_2$. According to (1-21), the fracture planes are orthogonal to \mathbf{q}_3 . For a given constant ζ , at any time t , the displacement field \mathbf{u} in (2-3) is constant on the plane $P_t = \{\mathbf{x} : \mathbf{x} \cdot \mathbf{n} - vt = \zeta\}$, called the wave front.

2A. The acoustic tensor. In this subsection we state some properties of the acoustic tensor $A(\mathbf{E}, \mathbf{n})$ defined in (2-11) and obtain its expression in the four regions W_i .

Proposition 2.1.

- (a) $A(\mathbf{E}, \mathbf{n})$ is symmetric.
- (b) For \mathbf{E} in $\bigcup_{i=1}^2 W_i$, let

$$D_E \mathbb{T}(\mathbf{E}) = \sum_{j=1}^6 \delta_j(\mathbf{E}) V_j(\mathbf{E}) \otimes V_j(\mathbf{E}), \tag{2-13}$$

be the spectral decomposition of $D_E \mathbb{T}(\mathbf{E})$, with $\delta_j(\mathbf{E})$ eigenvalues and $V_j(\mathbf{E})$ eigentensors of $D_E \mathbb{T}(\mathbf{E})$, $j = 1, \dots, 6$. Thus

$$A(\mathbf{E}, \mathbf{n}) = \rho^{-1} \sum_{j=1}^6 \delta_j(\mathbf{E}) V_j(\mathbf{E}) \mathbf{n} \otimes V_j(\mathbf{E}) \mathbf{n}. \tag{2-14}$$

- (c) $A(\mathbf{E}, \mathbf{n})$ is positive-semidefinite for $\mathbf{E} \in \bigcup_{i=0}^2 W_i$, and positive-definite for \mathbf{E} in W_3 .
- (d) $A(\mathbf{E}, \mathbf{n}) = A(\mathbf{E}, -\mathbf{n})$ for each unit vector \mathbf{n} .

- (e) Let Orth be the subset of Lin of orthogonal tensors \mathbf{Q} , $\mathbf{Q}\mathbf{Q}^T = \mathbf{Q}^T\mathbf{Q} = \mathbf{I}$. The acoustic tensor satisfies the relation

$$\mathbf{Q}\mathbf{A}(\mathbf{E}, \mathbf{n})\mathbf{Q}^T = \mathbf{A}(\mathbf{Q}\mathbf{E}\mathbf{Q}^T, \mathbf{Q}\mathbf{n}) \text{ for each } \mathbf{Q} \in \text{Orth}. \quad (2-15)$$

Proof.

- (a) By taking the symmetry of $D_E\mathbb{T}(\mathbf{E})$ into account, for each vector \mathbf{l} and \mathbf{p} we have,

$$\begin{aligned} \mathbf{l} \cdot \mathbf{A}(\mathbf{E}, \mathbf{n})\mathbf{p} &= \mathbf{l} \cdot \rho^{-1} D_E\mathbb{T}(\mathbf{E}) \left[\frac{\mathbf{p} \otimes \mathbf{n} + \mathbf{n} \otimes \mathbf{p}}{2} \right] \mathbf{n} \\ &= \mathbf{l} \otimes \mathbf{n} \cdot \rho^{-1} D_E\mathbb{T}(\mathbf{E}) \left[\frac{\mathbf{p} \otimes \mathbf{n} + \mathbf{n} \otimes \mathbf{p}}{2} \right] \\ &= \frac{\mathbf{l} \otimes \mathbf{n} + \mathbf{n} \otimes \mathbf{l}}{2} \cdot \rho^{-1} D_E\mathbb{T}(\mathbf{E}) \left[\frac{\mathbf{p} \otimes \mathbf{n} + \mathbf{n} \otimes \mathbf{p}}{2} \right] \\ &= \rho^{-1} D_E\mathbb{T}(\mathbf{E}) \left[\frac{\mathbf{l} \otimes \mathbf{n} + \mathbf{n} \otimes \mathbf{l}}{2} \right] \cdot \frac{\mathbf{p} \otimes \mathbf{n} + \mathbf{n} \otimes \mathbf{p}}{2} \\ &= \mathbf{p} \cdot \rho^{-1} D_E\mathbb{T}(\mathbf{E}) \left[\frac{\mathbf{l} \otimes \mathbf{n} + \mathbf{n} \otimes \mathbf{l}}{2} \right] \mathbf{n} \\ &= \mathbf{p} \cdot \mathbf{A}(\mathbf{E}, \mathbf{n})\mathbf{l}. \end{aligned} \quad (2-16)$$

- (b) From (2-13) it follows that

$$\begin{aligned} D_E\mathbb{T}(\mathbf{E}) \left[\frac{\mathbf{p} \otimes \mathbf{n} + \mathbf{n} \otimes \mathbf{p}}{2} \right] \mathbf{n} &= \sum_{j=1}^6 \delta_j(\mathbf{E}) \left(\mathbf{V}_j(\mathbf{E}) \cdot \left[\frac{\mathbf{p} \otimes \mathbf{n} + \mathbf{n} \otimes \mathbf{p}}{2} \right] \right) \mathbf{V}_j(\mathbf{E}) \mathbf{n} \\ &= \sum_{j=1}^6 \delta_j(\mathbf{E}) (\mathbf{V}_j(\mathbf{E}) \mathbf{n} \cdot \mathbf{p}) \mathbf{V}_j(\mathbf{E}) \mathbf{n} \\ &= \sum_{j=1}^6 \delta_j(\mathbf{E}) (\mathbf{V}_j(\mathbf{E}) \mathbf{n} \otimes \mathbf{V}_j(\mathbf{E}) \mathbf{n}) \mathbf{p}, \end{aligned} \quad (2-17)$$

for all vectors \mathbf{p} , and (2-14) follows from (2-11).

- (c) If $\mathbf{E} \in \bigcup_{i=0}^2 W_i$, from (2-16) for $\mathbf{l} = \mathbf{p}$, by taking the condition (1-27) into account, we obtain that $\mathbf{A}(\mathbf{E}, \mathbf{n})$ is positive-semidefinite. If $\mathbf{E} \in W_3$, $D_E\mathbb{T}(\mathbf{E}) = \mathbb{C}$ is positive-definite and $\mathbf{A}(\mathbf{E}, \mathbf{n})$ coincides with the acoustic tensor of an isotropic linear elastic material and is positive-definite (see (2-24)).
- (d) A trivial consequence of (2-11).
- (e) We note that from the isotropy of the stress function \mathbb{T} [Lucchesi et al. 2008],

$$\mathbb{T}(\mathbf{E}) = \mathbb{T}(\mathbf{Q}\mathbf{E}\mathbf{Q}^T) \text{ for each } \mathbf{E} \in \text{Sym}, \mathbf{Q} \in \text{Orth}, \quad (2-18)$$

the invariance of its derivative $D_E\mathbb{T}(\mathbf{E})$ [Gurtin 1981]

$$\mathbf{Q} D_E\mathbb{T}(\mathbf{E})[\mathbf{H}]\mathbf{Q}^T = D_E\mathbb{T}(\mathbf{Q}\mathbf{E}\mathbf{Q}^T)[\mathbf{Q}\mathbf{H}\mathbf{Q}^T], \quad (2-19)$$

follows for each $\mathbf{E} \in \bigcup_{i=0}^3 W_i$, $\mathbf{Q} \in \text{Orth}$, $\mathbf{H} \in \text{Sym}$.

Thus, for $\mathbf{E} \in \bigcup_{i=0}^3 W_i$ and \mathbf{n} unit vector, from (2-11) and (2-19), we obtain

$$\mathbf{A}(\mathbf{E}, \mathbf{n}) = \mathbf{Q}^T \mathbf{A}(\mathbf{Q}\mathbf{E}\mathbf{Q}^T, \mathbf{Q}\mathbf{n})\mathbf{Q} \text{ for each } \mathbf{Q} \in \text{Orth}. \quad (2-20)$$

Equation (2-20) extends an analogous relation proved in [Gurtin 1972] for isotropic linear elastic materials. From (2-20) it follows that if \mathbf{m} is an eigenvector of $\mathbf{A}(\mathbf{E}, \mathbf{n})$ corresponding to the eigenvalue v^2 , then $\mathbf{Q}\mathbf{m}$ is an eigenvector of $\mathbf{A}(\mathbf{Q}\mathbf{E}\mathbf{Q}^T, \mathbf{Q}\mathbf{n})$ corresponding to the same eigenvalue v^2 . \square

From Proposition 2.1, tensor $\mathbf{A}(\mathbf{E}, \mathbf{n})$ defined in (2-11) turns out to be symmetric and positive-semidefinite, hence, for each \mathbf{n} , there exist three orthogonal eigenvectors $\mathbf{m}_1, \mathbf{m}_2, \mathbf{m}_3$, and three associated non-negative eigenvalues v_1^2, v_2^2, v_3^2 , whose expressions are calculated in the following.

Due to the different expressions of $D_E \mathbb{T}(\mathbf{E})$ in the regions W_i , from (2-11) it follows that the acoustic tensor $\mathbf{A}(\mathbf{E}, \mathbf{n})$ has different expressions $A_i(\mathbf{E}, \mathbf{n})$ in the four regions W_i . In view of Proposition 2.1(b) we have:

$$\text{if } \mathbf{E} \in W_0, \text{ then } A_0(\mathbf{E}, \mathbf{n}) = \mathbf{0}, \quad (2-21)$$

$$\begin{aligned} \text{if } \mathbf{E} \in W_1, \text{ then } A_1(\mathbf{E}, \mathbf{n}) = E\rho^{-1} & \left(\mathbf{O}_{11}\mathbf{n} \otimes \mathbf{O}_{11}\mathbf{n} \right. \\ & \left. - \frac{e_1}{e_2 - e_1} \mathbf{O}_{12}\mathbf{n} \otimes \mathbf{O}_{12}\mathbf{n} - \frac{e_1}{e_3 - e_1} \mathbf{O}_{13}\mathbf{n} \otimes \mathbf{O}_{13}\mathbf{n} \right), \end{aligned} \quad (2-22)$$

$$\begin{aligned} \text{if } \mathbf{E} \in W_2, \text{ then } A_2(\mathbf{E}, \mathbf{n}) = 2\mu\rho^{-1} & \left(\mathbf{O}_{12}\mathbf{n} \otimes \mathbf{O}_{12}\mathbf{n} \right. \\ & - \frac{2(1+\alpha)e_1 + \alpha e_2}{(2+\alpha)(e_3 - e_1)} \mathbf{O}_{13}\mathbf{n} \otimes \mathbf{O}_{13}\mathbf{n} - \frac{\alpha e_1 + 2(1+\alpha)e_2}{(2+\alpha)(e_3 - e_2)} \mathbf{O}_{23}\mathbf{n} \otimes \mathbf{O}_{23}\mathbf{n} \\ & \left. + \frac{2+3\alpha}{2+\alpha} \frac{\mathbf{O}_{11} + \mathbf{O}_{22}}{\sqrt{2}} \mathbf{n} \otimes \frac{\mathbf{O}_{11} + \mathbf{O}_{22}}{\sqrt{2}} \mathbf{n} + \frac{\mathbf{O}_{11} - \mathbf{O}_{22}}{\sqrt{2}} \mathbf{n} \otimes \frac{\mathbf{O}_{11} - \mathbf{O}_{22}}{\sqrt{2}} \mathbf{n} \right), \end{aligned} \quad (2-23)$$

$$\text{if } \mathbf{E} \in W_3 \text{ then } A_3(\mathbf{E}, \mathbf{n}) = (2\mu + \lambda)\rho^{-1} \mathbf{n} \otimes \mathbf{n} + \mu\rho^{-1}(\mathbf{I} - \mathbf{n} \otimes \mathbf{n}). \quad (2-24)$$

Our goal is to find the eigenvalues $c_1^{(i)}(\mathbf{E}, \mathbf{n}) \geq c_2^{(i)}(\mathbf{E}, \mathbf{n}) \geq c_3^{(i)}(\mathbf{E}, \mathbf{n})$ and eigenvectors $\mathbf{m}_1^{(i)}(\mathbf{E}, \mathbf{n})$, $\mathbf{m}_2^{(i)}(\mathbf{E}, \mathbf{n})$, $\mathbf{m}_3^{(i)}(\mathbf{E}, \mathbf{n})$ of the acoustic tensor $A_i(\mathbf{E}, \mathbf{n})$, for $i = 1, 2, 3$.

For $\mathbf{E} \in W_1$, from (2-22) we get

$$\begin{aligned} A_1(\mathbf{E}, \mathbf{n}) = E\rho^{-1} & \left\{ \left[(\mathbf{n} \cdot \mathbf{q}_1)^2 - \frac{e_1}{2(e_2 - e_1)} (\mathbf{n} \cdot \mathbf{q}_2)^2 - \frac{e_1}{2(e_3 - e_1)} (\mathbf{n} \cdot \mathbf{q}_3)^2 \right] \mathbf{O}_{11} \right. \\ & - \frac{e_1}{2(e_2 - e_1)} (\mathbf{n} \cdot \mathbf{q}_1)^2 \mathbf{O}_{22} - \frac{e_1}{2(e_3 - e_1)} (\mathbf{n} \cdot \mathbf{q}_1)^2 \mathbf{O}_{33} - \frac{e_1}{\sqrt{2}(e_2 - e_1)} (\mathbf{n} \cdot \mathbf{q}_1)(\mathbf{n} \cdot \mathbf{q}_2) \mathbf{O}_{12} \\ & \left. - \frac{e_1}{\sqrt{2}(e_3 - e_1)} (\mathbf{n} \cdot \mathbf{q}_1)(\mathbf{n} \cdot \mathbf{q}_3) \mathbf{O}_{13} \right\}. \end{aligned} \quad (2-25)$$

Thus, if $\mathbf{n} = \mathbf{q}_1$, then

$$A_1(\mathbf{E}, \mathbf{q}_1) = E\rho^{-1} \left\{ \mathbf{O}_{11} - \frac{e_1}{2(e_2 - e_1)} \mathbf{O}_{22} - \frac{e_1}{2(e_3 - e_1)} \mathbf{O}_{33} \right\}, \quad (2-26)$$

whose eigenvalues and eigenvectors are

$$c_1^{(1)}(\mathbf{E}, \mathbf{q}_1) = E\rho^{-1}, \quad c_2^{(1)}(\mathbf{E}, \mathbf{q}_1) = -\frac{E\rho^{-1}e_1}{2(e_2 - e_1)}, \quad (2-27)$$

$$c_3^{(1)}(\mathbf{E}, \mathbf{q}_1) = -\frac{E\rho^{-1}e_1}{2(e_3 - e_1)}, \quad (2-28)$$

$$\mathbf{m}_1^{(1)}(\mathbf{E}, \mathbf{q}_1) = \mathbf{q}_1, \quad \mathbf{m}_2^{(1)}(\mathbf{E}, \mathbf{q}_1) = \mathbf{q}_2, \quad \mathbf{m}_3^{(1)}(\mathbf{E}, \mathbf{q}_1) = \mathbf{q}_3. \quad (2-29)$$

If $\mathbf{n} \cdot \mathbf{q}_1 = 0$, then

$$A_1(\mathbf{E}, \mathbf{n}) = -E\rho^{-1} \left[\frac{e_1}{2(e_2 - e_1)} (\mathbf{n} \cdot \mathbf{q}_2)^2 + \frac{e_1}{2(e_3 - e_1)} (\mathbf{n} \cdot \mathbf{q}_3)^2 \right] \mathbf{O}_{11}, \quad (2-30)$$

whose eigenvalues and eigenvectors are

$$c_1^{(1)}(\mathbf{E}, \mathbf{n}) = -\frac{E\rho^{-1}e_1}{2} \left[\frac{1}{e_2 - e_1} (\mathbf{n} \cdot \mathbf{q}_2)^2 + \frac{1}{e_3 - e_1} (\mathbf{n} \cdot \mathbf{q}_3)^2 \right], \quad (2-31)$$

$$c_2^{(1)}(\mathbf{E}, \mathbf{n}) = c_3^{(1)}(\mathbf{E}, \mathbf{n}) = 0, \quad (2-32)$$

$$\mathbf{m}_1^{(1)}(\mathbf{E}, \mathbf{n}) = \mathbf{q}_1, \quad \mathbf{m}_2^{(1)}(\mathbf{E}, \mathbf{n}) = \mathbf{q}_2, \quad \mathbf{m}_3^{(1)}(\mathbf{E}, \mathbf{n}) = \mathbf{q}_3. \quad (2-33)$$

In particular, if $\mathbf{n} = \mathbf{q}_2$, then

$$c_1^{(1)}(\mathbf{E}, \mathbf{q}_2) = -\frac{E\rho^{-1}e_1}{2(e_2 - e_1)}, \quad (2-34)$$

and for $\mathbf{n} = \mathbf{q}_3$, then

$$c_1^{(1)}(\mathbf{E}, \mathbf{q}_3) = -\frac{E\rho^{-1}e_1}{2(e_3 - e_1)}. \quad (2-35)$$

If $\mathbf{n} \cdot \mathbf{q}_2 = 0$, then the eigenvalues and eigenvectors of $A_1(\mathbf{E}, \mathbf{n})$ are

$$c_1^{(1)}(\mathbf{E}, \mathbf{n}) = \frac{E\rho^{-1}}{2} \left[(\mathbf{n} \cdot \mathbf{q}_1)^2 - \frac{e_1}{2(e_3 - e_1)} + \sqrt{\left((\mathbf{n} \cdot \mathbf{q}_1)^2 - \frac{e_1}{2(e_3 - e_1)} \right)^2 + 2\frac{e_1}{e_3 - e_1} (\mathbf{n} \cdot \mathbf{q}_1)^4} \right], \quad (2-36)$$

$$c_2^{(1)}(\mathbf{E}, \mathbf{n}) = -\frac{E\rho^{-1}e_1}{2(e_2 - e_1)} (\mathbf{n} \cdot \mathbf{q}_1)^2, \quad (2-37)$$

$$c_3^{(1)}(\mathbf{E}, \mathbf{n}) = \frac{E\rho^{-1}}{2} \left[(\mathbf{n} \cdot \mathbf{q}_1)^2 - \frac{e_1}{2(e_3 - e_1)} - \sqrt{\left((\mathbf{n} \cdot \mathbf{q}_1)^2 - \frac{e_1}{2(e_3 - e_1)} \right)^2 + 2\frac{e_1}{e_3 - e_1} (\mathbf{n} \cdot \mathbf{q}_1)^4} \right] \quad (2-38)$$

(where $c_2^{(1)} \leq c_3^{(1)}$ or $c_2^{(1)} \geq c_3^{(1)}$ depending on \mathbf{E}) and

$$\mathbf{m}_2^{(1)}(\mathbf{E}, \mathbf{n}) = \mathbf{q}_2, \quad \mathbf{m}_1^{(1)}(\mathbf{E}, \mathbf{n}), \mathbf{m}_3^{(1)}(\mathbf{E}, \mathbf{n}) \in \text{Span}(\mathbf{q}_1, \mathbf{q}_3). \quad (2-39)$$

Analogously, if $\mathbf{n} \cdot \mathbf{q}_3 = 0$, the eigenvalues and eigenvectors of $A_1(\mathbf{E}, \mathbf{n})$ are

$$c_1^{(1)}(\mathbf{E}, \mathbf{n}) = \frac{E\rho^{-1}}{2} \left[(\mathbf{n} \cdot \mathbf{q}_1)^2 - \frac{e_1}{2(e_2 - e_1)} + \sqrt{\left((\mathbf{n} \cdot \mathbf{q}_1)^2 - \frac{e_1}{2(e_2 - e_1)} \right)^2 + 2 \frac{e_1}{e_2 - e_1} (\mathbf{n} \cdot \mathbf{q}_1)^4} \right], \quad (2-40)$$

$$c_2^{(1)}(\mathbf{E}, \mathbf{n}) = \frac{E\rho^{-1}}{2} \left[(\mathbf{n} \cdot \mathbf{q}_1)^2 - \frac{e_1}{2(e_2 - e_1)} - \sqrt{\left((\mathbf{n} \cdot \mathbf{q}_1)^2 - \frac{e_1}{2(e_2 - e_1)} \right)^2 + 2 \frac{e_1}{e_2 - e_1} (\mathbf{n} \cdot \mathbf{q}_1)^4} \right], \quad (2-41)$$

$$c_3^{(1)}(\mathbf{E}, \mathbf{n}) = -\frac{E\rho^{-1}e_1}{2(e_3 - e_1)} (\mathbf{n} \cdot \mathbf{q}_1)^2, \quad (2-42)$$

(where $c_2^{(1)} \leq c_3^{(1)}$ or $c_2^{(1)} \geq c_3^{(1)}$ depending on \mathbf{E}) and

$$\mathbf{m}_1^{(1)}(\mathbf{E}, \mathbf{n}), \quad \mathbf{m}_2^{(1)}(\mathbf{E}, \mathbf{n}) \in \text{Span}(\mathbf{q}_1, \mathbf{q}_2), \quad \mathbf{m}_3^{(1)}(\mathbf{E}, \mathbf{n}) = \mathbf{q}_3. \quad (2-43)$$

For $\mathbf{n} \cdot \mathbf{q}_1 \neq 0$, $\mathbf{n} \cdot \mathbf{q}_2 \neq 0$, $\mathbf{n} \cdot \mathbf{q}_3 \neq 0$, the eigenvalues of $A_1(\mathbf{E}, \mathbf{n})$ can be determined by using the formulae in [Kachanov 1974]:

$$c_1^{(1)}(\mathbf{E}, \mathbf{n}) = \frac{2}{\sqrt{3}} \chi^{(1)} \cos(\theta^{(1)} - \frac{\pi}{3}) + \frac{1}{3} I_1^{(1)}, \quad (2-44)$$

$$c_2^{(1)}(\mathbf{E}, \mathbf{n}) = \frac{2}{\sqrt{3}} \chi^{(1)} \cos(\theta^{(1)} + \frac{\pi}{3}) + \frac{1}{3} I_1^{(1)}, \quad (2-45)$$

$$c_3^{(1)}(\mathbf{E}, \mathbf{n}) = -\frac{2}{\sqrt{3}} \chi^{(1)} \cos \theta^{(1)} + \frac{1}{3} I_1^{(1)}, \quad (2-46)$$

where

$$\chi^{(1)} = \sqrt{\frac{1}{3} ((I_1^{(1)})^2 - 3I_2^{(1)})}, \quad (2-47)$$

$$\cos 3\theta^{(1)} = -\frac{3\sqrt{3}\gamma^{(1)}}{2(\chi^{(1)})^3}, \quad (2-48)$$

$$\gamma^{(1)} = I_3^{(1)} - \frac{1}{3} I_1^{(1)} I_2^{(1)} + \frac{2}{27} (I_1^{(1)})^3, \quad (2-49)$$

with

$$\begin{aligned} I_1^{(1)} &= \text{tr } A_1(\mathbf{E}, \mathbf{n}) \\ &= E\rho^{-1} \left\{ (\mathbf{n} \cdot \mathbf{q}_1)^2 - \frac{e_1}{2(e_2 - e_1)} [(\mathbf{n} \cdot \mathbf{q}_1)^2 + (\mathbf{n} \cdot \mathbf{q}_2)^2] - \frac{e_1}{2(e_3 - e_1)} [(\mathbf{n} \cdot \mathbf{q}_1)^2 + (\mathbf{n} \cdot \mathbf{q}_3)^2] \right\}, \end{aligned} \quad (2-50)$$

$$I_2^{(1)} = \frac{1}{2} [(\text{tr } A_1(\mathbf{E}, \mathbf{n}))^2 - \text{tr } A_1(\mathbf{E}, \mathbf{n})^2], \quad (2-51)$$

$$I_3^{(1)} = \det A_1(\mathbf{E}, \mathbf{n}) = \frac{E^3 \rho^{-3} e_1^2 (\mathbf{n} \cdot \mathbf{q}_1)^6}{4(e_2 - e_1)(e_3 - e_1)}, \quad (2-52)$$

the principal invariants of $A_1(\mathbf{E}, \mathbf{n})$. The angle $\theta^{(1)}$ varies between 0 and $\pi/3$.

Since $\mathbf{n} \cdot \mathbf{q}_1 \neq 0$, then $I_3^{(1)} \neq 0$ and $A_1(\mathbf{E}, \mathbf{n})$ has no zero eigenvalues.

For $j = 1, 2, 3$, given $c_j^{(1)}(\mathbf{E}, \mathbf{n})$, the corresponding eigenvector $\mathbf{m}_j^{(1)}(\mathbf{E}, \mathbf{n})$ can be calculated by solving the system

$$(\mathbf{A}_1(\mathbf{E}, \mathbf{n}) - c_j^{(1)}(\mathbf{E}, \mathbf{n})\mathbf{I})\mathbf{m}_j^{(1)}(\mathbf{E}, \mathbf{n}) = \mathbf{0}. \quad (2-53)$$

Let us now consider the case in which $\mathbf{E} \in W_2$. From (2-23) we obtain

$$\begin{aligned}
 A_2(\mathbf{E}, \mathbf{n}) &= \rho^{-1} \left(\varphi(\mathbf{n} \cdot \mathbf{q}_1)^2 + \mu(\mathbf{n} \cdot \mathbf{q}_2)^2 - \mu \frac{2(1+\alpha)e_1 + \alpha e_2}{(2+\alpha)(e_3 - e_1)} (\mathbf{n} \cdot \mathbf{q}_3)^2 \right) \mathbf{O}_{11} \\
 &+ \rho^{-1} \left(\mu(\mathbf{n} \cdot \mathbf{q}_1)^2 + \varphi(\mathbf{n} \cdot \mathbf{q}_2)^2 - \mu \frac{\alpha e_1 + 2(1+\alpha)e_2}{(2+\alpha)(e_3 - e_2)} (\mathbf{n} \cdot \mathbf{q}_3)^2 \right) \mathbf{O}_{22} \\
 &- \rho^{-1} \left(\mu \frac{2(1+\alpha)e_1 + \alpha e_2}{(2+\alpha)(e_3 - e_1)} (\mathbf{n} \cdot \mathbf{q}_1)^2 + \mu \frac{\alpha e_1 + 2(1+\alpha)e_2}{(2+\alpha)(e_3 - e_2)} (\mathbf{n} \cdot \mathbf{q}_2)^2 \right) \mathbf{O}_{33} \\
 &+ \mu \rho^{-1} \sqrt{2} \frac{2+3\alpha}{2+\alpha} (\mathbf{n} \cdot \mathbf{q}_1)(\mathbf{n} \cdot \mathbf{q}_2) \mathbf{O}_{12} \\
 &- \mu \rho^{-1} \sqrt{2} \frac{2(1+\alpha)e_1 + \alpha e_2}{(2+\alpha)(e_3 - e_1)} (\mathbf{n} \cdot \mathbf{q}_1)(\mathbf{n} \cdot \mathbf{q}_3) \mathbf{O}_{13} \\
 &- \mu \rho^{-1} \sqrt{2} \frac{\alpha e_1 + 2(1+\alpha)e_2}{(2+\alpha)(e_3 - e_2)} (\mathbf{n} \cdot \mathbf{q}_2)(\mathbf{n} \cdot \mathbf{q}_3) \mathbf{O}_{23},
 \end{aligned} \tag{2-54}$$

with

$$\varphi = \frac{4\mu(1+\alpha)}{2+\alpha}. \tag{2-55}$$

If $\mathbf{n} = \mathbf{q}_1$, then

$$A_2(\mathbf{E}, \mathbf{q}_1) = \varphi \rho^{-1} \mathbf{O}_{11} + \mu \rho^{-1} \mathbf{O}_{22} - \mu \rho^{-1} \frac{2(1+\alpha)e_1 + \alpha e_2}{(2+\alpha)(e_3 - e_1)} \mathbf{O}_{33}, \tag{2-56}$$

whose eigenvalues and eigenvectors are

$$c_1^{(2)}(\mathbf{E}, \mathbf{q}_1) = \varphi \rho^{-1}, \quad c_2^{(2)}(\mathbf{E}, \mathbf{q}_1) = \mu \rho^{-1}, \tag{2-57}$$

$$c_3^{(2)}(\mathbf{E}, \mathbf{q}_1) = -\frac{\mu \rho^{-1}}{2+\alpha} \frac{2(1+\alpha)e_1 + \alpha e_2}{e_3 - e_1}, \tag{2-58}$$

$$\mathbf{m}_1^{(2)}(\mathbf{E}, \mathbf{q}_1) = \mathbf{q}_1, \quad \mathbf{m}_2^{(2)}(\mathbf{E}, \mathbf{q}_1) = \mathbf{q}_2, \quad \mathbf{m}_3^{(2)}(\mathbf{E}, \mathbf{q}_1) = \mathbf{q}_3. \tag{2-59}$$

If $\mathbf{n} = \mathbf{q}_2$, then

$$A_2(\mathbf{E}, \mathbf{q}_2) = \mu \rho^{-1} \mathbf{O}_{11} + \varphi \rho^{-1} \mathbf{O}_{22} - \mu \rho^{-1} \frac{\alpha e_1 + 2(1+\alpha)e_2}{(2+\alpha)(e_3 - e_2)} \mathbf{O}_{33}, \tag{2-60}$$

whose eigenvalues and eigenvectors are

$$c_1^{(2)}(\mathbf{E}, \mathbf{q}_2) = \varphi \rho^{-1}, \quad c_2^{(2)}(\mathbf{E}, \mathbf{q}_2) = \mu \rho^{-1}, \tag{2-61}$$

$$c_3^{(2)}(\mathbf{E}, \mathbf{q}_2) = -\frac{\mu \rho^{-1}}{2+\alpha} \frac{\alpha e_1 + 2(1+\alpha)e_2}{e_3 - e_2}, \tag{2-62}$$

$$\mathbf{m}_1^{(2)}(\mathbf{E}, \mathbf{q}_2) = \mathbf{q}_2, \quad \mathbf{m}_2^{(2)}(\mathbf{E}, \mathbf{q}_2) = \mathbf{q}_1, \quad \mathbf{m}_3^{(2)}(\mathbf{E}, \mathbf{q}_2) = \mathbf{q}_3. \tag{2-63}$$

If $\mathbf{n} = \mathbf{q}_3$, then

$$A_2(\mathbf{E}, \mathbf{q}_3) = -\mu \rho^{-1} \frac{2(1+\alpha)e_1 + \alpha e_2}{(2+\alpha)(e_3 - e_1)} \mathbf{O}_{11} - \mu \rho^{-1} \frac{\alpha e_1 + 2(1+\alpha)e_2}{(2+\alpha)(e_3 - e_2)} \mathbf{O}_{22}, \tag{2-64}$$

whose eigenvalues and eigenvectors are

$$c_1^{(2)}(\mathbf{E}, \mathbf{q}_3) = -\frac{\mu\rho^{-1}}{2+\alpha} \frac{2(1+\alpha)e_1 + \alpha e_2}{e_3 - e_1}, \quad c_2^{(2)}(\mathbf{E}, \mathbf{q}_3) = -\frac{\mu\rho^{-1}}{2+\alpha} \frac{\alpha e_1 + 2(1+\alpha)e_2}{e_3 - e_2}, \quad (2-65)$$

$$c_3^{(2)}(\mathbf{E}, \mathbf{q}_3) = 0, \quad (2-66)$$

$$\mathbf{m}_1^{(2)}(\mathbf{E}, \mathbf{q}_3) = \mathbf{q}_1, \quad \mathbf{m}_2^{(2)}(\mathbf{E}, \mathbf{q}_3) = \mathbf{q}_2, \quad \mathbf{m}_3^{(2)}(\mathbf{E}, \mathbf{q}_3) = \mathbf{q}_3. \quad (2-67)$$

If $\mathbf{n} \neq \mathbf{q}_1, \mathbf{q}_2, \mathbf{q}_3$, then the eigenvalues of $A_2(\mathbf{E}, \mathbf{n})$ can be determined by using the formulae in [Kachanov 1974]:

$$c_1^{(2)}(\mathbf{E}, \mathbf{n}) = \frac{2}{\sqrt{3}}\chi^{(2)} \cos(\theta^{(2)} - \frac{\pi}{3}) + \frac{1}{3}I_1^{(2)}, \quad (2-68)$$

$$c_2^{(2)}(\mathbf{E}, \mathbf{n}) = \frac{2}{\sqrt{3}}\chi^{(2)} \cos(\theta^{(2)} + \frac{\pi}{3}) + \frac{1}{3}I_1^{(2)}, \quad (2-69)$$

$$c_3^{(2)}(\mathbf{E}, \mathbf{n}) = -\frac{2}{\sqrt{3}}\chi^{(2)} \cos \theta^{(2)} + \frac{1}{3}I_1^{(2)}, \quad (2-70)$$

where

$$\chi^{(2)} = \sqrt{\frac{1}{3}((I_1^{(2)})^2 - 3I_2^{(2)})}, \quad (2-71)$$

$$\cos 3\theta^{(2)} = -\frac{3\sqrt{3}\gamma^{(2)}}{(2\chi^{(2)})^3}, \quad (2-72)$$

$$\gamma^{(2)} = I_3^{(2)} - \frac{1}{3}I_1^{(2)}I_2^{(2)} + \frac{2}{27}(I_1^{(2)})^3, \quad (2-73)$$

with

$$I_1^{(2)} = \text{tr } A_2(\mathbf{E}, \mathbf{n}).$$

$$I_2^{(2)} = \frac{1}{2}[(\text{tr } A_2(\mathbf{E}, \mathbf{n}))^2 - \text{tr } A_2(\mathbf{E}, \mathbf{n})^2], \quad (2-74)$$

$$I_3^{(2)} = \det A_2(\mathbf{E}, \mathbf{n}). \quad (2-75)$$

the principal invariants of $A_2(\mathbf{E}, \mathbf{n})$. The angle $\theta^{(2)}$ varies between 0 and $\pi/3$.

As in the case of $\mathbf{E} \in W_1$, for $j = 1, 2, 3$, given $c_j^{(2)}(\mathbf{E}, \mathbf{n})$, the corresponding eigenvector $\mathbf{m}_j^{(2)}(\mathbf{E}, \mathbf{n})$ can be calculated by solving the system

$$(A_2(\mathbf{E}, \mathbf{n}) - c_j^{(2)}(\mathbf{E}, \mathbf{n})\mathbf{I})\mathbf{m}_j^{(2)}(\mathbf{E}, \mathbf{n}) = \mathbf{0}. \quad (2-76)$$

Note that the acoustic tensor $A_3(\mathbf{E}, \mathbf{n})$ for $\mathbf{E} \in W_3$ coincides with the acoustic tensor of a linear elastic material with Lamé moduli μ and λ ; its eigenvalues are

$$c_1^{(3)} = \rho^{-1}(2\mu + \lambda), \quad c_2^{(3)} = c_3^{(3)} = \rho^{-1}\mu, \quad (2-77)$$

and the corresponding eigenvectors

$$\mathbf{m}_1^{(3)}(\mathbf{E}, \mathbf{n}) = \mathbf{n}, \quad \mathbf{m}_2^{(3)}(\mathbf{E}, \mathbf{n}) \text{ and } \mathbf{m}_3^{(3)}(\mathbf{E}, \mathbf{n}) \text{ belong to } \text{Span}(\mathbf{n})^\perp. \quad (2-78)$$

2B. Behavior of plane waves in the regions W_i . Let us now analyze the behavior of progressive waves in a body composed of a masonry-like material with homogeneous stress \mathbf{T} associated to a homogeneous strain field \mathbf{E} . This behavior is different in the four regions W_i introduced in Section 1, since it depends on $\mathbf{A}(\mathbf{E}, \mathbf{n})$, which has a different expression $\mathbf{A}_i(\mathbf{E}, \mathbf{n})$ in W_i (see (2-21), (2-22), (2-23) and (2-24)).

If $\mathbf{E} \in W_0$, from (2-21) it follows that no waves propagate in the medium.

For $\mathbf{E} \in W_i, i = 1, 2, 3$, Tables 1, 2 and 3 report the eigenvalues $c_1^{(i)} \geq c_2^{(i)} \geq c_3^{(i)}$ of $\mathbf{A}(\mathbf{E}, \mathbf{n})$, for each unit vector \mathbf{n} . The associated wave velocities are $v_j^{(i)} = \sqrt{c_j^{(i)}}$, for $i, j = 1, 2, 3$.

Let us consider the case of $\mathbf{E} \in W_1$.

For the eigenvalues $c_1^{(1)}, c_2^{(1)}, c_3^{(1)}$ in (2-27)–(2-28), it is a simple matter to prove that

$$c_1^{(1)}(\mathbf{E}, \mathbf{q}_1) < c_1^{(3)} = \rho^{-1}(2\mu + \lambda) \tag{2-79}$$

and

$$c_2^{(1)}(\mathbf{E}, \mathbf{q}_1) < c_2^{(3)} = \rho^{-1}\mu, \quad c_3^{(1)}(\mathbf{E}, \mathbf{q}_1) < c_3^{(3)} = \rho^{-1}\mu. \tag{2-80}$$

The first inequality in (2-80) follows from the condition $\alpha e_1 + 2(1 + \alpha)e_2 > 0$, which characterizes W_1 (see (1-16)).

As for $c_1^{(1)}$ in (2-31), simple calculations show that

$$c_1^{(1)}(\mathbf{E}, \mathbf{n}) < \rho^{-1}\mu. \tag{2-81}$$

For the eigenvalues in (2-36)–(2-38) and (2-40)–(2-42) we have

$$\begin{aligned} c_1^{(1)}(\mathbf{E}, \mathbf{n}) < c_1^{(3)} = \rho^{-1}(2\mu + \lambda), \quad c_2^{(1)}(\mathbf{E}, \mathbf{n}) < c_2^{(3)} = \rho^{-1}\mu, \\ c_3^{(1)}(\mathbf{E}, \mathbf{n}) < c_2^{(3)} = \rho^{-1}\mu. \end{aligned} \tag{2-82}$$

The polarization vector and the squared velocity of waves propagating in the masonry body subjected to a uniform strain field $\mathbf{E} \in W_1$ are summarized in Table 1, for varying directions of propagation \mathbf{n} .

$\mathbf{E} \in W_1$	$c_1^{(1)}$	$c_2^{(1)}$	$c_3^{(1)}$
$\mathbf{n} = \mathbf{q}_1$	$E\rho^{-1}$ longitudinal wave, \mathbf{q}_1	(2-27) transverse wave, \mathbf{q}_2	(2-28) transverse wave, \mathbf{q}_3
$\mathbf{n} \cdot \mathbf{q}_1 = 0$	(2-31) transverse wave, \mathbf{q}_1	0 no propagation	0 no propagation
$\mathbf{n} \cdot \mathbf{q}_2 = 0$	(2-36)	(2-37) transverse wave, \mathbf{q}_2	(2-38)
$\mathbf{n} \cdot \mathbf{q}_3 = 0$	(2-40)	(2-41)	(2-42) transverse wave, \mathbf{q}_3
$\mathbf{n} \cdot \mathbf{q}_1 \neq 0$ $\mathbf{n} \cdot \mathbf{q}_2 \neq 0$ $\mathbf{n} \cdot \mathbf{q}_3 \neq 0$	(2-44)	(2-45)	(2-46)

Table 1. Wave velocities squared for $\mathbf{E} \in W_1$.

If $\mathbf{n} = \mathbf{q}_1$, there are one longitudinal wave and two transverse waves,

$$A_1(\mathbf{E}, \mathbf{q}_1)\mathbf{q}_1 = \rho^{-1} \mathbf{E}\mathbf{q}_1, \tag{2-83}$$

$$A_1(\mathbf{E}, \mathbf{q}_1)\mathbf{q}_2 = -\frac{E\rho^{-1}e_1}{2(e_2 - e_1)}\mathbf{q}_2, \quad A_1(\mathbf{E}, \mathbf{q}_1)\mathbf{q}_3 = -\frac{E\rho^{-1}e_1}{2(e_3 - e_1)}\mathbf{q}_3. \tag{2-84}$$

Due to (2-79) and (2-80), the velocities of the longitudinal and transverse waves are lower than those of the corresponding waves in a linear elastic material. In particular, if $e_2 = e_3$, the transverse waves have equal velocities; if not, the lowest velocity is associated with the direction of motion \mathbf{q}_3 , which corresponds to the highest values of the fracture strain (see (1-20)).

If $\mathbf{n} \cdot \mathbf{q}_1 = 0$, only a transverse wave can propagate with square velocity (2-31), which, because of (2-81), is less than the squared velocity of the transverse linear elastic wave.

In the case of $\mathbf{n} \cdot \mathbf{q}_2 = 0$ or $\mathbf{n} \cdot \mathbf{q}_3 = 0$, three waves propagate, a single transverse one with squared velocity less than $\rho^{-1}\mu$, while the other two have squared velocities respectively less than $\rho^{-1}(2\mu + \lambda)$, and less than $\rho^{-1}\mu$ (see (2-82)).

Let us consider $\mathbf{E} \in W_2$. For the eigenvalues $c_1^{(2)}, c_2^{(2)}, c_3^{(2)}$, in (2-57)–(2-58), it is an easy matter to prove that

$$c_1^{(2)}(\mathbf{E}, \mathbf{q}_1) < c_1^{(3)} = \rho^{-1}(2\mu + \lambda), \quad c_3^{(2)}(\mathbf{E}, \mathbf{q}_1) < c_2^{(3)} = \rho^{-1}\mu \tag{2-85}$$

where the last inequality comes from the condition $2e_3 + \alpha(e_1 + e_2 + e_3) > 0$, which holds in W_2 (see (1-17)).

Analogously, for $c_3^{(2)}$ in (2-62) we have

$$c_3^{(2)}(\mathbf{E}, \mathbf{n}) < c_3^{(3)} = \rho^{-1}\mu. \tag{2-86}$$

The polarization vector and the squared velocities of waves that propagate in the masonry medium for $\mathbf{E} \in W_2$ are summarized in Table 2, for different values of the propagation vector \mathbf{n} .

If $\mathbf{n} = \mathbf{q}_1$ or $\mathbf{n} = \mathbf{q}_2$, there are one longitudinal wave and two transverse waves:

$$A_2(\mathbf{E}, \mathbf{q}_1)\mathbf{q}_1 = \varphi\rho^{-1}\mathbf{q}_1, \quad A_2(\mathbf{E}, \mathbf{q}_1)\mathbf{q}_2 = \mu\rho^{-1}\mathbf{q}_2, \tag{2-87}$$

$$A_2(\mathbf{E}, \mathbf{q}_1)\mathbf{q}_3 = -\frac{\mu\rho^{-1}}{2 + \alpha} \frac{2(1 + \alpha)e_1 + \alpha e_2}{e_3 - e_1} \mathbf{q}_3; \tag{2-88}$$

$\mathbf{E} \in W_2$	$c_1^{(2)}$	$c_2^{(2)}$	$c_3^{(2)}$
$\mathbf{n} = \mathbf{q}_1$	$\varphi\rho^{-1}$ longitudinal wave, \mathbf{q}_1	$\mu\rho^{-1}$ transverse wave, \mathbf{q}_2	$(2-58)$ transverse wave, \mathbf{q}_3
$\mathbf{n} = \mathbf{q}_2$	$\varphi\rho^{-1}$ longitudinal wave, \mathbf{q}_2	$\mu\rho^{-1}$ transverse wave, \mathbf{q}_1	$(2-62)$ transverse wave, \mathbf{q}_3
$\mathbf{n} = \mathbf{q}_3$	$(2-65)$ transverse wave, \mathbf{q}_1	$(2-65)$ transverse wave, \mathbf{q}_2	0 no propagation
$\mathbf{n} \neq \mathbf{q}_1, \mathbf{q}_2, \mathbf{q}_3$	$(2-68)$	$(2-69)$	$(2-70)$

Table 2. Wave velocities squared for $\mathbf{E} \in W_2$.

$$A_2(\mathbf{E}, \mathbf{q}_2)\mathbf{q}_2 = \varphi\rho^{-1}\mathbf{q}_2, \quad A_2(\mathbf{E}, \mathbf{q}_2)\mathbf{q}_1 = \mu\rho^{-1}\mathbf{q}_1, \tag{2-89}$$

$$A_2(\mathbf{E}, \mathbf{q}_2)\mathbf{q}_3 = -\frac{\mu\rho^{-1}}{2+\alpha} \frac{\alpha e_1 + 2(1+\alpha)e_2}{e_3 - e_2} \mathbf{q}_3. \tag{2-90}$$

Due to (2-85) and (2-86), the velocities of longitudinal and transverse waves are less than those of the corresponding waves in a linear elastic material.

If $\mathbf{n} = \mathbf{q}_3$, no longitudinal waves propagate, and two transverse waves propagate with velocities (2-65) that, in view of (2-85) and (2-86), are less than the velocity of the transverse linear elastic waves.

Note that even though the elasticity tensor is not strongly elliptic in W_1 and W_2 , and hence the hypotheses of the Fedorov–Stippes theorem [Gurtin 1972] are not satisfied, longitudinal and transverse progressive waves do exist. In particular, for $\mathbf{E} \in W_1$, then a longitudinal wave exists only for $\mathbf{n} = \mathbf{q}_1$. The other two progressive waves in direction \mathbf{q}_1 , whose directions of motion are equal to \mathbf{q}_2 and \mathbf{q}_3 , are transverse. For $\mathbf{n} \in W_2$, two longitudinal waves exist, one for $\mathbf{n} = \mathbf{q}_1$, and another for $\mathbf{n} = \mathbf{q}_2$.

For $\mathbf{E} \in W_3$ the material behaves like an isotropic linear elastic material, and there are but two types of progressive waves: longitudinal and transverse, as shown in Table 3.

$\mathbf{E} \in W_3$	$c_1^{(3)}$	$c_2^{(3)}$	$c_3^{(3)}$
\mathbf{n}	$(2\mu + \lambda)\rho^{-1}$ longitudinal wave	$\mu\rho^{-1}$ transverse wave	$\mu\rho^{-1}$ transverse wave

Table 3. Wave velocities squared for $\mathbf{E} \in W_3$.

3. The two-dimensional case

Let us consider a plane strain state and, for fixed \mathbf{q}_3 , strain tensors \mathbf{E} such that $\mathbf{E}\mathbf{q}_3 = \mathbf{0}$. Let us indicate with the same symbols \mathbf{E} , \mathbf{T} and \mathbf{E}^f the restriction of \mathbf{E} , \mathbf{T} and \mathbf{E}^f to the two-dimensional subspace of the three-dimensional vector space orthogonal to \mathbf{q}_3 .

Let $e_1 \leq e_2$ be the ordered eigenvalues of \mathbf{E} , and $\mathbf{q}_1, \mathbf{q}_2$ the corresponding eigenvectors and put

$$\mathbf{O}_{11} = \mathbf{q}_1 \otimes \mathbf{q}_1, \quad \mathbf{O}_{22} = \mathbf{q}_2 \otimes \mathbf{q}_2, \quad \mathbf{O}_{12} = 1/\sqrt{2}(\mathbf{q}_1 \otimes \mathbf{q}_2 + \mathbf{q}_2 \otimes \mathbf{q}_1). \tag{3-1}$$

Define the sets

$$S_0 = \{\mathbf{E} : e_1 \geq 0\}, \tag{3-2}$$

$$S_1 = \{\mathbf{E} : e_1 \leq 0, \alpha e_1 + (2 + \alpha)e_2 \geq 0\}, \tag{3-3}$$

$$S_2 = \{\mathbf{E} : \alpha e_1 + (2 + \alpha)e_2 \leq 0\}, \tag{3-4}$$

depicted on the next page in Figure 2. Given \mathbf{E} , the corresponding stress $\mathbf{T} = \mathbb{T}(\mathbf{E})$ satisfying the constitutive equation of masonry-like materials in the plane strain case is given as follows [Lucchesi et al. 2008]:

$$\text{if } \mathbf{E} \in S_0, \text{ then } \mathbf{T} = \mathbf{0}; \tag{3-5}$$

$$\text{if } \mathbf{E} \in S_1, \text{ then } \mathbf{T} = \varphi e_1 \mathbf{O}_{11}, \quad \text{with } \varphi \text{ as in (2-55);} \tag{3-6}$$

$$\text{if } \mathbf{E} \in S_2, \text{ then } \mathbf{T} = \mu[(2 + \alpha)e_1 + \alpha e_2]\mathbf{O}_{11} + \mu[\alpha e_1 + (2 + \alpha)e_2]\mathbf{O}_{22}. \tag{3-7}$$

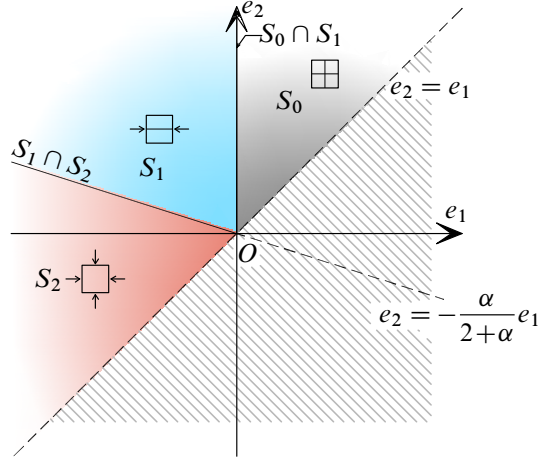


Figure 2. Subdivision of the half-plane $e_1 \leq e_2$ into the regions S_0 , S_1 and S_2 .

As for the fracture strain, we have

$$\text{if } \mathbf{E} \in S_0, \text{ then } \mathbf{E}^f = \mathbf{E}, \quad (3-8)$$

$$\text{if } \mathbf{E} \in S_1, \text{ then } \mathbf{E}^f = (e_2 + \frac{\alpha}{2+\alpha}e_1)\mathbf{O}_{22}, \quad (3-9)$$

$$\text{if } \mathbf{E} \in S_2, \text{ then } \mathbf{E}^f = \mathbf{0}. \quad (3-10)$$

For Z_i the interior of S_i , the derivative $D_E \mathbb{T}(\mathbf{E})$ in regions Z_i has been calculated in [Lucchesi et al. 2008] and has the expressions:

$$\text{if } \mathbf{E} \in Z_0, \text{ then } D_E \mathbb{T}(\mathbf{E}) = \mathbb{O}, \quad (3-11)$$

$$\text{if } \mathbf{E} \in Z_1, \text{ then } D_E \mathbb{T}(\mathbf{E}) = \varphi \mathbf{O}_{11} \otimes \mathbf{O}_{11} - \varphi \frac{e_1}{e_2 - e_1} \mathbf{O}_{12} \otimes \mathbf{O}_{12}, \quad (3-12)$$

$$\text{if } \mathbf{E} \in Z_2, \text{ then } D_E \mathbb{T}(\mathbf{E}) = \mathbb{C}. \quad (3-13)$$

For $\mathbf{E} \in \bigcup_{i=0}^2 Z_i$ and unit vector \mathbf{n} , the acoustic tensor $\mathbf{A}(\mathbf{E}, \mathbf{n})$ defined in (2-11) has different expressions $\mathbf{A}_i(\mathbf{E}, \mathbf{n})$ in the three regions Z_i [Degl'Innocenti et al. 2006]:

$$\text{if } \mathbf{E} \in Z_0, \text{ then } \mathbf{A}_0(\mathbf{E}, \mathbf{n}) = \mathbf{0}, \quad (3-14)$$

$$\begin{aligned} \text{if } \mathbf{E} \in Z_1, \text{ then } \mathbf{A}_1(\mathbf{E}, \mathbf{n}) = & \varphi \rho^{-1} \left[(\mathbf{q}_1 \cdot \mathbf{n})^2 - \frac{e_1}{2(e_2 - e_1)} (\mathbf{q}_2 \cdot \mathbf{n})^2 \right] \mathbf{O}_{11} \\ & - \varphi \rho^{-1} \frac{e_1}{2(e_2 - e_1)} (\mathbf{q}_1 \cdot \mathbf{n})^2 \mathbf{O}_{22} - \varphi \rho^{-1} \frac{e_1}{\sqrt{2}(e_2 - e_1)} (\mathbf{q}_1 \cdot \mathbf{n})(\mathbf{q}_2 \cdot \mathbf{n}) \mathbf{O}_{12}, \end{aligned} \quad (3-15)$$

$$\text{if } \mathbf{E} \in Z_2, \text{ then } \mathbf{A}_2(\mathbf{E}, \mathbf{n}) = (2\mu + \lambda)\rho^{-1} \mathbf{n} \otimes \mathbf{n} + \mu\rho^{-1} (\mathbf{I} - \mathbf{n} \otimes \mathbf{n}). \quad (3-16)$$

As in the three-dimensional case, our goal is to determine the eigenvalues $c_1^{(i)}(\mathbf{E}, \mathbf{n}) \geq c_2^{(i)}(\mathbf{E}, \mathbf{n})$ and eigenvectors $\mathbf{m}_1^{(i)}(\mathbf{E}, \mathbf{n}), \mathbf{m}_2^{(i)}(\mathbf{E}, \mathbf{n})$ of the acoustic tensor $\mathbf{A}_i(\mathbf{E}, \mathbf{n})$, for $i = 1, 2$.

Let us now consider $\mathbf{E} \in Z_1$. The components $A_{ij}(\mathbf{E}, \mathbf{n}) = \mathbf{q}_i \cdot \mathbf{A}_1(\mathbf{E}, \mathbf{n})\mathbf{q}_j$ of the acoustic tensor $\mathbf{A}_1(\mathbf{E}, \mathbf{n})$ in (3-15) with respect to the basis $(\mathbf{q}_1, \mathbf{q}_2)$ are

$$A_{11}(\mathbf{E}, \mathbf{n}) = \varphi\rho^{-1}(\mathbf{q}_1 \cdot \mathbf{n})^2 - \varphi\rho^{-1} \frac{e_1}{2(e_2 - e_1)} (\mathbf{q}_2 \cdot \mathbf{n})^2, \quad (3-17)$$

$$A_{22}(\mathbf{E}, \mathbf{n}) = -\varphi\rho^{-1} \frac{e_1}{2(e_2 - e_1)} (\mathbf{q}_1 \cdot \mathbf{n})^2, \quad (3-18)$$

$$A_{12}(\mathbf{E}, \mathbf{n}) = -\varphi\rho^{-1} \frac{e_1}{2(e_2 - e_1)} (\mathbf{q}_1 \cdot \mathbf{n})(\mathbf{q}_2 \cdot \mathbf{n}). \quad (3-19)$$

If $\mathbf{n} = \mathbf{q}_1$, then

$$\mathbf{A}_1(\mathbf{E}, \mathbf{q}_1) = \varphi\rho^{-1} \mathbf{O}_{11} - \varphi\rho^{-1} \frac{e_1}{2(e_2 - e_1)} \mathbf{O}_{22}, \quad (3-20)$$

whose eigenvalues, both greater than zero, and eigenvectors are

$$c_1^{(1)}(\mathbf{E}, \mathbf{q}_1) = \varphi\rho^{-1}, \quad c_2^{(1)}(\mathbf{E}, \mathbf{q}_1) = -\varphi\rho^{-1} \frac{e_1}{2(e_2 - e_1)}, \quad (3-21)$$

$$\mathbf{m}_1^{(1)}(\mathbf{E}, \mathbf{q}_1) = \mathbf{q}_1, \quad \mathbf{m}_2^{(1)}(\mathbf{E}, \mathbf{q}_1) = \mathbf{q}_2. \quad (3-22)$$

If $\mathbf{n} = \mathbf{q}_2$, then

$$\mathbf{A}_1(\mathbf{E}, \mathbf{q}_2) = -\varphi\rho^{-1} \frac{e_1}{2(e_2 - e_1)} \mathbf{O}_{11}, \quad (3-23)$$

whose eigenvalues and eigenvectors are

$$c_1^{(1)}(\mathbf{E}, \mathbf{q}_2) = -\varphi\rho^{-1} \frac{e_1}{2(e_2 - e_1)}, \quad c_2^{(1)}(\mathbf{E}, \mathbf{q}_2) = 0, \quad (3-24)$$

$$\mathbf{m}_1^{(1)}(\mathbf{E}, \mathbf{q}_2) = \mathbf{q}_1, \quad \mathbf{m}_2^{(1)}(\mathbf{E}, \mathbf{q}_2) = \mathbf{q}_2. \quad (3-25)$$

If $\mathbf{n} \neq \mathbf{q}_1$ and $\mathbf{n} \neq \mathbf{q}_2$, the eigenvalues and eigenvectors of (3-15) are

$$c_1^{(1)}(\mathbf{E}, \mathbf{n}) = \frac{\varphi\rho^{-1}}{2} \left\{ (\mathbf{n} \cdot \mathbf{q}_1)^2 - \frac{e_1}{2(e_2 - e_1)} + \sqrt{\frac{e_2 + e_1}{e_2 - e_1} (\mathbf{n} \cdot \mathbf{q}_1)^4 - \frac{e_1}{e_2 - e_1} (\mathbf{n} \cdot \mathbf{q}_1)^2 + \frac{e_1^2}{4(e_2 - e_1)^2}} \right\}, \quad (3-26)$$

$$c_2^{(1)}(\mathbf{E}, \mathbf{n}) = \frac{\varphi\rho^{-1}}{2} \left[(\mathbf{n} \cdot \mathbf{q}_1)^2 - \frac{e_1}{2(e_2 - e_1)} - \sqrt{\frac{e_2 + e_1}{e_2 - e_1} (\mathbf{n} \cdot \mathbf{q}_1)^4 - \frac{e_1}{e_2 - e_1} (\mathbf{n} \cdot \mathbf{q}_1)^2 + \frac{e_1^2}{4(e_2 - e_1)^2}} \right], \quad (3-27)$$

$$\mathbf{m}_1^{(1)}(\mathbf{E}, \mathbf{n}) = \frac{1}{m_1} \left(\mathbf{q}_1 + \frac{c_1^{(1)}(\mathbf{E}, \mathbf{n}) - A_{11}(\mathbf{E}, \mathbf{n})}{A_{12}(\mathbf{E}, \mathbf{n})} \mathbf{q}_2 \right), \quad (3-28)$$

$$\mathbf{m}_2^{(1)}(\mathbf{E}, \mathbf{n}) = \frac{1}{m_2} \left(\frac{c_2^{(1)}(\mathbf{E}, \mathbf{n}) - A_{22}(\mathbf{E}, \mathbf{n})}{A_{12}(\mathbf{E}, \mathbf{n})} \mathbf{q}_1 + \mathbf{q}_2 \right), \quad (3-29)$$

where $A_{11}(\mathbf{E}, \mathbf{n})$, $A_{22}(\mathbf{E}, \mathbf{n})$ and $A_{12}(\mathbf{E}, \mathbf{n})$ (which is different from zero since $\mathbf{n} \neq \mathbf{q}_1$ and $\mathbf{n} \neq \mathbf{q}_2$ and

$\mathbf{E} \in Z_1$) are given by (3-17), (3-18) and (3-19) and

$$m_1 = \sqrt{1 + \frac{(c_1^{(1)}(\mathbf{E}, \mathbf{n}) - A_{11}(\mathbf{E}, \mathbf{n}))^2}{A_{12}(\mathbf{E}, \mathbf{n})^2}}, \tag{3-30}$$

$$m_2 = \sqrt{1 + \frac{(c_2^{(1)}(\mathbf{E}, \mathbf{n}) - A_{22}(\mathbf{E}, \mathbf{n}))^2}{A_{12}(\mathbf{E}, \mathbf{n})^2}}. \tag{3-31}$$

Note that, taking (3-3) into account, it is a simple matter to prove that

$$c_1^{(1)}(\mathbf{E}, \mathbf{n}) < (2\mu + \lambda)\rho^{-1}, \quad c_2^{(1)}(\mathbf{E}, \mathbf{n}) < \mu\rho^{-1}, \tag{3-32}$$

for $c_1^{(1)}$ and $c_2^{(1)}$ given in (3-21), (3-24), and (3-26)–(3-27).

If $\mathbf{E} \in Z_2$, the acoustic tensor $A_2(\mathbf{E}, \mathbf{n})$ coincides with the acoustic tensor of a linear elastic material subjected to a plane strain state. Its eigenvalues are

$$c_1^{(2)} = (2\mu + \lambda)\rho^{-1}, \quad c_2^{(2)} = c_3^{(3)} = \mu\rho^{-1}, \tag{3-33}$$

and the corresponding eigenvectors are

$$\mathbf{m}_1^{(1)}(\mathbf{E}, \mathbf{n}) = \mathbf{n}, \quad \mathbf{m}_2^{(2)}(\mathbf{E}, \mathbf{n}) \text{ belonging to } \text{Span}(\mathbf{n})^\perp. \tag{3-34}$$

Thus, the behavior of progressive waves in a body composed of a masonry-like material with homogeneous stress \mathbf{T} associated to a homogeneous plane strain field $\mathbf{E} \in \bigcup_{i=0}^2 Z_i$ can be summarized in Table 4, which reports the polarization vector and the squared velocity of waves propagating in masonry solids for different directions of propagation \mathbf{n} . If $\mathbf{E} \in Z_0$, no propagation occurs. If $\mathbf{E} \in Z_1$, for $\mathbf{n} = \mathbf{q}_1$

$\mathbf{E} \in Z_0$	$c_1^{(0)}$	$c_2^{(0)}$
\mathbf{n}	0 no propagation	0 no propagation
$\mathbf{E} \in Z_1$	$c_1^{(1)}$	$c_2^{(1)}$
$\mathbf{n} = \mathbf{q}_1$	$\varphi\rho^{-1}$ longitudinal wave, \mathbf{q}_1	$-\varphi\rho^{-1}e_1/(2(e_2 - e_1))$ transverse wave, \mathbf{q}_2
$\mathbf{n} = \mathbf{q}_2$	$-\varphi\rho^{-1}e_1/(2(e_2 - e_1))$ transverse wave, \mathbf{q}_1	0 no propagation
$\mathbf{n} \neq \mathbf{q}_1, \mathbf{q}_2$	(3-26)	(3-27)
$\mathbf{E} \in Z_2$	$c_1^{(2)}$	$c_2^{(2)}$
\mathbf{n}	$(2\mu + \lambda)\rho^{-1}$ longitudinal wave	$\mu\rho^{-1}$ transverse wave

Table 4. Wave velocities squared for $\mathbf{E} \in Z_i, i = 0, 1, 2$.

there is one longitudinal wave and one transverse wave,

$$A_1(\mathbf{E}, \mathbf{q}_1)\mathbf{q}_1 = \varphi\rho^{-1}\mathbf{q}_1, \tag{3-35}$$

$$A_1(\mathbf{E}, \mathbf{q}_1)\mathbf{q}_2 = -\frac{\varphi\rho^{-1}e_1}{2(e_2 - e_1)}\mathbf{q}_2. \tag{3-36}$$

Due to (3-32), the velocities of the longitudinal and transverse waves are less than those of the corresponding waves in a linear elastic material. For $\mathbf{n} = \mathbf{q}_2$, only one transverse wave propagates, with squared velocity (3-24), which because of (3-32), is less than the squared velocity of the transverse linear elastic wave. For $\mathbf{n} \neq \mathbf{q}_1$ and $\mathbf{n} \neq \mathbf{q}_2$, two waves propagate with the squared velocities (3-26) and (3-27), that are less than the squared velocities of the longitudinal and transverse waves in a linear elastic material (see (3-32)).

For $\mathbf{E} \in Z_2$, masonry material behaves like a linear elastic material and for each unit vector \mathbf{n} , there are a longitudinal wave and a transverse wave with the squared velocities in (3-33).

Now, we wish to analyze the behavior of eigenvalues $c_1^{(1)}(\mathbf{E}, \mathbf{n})$ and $c_2^{(1)}(\mathbf{E}, \mathbf{n})$ of $A_1(\mathbf{E}, \mathbf{n})$, as \mathbf{n} varies.

Let us put

$$z = (\mathbf{n} \cdot \mathbf{q}_1)^2, \quad z \in [0, 1], \tag{3-37}$$

and

$$k = -e_2/e_1, \tag{3-38}$$

with k satisfying the inequality

$$k > \frac{\alpha}{2+\alpha}, \tag{3-39}$$

because \mathbf{E} belongs to Z_1 .

By taking (3-37) and (3-38) into account, the eigenvalue $c_1^{(1)}(\mathbf{E}, \mathbf{n})$ in (3-26) can be expressed in terms of z and k via the expression

$$f_1(z; k) = \frac{\varphi\rho^{-1}}{2} \left(z + \frac{1}{2(k+1)} + \sqrt{\frac{k-1}{k+1}z^2 + \frac{1}{k+1}z + \frac{1}{4(k+1)^2}} \right). \tag{3-40}$$

For each k satisfying (3-39), $f_1(z; k)$ is an increasing function of z , with

$$f_1(0; k) = c_1^{(1)}(\mathbf{E}, \mathbf{q}_2) = \frac{\varphi\rho^{-1}}{2(k+1)}, \tag{3-41}$$

$$f_1(1; k) = c_1^{(1)}(\mathbf{E}, \mathbf{q}_1) = \varphi\rho^{-1}, \tag{3-42}$$

thus,

$$f_1(z; k) \leq \varphi\rho^{-1} \text{ for each } z \in [0, 1], \tag{3-43}$$

and

$$\begin{aligned} \lim_{k \rightarrow \frac{\alpha}{2+\alpha}} f_1(0; k) &= \mu\rho^{-1}, \\ \lim_{k \rightarrow \infty} f_1(z; k) &= \varphi\rho^{-1}z \quad \text{for each } z \in [0, 1]. \end{aligned} \tag{3-44}$$

Analogously, the eigenvalue $c_2^{(1)}(\mathbf{E}, \mathbf{n})$ in (3-27) can be expressed in terms of z and k via the expression

$$f_2(z; k) = \frac{\varphi\rho^{-1}}{2} \left(z + \frac{1}{2(k+1)} - \sqrt{\frac{k-1}{k+1}z^2 + \frac{1}{k+1}z + \frac{1}{4(k+1)^2}} \right). \tag{3-45}$$

In particular, for each k satisfying (3-39),

$$f_2(0; k) = c_2^{(1)}(\mathbf{E}, \mathbf{q}_2) = 0, \tag{3-46}$$

$$f_2(1; k) = c_2^{(1)}(\mathbf{E}, \mathbf{q}_1) = \frac{\varphi\rho^{-1}}{2(k+1)}, \tag{3-47}$$

and

$$f_2(z; k) \leq \frac{\varphi\rho^{-1}}{2(k+1)} \text{ for each } z \in [0, 1], \tag{3-48}$$

moreover,

$$\lim_{k \rightarrow \infty} f_2(z; k) = 0, \quad \lim_{k \rightarrow \alpha/(2+\alpha)} f_2(1; k) = \mu\rho^{-1} \text{ for each } z \in [0, 1]. \tag{3-49}$$

As for the elastic constants, we have assumed $E/\rho = 500000 \text{ (m/s)}^2$ and $\nu = 0.2$ for the Poisson's ratio. Consequently, we have $\mu/\rho = E/(2\rho(1+\nu)) = 208333 \text{ (m/s)}^2$, $\lambda/\rho = \nu E/(\rho(1+\nu)(1-2\nu)) = 138889 \text{ (m/s)}^2$, $\varphi/\rho = 520833 \text{ (m/s)}^2$, $(2\mu + \lambda)/\rho = 555556 \text{ (m/s)}^2$ and $\alpha = 0.7$.

Figures 3 and 4 show the behavior of $f_1(z; k)$ and $f_2(z; k)$ versus z for different values of k compared with the eigenvalues $(2\mu + \lambda)\rho^{-1}$ and $\mu\rho^{-1}$ of the acoustic tensor corresponding to a linear elastic material. The dashed line represents the function $\lim_{k \rightarrow \infty} f_1(z; k)$ in (3-44). In particular, we have chosen $k = 0.25$ (corresponding to $\alpha/(2 + \alpha)$) and $k = 0.3, 0.5, 1, 2, 10$. Both (3-44) and (3-49) are in agreement with the jump conditions (3-65) and (3-67), reported in the Appendix, of the acoustic tensor at the interfaces $S_0 \cap S_1$ and $S_1 \cap S_2$, which are reached when $k \rightarrow \infty$ and $k \rightarrow \alpha/(2 + \alpha)$. Note that waves propagating in a masonry-like material are slower than waves propagating in a linear elastic material and that their velocities decrease as k increases.

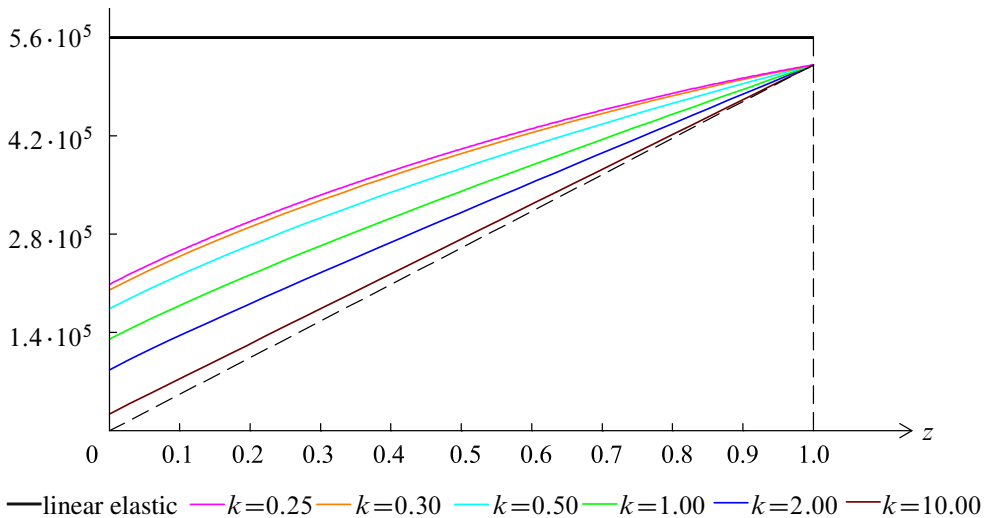


Figure 3. Function $f_1(z; k)$ vs. $z \in [0, 1]$ for different values of k .

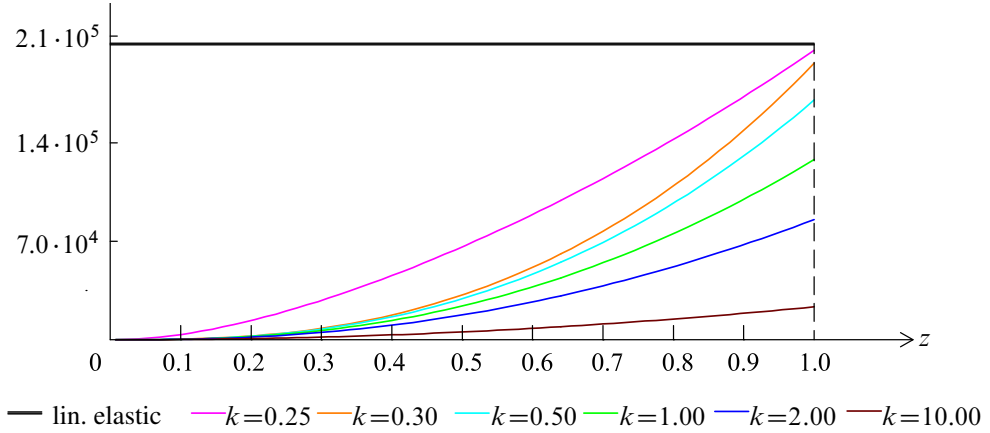


Figure 4. Function $f_2(z; k)$ vs. $z \in [0, 1]$ for different values of k .

Figure 5 shows a plot of the curves $\mathcal{C}_1(k)$ composed of the points having coordinates

$$(\tau f_1(\tau^2; k), \sqrt{1 - \tau^2} f_1(\tau^2; k)) \tag{3-50}$$

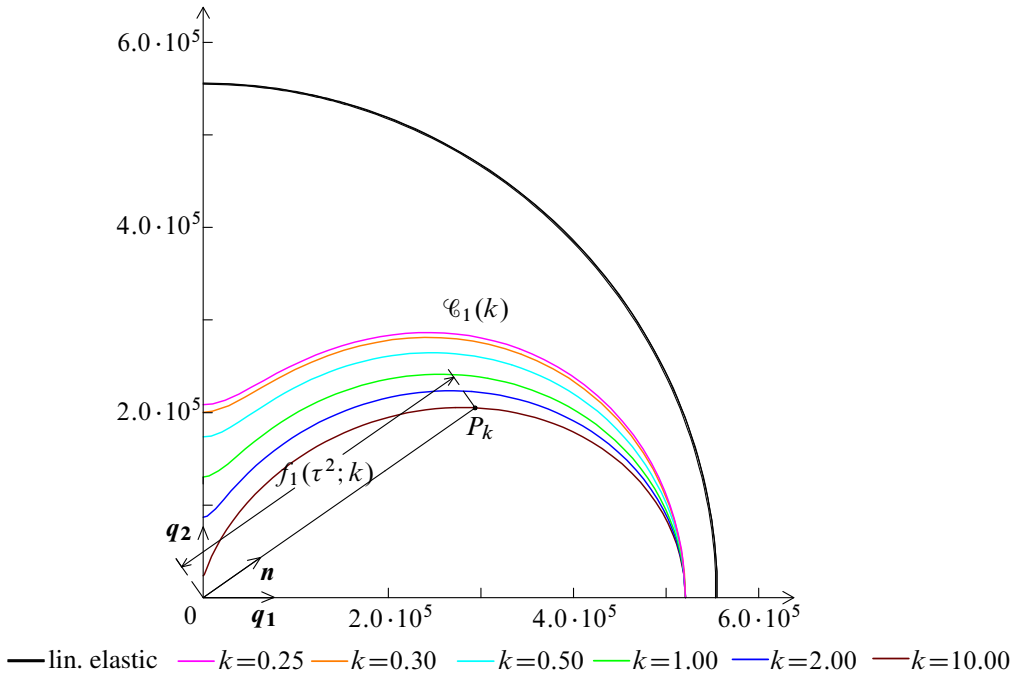


Figure 5. Curve $\mathcal{C}_1(k)$ formed by the points with coordinates in (3-50), for $k = 0.25, 0.30, 0.50, 1.00, 2.00,$ and 10.00 , from the top down. The thick black curve represents the linear elastic case.

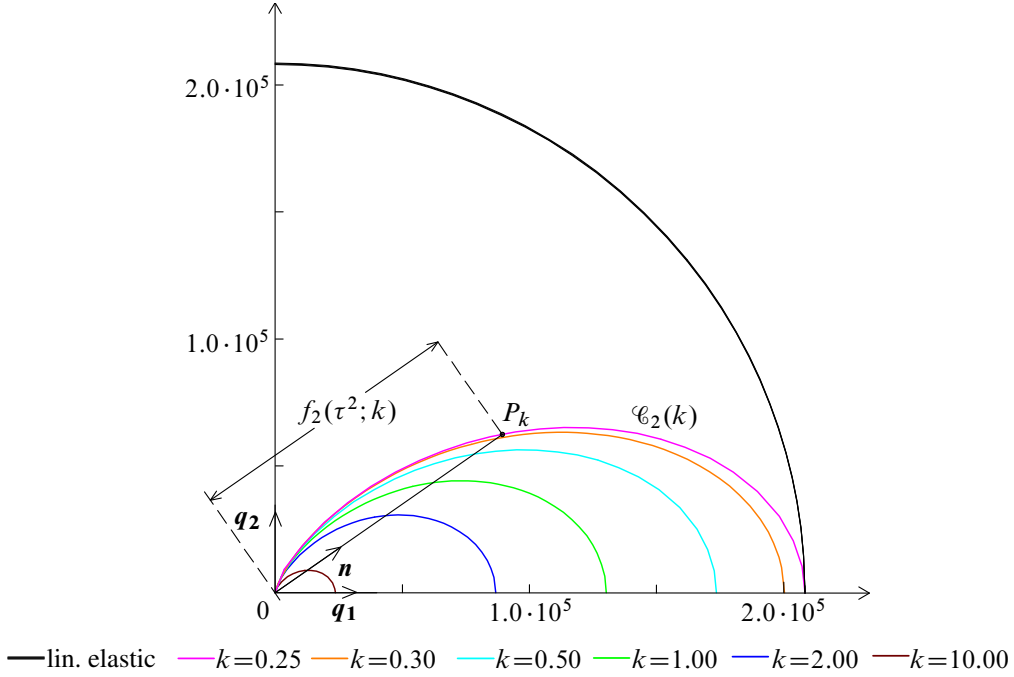


Figure 6. Curve $\mathcal{C}_2(k)$ formed by the points with coordinates in (3-51), for $k = 0.25, 0.30, 0.50, 1.00, 2.00,$ and 10.00 , from the top down. The thick black curve represents the linear elastic case.

with respect to the Cartesian coordinate frame $\{q_1, q_2, O\}$, with $\tau = n \cdot q_1 \in [0, 1]$ for $k = 0.25, 0.3, 0.5, 1, 2, 10$. For P_k the intersection point of curve $\mathcal{C}_1(k)$ and the line passing from the origin and parallel to the unit vector n of components $(n \cdot q_1, n \cdot q_2)$, the length of the segment OP_k is $f_1((n \cdot q_1)^2; k)$, which coincides with the maximum squared velocity of a wave propagating along n .

Analogously, Figure 6 plots the curves $\mathcal{C}_2(k)$, composed of the points having coordinates

$$(\tau f_2(\tau^2; k), \sqrt{1 - \tau^2} f_2(\tau^2; k)) \tag{3-51}$$

with respect to the Cartesian coordinate frame $\{q_1, q_2, O\}$, with $\tau = n \cdot q_1 \in [0, 1]$ for $k = 0.25, 0.3, 0.5, 1, 2, 10$. For P_k the intersection point of curve $\mathcal{C}_2(k)$ and the line passing from the origin and parallel to the unit vector n of components $(n \cdot q_1, n \cdot q_2)$, the length of the segment OP_k is $f_2((n \cdot q_1)^2; k)$, which coincides with the minimum squared velocity of a wave propagating along n .

Figure 7 shows the quantities

$$d_1(\tau; k) = \frac{|\sqrt{f_1(\tau^2; k)} - \sqrt{(2\mu + \lambda)\rho^{-1}}|}{\sqrt{(2\mu + \lambda)\rho^{-1}}}, \quad d_2(\tau; k) = \frac{|\sqrt{f_2(\tau^2; k)} - \sqrt{\mu\rho^{-1}}|}{\sqrt{\mu\rho^{-1}}} \tag{3-52}$$

as a function of τ for different values of k . They measure the relative distance between the maximum (top half) and minimum (bottom half) squared velocities of waves propagating in a masonry-like and a linear elastic material. Figure 7 shows that, for a given k , the relative distances $d_1(\tau; k)$ and $d_2(\tau; k)$

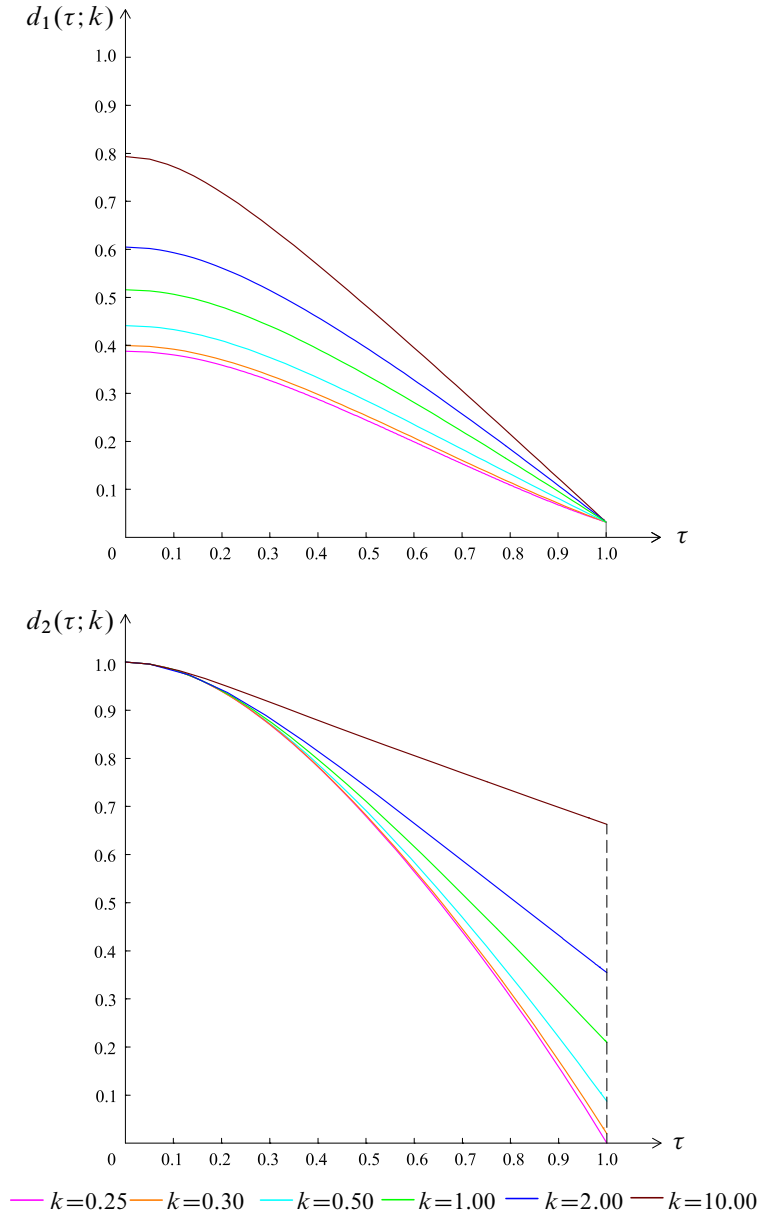


Figure 7. Functions $d_1(\tau; k)$ and $d_2(\tau; k)$ vs. $\tau \in [0, 1]$ for $k = 0.25, 0.30, 0.50, 1.00, 2.00,$ and 10.00 , from the bottom up.

have a maximum for $\tau = \mathbf{n} \cdot \mathbf{q}_1 = 0$, namely when the propagation vector is orthogonal to the direction of maximum compression \mathbf{q}_1 , and have a minimum when the propagation vector coincides with \mathbf{q}_1 .

Figure 8 shows the behavior of the scalar product $r(\tau; k) = \mathbf{m}_1^{(1)}(\mathbf{E}, \mathbf{n}) \cdot \mathbf{n}$ as a function of $\tau = \mathbf{n} \cdot \mathbf{q}_1 \in [0, 1]$; it is a measure of the deviation of the eigenvector $\mathbf{m}_1^{(1)}(\mathbf{E}, \mathbf{n})$ from the direction of propagation \mathbf{n} , along which the longitudinal wave travels in the linear elastic case.

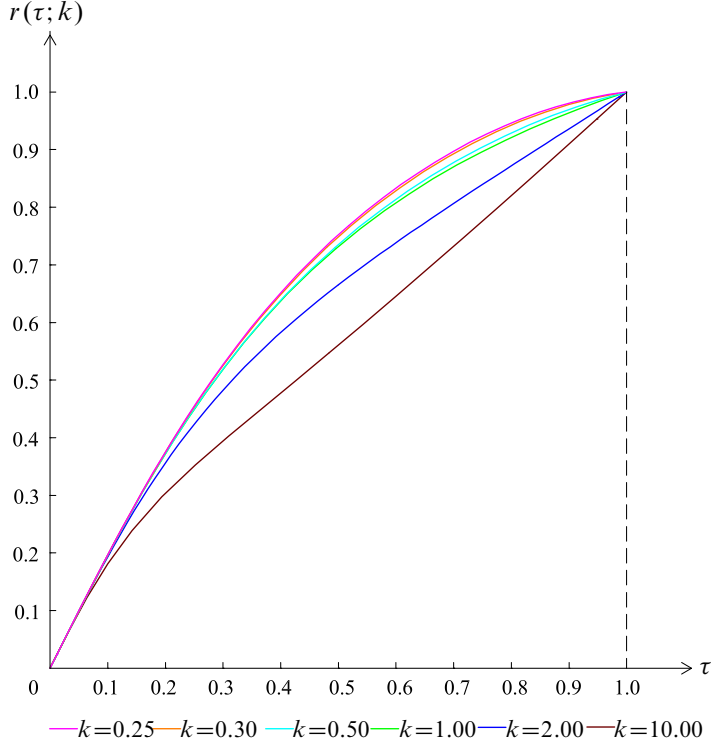


Figure 8. Function $r(\tau; k)$ vs. $\tau \in [0, 1]$ for different values of k .

Let us now consider the homogenous wave

$$\mathbf{u}(\mathbf{x}, t) = \mathbf{m} \sin(\mathbf{n} \cdot \mathbf{x} - vt). \tag{3-53}$$

We wish to analyze the behavior of \mathbf{u} as function of time t in order to highlight the differences between a linear elastic and a masonry-like material. For $\mathbf{n} = \mathbf{q}_1$, we can distinguish the longitudinal wave

$$\mathbf{u}_L(x_1, t) = \mathbf{q}_1 \sin(x_1 - \sqrt{\varphi\rho^{-1}}t), \tag{3-54}$$

and the transverse wave

$$\mathbf{u}_T(x_1, t) = \mathbf{q}_2 \sin\left(x_1 - \sqrt{\frac{\varphi\rho^{-1}}{2(k+1)}}t\right), \tag{3-55}$$

with $x_1 = \mathbf{q}_1 \cdot \mathbf{x}$ and $t \geq 0$. The longitudinal and transverse waves in the case of linear elastic materials are respectively

$$\mathbf{u}_L^e(x_1, t) = \mathbf{q}_1 \sin(x_1 - \sqrt{(2\mu + \lambda)\rho^{-1}}t), \tag{3-56}$$

$$\mathbf{u}_T^e(x_1, t) = \mathbf{q}_2 \sin(x_1 - \sqrt{\mu\rho^{-1}}t), \tag{3-57}$$

Figure 9 shows the functions $\mathbf{u}_L(x_1, t)$ (red line) and $\mathbf{u}_L^e(x_1, t)$ (black line) versus t at $x_1 = 0$. Figure 10

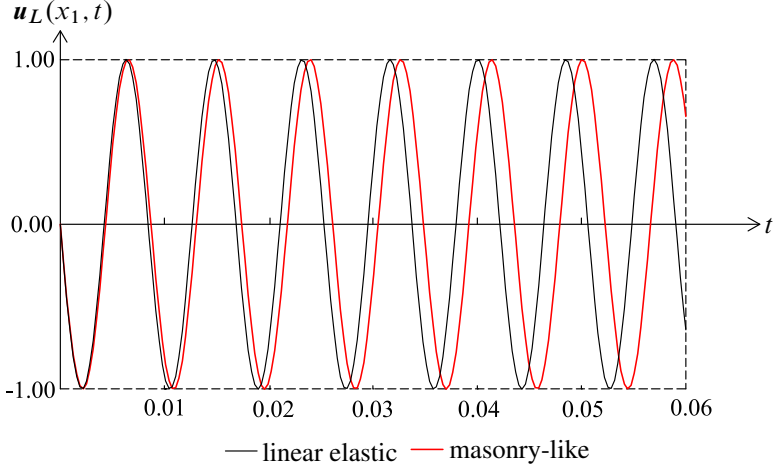


Figure 9. Longitudinal wave propagating along $\mathbf{n} = \mathbf{q}_1$, $u_L(x_1, t)$ at $x_1 = 0$ vs. t for different values of k .

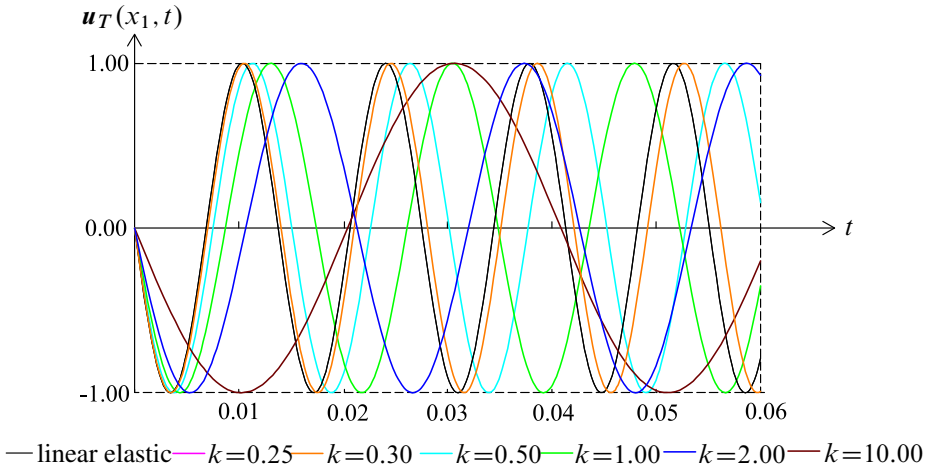


Figure 10. Transverse wave propagating along $\mathbf{n} = \mathbf{q}_1$, $u_T(x_1, t)$ at $x_1 = 0$ vs. t for different values of k .

shows the functions $u_T(x_1, t)$ and $u_T^e(x_1, t)$ versus t at $x_1 = 0$. Displacement $u_T(x_1, t)$ is plotted for $k = 0.25, 0.3, 0.5, 1, 2, 10$.

For $\mathbf{n} = \mathbf{q}_2$, there is only one transverse wave,

$$u_T(x_2, t) = \mathbf{q}_1 \sin\left(x_2 - \sqrt{\frac{\varphi\rho^{-1}}{2(k+1)}}t\right), \tag{3-58}$$

with $x_2 = \mathbf{q}_2 \cdot \mathbf{x}$, and no longitudinal waves propagate in the material,

$$u_L(x_2, t) = \mathbf{0}. \tag{3-59}$$

As for the linear elastic case, we have

$$\mathbf{u}_L^e(x_2, t) = \mathbf{q}_2 \sin(x_2 - \sqrt{(2\mu + \lambda)\rho^{-1}}t), \quad (3-60)$$

$$\mathbf{u}_T^e(x_2, t) = \mathbf{q}_1 \sin(x_1 - \sqrt{\mu\rho^{-1}}t). \quad (3-61)$$

By replacing φ with E , we obtain the results for the plane stress state. Note that in view of the inequality $\varphi > E$, the velocities of elastic waves, both longitudinal and transverse, in the plane strain state are greater than the velocities in the plane stress state.

Conclusions

The propagation of elastic waves in an infinite masonry-like body subjected to a given homogeneous strain field has been investigated. Masonry-like materials are characterized by the fact that they cannot withstand tensile stresses and, as a consequence, they can crack. The stress function \mathbb{T} defined on Sym with values in the subset of the negative-semidefinite symmetric tensors is nonlinear and differentiable on an open subset W of Sym . Starting with the differentiability of \mathbb{T} with respect to \mathbf{E} on W and using the explicit expression for $D_E\mathbb{T}(\mathbf{E})$, we obtain the condition that a progressive wave must satisfy in order to propagate in a masonry body subjected to a given homogeneous strain field \mathbf{E} . The propagation condition involves the acoustic tensor, which is a function of \mathbf{E} and the direction of propagation \mathbf{n} . We show that the behavior of progressive waves propagating in the solid depends on the state of prestrain \mathbf{E} and on the corresponding crack distribution. In particular, due to the presence of cracks, the propagation velocity of waves in masonry-like solids is lower than in linear elastic materials. A peculiar aspect of masonry-like solids is that there exist directions \mathbf{n} along which waves cannot propagate. The preliminary results obtained in this paper can constitute a basis for the study of the propagation of small elastic waves in masonry constructions. The problem is quite relevant to technical applications: in fact, measurement of the wave propagation velocities in masonry buildings can furnish important information about the mechanical behavior of their undamaged and cracked portions.

Appendix

As pointed out in [Lucchesi et al. 2008], no tangential discontinuity affects $D_E\mathbb{T}(\mathbf{E})$ across the interfaces $S_0 \cap S_1$ and $S_1 \cap S_2$. In fact its jumps are

$$[D_E\mathbb{T}(\mathbf{E})] = \varphi \mathbf{O}_{11} \otimes \mathbf{O}_{11} \text{ for } \mathbf{E} \in S_0 \cap S_1, \quad (3-62)$$

and

$$[D_E\mathbb{T}(\mathbf{E})] = \mu \left\{ \frac{\alpha^2}{2+\alpha} \mathbf{O}_{11} \otimes \mathbf{O}_{11} + (2+\alpha) \mathbf{O}_{22} \otimes \mathbf{O}_{22} + \alpha (\mathbf{O}_{11} \otimes \mathbf{O}_{22} + \mathbf{O}_{22} \otimes \mathbf{O}_{11}) \right\} \text{ for } \mathbf{E} \in S_1 \cap S_2. \quad (3-63)$$

For the jumps that the acoustic tensor inherits from $D_E\mathbb{T}(\mathbf{E})$, from (3-14), (3-15) and (3-16) we get

$$[\mathbf{A}(\mathbf{E}, \mathbf{n})] = \varphi \rho^{-1} (\mathbf{q}_1 \cdot \mathbf{n})^2 \mathbf{O}_{11} \text{ for } \mathbf{E} \in S_0 \cap S_1, \quad (3-64)$$

and, in particular,

$$[\mathbf{A}(\mathbf{E}, \mathbf{q}_1)] = \varphi \rho^{-1} \mathbf{O}_{11}, [\mathbf{A}(\mathbf{E}, \mathbf{q}_2)] = \mathbf{0}. \quad (3-65)$$

Moreover,

$$\begin{aligned}
 [A(\mathbf{E}, \mathbf{n})] = & \mu\rho^{-1} \left[1 + \frac{(1+\alpha)(\alpha-2)}{2+\alpha} (\mathbf{q}_1 \cdot \mathbf{n})^2 + \frac{2(1+\alpha)e_1}{(2+\alpha)(e_2-e_1)} (\mathbf{q}_2 \cdot \mathbf{n})^2 \right] \mathbf{O}_{11} \\
 & + \mu\rho^{-1} \left[1 + \frac{2(1+\alpha)e_1}{(2+\alpha)(e_2-e_1)} (\mathbf{q}_1 \cdot \mathbf{n})^2 + (1+\alpha)(\mathbf{q}_2 \cdot \mathbf{n})^2 \right] \mathbf{O}_{22} \\
 & - \varphi\rho^{-1} \frac{\alpha e_1}{\sqrt{2}(e_2-e_1)} (\mathbf{q}_1 \cdot \mathbf{n})(\mathbf{q}_2 \cdot \mathbf{n}) \mathbf{O}_{12} \text{ for } \mathbf{E} \in S_1 \cap S_2, \quad (3-66)
 \end{aligned}$$

and

$$[A(\mathbf{E}, \mathbf{q}_1)] = \mu\rho^{-1} \frac{\alpha^2}{2+\alpha} \mathbf{O}_{11}, \quad [A(\mathbf{E}, \mathbf{q}_2)] = (2\mu + \lambda)\rho^{-1} \mathbf{O}_{22}. \quad (3-67)$$

References

- [Binante et al. 2014] V. Binante, M. Girardi, C. Padovani, G. Pasquinelli, D. Pellegrini, and M. Porcelli, *NOSA-ITACA 1.0 documentation*, 2014, <http://www.nosaitaca.it/software/>.
- [Callieri et al. 2010] M. Callieri, M. Corsini, M. Girardi, C. Padovani, A. Pagni, G. Pasquinelli, and R. Scopigno, “The “Rognosa” tower in San Gimignano: digital acquisition and structural analysis”, in *Proceedings of the 10th International Conference on Computational Structures Technologies* (Valencia, 2010), edited by B. H. V. Topping et al., Saxe-Coburg, Stirling, United Kingdom, 2010.
- [Casarosa et al. 1998] C. Casarosa, M. Lucchesi, C. Padovani, A. Pagni, and G. Pasquinelli, “Longitudinal vibrations of masonry beams”, pp. 43–50 in *Computer methods in structural masonry 4: Proceedings of the International Symposium* (Florence, 1997), edited by G. N. Pande et al., Routledge, New York, 1998.
- [Chadwick 1989] P. Chadwick, “Wave propagation in transversely isotropic elastic media, I: Homogeneous plane waves”, *Proc. R. Soc. Lond. A* **422**:1862 (1989), 23–66.
- [Crampin 1981] S. Crampin, “A review of wave motion in anisotropic and cracked elastic-media”, *Wave Motion* **3** (1981), 343–391.
- [De Falco et al. 2014] A. De Falco, M. Girardi, and D. Pellegrini, “Nonlinear analyses on the medieval “Ponte del Diavolo” in Borgo a Mozzano (Italy)”, in *Proceedings of the 12th International Conference on Computational Structures Technology* (Naples, 2014), edited by B. H. V. Topping and P. Iványi, Civil-Comp Press, Stirlingshire, UK, 2014.
- [Degl’Innocenti et al. 2006] S. Degl’Innocenti, P. C., and G. Pasquinelli, “Numerical methods for the dynamic analysis of masonry structures”, *Struct. Eng. Mech.* **22**:1 (2006), 107–130.
- [Del Piero 1989] G. Del Piero, “Constitutive equation and compatibility of the external loads for linear elastic masonry-like materials”, *Meccanica (Milano)* **24**:3 (1989), 150–162.
- [Ewing et al. 1957] W. M. Ewing, W. S. Jardetzky, and F. Press, *Elastic waves in layered media*, Lamont Geological Observatory Contribution McGraw-Hill Series in the Geological Sciences **189**, McGraw-Hill, New York, 1957.
- [Gurtin 1972] M. E. Gurtin, “The linear theory of elasticity”, pp. 1–296 in *Handbuch der Physik*, vol. VIa/2, edited by C. Truesdell and S. Flügge, Springer, Heidelberg, Germany, 1972.
- [Gurtin 1981] M. E. Gurtin, *An introduction to continuum mechanics*, Mathematics in Science and Engineering **158**, Academic Press, New York, 1981.
- [Itskov 2015] M. Itskov, *Tensor algebra and tensor analysis for engineers*, 4th ed., Mathematical Engineering, Springer, Cham, Switzerland, 2015.
- [Ivanovic et al. 2001] S. S. Ivanovic, M. D. Trifunac, and M. I. Todorovska, “On identification of damage in structures via wave travel times”, in *Strong motion instrumentation for civil engineering structures* (Istanbul, 1999), edited by M. Erdik et al., Kluwer, Dordrecht, 2001.
- [Kachanov 1974] L. M. Kachanov, *Fundamentals of the theory of plasticity*, Mir, Moscow, 1974.

- [Lucchesi et al. 1999] M. Lucchesi, C. Padovani, A. Pagni, and G. Pasquinelli, “The entropy condition and Lax’s E-condition for longitudinal oscillations of bimodular rods”, pp. 1389–1392 in *Proceedings of PACAM VI / DINAME 8 (6th Pan-American Congress of Applied Mechanics and VIII International Conference of Dynamic Problems in Mechanics)* (Rio de Janeiro, 1999), edited by H. Weber et al., Applied Mechanics of the Americas **8**, 1999.
- [Lucchesi et al. 2008] M. Lucchesi, C. Padovani, G. Pasquinelli, and N. Zani, *Masonry constructions: Mechanical models and numerical applications*, Springer, Berlin, 2008.
- [Ogden and Singh 2011] R. W. Ogden and B. Singh, “Propagation of waves in an incompressible transversely isotropic elastic solid with initial stress: Biot revisited”, *J. Mech. Mater. Struct.* **6**:1–4 (2011), 453–477.
- [Padovani and Šilhavý 2015] C. Padovani and M. Šilhavý, “On the derivative of the stress-strain relation in a no-tension material”, *Math. Mech. Solids* (2015).
- [Pao et al. 1984] Y. H. Pao, W. Sachse, and H. Fukuoka, “Acoustoelasticity and ultrasonic measurements of residual stresses”, pp. 61–143 in *Physical acoustics*, vol. 17, edited by W. P. Mason and R. N. Thurston, Academic Press, New York, 1984.
- [Royer and Dieulesaint 2000] D. Royer and E. Dieulesaint, *Elastic waves in solids, I: Free and guided propagation*, Springer, Berlin, 2000.
- [Safack 1999] E. Safack, “Wave propagation formulation of seismic response of multi-story buildings”, *J. Struct. Eng. (ASCE)* **125**:4 (1999), 426–437.
- [Safak et al. 2009] E. Safak, E. Cakti, and Y. Kaya, “Seismic wave velocities in historical structures: a new parameter for identification and damage detection”, pp. 757–764 in *3rd International Modal Analysis Conference (IOMAC 2009)* (Portonovo, Italy, 2009), edited by C. Gentile et al., Curran Associates, Red Hook, NY, 2009.
- [Šilhavý 1997] M. Šilhavý, *The mechanics and thermodynamics of continuous media*, Springer, Berlin, 1997.
- [Truesdell and Toupin 1960] C. Truesdell and R. Toupin, “The classical field theories”, pp. 226–793; appendix, pp. 794–858 in *Handbuch der Physik*, vol. III/1, edited by S. Flügge, Springer, Berlin, 1960.
- [Winkler and Liu 1996] K. W. Winkler and X. Liu, “Measurements of third-order elastic constants in rocks”, *J. Acoust. Soc. Am.* **100** (1996), 1392–1398.

Received 23 Dec 2015. Revised 20 Apr 2016. Accepted 26 Apr 2016.

MARIA GIRARDI: maria.girardi@isti.cnr.it

Institute of Information Science and Technologies “A. Faedo”, Via Moruzzi, 1, 56126 Pisa, Italy

CRISTINA PADOVANI: cristina.padovani@isti.cnr.it

Institute of Information Science and Technologies “A. Faedo”, Via Moruzzi, 1, 56126 Pisa, Italy

DANIELE PELLEGRINI: daniele.pellegrini@isti.cnr.it

Institute of Information Science and Technologies “A. Faedo”, Via Moruzzi, 1, 56126 Pisa, Italy

TWO-DIMENSIONAL FRETTING CONTACT OF PIEZOELECTRIC MATERIALS UNDER A RIGID CONDUCTING CYLINDRICAL PUNCH

JIE SU, LIAO-LIANG KE AND YUE-SHENG WANG

This paper investigates the fretting contact between a transversely isotropic piezoelectric half-plane and a rigid cylindrical punch in a plane strain state. It is assumed that the punch is a perfect conductor with a constant electric potential within the contact region. Since the fretting contact problem is frictional and history dependent, the two bodies are brought into contact first by a monotonically increasing normal load, and then by a cyclic tangential load, which is less than that necessary to cause complete sliding. It is assumed that the contact region contains an inner stick region and two outer slip regions in which Coulomb's friction law is applied. With the use of the superposition principle and Fourier integral transform technique, the problem is reduced to a set of coupled Cauchy singular integral equations. An iterative method is used to determine the unknown stick/slip region, normal contact pressure, electric charge and tangential traction. The effects of the friction coefficient, electric load and conductivity of the punch on the surface electromechanical fields are discussed during different loading phases.

1. Introduction

Piezoelectric materials are important smart materials and have been widely used in various electromechanical devices such as actuators, sensors, transducers and micropower generators. Piezoelectric devices are often subjected to highly localized loading indented by a concentration load or rigid punches. Thus, failure and degradation of the piezoelectric components may be caused by the inharmonious contact between piezoelectric devices and the punch due to the innate brittleness of the piezoelectric ceramics. As a result of the aforementioned reasons, many theoretical investigations concerning indentation, frictionless contact and frictional contact of piezoelectric materials have received considerable concerns and been solved perfectly.

Using the state space framework, Sosa and Castro [1994] obtained the solutions of a piezoelectric half-plane loaded by a concentrated line force and a concentrated line charge. Fan et al. [1996] investigated the two-dimensional contact problem of an anisotropic piezoelectric half-plane by the nonslip or slip indenter. Chen [1999] analyzed the contact problem of an inclined rigid conducting circular flat punch indenting a transversely isotropic piezoelectric half-space. Ding et al. [2000] investigated the three-dimensional frictionless contact problem including a spherical indenter, a conical indenter and an upright circular flat indenter on a transversely isotropic piezoelectric half-space. The contact problem of piezoelectric materials was also examined by Giannakopoulos and Suresh [1999], Chen [2000], Ramirez and Heyliger [2003], Wang et al. [2008], Zhou and Lee [2012] and Wu et al. [2012] for the frictionless case; Makagon

Liao-Liang Ke is the corresponding author.

Keywords: fretting contact, cyclic load, piezoelectric materials, conducting punch, singular integral equation.

et al. [2009], Zhou and Lee [2011; 2014] and Ma et al. [2014] for the sliding frictional case; and Chen and Yu [2005] and Guo and Jin [2009] for the adhesive case.

Fretting is a frictional contact phenomenon that occurs when two bodies are brought into contact by a normal load, and are subjected to cyclic tangential loads causing small relative oscillations with respect to each other. The whole contact surface is divided into an inner stick region, where there is no relative motion between the two bodies, and two outer slip regions at the two edges. The surface tractions near the ends of contact, where the contact surfaces undergo the relative tangential motion, initiate surface cracks that are known as fretting fatigue. Contact damage and fretting fatigue, which occur in engineering structures, gas turbine engines, electric power, aircraft, traffic tools, etc., are the main causes of failure of key components. In some engineering components, the normal load for contacting bodies often does not vary significantly, whereas the tangential load varies cyclically with time. An initial theoretical investigation of the fretting contact was made by Cattaneo [1938], who extended the Hertz contact theory to include a monotonically increasing tangential force. Subsequently, the fretting contact of elastically similar bodies under tangential loading was considered by Mindlin and Deresiewicz [1953], Mindlin et al. [1951], Ciavarella [1998a; 1998b] and Ciavarella and Hills [1999]. The fretting contact of elastically dissimilar bodies was studied by Spence [1973] for monotonically normal loading, Spence [1986] for monotonically tangential loading, Keer and Farris [1987], Hanson et al. [1989], Nowell et al. [1988] for cyclic tangential loading.

Since piezoelectric devices are often in vibration environments, fretting contact damage inevitably occurs in these devices. Unfortunately, so far the work done on the fretting contact of piezoelectric materials is quite limited despite the importance of their application in smart devices. We only found that Su et al. [2015] analyzed the two-dimensional fretting contact between a transversely isotropic piezoelectric half-plane and a rigid insulating cylindrical punch. This paper further studies the fretting contact of a piezoelectric half-plane under a rigid conducting cylindrical punch with a constant electric potential. It is assumed that the whole contact region contains a centrally located stick region between the two regions of slip in which Coulomb's friction law is applied. The two dissimilar bodies are first acted upon by a monotonically increasing normal load, and then by a cyclic tangential load. The fretting contact problem is reduced to a set of coupled Cauchy singular integral equations which are then solved by using an iterative method. The numerical results highlight the effects of the friction coefficient, electric loading and conductivity of the punch on the normal contact pressure, electric charge, tangential traction, in-plane stress and in-plane electric displacement.

Unlike the insulating punch problem in Su et al. [2015], the conductivity of the punch will lead to electric charge distribution at the contact surface. Moreover, the conducting punch problem is governed by the coupled Cauchy singular integral equations with unknown contact pressure and electric charge, which is more difficult to solve than the insulating punch problem. The present results indicate that the insulation of the punch may lead to the concentration of the tangential traction, which may cause a serious influence on the fretting contact damage.

2. Problem formulation

Figure 1 shows the two-dimensional fretting contact between a transversely isotropic piezoelectric half-plane and an infinitely long rigid conducting cylindrical punch with the radius R in a plane strain state.

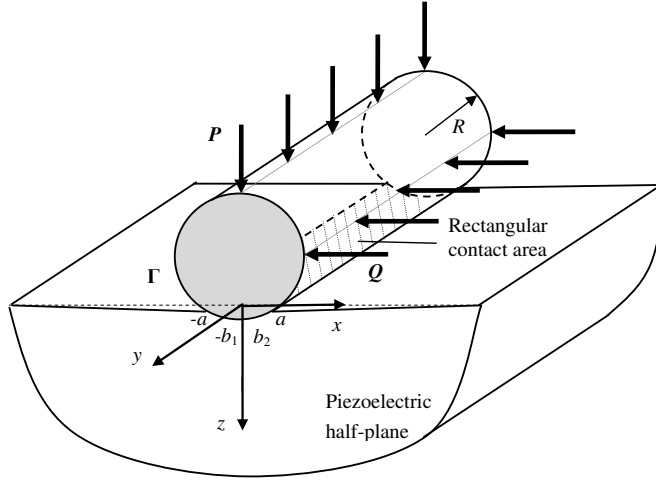


Figure 1. Sketch map of the fretting contact between a homogeneous piezoelectric half-plane and a rigid conducting cylindrical punch in a plane strain state.

The x -axis is along the longitudinal direction at the contact surface while the z -axis is along the thickness direction and points downwards. The two bodies are brought into contact first by a monotonically increasing normal load P to form a contact region $-a \leq x \leq a$, and then by a cyclic tangential load Q which is less than that necessary to cause complete sliding, i.e., $|Q| < \eta P$ where η is the friction coefficient. It is assumed that the punch is a perfect conductor with a constant electric potential ϕ_0 within the contact region. The resultant electric charge Γ is also applied on the punch. The normal displacement component is known from the given punch profile within the contact region whereas the surface normal and tangential tractions are zero outside the contact region.

To solve the present fretting contact problem, the first step is to derive the fundamental solutions of the piezoelectric half-plane subjected to a normal linear load P , a tangential linear load Q and a linear electric charge Γ . Recently, Ma et al. [2014] developed these fundamental solutions which are written as (refer to [Ma et al. 2014, Equations (27)–(29)])

$$u_{x0} = -\frac{if_{11}P}{\pi} \int_0^{+\infty} \frac{\sin(sx)}{s} ds - \frac{f_{12}Q}{\pi} \int_0^{+\infty} \frac{\cos(sx)}{s} ds - \frac{if_{13}\Gamma}{\pi} \int_0^{+\infty} \frac{\sin(sx)}{s} ds, \quad (1)$$

$$u_{z0} = -\frac{f_{21}P}{\pi} \int_0^{+\infty} \frac{\cos(sx)}{s} ds - \frac{if_{22}Q}{\pi} \int_0^{+\infty} \frac{\sin(sx)}{s} ds - \frac{f_{23}\Gamma}{\pi} \int_0^{+\infty} \frac{\cos(sx)}{s} ds, \quad (2)$$

$$\phi_0 = -\frac{f_{31}P}{\pi} \int_0^{+\infty} \frac{\cos(sx)}{s} ds - \frac{if_{32}Q}{\pi} \int_0^{+\infty} \frac{\sin(sx)}{s} ds - \frac{f_{33}\Gamma}{\pi} \int_0^{+\infty} \frac{\cos(sx)}{s} ds. \quad (3)$$

Here $u_{x0} = u_x(x, 0)$ and $u_{z0} = u_z(x, 0)$ are the surface displacement components in the x - and z -directions, respectively; $\phi_0 = \phi(x, 0)$ is the surface electric potential of the piezoelectric half-plane; $i = \sqrt{-1}$ and s is the transform variable; f_{ij} ($i, j = 1, 2, 3$) are the parameters given in the Appendix.

Let $p(x)$, $q(x)$ and $g(x)$ be the normal contact pressure, tangential traction and electric charge within the contact region, respectively. The superposition principle gives the surface displacement components

and surface electric potential

$$u_{x0} = -\frac{if_{11}}{\pi} \int_{-a}^a p(t) \int_0^{+\infty} \frac{\sin[s(x-t)]}{s} ds dt - \frac{f_{12}}{\pi} \int_{-a}^a q(t) \int_0^{+\infty} \frac{\cos[s(x-t)]}{s} ds dt - \frac{if_{13}}{\pi} \int_{-a}^a g(t) \int_0^{+\infty} \frac{\sin[s(x-t)]}{s} ds dt, \quad (4)$$

$$u_{z0} = -\frac{f_{21}}{\pi} \int_{-a}^a p(t) \int_0^{+\infty} \frac{\cos[s(x-t)]}{s} ds dt - \frac{if_{22}}{\pi} \int_{-a}^a q(t) \int_0^{+\infty} \frac{\sin[s(x-t)]}{s} ds dt - \frac{f_{23}}{\pi} \int_{-a}^a g(t) \int_0^{+\infty} \frac{\cos[s(x-t)]}{s} ds dt, \quad (5)$$

$$\phi_0 = -\frac{f_{31}}{\pi} \int_{-a}^a p(t) \int_0^{+\infty} \frac{\cos[s(x-t)]}{s} ds dt - \frac{if_{32}}{\pi} \int_{-a}^a q(t) \int_0^{+\infty} \frac{\sin[s(x-t)]}{s} ds dt - \frac{f_{33}}{\pi} \int_{-a}^a g(t) \int_0^{+\infty} \frac{\cos[s(x-t)]}{s} ds dt. \quad (6)$$

Differentiating Equations (4)–(6) with respect to x yields

$$\frac{\partial u_{x0}}{\partial x} = -\frac{if_{11}}{\pi} \int_{-a}^a p(t) \int_0^{+\infty} \cos[s(x-t)] ds dt + \frac{f_{12}}{\pi} \int_{-a}^a q(t) \int_0^{+\infty} \sin[s(x-t)] ds dt - \frac{if_{13}}{\pi} \int_{-a}^a g(t) \int_0^{+\infty} \cos[s(x-t)] ds dt, \quad (7)$$

$$\frac{\partial u_{z0}}{\partial x} = \frac{f_{21}}{\pi} \int_{-a}^a p(t) \int_0^{+\infty} \sin[s(x-t)] ds dt - \frac{if_{22}}{\pi} \int_{-a}^a q(t) \int_0^{+\infty} \cos[s(x-t)] ds dt + \frac{f_{23}}{\pi} \int_{-a}^a g(t) \int_0^{+\infty} \sin[s(x-t)] ds dt, \quad (8)$$

$$\frac{\partial \phi_0}{\partial x} = \frac{f_{31}}{\pi} \int_{-a}^a p(t) \int_0^{+\infty} \sin[s(x-t)] ds dt - \frac{if_{32}}{\pi} \int_{-a}^a q(t) \int_0^{+\infty} \cos[s(x-t)] ds dt + \frac{f_{33}}{\pi} \int_{-a}^a g(t) \int_0^{+\infty} \sin[s(x-t)] ds dt. \quad (9)$$

Using the Fourier representation of generalized functions gives [Gradshteyn and Ryzhik 2000; Choi and Paulino 2008]

$$\int_0^{\infty} \sin[s(x-t)] ds = \frac{1}{x-t}, \quad \int_0^{\infty} \cos[s(x-t)] ds = \pi \delta(x-t), \quad (10)$$

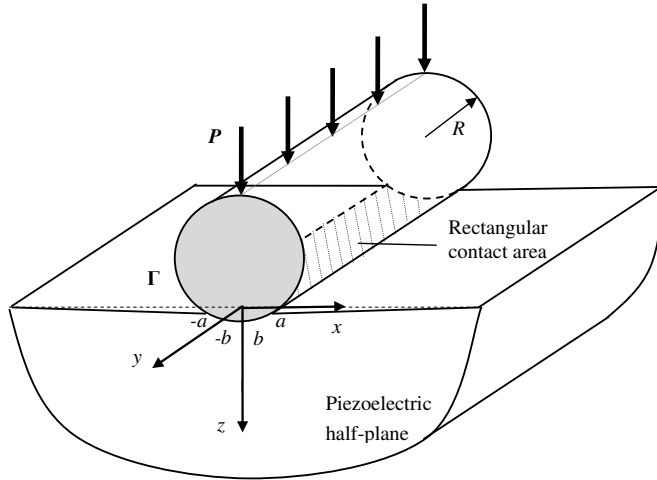


Figure 2. The normal contact with a monotonically increasing normal load P in a plane strain state.

Equations (7)–(9) can be reduced to the following coupled Cauchy singular integral equations for the unknowns $p(x)$, $q(x)$ and $g(x)$

$$-i f_{11} p(x) - i f_{13} g(x) - \frac{f_{12}}{\pi} \int_{-a}^a \frac{q(t)}{t-x} dt = \frac{\partial u_{x0}}{\partial x}, |x| \leq a, \tag{11}$$

$$-\frac{f_{21}}{\pi} \int_{-a}^a \frac{p(t)}{t-x} dt - i f_{22} q(x) - \frac{f_{23}}{\pi} \int_{-a}^a \frac{g(t)}{t-x} dt = \frac{\partial u_{z0}}{\partial x}, |x| \leq a, \tag{12}$$

$$-\frac{f_{31}}{\pi} \int_{-a}^a \frac{p(t)}{t-x} dt - i f_{32} q(x) - \frac{f_{33}}{\pi} \int_{-a}^a \frac{g(t)}{t-x} dt = \frac{\partial \phi_0}{\partial x}, |x| \leq a. \tag{13}$$

The resultant force P , Q and resultant electric charge Γ related to $p(x)$, $q(x)$ and $g(x)$ are given by

$$\int_{-a}^a p(t) dt = P, \tag{14}$$

$$\int_{-a}^a q(t) dt = Q, \tag{15}$$

$$\int_{-a}^a g(t) dt = \Gamma. \tag{16}$$

Equations (11)–(16) are the general governing equations for the fretting contact problem of the piezoelectric half-plane acted upon by a rigid conducting punch. Since the fretting contact is frictional and loading history dependent, the analysis is often divided into the normal loading process and tangential loading process. These two processes are discussed in the next two sections.

3. Normal loading

For the first step of fretting contact analysis, we consider the normal contact with a monotonically increasing normal load P to form a contact region $-a \leq x \leq a$, while the tangential load Q is neglected

as shown in Figure 2. Due to two dissimilar contact bodies pressed together under the action of a purely normal load, the corresponding surface particles will undergo different tangential displacements, and this relative tangential motion will lead to the development of the tangential traction at the interface. That is to say, an applied normal load will lead to both normal and tangential displacements. Therefore, the normal contact of two dissimilar bodies is fully coupled to the normal contact pressure and tangential traction. It is assumed that the whole contact region contains a centrally located stick region ($|x| \leq b$) between two slip regions ($b < |x| \leq a$) in which Coulomb’s friction law is applied. The slip direction must also be consistent with the direction of the frictional force in the slip regions, which means that the slips in both slip regions are in opposite directions.

Referring to [Nowell et al. 1988] and [Hills et al. 1993], the tangential traction in the slip and stick regions is written as

$$q(x) = \begin{cases} -\eta p(x)\text{sign}(x) & b < |x| \leq a, \\ -\eta p(b)(x/b) + q^*(x) & |x| \leq b, \end{cases} \tag{17}$$

where $q^*(x)$ is an unknown function equal to zero at $x = \pm b$.

For a cylindrical punch, the derivative of u_{z0} may be approximately represented as [Johnson 1985]

$$\frac{\partial u_{z0}}{\partial x} = \frac{x}{R}, \quad |x| \leq a. \tag{18}$$

The surface electric potential ϕ_0 is a constant inside the contact region, so we have

$$\frac{\partial \phi_0}{\partial x} = 0, \quad |x| \leq a. \tag{19}$$

Spence [1973] proposed the self-similarity assumption that the stress fields were self-similar at each stage during monotonically increasing normal loading. In the inner stick region, the prior prestrain of surface points before they enter the stick region is proportional to $|x|$ as given by

$$\frac{\partial u_{x0}}{\partial x} = C|x|, \quad |x| \leq b, \tag{20}$$

where C is unknown and denotes the slope of the tangential displacement gradient at this stage. In the slip regions $b < |x| \leq a$, $\partial u_{x0}/\partial x$ cannot be specified.

With the aid of (18) and (19), (12) and (13) can be rewritten as

$$\frac{1}{\pi} \int_{-a}^a \frac{p(t)}{t-x} dt = \frac{f_{33}x}{\gamma_1 R} - i \frac{\gamma_2}{\gamma_1} q(x), \quad |x| \leq a, \tag{21}$$

$$-\frac{f_{23}}{\pi} \int_{-a}^a \frac{g(t)}{t-x} dt = \frac{x}{R} + \frac{f_{21}}{\pi} \int_{-a}^a \frac{p(t)}{t-x} dt + i f_{22} q(x), \quad |x| \leq a, \tag{22}$$

where

$$\gamma_1 = f_{31}f_{23} - f_{21}f_{33}, \quad \gamma_2 = f_{32}f_{23} - f_{22}f_{33}.$$

For the conducting cylindrical punch, the contact pressure is smooth at $x = \pm a$, while the electric charge can be divided into two parts [Ke et al. 2008]

$$g(x) = g_1(x) + g_2(x), \tag{23}$$

where $g_1(x)$ is induced by the normal load P and is smooth at $x = \pm a$, while $g_2(x)$ is induced by the constant electric potential ϕ_0 and has the square root singularity at both ends.

Then, by representing $t = a\theta$ and $x = a\tau$ ($-1 \leq (\tau, \theta) \leq 1$), (21), (14), (22) and (16) are normalized as

$$\frac{1}{\pi} \int_{-1}^1 \frac{p(\theta)}{\theta - \tau} d\theta = h_0(\tau), \tag{24}$$

$$\int_{-1}^1 p(\theta) d\theta = \frac{P}{a}, \tag{25}$$

$$-\frac{f_{23}}{\pi} \int_{-1}^1 \frac{g_1(\theta)}{\theta - \tau} d\theta = h_1(\tau), \tag{26}$$

$$\int_{-1}^1 g_1(\theta) d\theta = \frac{\Gamma_1}{a}, \tag{27}$$

$$-\frac{f_{23}}{\pi} \int_{-1}^1 \frac{g_2(\theta)}{\theta - \tau} d\theta = 0, \tag{28}$$

$$\int_{-1}^1 g_2(\theta) d\theta = \frac{\Gamma - \Gamma_1}{a}, \tag{29}$$

where

$$h_0(\tau) = \frac{f_{33}a\tau}{\gamma_1 R} - i \frac{\gamma_2}{\gamma_1} q(\tau), \tag{30}$$

$$h_1(\tau) = \frac{a\tau}{R} + \frac{f_{21}}{\pi} \int_{-1}^1 \frac{p(\theta)}{\theta - \tau} d\theta + i f_{22} q(\tau). \tag{31}$$

Next, substituting (17) into (11) yields the equation about $q^*(x)$,

$$\frac{1}{\pi} \int_{-b}^b \frac{q^*(t)}{t - x} dt = N_1(x), \quad |x| \leq b, \tag{32}$$

where

$$N_1(x) = -\frac{C|x|}{f_{12}} - i \frac{f_{11}}{f_{12}} p(x) - i \frac{f_{13}}{f_{12}} g(x) + \frac{\eta}{\pi} \int_b^a \frac{p(t)}{t - x} dt - \frac{\eta}{\pi} \int_{-a}^{-b} \frac{p(t)}{t - x} dt + \frac{\eta p(b)}{b\pi} \int_{-b}^b \frac{t}{t - x} dt. \tag{33}$$

By introducing the normalized quantities $t = b\kappa$ and $x = b\alpha$, (32) may be expressed as

$$\frac{1}{\pi} \int_{-1}^1 \frac{q^*(\kappa)}{\kappa - \alpha} d\kappa = N_1(\alpha), \quad |\alpha| \leq 1. \tag{34}$$

In addition, the following consistency condition should be satisfied [Muskhelishvili 1958]:

$$\int_{-1}^1 \frac{N_1(\zeta)}{\sqrt{1 - \zeta^2}} d\zeta = 0. \tag{35}$$

Using the method of Erdogan and Gupta [1972], this integral equation may be reduced to a set of linear equations that satisfy the consistency condition (35). Through setting $q^*(\kappa) = \varphi(\kappa)\sqrt{1 - \kappa^2}$, we

can discretize (34) to give

$$\sum_{l=1}^M \frac{(1 - \kappa_l^2)\varphi(\kappa_l)}{(M+1)(\kappa_l - \alpha_r)} = N_1(\alpha_r), \quad |\alpha_r| \leq 1, \quad (36)$$

where $\kappa_l = \cos[l\pi/(M+1)]$, $\alpha_r = \cos[(2r-1)\pi/2(M+1)]$, $r = 1, 2, \dots, M+1$, and M is the total number of the discrete points of $\varphi(\kappa_l)$ in $(-1, 1)$. By setting $p(\theta) = \psi(\theta)\sqrt{1-\theta^2}$ and $g_1(\theta) = \lambda(\theta)\sqrt{1-\theta^2}$, (24)–(27) are also discretized as

$$\sum_{l=1}^M \frac{(1 - \theta_l^2)\psi(\theta_l)}{(M+1)(\theta_l - \tau_r)} = h_0(\tau_r), \quad |\tau_r| \leq 1, \quad (37)$$

$$\sum_{l=1}^M \frac{(1 - \theta_l^2)\psi(\theta_l)}{M+1} = \frac{P}{a\pi}, \quad (38)$$

$$\sum_{l=1}^M \frac{f_{23}(1 - \theta_l^2)\lambda(\theta_l)}{(M+1)(\theta_l - \tau_r)} = h_1(\tau_r), \quad |\tau_r| \leq 1, \quad (39)$$

$$\sum_{l=1}^M \frac{(1 - \theta_l^2)\lambda(\theta_l)}{M+1} = \frac{\Gamma_1}{a\pi}, \quad (40)$$

where $\theta_l = \cos[l\pi/(M+1)]$, $\tau_r = \cos[(2r-1)\pi/2(M+1)]$, $r = 1, 2, \dots, M+1$, where M is the total number of the discrete points of $\psi(\theta_l)$ and $\lambda(\theta_l)$ in $(-1, 1)$.

Because $g_2(x)$ has the square root singularity at both ends, we can set $g_2(\theta) = \vartheta(\theta)/\sqrt{1-\theta^2}$. Then (28) and (29) can be reduced to

$$\frac{1}{M} \sum_{l=1}^M \frac{f_{23}\vartheta(\theta_l)}{(\theta_l - \tau_r)} = 0, \quad |\tau_r| \leq 1, \quad (41)$$

$$\frac{1}{M} \sum_{l=1}^M \vartheta(\theta_l) = \frac{\Gamma - \Gamma_1}{a\pi}, \quad (42)$$

where $\theta_l = \cos[(2l-1)\pi/2M]$, $\tau_r = \cos[r\pi/M]$, $r = 1, 2, \dots, M-1$, where M is the total number of the discrete points of $\vartheta(\theta_l)$ in $(-1, 1)$.

In (36), (37), (39) and (41), we have $4M+2$ equations and $4M+3$ unknowns, $\varphi(\kappa_1), \dots, \varphi(\kappa_M)$, $\psi(\theta_1), \dots, \psi(\theta_M)$, $\lambda(\theta_1), \dots, \lambda(\theta_M)$, $\vartheta(\theta_1), \dots, \vartheta(\theta_M)$, a , b and C ; the problem is also underconstrained. As we know, the tangential traction must be continuous at the stick-slip interface, which leads to the requirements $\varphi(\pm 1) = 0$ [Keer and Farris 1987; Hanson et al. 1989]. This condition can therefore be utilized to determine b and $q(x)$, to make the analysis self-contained. This technique would require a sequence of iteration, which can be specified as follows:

- (1) Input the values of a and b . The frictionless solutions of the contact pressure $p^0(\theta)$ and electric charge $g^0(\theta)$ from Ke et al. [2008] are selected as the initial values for $p(\theta)$ and $g(\theta)$.
- (2) Solve (36) to obtain the tangential traction $q^1(\kappa)$ for $q(\kappa)$, and substitute $q^1(\kappa)$ into (37), (39) and (41). Then, $p^1(\theta)$ and $g^1(\theta)$ can be solved from this set of equations.

- (3) Calculate $\varphi(\pm 1)$ from (36). If $\varphi(\pm 1) = 0$, go to the next step; if $\varphi(\pm 1) \neq 0$, return to steps 1 and 2. Then, the new values must be selected for b and a , and the procedure is repeated.
- (4) Calculate $p^n(\theta)$, $g^n(\theta)$ and $q^n(\kappa)$ (the superscript n denotes the n -th iteration), together with C , which satisfy (36), (37), (39) and (41) and are the solutions of the coupled normal contact problem. Then, we can get P and Γ from (38), (40) and (42).

4. Tangential loading

4.1. A monotonically increasing tangential load. At the end of the normal loading phase, the whole contact region is divided into the inner stick region $|x| \leq b$ and two outer slip regions $b < x \leq a$ and $-a \leq x < -b$. Then, we apply a cyclic tangential load Q ($|Q| < \eta P$) to the punch as shown in Figure 1. The tangential loading history is depicted in Figure 3 to define the tangential load Q as a function of time. In the first step of the tangential loading problem, the cylindrical punch is acted upon by a constant normal load P , and then subjected to a monotonically increasing tangential load from zero to a maximum value Q_{\max} , i.e., point A in Figure 3.

The normal contact pressure, tangential traction and electric charge distributions at the end of the normal loading phase can be found from the fully coupled normal contact in previous section. The resulting values of the relative tangential displacement gradient $\partial u_{x0}/\partial x$ in the whole contact region are then calculated using (11) and stored. We expect an inner stick region at the interval $-b_1 \leq x \leq b_2$ bordered by two slip regions ($-a \leq x < -b_1$ and $b_2 < x \leq a$) with the same slip direction as shown in Figure 1. In the slip regions, the tangential traction $q(x)$ is strictly related to the local normal contact pressure $p(x)$ by Coulomb’s friction law. Hence, (11) is rewritten as

$$\frac{1}{\pi} \int_{-b_1}^{b_2} \frac{q^{**}(t)}{t-x} dt = N_2(x), \quad -b_1 \leq x \leq b_2, \tag{43}$$

where

$$q^{**}(x) = -\eta p(x) + q(x), \tag{44}$$

$$N_2(x) = -\frac{1}{f_{12}} \frac{\partial u_{x0}}{\partial x} - \frac{if_{11}}{f_{12}} p(x) - \frac{if_{13}}{f_{12}} g(x) - \frac{\eta}{\pi} \int_{-a}^a \frac{p(t)}{t-x} dt. \tag{45}$$

Once the tangential load is applied, the normal contact pressure and electric charge distributions may become asymmetric. Therefore, the contact patch may be not central about the center-line of the punch

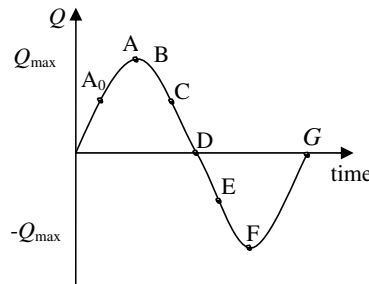


Figure 3. Load history of the tangential load Q as a function of time.

which allows for an eccentricity e between the center-line and the origin [Nowell et al. 1988]. Thus, (21) and (22) have the form

$$\frac{1}{\pi} \int_{-a}^a \frac{p(t)}{t-x} dt = \frac{f_{33}(x-e)}{\gamma_1 R} - i \frac{\gamma_2}{\gamma_1} q(x), \quad |x| \leq a, \tag{46}$$

$$-\frac{f_{23}}{\pi} \int_{-a}^a \frac{g(t)}{t-x} dt = \frac{x-e}{R} + \frac{f_{21}}{\pi} \int_{-a}^a \frac{p(t)}{t-x} dt + i f_{22} q(x), \quad |x| \leq a. \tag{47}$$

In addition, the static equilibrium for the normal contact pressure and tangential traction must be satisfied by (14) and (15). Substituting (44) and (14) into (15) yields

$$\int_{-b_1}^{b_2} q^{**}(t) dt = Q - \eta P. \tag{48}$$

Introducing the following normalized quantities

$$t = \frac{b_1 + b_2}{2} \kappa + \frac{b_2 - b_1}{2}, \quad x = \frac{b_1 + b_2}{2} \alpha + \frac{b_2 - b_1}{2}, \tag{49}$$

Equations (43) and (48) may be expressed in the form of

$$\frac{1}{\pi} \int_{-1}^1 \frac{q^{**}(\kappa)}{\kappa - \alpha} d\kappa = N_2(\alpha), \quad |\alpha| \leq 1, \tag{50}$$

$$\int_{-1}^1 q^{**}(\kappa) d\kappa = \frac{2(Q - \eta P)}{b_1 + b_2}. \tag{51}$$

Using (23), (46) and (47) are normalized by introducing $t = a\theta$ and $x = a\tau$,

$$\frac{1}{\pi} \int_{-1}^1 \frac{p(\theta)}{\theta - \tau} d\theta = h_2(\tau), \quad |\tau| \leq 1, \tag{52}$$

$$-\frac{f_{23}}{\pi} \int_{-1}^1 \frac{g_1(\theta)}{\theta - \tau} d\theta = h_3(\tau), \quad |\tau| \leq 1, \tag{53}$$

where

$$h_2(\tau) = \frac{f_{33}(a\tau - e)}{\gamma_1 R} - i \frac{\gamma_2}{\gamma_1} q(\tau), \tag{54}$$

$$h_3(\tau) = \frac{a\tau - e}{R} + \frac{f_{21}}{\pi} \int_{-1}^1 \frac{p(\theta)}{\theta - \tau} d\theta + i f_{22} q(\tau). \tag{55}$$

Equations (52) and (53) are also discretized by setting $p(\theta) = \psi(\theta)\sqrt{1-\theta^2}$ and $g_1(\theta) = \lambda(\theta)\sqrt{1-\theta^2}$ to give

$$\sum_{l=1}^M \frac{(1-\theta_l^2)\psi(\theta_l)}{(M+1)(\theta_l - \tau_r)} = h_2(\tau_r), \quad |\tau_r| \leq 1, \tag{56}$$

$$\sum_{l=1}^M -\frac{f_{23}(1-\theta_l^2)\lambda(\theta_l)}{(M+1)(\theta_l - \tau_r)} = h_3(\tau_r), \quad |\tau_r| \leq 1, \tag{57}$$

where $\theta_l = \cos[l\pi/(M+1)]$, $\tau_r = \cos[(2r-1)\pi/2(M+1)]$, $r = 1, 2, \dots, M+1$, where M is the total number of the discrete points of $\psi(\theta_l)$ and $\lambda(\theta_l)$ in $(-1, 1)$.

Equations (50) and (51) are also discretized by setting $q^{**}(\kappa) = \varphi(\kappa)\sqrt{1-\kappa^2}$ to give

$$\sum_{l=1}^M \frac{(1-\kappa_l^2)\varphi(\kappa_l)}{(M+1)(\kappa_l-\alpha_r)} = N_2(\alpha_r), \quad |\alpha_r| \leq 1, \quad (58)$$

$$\sum_{l=1}^M \frac{(1-\kappa_l^2)\varphi(\kappa_l)}{M+1} = \frac{2(Q-\eta P)}{(b_1+b_2)\pi}, \quad (59)$$

where $\kappa_l = \cos[l\pi/(M+1)]$, $\alpha_r = \cos[(2r-1)\pi/2(M+1)]$, $r = 1, 2, \dots, M+1$, and M is the total number of the discrete points of $\varphi(\kappa_l)$ in $(-1, 1)$. In (41), (56), (57) and (58), there are $4M+2$ equations for $4M+3$ unknowns, $\varphi(\kappa_1), \dots, \varphi(\kappa_M)$, $\psi(\theta_1), \dots, \psi(\theta_M)$, $\lambda(\theta_1), \dots, \lambda(\theta_M)$, $\vartheta(\theta_1), \dots, \vartheta(\theta_M)$, b_1 , b_2 and e . It should be noted that the discretization of (58) yields $M+1$ equations for M unknowns $\varphi(\kappa_l)$, since in this case there is no constant C to be determined, as the stick zone is receding. The iterative procedure is given below:

- (1) Input a value of b_1 and a trial value of b_2 , and drop the $(M+1)$ -th equation of (58).
- (2) Compute the solution of the coupled equations (41), (56), (57) and (58) by using the iterative procedure described in Section 3.
- (3) Check whether the solution satisfies the $(M+1)$ -th equation of (58). If it satisfies, we obtain the consistent solution; then go to the next step. Otherwise, a new value of b_2 must be chosen for step 1 and the iteration procedure is continued till the consistent solution is achieved.
- (4) Compute the applied normal load P , electric charge Γ and tangential load Q from (38), (40), (42) and (59).

4.2. A cyclic tangential load. In the previous subsection, we analyzed the tangential load Q , which increased monotonically from 0 to Q_{\max} . However, the tangential load is generally cyclic between limits in fretting fatigue. So, we further consider a cyclic tangential load varying between the limits $\pm Q_{\max}$ applied to the rigid conducting cylindrical punch. Starting immediately at unloading, the pressure cannot sustain the stick at the outer edge of contact where the tangential traction becomes $q(x) = -\eta p(x)$. Since the frictional contact problem depends on the loading history, the contact tractions and electric charge can be first obtained at the end of the monotonically increasing tangential loading phase ($Q = Q_{\max}$); $\partial u_{x0}/\partial x$ can be calculated and stored by considering (43). Equation (11) is resolved in the new stick region, $-c_1 \leq x \leq c_2$, and reverse slip regions, $-a \leq x < -c_1$ and $c_2 < x \leq a$, and thus can be expressed as

$$\frac{1}{\pi} \int_{-c_1}^{c_2} \frac{q^{***}(t)}{t-x} dt = N_3(x), \quad -c_1 \leq x \leq c_2, \quad (60)$$

where

$$q^{***}(x) = q(x) + \eta p(x), \quad (61)$$

$$N_3(x) = -\frac{1}{f_{12}} \frac{\partial u_{x0}}{\partial x} - i \frac{f_{11}}{f_{12}} p(x) - i \frac{f_{13}}{f_{12}} g(x) + \frac{\eta}{\pi} \int_{-a}^a \frac{p(t)}{t-x} dt. \quad (62)$$

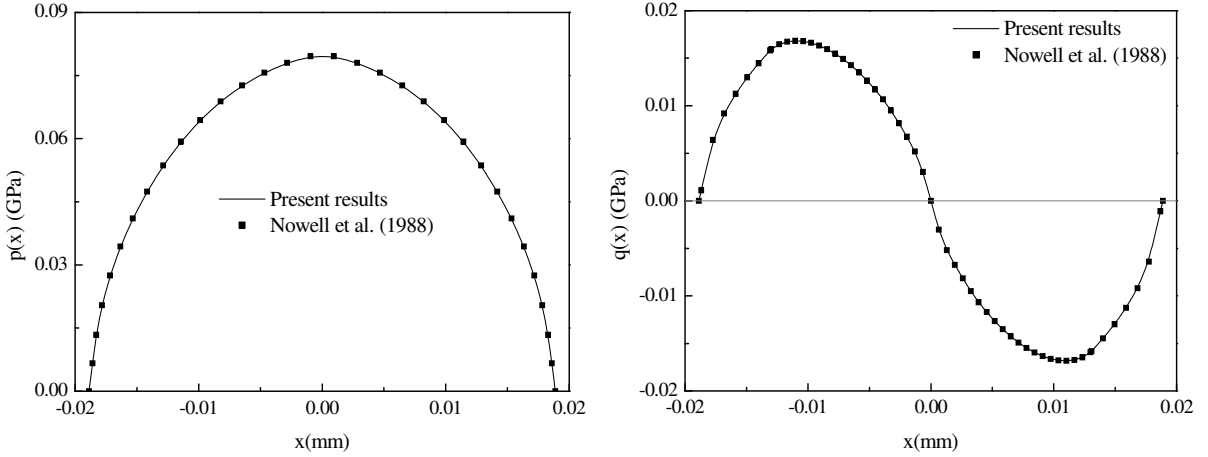


Figure 4. Comparison of the present results with the results obtained in [Nowell et al. 1988]: (left) normal contact pressure; and (right) tangential traction.

In addition, the static equilibrium for the contact tractions must satisfy

$$\int_{-c_1}^{c_2} q^{***}(t) dt = Q + \eta P. \tag{63}$$

Equation (60) is also solved together with (41), (56) and (57) by using the iterative procedure developed in Section 4.1. Note that this process may be continued for the reverse loading phase (DF in Figure 3), reverse unloading phase (FG in Figure 3) and other loading cycles.

5. In-plane stress and in-plane electric displacement

After we obtain the tangential contact stress $\sigma_{zx0} = -q(x)$, along with the normal contact stress $\sigma_{zz0} = -p(x)$ and electrical displacement $D_{z0} = -g(x)$ for the normal and tangential loading processes, the in-plane stress σ_{xx0} and in-plane electric displacement D_{x0} at the contact surface can be solved as

$$\sigma_{xx0}(x) = -(\Delta_1 + if_{11}\Delta_3)p(x) - (\Delta_2 + if_{13}\Delta_3)g(x) - \frac{\Delta_3 f_{12}}{\pi} \int_{-a}^a \frac{q(t)}{t-x} dt, \tag{64}$$

$$D_{x0}(x) = -\left(\frac{e_{15}}{c_{44}} - if_{32}\Delta_4\right)q(x) + \frac{\Delta_4 f_{31}}{\pi} \int_{-a}^a \frac{p(t)}{t-x} dt + \frac{\Delta_4 f_{33}}{\pi} \int_{-a}^a \frac{g(t)}{t-x} dt, \tag{65}$$

where

$$\begin{aligned} \Delta_1 &= \frac{e_{31}e_{33} + c_{13}\epsilon_{33}}{e_{33}^2 + c_{33}\epsilon_{33}}, & \Delta_2 &= \frac{c_{13}e_{33} - c_{33}e_{31}}{e_{33}^2 + c_{33}\epsilon_{33}}, \\ \Delta_3 &= \frac{c_{11}e_{33}^2 - c_{13}^2\epsilon_{33} + c_{33}e_{31}^2 + c_{11}c_{33}\epsilon_{33} - 2c_{13}e_{31}e_{33}}{e_{33}^2 + c_{33}\epsilon_{33}}, & \Delta_4 &= \frac{e_{15}^2}{c_{44}} + \epsilon_{11}. \end{aligned}$$

6. Results and discussion

Before the analysis of the fretting contact of piezoelectric materials, we first verify the effectiveness of the present method. If we neglect the anisotropy and piezoelectric effect of materials, the present contact

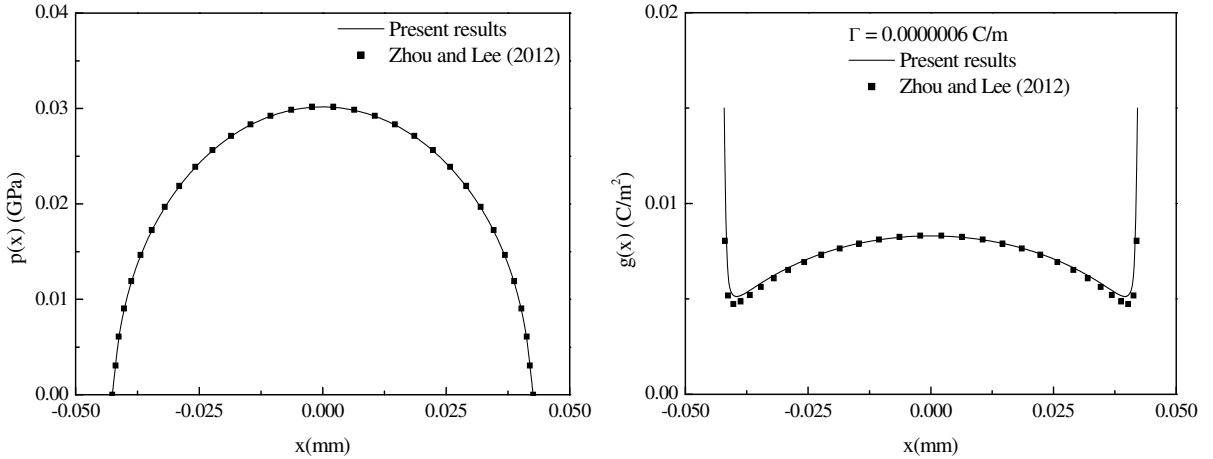


Figure 5. Comparison of the present results with the results obtained in [Zhou and Lee 2012]: (left) normal contact pressure; and (right) electric charge distributions.

problem can be easily reduced to the fretting contact of an isotropic elastic half-plane under a rigid cylindrical punch. Figure 4 plots the normal contact pressure and tangential traction for the coupled normal contact with $\eta = 0.3$, $R = 10$ mm and $P = 2.24 \cdot 10^3$ N/m. The elastic half-plane is made of aluminum with the shear modulus $\mu = 27.3$ GPa and Poisson's ratio $\nu = 0.3$. The results in [Nowell et al. 1988] are also provided in Figure 4 for a direct comparison. It is observed that the present results agree well with the results given in [Nowell et al. 1988].

If we neglect the friction, the present contact problem is reduced to the frictionless contact of piezoelectric materials. Zhou and Lee [2012] obtained the exact solutions for the frictionless contact of a piezoelectric half-plane under a rigid conducting cylindrical punch. Figure 5 presents the normal contact pressure and electric charge distributions for the frictionless contact of piezoelectric materials with $R = 60$ mm, $P = 2000$ N/m and $\Gamma = 6 \cdot 10^{-7}$ C/m. The present results show good agreement with the exact solutions.

In what follows, we will discuss the fretting contact behavior of a piezoelectric half-plane under a rigid conducting cylindrical punch. The half-plane is made of piezoceramic PZT-4 whose electromechanical properties are listed in Table 1 [Ke et al. 2008]. Unless otherwise stated, the resultant normal load, resultant electric charge and radius of the punch are selected as $P = 2000$ N/m, $\Gamma = 6 \cdot 10^{-7}$ C/m and $R = 60$ mm. Note that Su et al. [2015] studied the fretting contact of a piezoelectric half-plane under an insulating punch. Their results are also given in Figures 8, 9, 10, 16 and 19 to show the effect of the conductivity of the punch.

6.1. Normal loading. Figure 6 plots the effect of the friction coefficient η on the normal contact pressure $p(x)$, electric charge $g(x)$ and tangential traction $q(x)$. As can be expected, the electric charge is singular at the edge of the contact region, whereas the normal contact pressure and tangential traction are quite smooth. It is observed that $p(x)$ and $g(x)$ are symmetric, and $q(x)$ is antisymmetric with respect to $x = 0$. The friction coefficient has a slight effect on $p(x)$ and $g(x)$. However, it has a marked effect on $q(x)$. The peak value of $q(x)$ occurs at the interface between the stick region and slip region, and increases rapidly with the increase of η .

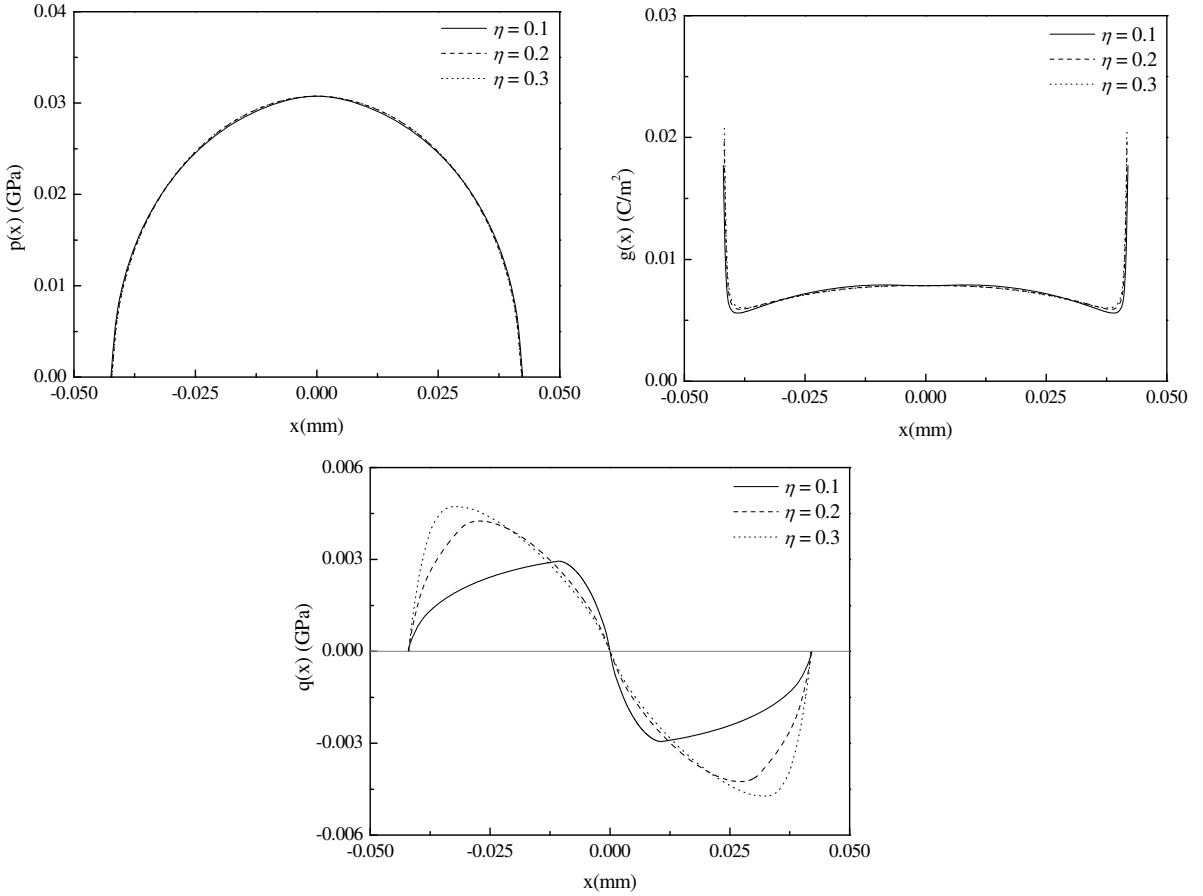


Figure 6. The effect of the friction coefficient η on the (left) normal contact pressure, (right) electric charge distributions and (bottom) tangential traction with $R = 60$ mm, $P = 2000$ N/m and $\Gamma = 6 \cdot 10^{-7}$ C/m.

c_{11} (GPa)	c_{13} (GPa)	c_{33} (GPa)	c_{44} (GPa)
139	74.3	115	25.6
e_{31} (C/m ²)	e_{33} (C/m ²)	e_{15} (C/m ²)	
-5.2	15.1	12.7	
ϵ_{11} (10^{-10} C/Vm)	ϵ_{33} (10^{-10} C/Vm)		
64.61	56.2		

Table 1. Piezoelectric material properties of PZT-4.

The effect of the friction coefficient η on the in-plane stress σ_{xx0} and in-plane electric displacement D_{x0} is given in Figure 7. The in-plane stress σ_{xx0} is symmetric with $x = 0$ and compressive at all regions. The maximum value of σ_{xx0} increases with the decrease of η , and occurs at the interface between the stick region and slip region. The in-plane electric displacement D_{x0} is insensitive to the friction coefficient. It

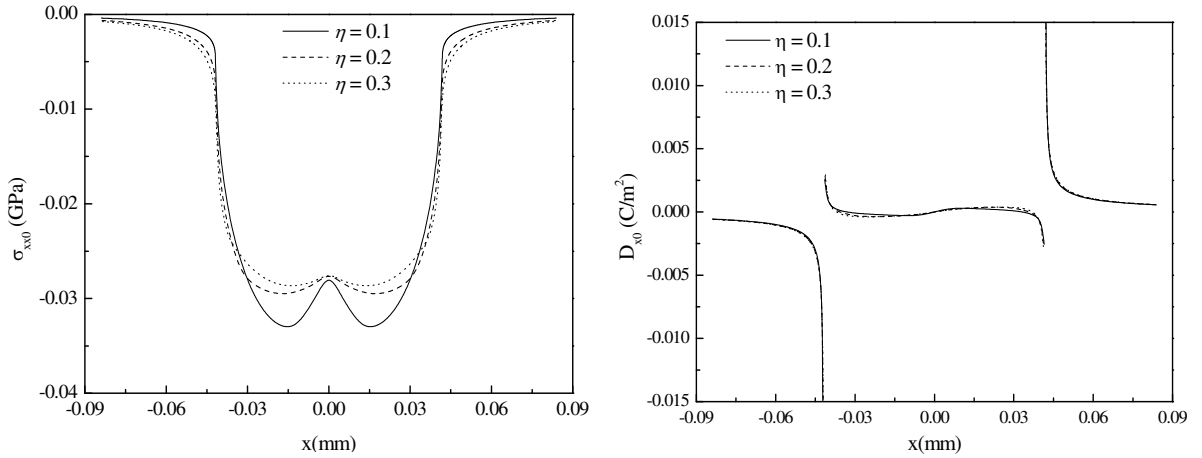


Figure 7. The effect of the friction coefficient η on the (left) in-plane stress σ_{xx0} and (right) in-plane electric displacement D_{x0} with $R = 60$ mm, $P = 2000$ N/m and $\Gamma = 6 \cdot 10^{-7}$ C/m.

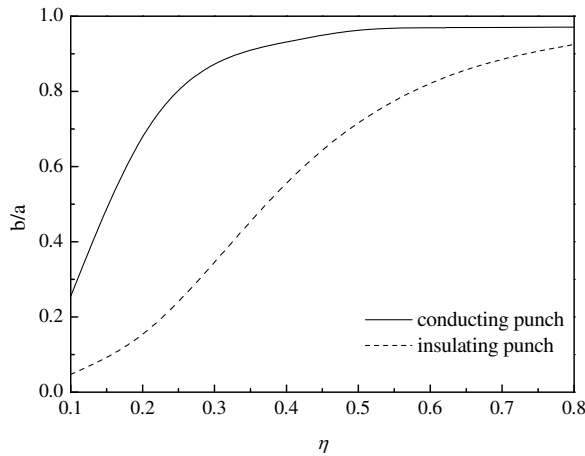


Figure 8. The relations between the stick region size and the friction coefficient with $R = 60$ mm, $P = 2000$ N/m and $\Gamma = 6 \cdot 10^{-7}$ C/m.

has the antisymmetric distribution with the positive value at the region $x > a$ and negative value at the region $x < a$. The maximum value of D_{x0} occurs at the two edges of the contact region.

Figure 8 depicts the relation between the stick region size b/a and friction coefficient η for both insulating and conducting punches. For both punches, the value of b/a increases with the increase of η , and is close to the value of fully adhesive contact (i.e., $b/a \approx 1$) for large η . It can be concluded that the higher the friction coefficient is the less likely the slip occurs. It is found that the conducting punch has a greater value of b/a than the insulating punch for a given η . Therefore, the conductivity of the punch has a significant effect on the fretting contact behavior of piezoelectric materials.

Figure 9 presents the relation between the slope of the tangential displacement gradient C and the friction coefficient η for both insulating and conducting punches. With the increase of η , the value of

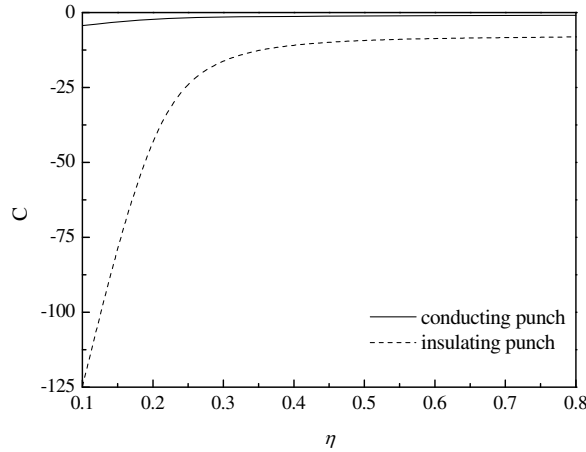


Figure 9. The relations between the slope of the tangential displacement gradient and the friction coefficient with $R = 60$ mm, $P = 2000$ N/m and $\Gamma = 6 \cdot 10^{-7}$ C/m.

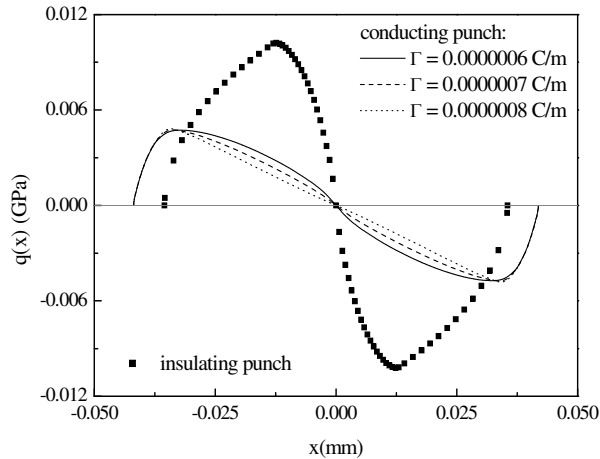


Figure 10. The effect of the resultant electric charge Γ on the tangential traction with $R = 60$ mm, $\eta = 0.3$, $P = 2000$ N/m.

C decreases rapidly when $\eta < 0.3$ (especially for the insulating punch), and then changes slightly when $0.3 \leq \eta \leq 0.8$. Moreover, the value C of the insulating punch is larger than that of the conducting punch for a given η .

Figure 10 analyzes the effect of the resultant electric charge Γ on the tangential traction for both insulating and conducting punches with $\eta = 0.3$. We found that the peak value of $q(x)$ for the insulating punch is greater than that of the conducting punch, but the size of the stick region is smaller than that of the conducting punch. With the increase of Γ , the value of $q(x)$ decreases at the stick region and changes slightly at the slip region. The results indicate that the insulation of the punch may lead to a concentration of the tangential traction, which may cause a serious influence on the fretting contact damage.

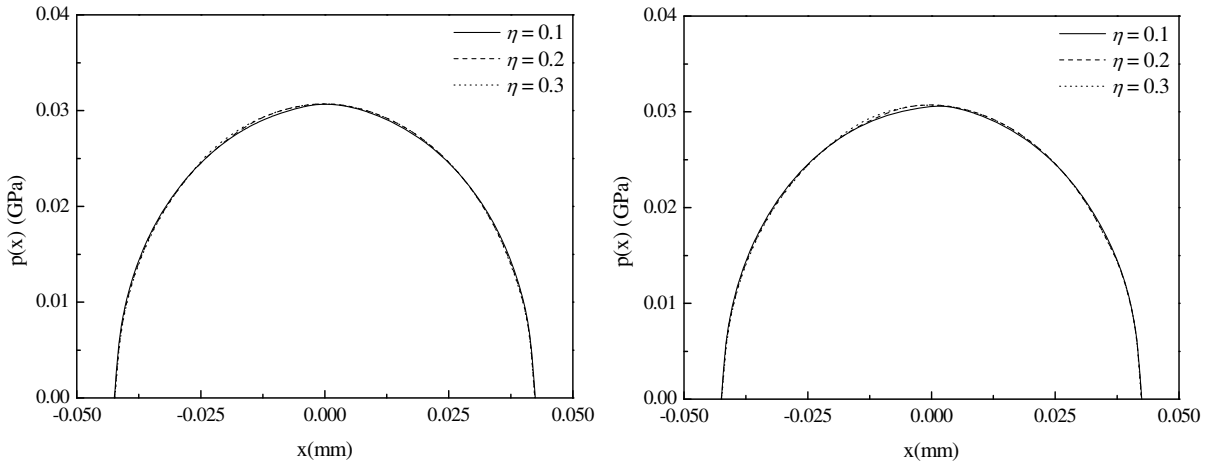


Figure 11. Normal contact pressure during monotonically increasing tangential loading with $R = 60$ mm, $P = 2000$ N/m and $\Gamma = 6 \cdot 10^{-7}$ C/m: (left) $Q/\eta P = 0.3$, point A_0 in Figure 3; and (right) $Q/\eta P = 0.5$, point A in Figure 3.

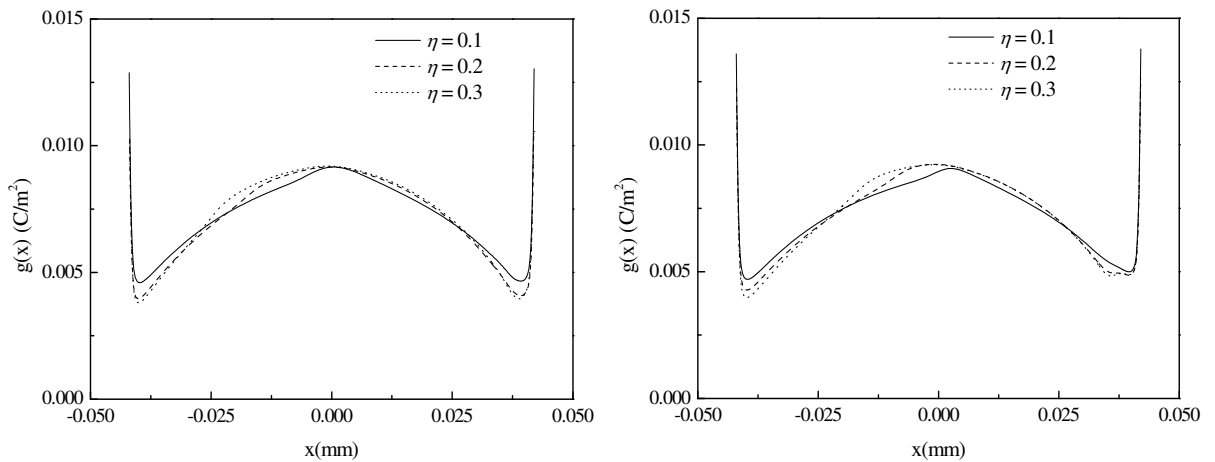


Figure 12. Electric charge distribution during monotonically increasing tangential loading with $R = 60$ mm, $P = 2000$ N/m and $\Gamma = 6 \cdot 10^{-7}$ C/m: (left) $Q/\eta P = 0.3$, point A_0 in Figure 3; and (right) $Q/\eta P = 0.5$, point A in Figure 3.

6.2. Tangential loading. Figures 11–13 discuss the effect of the friction coefficient η on the normal contact pressure $p(x)$, electric charge $g(x)$ and tangential traction $q(x)$ at the loading phase (points A_0 and A in Figure 3), respectively. Because of the action of the tangential load, the normal contact pressure, electric charge distributions and tangential traction are asymmetric during the loading phase. The friction coefficient has a minor effect on the normal contact pressure and electric charge distributions, but it has a significant effect on the tangential traction. It shows that the maximum value of the tangential traction increases with the increase of the friction coefficient and appears at the interface of the stick/slip region. Additionally, because the eccentricity e is very small, the normal contact pressure and electric charge

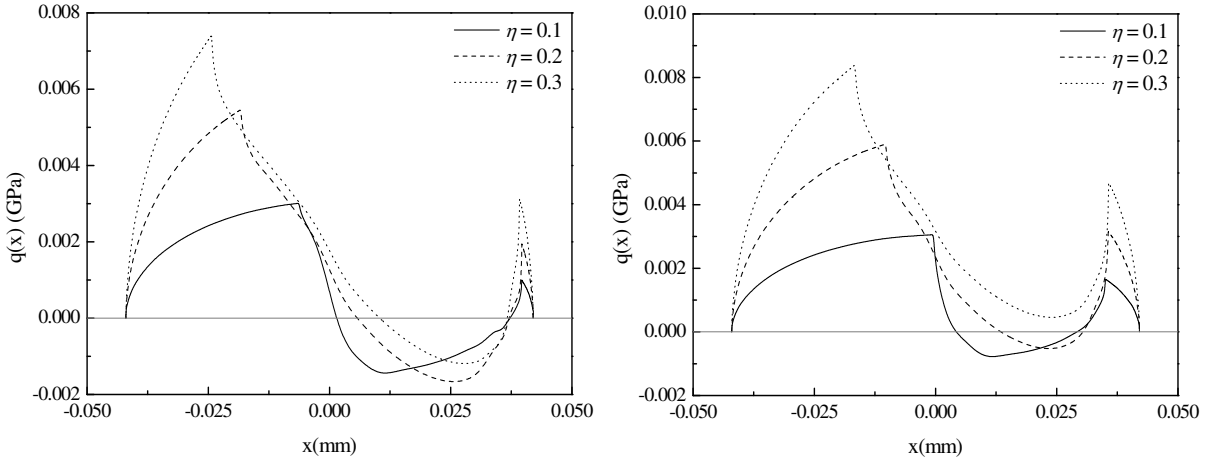


Figure 13. Tangential traction during monotonically increasing tangential loading with $R = 60$ mm, $P = 2000$ N/m and $\Gamma = 6 \cdot 10^{-7}$ C/m: (left) $Q/\eta P = 0.3$, point A_0 in Figure 3; and (right) $Q/\eta P = 0.5$, point A in Figure 3.

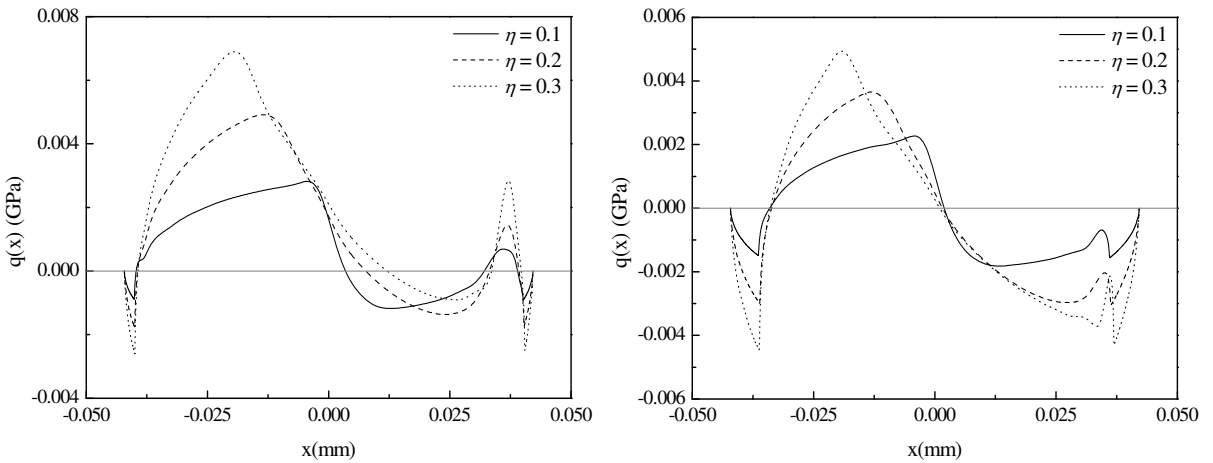


Figure 14. Tangential traction during cyclic tangential loading with $R = 60$ mm, $P = 2000$ N/m and $\Gamma = 6 \cdot 10^{-7}$ C/m: (left) $Q/\eta P = 0.3$, point C in Figure 3; and (right) $Q/\eta P = 0.0$, point D in Figure 3.

at the tangential loading phase is very close to those at the normal loading phase. Hence, the normal contact pressure and electric charge distributions will not be discussed in the following analysis.

Figures 14 and 15 analyze the effect of the friction coefficient η on the tangential traction at the unloading and reverse loading phases (points C, D, E and F in Figure 3). At first, near the two edges of the contact region, we see that the reverse slip occurs during the unloading phase; and the tangential traction becomes $q(x) = -\eta p(x)$. Due to the effect of the loading history, the distribution of the tangential traction becomes quite complex at the stick region, and a localized increase or decrease occurs at the interface of the stick/slip region during the unloading phase. Comparing Figure 13 (right) to Figure 15 (right), we

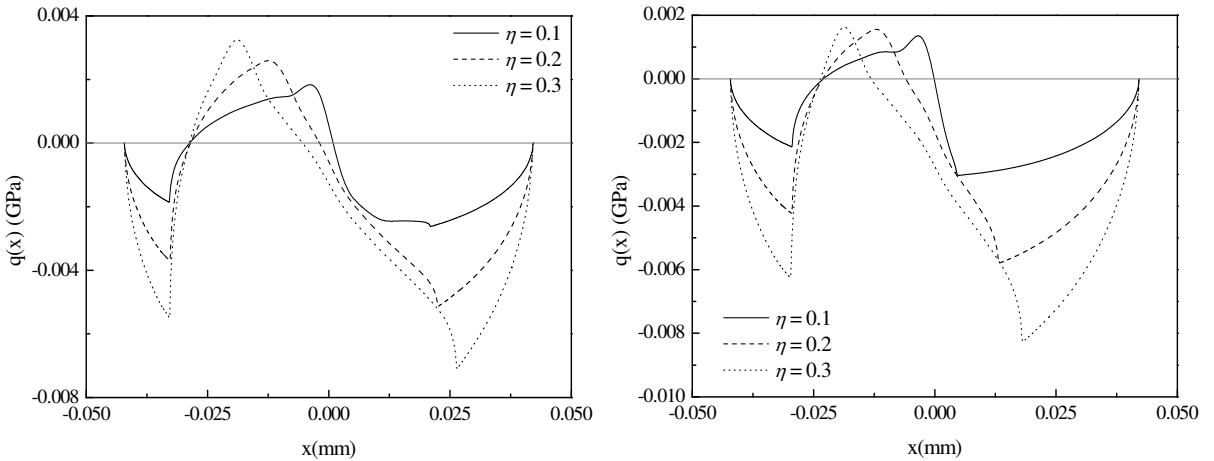


Figure 15. Tangential traction during cyclic tangential loading with $R = 60$ mm, $P = 2000$ N/m and $\Gamma = 6 \cdot 10^{-7}$ C/m: (left) $Q/\eta P = -0.3$, point E in Figure 3; and (right) $Q/\eta P = -0.5$, point F in Figure 3.

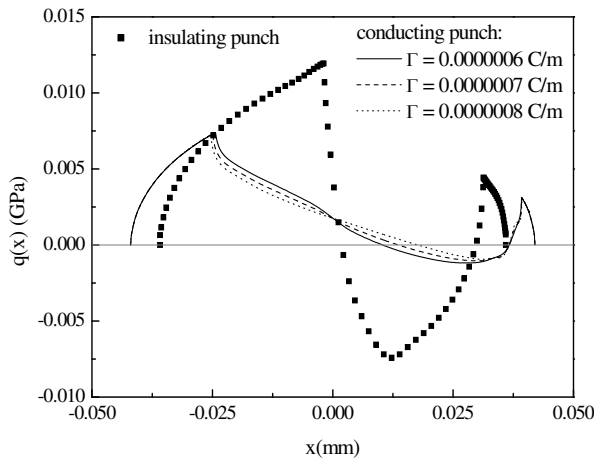


Figure 16. Tangential traction during monotonically increasing tangential loading with $R = 60$ mm, $P = 2000$ N/m, $\eta = 0.3$ and $Q/\eta P = 0.3$, point A₀ in Figure 3.

can observe that the distribution of tangential traction is completely reversed when the tangential load is completely reversed from $Q = Q_{max}$ to $Q = -Q_{max}$.

Figure 16 shows the effect of the resultant electric charge Γ on the tangential traction $q(x)$ during the loading phase (points A₀ in Figure 3) for both insulating and conducting punches. Similar to the normal loading phase, the peak value of $q(x)$ for the insulating punch is greater than that of the conducting punch during the tangential loading phase. With the increase in Γ , the value of $q(x)$ has a slight change at the stick region, and is almost unchanged at the slip region.

Figure 17 plots the effect of the friction coefficient η on the in-plane stress σ_{xx0} when $Q/\eta P = \pm 0.5$. For $Q/\eta P = 0.5$, σ_{xx0} is compressive at the region $x < 0$, but changes from compressive to tensile and

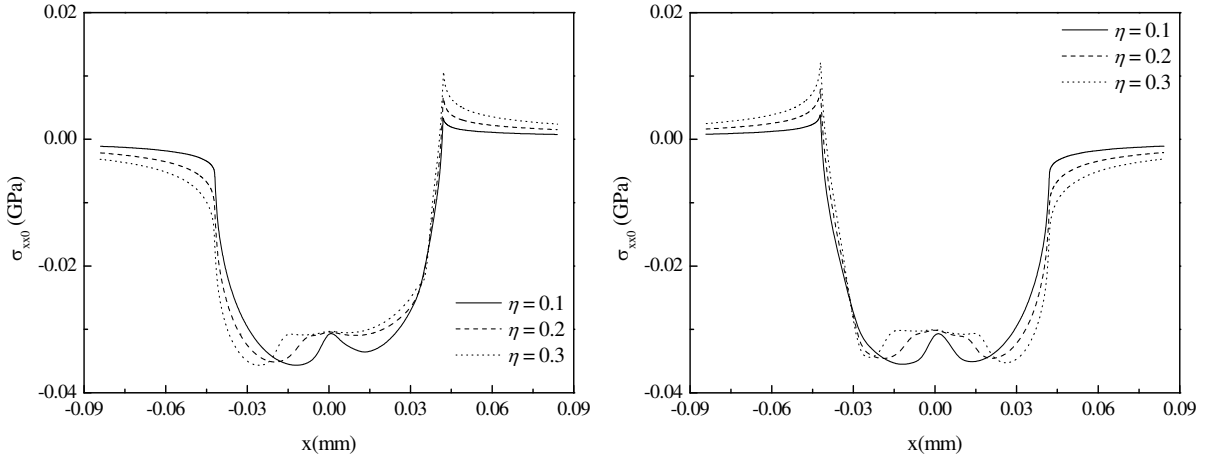


Figure 17. The effect of the friction coefficient η on the in-plane stress σ_{xx0} with $R = 60$ mm, $P = 2000$ N/m and $\Gamma = 6 \cdot 10^{-7}$ C/m: (left) $Q/\eta P = 0.5$, point A in Figure 3; and (right) $Q/\eta P = -0.5$, point F in Figure 3.

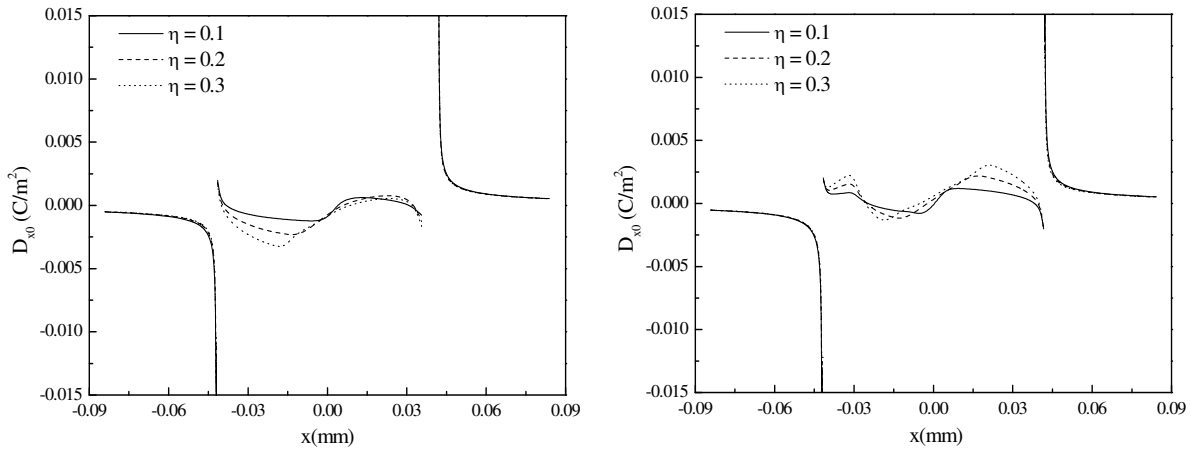


Figure 18. The effect of the friction coefficient η on the in-plane electric displacement D_{x0} with $R = 60$ mm, $P = 2000$ N/m and $\Gamma = 6 \cdot 10^{-7}$ C/m: (left) $Q/\eta P = 0.5$, point A in Figure 3; and (right) $Q/\eta P = -0.5$, point F in Figure 3.

increases as η increases throughout most of the region $x > 0$. The behavior of σ_{xx0} for $Q/\eta P = -0.5$ is opposite of that for $Q/\eta P = 0.5$. In particular, the maximum tensile stress σ_{xx0} increases with the increase of η , and occurs at $x = a$ for $Q/\eta P = 0.5$ and at $x = -a$ for $Q/\eta P = -0.5$. The maximum tensile stress implies the possible site of the fretting crack initiation.

Figure 18 analyzes the effect of the friction coefficient η on the in-plane electric displacement D_{x0} when $Q/\eta P = \pm 0.5$. During tangential loading phase, the in-plane electric displacement distribution is quite similar to that of the normal loading phase. The friction coefficient η also has little effect on the in-plane electric displacement.

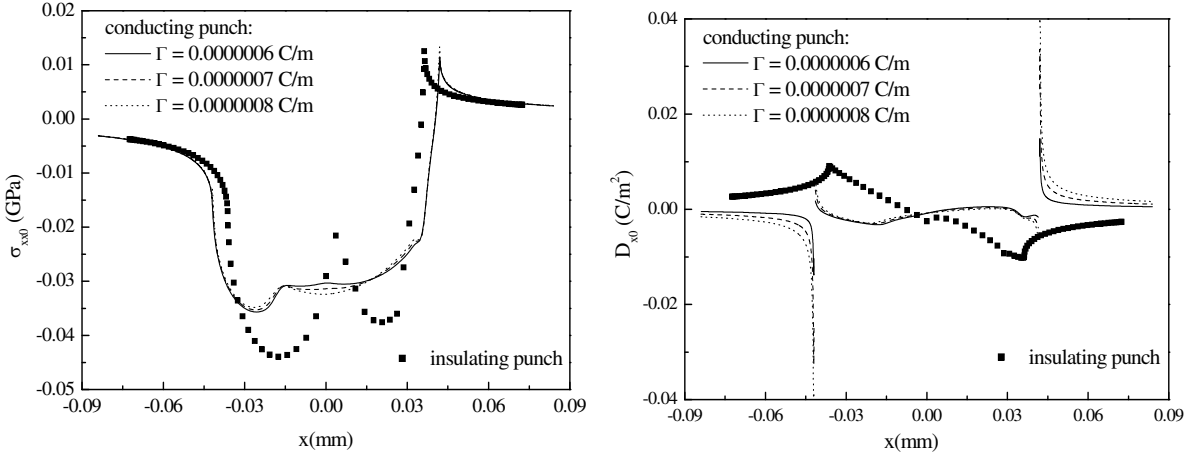


Figure 19. The effect of the resultant electric charge Γ on the (left) in-plane stress σ_{xx0} and (right) in-plane electric displacement D_{x0} with $R = 60$ mm, $P = 2000$ N/m, $\eta = 0.3$ and $Q/\eta P = 0.5$, point A in Figure 3.

Figure 19 discusses the effect of the resultant electric charge Γ on the in-plane stress σ_{xx0} and the in-plane electric displacement D_{x0} for both insulating and conducting punches with $Q/\eta P = 0.5$ and $\eta = 0.3$. We can observe that the in-plane stress distribution of the insulating punch is similar to that of the conducting punch. The maximum tensile stress of the insulating punch is greater than that of the conducting punch. However, the in-plane electric displacement distribution is totally different than that of the conducting punch. The in-plane electric displacement is singular at the edge of the contact region for the conducting punch whereas it is quite smooth for the insulating punch. The change of Γ has a slight effect on both σ_{xx0} and D_{x0} .

7. Conclusions

In this paper, the two-dimensional fretting contact between a homogeneous transversely isotropic piezoelectric half-plane and a rigid conducting cylindrical punch was considered. The two dissimilar bodies are first acted upon by a monotonically increasing normal load, and then by a cyclic tangential load. The fretting contact problem is reduced to a set of coupled Cauchy singular integral equations which are solved by using an iterative method to determine the contact tractions, electric charge and unknown stick/slip region. It was found that:

- (1) The electric charge is singular at the edge of the contact region whereas the normal contact pressure and tangential traction is quite smooth.
- (2) The friction coefficient has a slight effect on the normal contact pressure and electric charge. The peak value of the tangential traction occurs at the interface between the stick region and slip region, and increases rapidly with the increase of the friction coefficient.
- (3) With the increase of the applied electric charge, the value of the tangential traction decreases at the stick region and changes slightly at the slip region.

- (4) The peak values of tangential traction for the insulating punch is greater than that of the conducting punch, but the size of the stick region is smaller than that of the conducting punch.
- (5) The maximum values of the in-plane tensile stress and the in-plane electric displacement occur at the edges of the contact region during the tangential loading phase, which implies a possible site of electromechanical damage.

Acknowledgments

The work described in this paper is supported by the Fundamental Research Funds for the Central Universities under grant number 2016YJS113.

Appendix

The parameters f_{ij} may be written in the form

$$f_{ij} = sF_{ij}, \quad i, j = 1, 2, 3, \quad (\text{A.1})$$

where

$$[F] = \begin{bmatrix} 1 & 1 & 1 \\ a_1 & a_2 & a_3 \\ b_1 & b_2 & b_3 \end{bmatrix} \begin{bmatrix} c_{13}is + c_{33}a_1n_1 + e_{33}b_1n_1 & c_{13}is + c_{33}a_2n_2 + e_{33}b_2n_2 & c_{13}is + c_{33}a_3n_3 + e_{33}b_3n_3 \\ c_{44}n_1 + c_{44}isa_1 + e_{15}isb_1 & c_{44}n_2 + c_{44}isa_2 + e_{15}isb_2 & c_{44}n_3 + c_{44}isa_3 + e_{15}isb_3 \\ e_{31}is + e_{33}a_1n_1 - \epsilon_{33}b_1n_1 & e_{31}is + e_{33}a_2n_2 - \epsilon_{33}b_2n_2 & e_{31}is + e_{33}a_3n_3 - \epsilon_{33}b_3n_3 \end{bmatrix}^{-1},$$

and $[]^{-1}$ is the inverse matrix.

For the piezoceramic PZT-4 half-plane, the parameters f_{ij} can be written as

$$\begin{aligned} f_{11} &= -7.5241 \cdot 10^{-12}i, & f_{12} &= 1.8396 \cdot 10^{-11}, & f_{13} &= 1.7328 \cdot 10^{-2}i, \\ f_{21} &= 1.7728 \cdot 10^{-11}, & f_{22} &= 7.4241 \cdot 10^{-12}i, & f_{23} &= 2.2085 \cdot 10^{-2}, \\ f_{31} &= 2.2085 \cdot 10^{-2}, & f_{32} &= -1.7328 \cdot 10^{-2}i, & f_{33} &= -8.8307 \cdot 10^7. \end{aligned} \quad (\text{A.2})$$

References

- [Cattaneo 1938] C. Cattaneo, "Sul contatto di due corpi elastici: distribuzione locale degli sforzi", *Rend. Accad. Naz. Lincei* **27**:6 (1938), 342–348, 434–436, 474–478.
- [Chen 1999] W.-Q. Chen, "Inclined circular flat punch on a transversely isotropic piezoelectric half-space", *Arch. Appl. Mech.* **69**:7 (1999), 455–464.
- [Chen 2000] W.-Q. Chen, "On piezoelectric contact problem for a smooth punch", *Int. J. Solids Struct.* **37**:16 (2000), 2331–2340.
- [Chen and Yu 2005] Z.-R. Chen and S.-W. Yu, "Micro-scale adhesive contact of a spherical rigid punch on a piezoelectric half-space", *Compos. Sci. Technol.* **65**:9 (2005), 1372–1381.
- [Choi and Paulino 2008] H. J. Choi and G. H. Paulino, "Thermoelastic contact mechanics for a flat punch sliding over a graded coating/substrate system with frictional heat generation", *J. Mech. Phys. Solids* **56**:4 (2008), 1673–1692.
- [Ciavarella 1998a] M. Ciavarella, "The generalized Cattaneo partial slip plane contact problem, I: Theory", *Int. J. Solids Struct.* **35**:18 (1998), 2349–2362.
- [Ciavarella 1998b] M. Ciavarella, "The generalized Cattaneo partial slip plane contact problem, II: Examples", *Int. J. Solids Struct.* **35**:18 (1998), 2363–2378.

- [Ciavarella and Hills 1999] M. Ciavarella and D. A. Hills, “Brief note: some observations on oscillating tangential forces and wear in general plane contacts”, *Eur. J. Mech. A-Solid* **18**:3 (may 1999), 491–497.
- [Ding et al. 2000] H.-J. Ding, P.-F. Hou, and F.-L. Guo, “The elastic and electric fields for three-dimensional contact for transversely isotropic piezoelectric materials”, *Int. J. Solids Struct.* **37**:23 (2000), 3201–3229.
- [Erdogan and Gupta 1972] F. Erdogan and G. D. Gupta, “On the numerical solution of singular integral equations”, *Q. Appl. Math.* **29** (1972), 525–534.
- [Fan et al. 1996] H. Fan, K.-Y. Sze, and W. Yang, “Two-dimensional contact on a piezoelectric half-space”, *Int. J. Solids Struct.* **33**:9 (1996), 1305–1315.
- [Giannakopoulos and Suresh 1999] A. E. Giannakopoulos and S. Suresh, “Theory of indentation of piezoelectric materials”, *Acta Mater.* **47**:7 (1999), 2153–2164.
- [Gradshteyn and Ryzhik 2000] I. S. Gradshteyn and I. M. Ryzhik (editors), *Table of integrals, series, and products*, Academic Press, New York, 2000.
- [Guo and Jin 2009] X. Guo and F. Jin, “A generalized JKR-model for two-dimensional adhesive contact of transversely isotropic piezoelectric half-space”, *Int. J. Solids Struct.* **46**:20 (2009), 3607–3619.
- [Hanson et al. 1989] M. T. Hanson, L. M. Keer, and T. N. Farris, “Energy dissipation in non-Hertzian fretting contact”, *Tribol. T.* **32**:2 (1989), 147–154.
- [Hills et al. 1993] D. A. Hills, D. Nowell, and A. Sackfield (editors), *Mechanics of elastic contacts*, Butterworth-Heinemann, Oxford, 1993.
- [Johnson 1985] K. L. Johnson, *Contact mechanics*, Cambridge University Press, 1985.
- [Ke et al. 2008] L.-L. Ke, J. Yang, S. Kitipornchai, and Y.-S. Wang, “Electro-mechanical frictionless contact behavior of a functionally graded piezoelectric layered half-plane under a rigid punch”, *Int. J. Solids Struct.* **45**:11–12 (2008), 3313–3333.
- [Keer and Farris 1987] L. M. Keer and T. N. Farris, “Effects of finite thickness and tangential loading on development of zones of microslip in fretting”, *ASLE Transactions* **30**:2 (1987), 203–210.
- [Ma et al. 2014] J. Ma, L.-L. Ke, and Y.-S. Wang, “Electro-mechanical sliding frictional contact of a piezoelectric half-plane under a rigid conducting punch”, *Appl. Math. Model.* **38**:23 (2014), 5471–5489.
- [Makagon et al. 2009] A. Makagon, M. Kachanov, E. Karapetian, and S. V. Kalinin, “Piezoelectric indentation of a flat circular punch accompanied by frictional sliding and applications to scanning probe microscopy”, *Int. J. Eng. Sci.* **47**:2 (2009), 221–239.
- [Mindlin and Deresiewicz 1953] R. D. Mindlin and H. Deresiewicz, “Elastic spheres in contact under varying oblique forces”, *J. Appl. Mech. (ASME)* **20**:3 (1953), 327–344.
- [Mindlin et al. 1951] R. D. Mindlin, W. P. Mason, T. F. Osmer, and H. Deresiewicz, “Effects of an oscillating tangential force on the contact surfaces of elastic spheres”, *J. Appl. Mech. (ASME)* **18**:3 (1951), 331.
- [Muskhelishvili 1958] N. I. Muskhelishvili, *Singular integral equations: boundary problems of functions theory and their applications to mathematical physics*, Wolters-Noordhoff Publishing, Groningen, 1958.
- [Nowell et al. 1988] D. Nowell, D. A. Hills, and A. Sackfield, “Contact of dissimilar elastic cylinders under normal and tangential loading”, *J. Mech. Phys. Solids* **36**:1 (1988), 59–75.
- [Ramirez and Heyliger 2003] G. Ramirez and P. Heyliger, “Frictionless contact in a layered piezoelectric half-space”, *Smart Mater. Struct.* **12**:4 (2003), 612–625.
- [Sosa and Castro 1994] H. A. Sosa and M. A. Castro, “On concentrated loads at the boundary of a piezoelectric half-plane”, *J. Mech. Phys. Solids* **42**:7 (1994), 1105–1122.
- [Spence 1973] D. A. Spence, “An eigenvalue problem for elastic contact with finite friction”, *Proc. Cambridge Philos. Soc.* **73**:1 (1973), 249–268.
- [Spence 1986] D. A. Spence, “Frictional contact with transverse shear”, *Q. J. Mech. Appl. Math.* **39**:2 (1986), 233–253.
- [Su et al. 2015] J. Su, L.-L. Ke, and Y.-S. Wang, “Two-dimensional fretting contact analysis of piezoelectric materials”, *Int. J. Solids Struct.* **73–74** (2015), 41–54.
- [Wang et al. 2008] B. B. L. Wang, J. C. Han, S. Y. Du, H. Y. Zhang, and Y. G. Sun, “Electromechanical behaviour of a finite piezoelectric layer under a flat punch”, *Int. J. Solids Struct.* **45**:25–26 (2008), 6384–6398.

- [Wu et al. 2012] Y. F. Wu, H. Y. Yu, and W. Q. Chen, “Mechanics of indentation for piezoelectric thin films on elastic substrate”, *Int. J. Solids Struct.* **49**:1 (2012), 95–110.
- [Zhou and Lee 2011] Y. T. Zhou and K. Y. Lee, “Thermo-electro-mechanical contact behavior of a finite piezoelectric layer under a sliding punch with frictional heat generation”, *J. Mech. Phys. Solids* **59**:5 (2011), 1037–1061.
- [Zhou and Lee 2012] Y.-T. Zhou and K. Y. Lee, “Theory of moving contact of anisotropic piezoelectric materials via real fundamental solutions approach”, *Eur. J. Mech. — A/Solids* **35** (2012), 22–36.
- [Zhou and Lee 2014] Y.-T. Zhou and K. Y. Lee, “Investigation of frictional sliding contact problems of triangular and cylindrical punches on monoclinic piezoelectric materials”, *Mech. Mater.* **69**:1 (2014), 237–250.

Received 11 Jan 2016. Revised 10 May 2016. Accepted 16 May 2016.

JIE SU: 14115272@bjtu.edu.cn

Institute of Engineering Mechanics, Beijing Jiaotong University, Haidan District, Beijing, 100044, PR China

LIAO-LIANG KE: llke@bjtu.edu.cn

Institute of Engineering Mechanics, Beijing Jiaotong University, Haidan District, Beijing, 100044, PR China

YUE-SHENG WANG: ywang@bjtu.edu.cn

Institute of Engineering Mechanics, Beijing Jiaotong University, Haidan District, Beijing, 100044, PR China

AN ANISOTROPIC MODEL FOR THE MULLINS EFFECT IN MAGNETOACTIVE RUBBER-LIKE MATERIALS

M. H. B. M. SHARIFF AND ROGER BUSTAMANTE

An anisotropic phenomenological model is proposed to describe the Mullins phenomena for magnetoactive elastomers. The model is based on the use of direction-dependent damage parameters and a set of spectral invariants presented recently in the literature. The effect of the magnetic field on the Mullins phenomena for simple tension and simple shear is discussed.

1. Introduction

Magnetoactive (MS) elastomers correspond to a class of rubber-like materials, which are filled with magnetoactive particles during the curing process, where the particles are usually made of iron and carbonyl iron (see, for example, [Bellan and Bossis 2002; Boczkowska and Awietjan 2012]). When such an elastomer solidifies, the MS particles remain locked inside it. Subsequently, if an external magnetic field is applied, it is possible to obtain relatively large deformations [Bellan and Bossis 2002; Boczkowska and Awietjan 2012] that can be controlled by this external field, and for this reason this class of elastomers is classified as a smart material [Ginder et al. 2001; Ghaforianfar et al. 2013]. There are many possible applications for these elastomers, such as in the design of flexible robots and in vibration suppression [Böse et al. 2012; Farshad and Roux 2004; Kashima et al. 2012; Zhu et al. 2012].

Due to the potential applications of these MS elastomers, in the last few years there has been an interest in the mathematical modeling of the mechanical behavior of such materials. Some relatively recent works on this topic are the series of papers by Dorfmann and Ogden [2003; 2004a; 2004b; 2005], Triantafyllidis and coworkers [Kankanala and Triantafyllidis 2004; Danas et al. 2012], Steigmann [2004] and Vu and Steinmann [2010]¹.

In most of these works, the MS elastomers were assumed to be hyperelastic bodies; however, when mixing a rubber-like material with MS particles, we expect to observe some inelastic phenomena since most elastomers, especially elastomers with fillers, exhibit an anisotropic stress-softening phenomenon widely known as the Mullins effect [Mullins 1947; Coquelle and Bossis 2006]. Quite often, the stress is softened significantly, hence modeling MS elastomers as purely elastic deformations can be erroneous. In addition to this, modeling the nonvirgin reference stress-free state of an MS material as isotropic is not accurate, since generally it is not isotropic in the stress-free reference state and the type of anisotropy depends on the history of strain.

Keywords: magnetoactive materials, Mullins effect, anisotropic stress-softening, spectral invariants.

¹See the book by Ogden and Steigmann [2010] for more references on this topic; the interested reader can also see [Brown 1966; Eringen and Maugin 1990; Maugin 1988] for some older works on the interaction of electromagnetic fields and continua.

In the present communication, the mechanical behavior of MS elastomers is modeled via an anisotropic Mullins model, which is based on the direction-dependent model proposed by Shariff [2014]. In particular, we are interested in studying the influence of the magnetic field on the anisotropic stress softening behavior of MS elastomers, where we currently believe there is no model that could describe three-dimensional anisotropic stress-softening behavior (Mullins effect) of MS materials in the presence of a magnetic field. Our proposed model is based on the model of Shariff [2014], where he uses direction-dependent damage parameters (that depend on the history of strain) to simulate the anisotropic behavior that manifests due to the Mullins effect. His model is able to reasonably predict a variety of nonproportional (i.e., successive loadings with different directions of stretching or types of loading) experimental data on the anisotropic Mullins effect for different types of rubber-like materials. The constitutive equations for MS elastomers proposed in the present paper are characterized using a set of (useful) experimentally spectral invariants recently developed in the literature by Shariff and coworkers [Bustamante and Shariff 2015; Shariff 2008]. Most MS elastomers are nearly incompressible, however, in this communication it is assumed, for simplicity, that they are incompressible.

This paper is divided in the following parts: in Section 2 the main elements of the theory of Dorfmann and Ogden [2003; 2004b; 2004a; 2005] for MS elastomers are presented. In Section 3 the model for the Mullins effect is shown, while in Section 4 some boundary value problems are studied. Finally, in Section 5 some final comments are given.

2. Preliminary

2.1. Kinematics. In this paper, all subscripts i, j and k take the values 1, 2, 3, unless stated otherwise.

Let \mathcal{B} denote the MS body, and $\mathbf{x} \in \mathcal{B}_t$ denote the position of a particle $X \in \mathcal{B}$ in the current configuration \mathcal{B}_t . The position of the same particle in the reference configuration is denoted as $\mathbf{X} \in \mathcal{B}_r$, where \mathcal{B}_r is the body in the reference configuration, which is assumed to be undeformed and unstressed. It is assumed that there exists a one-to-one mapping χ such that $\mathbf{x} = \chi(\mathbf{X}, t)$ for any time $t > 0$. The deformation gradient, the left Cauchy–Green \mathbf{B} and right Cauchy–Green \mathbf{C} deformation tensors are respectively defined as

$$\mathbf{F} = \frac{\partial \mathbf{x}}{\partial \mathbf{X}}, \quad \mathbf{B} = \mathbf{F}\mathbf{F}^T = \mathbf{V}^2, \quad \mathbf{C} = \mathbf{F}^T\mathbf{F} = \mathbf{U}^2, \quad (1)$$

where χ is assumed such that $J = \det \mathbf{F} > 0$.

In this communication, only quasistatic deformations and time-independent fields are considered, and the mechanical body forces are assumed to be negligible.

2.2. Governing equations for magnetosensitive elastomers.

2.2.1. The Maxwell equations. The theory of magnetosensitive elastomers (with no dependence on time) employed here makes use of three vector fields in the current configuration—the magnetic field \mathbf{h} , the induction \mathbf{b} and the magnetic polarization \mathbf{m} —to describe the magnetic effects in an MS body. In the absence of electric interactions and time effects, the magnetic field and the magnetic induction have to satisfy the simplified form of the Maxwell equations

$$\operatorname{div} \mathbf{b} = 0, \quad \operatorname{curl} \mathbf{h} = \mathbf{0}, \quad (2)$$

where, respectively, div and curl are the divergence and curl operators with respect to \mathbf{x} . Using the global form of (2), it is possible to define the following Lagrangian counterparts (in the reference configuration) of the magnetic field \mathbf{h}_l , and the magnetic induction \mathbf{b}_l

$$\mathbf{h}_l = \mathbf{F}^T \mathbf{h}, \quad \mathbf{b}_l = \mathbf{F}^{-1} \mathbf{b}. \quad (3)$$

The above variables satisfy [Dorfmann and Ogden 2004a]

$$\text{Div } \mathbf{b}_l = 0, \quad \text{Curl } \mathbf{h}_l = \mathbf{0}, \quad (4)$$

where Div and Curl are the divergence and curl operators with respect to \mathbf{X} , respectively.

In vacuum, the magnetic field and the magnetic induction are related by the equation

$$\mathbf{b} = \mu_0 \mathbf{h}, \quad (5)$$

where μ_0 is the magnetic permeability in vacuo. For condensed matter, an additional field is required, which is the magnetization field \mathbf{m} and it is related to \mathbf{b} and \mathbf{h} through (see [Kovetz 2000] for more details on the theory of electromagnetism)

$$\mathbf{b} = \mu_0(\mathbf{h} + \mathbf{m}). \quad (6)$$

2.2.2. The theory of magnetoelastic interactions by Dorfmann and Ogden . In nonlinear magnetoelasticity, there are different ways to express the equation of motion, the relation between the stresses, the strains and the magnetic variables; there are also different possible definitions for the stress tensor [Hutter et al. 2006]. In this communication, as a basis for our work the theory developed by Dorfmann and Ogden [2004a] is used, where they define a total stress tensor \mathbf{T} that incorporates in its definition the magnetic body forces (which are expressed as the divergence of a Maxwell stress tensor). The total (symmetrical) stress tensor \mathbf{T} is related to the nonsymmetrical (elastic) Cauchy $\boldsymbol{\sigma}$ stress via the relation [Dorfmann and Ogden 2004b]

$$\mathbf{T} = \boldsymbol{\sigma} + \frac{1}{\mu_0} [\mathbf{b} \otimes \mathbf{b} - \frac{1}{2}(\mathbf{b} \cdot \mathbf{b})\mathbf{I}] + (\mathbf{m} \cdot \mathbf{b})\mathbf{I} - \mathbf{b} \otimes \mathbf{m}, \quad (7)$$

where \otimes and \cdot denote the dyadic and dot products, respectively. The nonsymmetrical mechanical Cauchy stress $\boldsymbol{\sigma}$ is part of the symmetrical total stress, and its role is important in deriving the proposed total energy (see (16) below). A key ingredient of this theory is the definition of a total energy function (see [Dorfmann and Ogden 2004a, Equation 3.10] and Section 3.3 below), where relatively simple expressions for the total stress and one of the magnetic variables are obtained.

2.2.3. Equation of equilibrium and continuity conditions. The total stress tensor \mathbf{T} must satisfy the balance equation [Dorfmann and Ogden 2004a, Equation 2.13]

$$\text{div } \mathbf{T} = \mathbf{0}. \quad (8)$$

Through the surface of the body $\partial\mathcal{B}_t$ the magnetic variables and the total stress tensor must satisfy the continuity conditions [Kovetz 2000]

$$\mathbf{n} \cdot [\![\mathbf{b}]\!] = 0, \quad \mathbf{n} \times [\![\mathbf{h}]\!] = \mathbf{0}, \quad \mathbf{T}\mathbf{n} = \hat{\mathbf{t}} + \mathbf{T}_M \mathbf{n}, \quad (9)$$

where \mathbf{n} is the unit outward normal vector to $\partial\mathcal{B}_t$, $\hat{\mathbf{t}}$ is the external mechanical traction, $[\![\]\!]$ denotes the difference of a quantity from outside and inside a body, and \mathbf{T}_m is the Maxwell stress tensor with the

relation [Kovetz 2000]

$$T_M = \mathbf{h} \otimes \mathbf{b} - \frac{1}{2}(\mathbf{h} \cdot \mathbf{b})\mathbf{I}. \tag{10}$$

3. Anisotropic stress softening model

When rubber is loaded in simple tension from its virgin state, and is then unloaded and reloaded, due to some damage, the stress required is less than that of the initial loading for stretches up to the maximum stretch achieved on the initial loading. This stress softening phenomenon is referred to as the Mullins effect. Here, a brief description on the behavior of the ideal Mullins effect is given; the unloading and reloading (in the same direction and up to the same “maximal” strain) paths coincide, and there is no permanent set. This description is made clear in Figure 1 below. In this section, we also define direction-dependent damage parameters, introduce the concept of the damage function [Shariff 2006; 2014] and construct a total energy function using a set of spectral invariants. In this communication, the term “damage” is interpreted in its widest sense; for example, it may mean “rupture of molecular bonds that reform to create new microstructure” or “conversion of hard phase to soft phase” or “any change in the ground state mechanical properties that are induced by strain”. We are only concerned with strain induced damages that lead to stress softening.

3.1. Description of the ideal Mullins effect in nonproportional uniaxial loadings with no permanent set.

Consider the case when there is no magnetic field ($h = 0$) and a magnetosensitive (MS) material is being prestretched uniaxially as shown on the primary (virgin material response) loading path Oa in Figure 1. On unloading from a the elastic path aEO is followed; we call this path elastic because when the material is loaded again up to point a the path aEO is retraced as $O Ea$, hence the material behaves elastically and its ground-state-material-constant values are fixed during this deformation. From the point a the material is loaded to the point b via the primary loading path Oab . When the material is unloaded from b , the elastic bEO path is followed. After unloading completely, a simple tension deformation is applied in a direction 30° from the prestretch loading direction on a smaller specimen cut

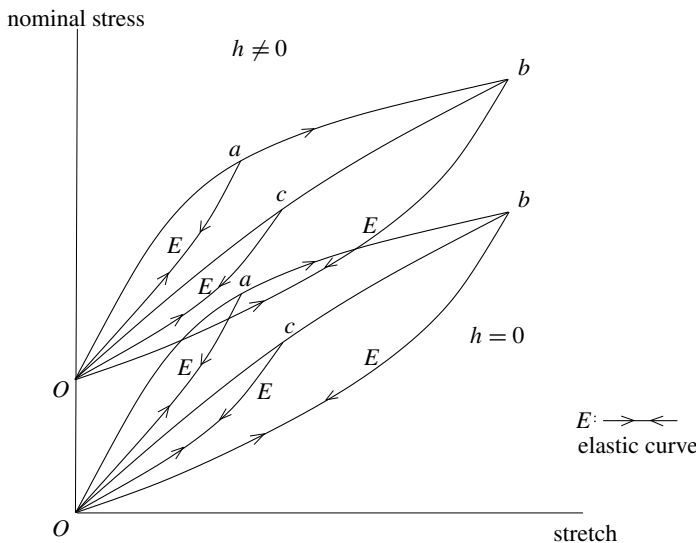


Figure 1. Schematic loading-unloading curves in simple tension of an MS Mullins material.

from the prestretched material. This sequence of deformations was done experimentally by Machado et al. [2012] on a non-MS material. The nonelastic 30° path is depicted by the path Ocb and the elastic paths (unloading from c and b) are depicted by cEO and bEO . The elastic properties for the elastic paths $O Ea$, $O Eb$ and $O Ec$ are different. The nominal stress on any path can be obtained by differentiating the area under an elastic path. From Figure 1, the stress-strain behavior in different loading directions are not the same, which suggests that the damage caused by strain is anisotropic. The areas under different elastic paths can be represented by different direction dependent total elastic energy functions, although the material itself is not elastic. Note that the ground state material properties may change during deformation. With these in mind, following the work of Shariff [2006; 2014], we introduce a “free” energy function for an inelastic solid that can be portrayed by an infinite family of total elastic energy functions parameterized by the direction-dependent damage parameter defined in Section 3.2.

When a magnetic field ($h \neq 0$) is applied on the undeformed reference configuration, the material will deform due to the magnetic forces. In this case, an external stress is required to maintain that undeformed configuration $\mathbf{F} = \mathbf{I}$. Consider the sequence of uniaxial deformations described previously, where the directions of the magnetic field are always in the uniaxial directions. The behavior of the loading paths are similar to the loading paths mentioned before, but due to the presence of a magnetic field the uniaxial stresses are generally higher (as depicted in Figure 1) than the stresses when there is no magnetic field [Bellan and Bossis 2002].

3.2. Direction-dependent damage parameter and damage function. Based on simple tension deformations, in the original work by Mullins [1947], it was assumed that stress softening takes place if the current (principle) tensile stretch is less than the maximum stretch. In view of this, most previous models [Mullins 1947; Govindjee and Simo 1991; Johnson and Beatty 1993; Itskov et al. 2010] used maximum tensile stretch as their damage parameter. However, in simple tension there are three principal stretches, one in tension and two in compression; hence one should consider both the maximum tensile and minimum compressive stretches. It is worth noting that the Pawelski [2001] experiment showed that stress softening also occurs in compression. This suggests that minimum compressive stretch should not be ignored in stress softening modeling and hence, in our model, we include both the maximum and minimum stretches. They are related to the proposed direction-dependent damage parameter α_i as explained below.

The principal stretches satisfy the following inequality

$$s_i^{(\min)} \leq \lambda_i \leq s_i^{(\max)}, \quad (11)$$

where

$$s_i^{(\max)} = \max_{0 \leq z \leq t} \sqrt{\mathbf{e}_i \cdot \mathbf{C}(z) \mathbf{e}_i} \quad \text{and} \quad s_i^{(\min)} = \min_{0 \leq z \leq t} \sqrt{\mathbf{e}_i \cdot \mathbf{C}(z) \mathbf{e}_i}. \quad (12)$$

Physically, $s_i^{(\max)}$ and $s_i^{(\min)}$ are the maximum and minimum “stretch” values of the \mathbf{e}_i line element throughout the history of the deformation, respectively. From the above equation it is clear that $s_i^{(\max)} \geq 1$, $s_i^{(\min)} \leq 1$ and λ_i is bounded by $s_i^{(\min)}$ and $s_i^{(\max)}$. Consider, for example, a material being prestretched by a simple tension deformation process. A simple tension deformation is then applied on this prestretch material in the same direction as the prestretch direction, where the deformation is described by

$$\mathbf{U}(\lambda) \equiv (\lambda, 1/\sqrt{\lambda}, 1/\sqrt{\lambda}), \quad (13)$$

where $1 \leq \lambda \leq \lambda_m = s_1^{(\max)}$, $s_2^{(\min)} = s_3^{(\min)} = 1/\sqrt{\lambda_m} \leq 1/\sqrt{\lambda} \leq 1$ and $s_1^{(\min)} = s_2^{(\max)} = s_3^{(\max)} = 1$. In (12), $s_i^{(\max)}$ and $s_i^{(\min)}$ are related to the amount of damage; the interval in (11) widens as the amount of damage increases.

For a non-MS Mullins material, Shariff [2006; 2014] proposed an anisotropic stress softening damage model using the direction-dependent damage parameter α_i , where

$$\alpha_i = \begin{cases} s_i^{(\max)} & \text{when } \lambda_i > 1, \\ s_i^{(\min)} & \text{when } \lambda_i < 1. \end{cases} \tag{14}$$

Note that in (14) we do not consider $\lambda_i = 1$, because our model is constructed in such a way that α_i does not contribute to the stress softening when $\lambda_i = 1$ (see Section 3.5 below). In the case when $\lambda_i = \lambda_j$ ($i \neq j$), the directions of \mathbf{e}_i and \mathbf{e}_j are not unique. In view of this, we let

$$\alpha_i = \alpha_j = \begin{cases} 1/\sqrt{s_k^{(\min)}} & \text{when } \lambda_i = \lambda_j > 1, \\ 1/\sqrt{s_k^{(\max)}} & \text{when } \lambda_i = \lambda_j < 1, \end{cases} \tag{15}$$

where $i \neq j \neq k \neq i$. In the case when all the principal stretches are equal, the principal directions \mathbf{e}_i are all nonunique. However, for an incompressible material this can only happen when $\lambda_1 = \lambda_2 = \lambda_3 = 1$ and, as mentioned above, the corresponding α_i in this case do not contribute to the stress softening; hence their values are not given here.

Stress softening models usually have softening functions which control the softening behavior. The softening function is governed by the amount of damage [Simo 1987; Ogden and Roxburgh 1999; Itskov et al. 2010]. The rate of change of the amount of damage with respect to time or any deformation parameter that increases with primary loading should be nonnegative. In our model, in view of the definition of the damage parameter α_i , a measure of an amount of damage (damage function) related to the \mathbf{e}_i line element is proposed. The proposed damage function g (which may depend on material properties) is defined such that $0 = g(1) \leq g(x)$, $x \in R$, $x > 0$. The function g has also the properties that $\hat{g}'(\alpha) \geq 0$, where $\hat{g}(\alpha) = g((1 - \alpha) + \alpha w)$, $0 < \alpha \leq 1$ and $w > 0$ ($\neq 1$) is a constant. The function $\hat{g}'(\alpha)$ need not be defined at $\alpha = 0$. If it is defined then $\hat{g}'(0) = 0$. In view of our definition, g increases monotonically as x moves away from the point $x = 1$; hence, $g(\lambda_i) \leq g(\alpha_i)$. Physically, $g(\alpha_i)$ can be considered as a measure of an amount of damage related to the \mathbf{e}_i line element; for a strictly monotonic g , the higher the value of g the bigger the damage induced on the \mathbf{e}_i line element. Specific forms of g are given below in (64) and (72).

3.3. Constitutive equations and spectral invariants . For an isothermal problem the Clausius–Duhem inequality take the form

$$\boldsymbol{\sigma} : \mathbf{D} - \rho_0 \dot{\psi} - \mathbf{m} \cdot \dot{\mathbf{b}} \geq 0, \tag{16}$$

where the superposed dot represents the time derivative, $:$ denotes the inner product of two second order tensors, ρ_0 is the density of the incompressible material, ψ is the Helmholtz free energy function, $\mathbf{D} = \text{grad } \mathbf{v}$, grad is the gradient operator with respect to \mathbf{x} and \mathbf{v} is the velocity. Following [Dorfmann and Ogden 2004a] and [Shariff 2014] the Helmholtz free energy can be expressed as

$$\rho_0 \psi = \psi_a(\mathbf{F}, \mathbf{b}, \mathbf{g}), \tag{17}$$

where the vector $\mathbf{g} \equiv [g(\alpha_1), g(\alpha_2), g(\alpha_3)]^T$ is an internal variable. Taking note that, for an incompressible material $\text{tr}(\mathbf{D}) = 0$, and since $\boldsymbol{\sigma} : \mathbf{D} = (\mathbf{F}^{-1}\boldsymbol{\sigma})^T : \dot{\mathbf{F}}$, (16) and (17) give the relations

$$\left(\boldsymbol{\sigma} + p\mathbf{I} - \mathbf{F} \frac{\partial \psi_a}{\partial \mathbf{F}} \right) : \dot{\mathbf{F}} - \left(\mathbf{m} + \frac{\partial \psi_a}{\partial \mathbf{b}} \right) \cdot \dot{\mathbf{b}} - \sum_{i=1}^3 \frac{\partial \psi_a}{\partial g(\alpha_i)} \dot{g}(\alpha_i) \geq 0, \quad (18)$$

$$\boldsymbol{\sigma} = -p\mathbf{I} + \mathbf{F} \frac{\partial \psi_a}{\partial \mathbf{F}}, \quad \mathbf{m} = -\frac{\partial \psi_a}{\partial \mathbf{b}}, \quad (19)$$

and the inequality

$$-\sum_{i=1}^3 \frac{\partial \psi_a}{\partial g(\alpha_i)} \dot{g}(\alpha_i) \geq 0. \quad (20)$$

In view of the property of g , $\dot{g}(\alpha_i) \geq 0$, and to satisfy (20), the condition

$$\frac{\partial \psi_a}{\partial g(\alpha_i)} \leq 0 \quad (21)$$

is imposed. If we define

$$\Phi(\mathbf{F}, \mathbf{b}_l, \mathbf{g}) = \psi_a(\mathbf{F}, \mathbf{F}\mathbf{b}_l, \mathbf{g}), \quad (22)$$

the nonsymmetric Cauchy stress [Dorfmann and Ogden 2004a] takes the form

$$\boldsymbol{\sigma} = -p\mathbf{I} + \mathbf{F} \frac{\partial \Phi}{\partial \mathbf{F}} - (\mathbf{m} \cdot \mathbf{b})\mathbf{I} + \mathbf{b} \otimes \mathbf{m}, \quad (23)$$

where p is the associated Lagrange multiplier due to the incompressibility constraint and \mathbf{I} is the second order identity tensor.

Following [Dorfmann and Ogden 2004a], an amended free energy function

$$\Omega_m(\mathbf{F}, \mathbf{b}_l, \mathbf{g}) = \Phi(\mathbf{F}, \mathbf{b}_l, \mathbf{g}) + \frac{1}{2\mu_0} \mathbf{b}_l \cdot \mathbf{C} \mathbf{b}_l \quad (24)$$

is defined and using (24) the simplified relation

$$\mathbf{h}_l = \frac{\partial \Omega_m}{\partial \mathbf{b}_l} \quad (25)$$

is obtained.

In this paper, \mathbf{h}_l is chosen (instead of \mathbf{b}_l) as the independent variable and a complementary (total) energy function $\Omega_e = \Omega_a(\mathbf{F}, \mathbf{h}_l)$ is defined through the partial Legendre transformation as

$$\Omega_e = \Omega_a(\mathbf{F}, \mathbf{h}_l, \mathbf{g}) = \Omega_m(\mathbf{F}, \mathbf{b}_l, \mathbf{g}) - \mathbf{b}_l \cdot \mathbf{h}_l, \quad (26)$$

where, in view of the inequality (21), the inequality

$$\frac{\partial \Omega_e}{\partial g(\alpha_i)} \leq 0 \quad (27)$$

is automatically satisfied. The relation

$$\mathbf{b}_l = -\frac{\partial \Omega_e}{\partial \mathbf{h}_l} \quad (28)$$

is obtained from (26).

If Ω_e is treated as a function of \mathbf{C} , the objectivity condition is automatically satisfied and can be written as

$$\Omega_e = \Omega_c(\mathbf{C}, \mathbf{a}, \mathbf{g}, h) = \Omega_a(\mathbf{F}, \mathbf{h}_l, \mathbf{g}), \quad (29)$$

where the unit vector $\mathbf{a} = \mathbf{h}_l/h$ and $h = |\mathbf{h}_l|$. Following the work of Spencer [1971], Ω_e can be expressed in terms classical invariants, i.e.,

$$\Omega_e = \Omega_d(I_1, I_2, I_4, I_5, \mathbf{g}, h), \quad (30)$$

where

$$I_1 = \text{tr}(\mathbf{C}), \quad I_2 = \frac{I_1^2 - \text{tr}(\mathbf{C}^2)}{2}, \quad I_4 = \mathbf{a} \cdot \mathbf{C}\mathbf{a}, \quad I_5 = \mathbf{a} \cdot \mathbf{C}^2\mathbf{a} \quad (31)$$

and tr denotes the trace of a second order tensor. Except for I_4 , the rest of the above classical invariants have no immediate physical interpretation. Hence, they are not attractive in seeking to design a rational program of experiments² for MS solids. For example, it is not straightforward to design an experiment to construct (rigorously) a specific functional form of the total energy Ω_e , where the experiment requires varying a single classical invariant while keeping the remaining classical invariants fixed [Holzapfel and Ogden 2009; Humphrey et al. 1990; Lin and Yin 1998]. In this paper our total energy function is characterized using a set of spectral invariants, where each invariant has a clear physical meaning and have an experimental advantage [Shariff 2008] over the standard (classical and its variants) invariants commonly used in dealing with anisotropic problems. Note that

$$\mathbf{C} = \sum_{i=1}^3 \lambda_i^2 \mathbf{e}_i \otimes \mathbf{e}_i, \quad (32)$$

where λ_i is a principal value (stretch) of the right stretch tensor \mathbf{U} , and \mathbf{e}_i is a principal direction of \mathbf{U} . In view of (29) and (32),

$$\Omega_e = \Omega_f(\lambda_1, \lambda_2, \lambda_3, \mathbf{e}_1 \otimes \mathbf{e}_1, \mathbf{e}_2 \otimes \mathbf{e}_2, \mathbf{e}_3 \otimes \mathbf{e}_3, \mathbf{a}, \mathbf{g}, h). \quad (33)$$

Hence, following the work presented in [Shariff 2008], Ω_e can be written in terms of h and the corresponding spectral invariants, i.e.,

$$\Omega_e = \Omega(\lambda_1, \lambda_2, \lambda_3, \zeta_1, \zeta_2, \zeta_3, \mathbf{g}, h), \quad (34)$$

where $\zeta_i = (\mathbf{a} \cdot \mathbf{e}_i)^2$. The physical meaning of λ_i is obvious, and it is clear that ζ_i is the square of the cosine of the angle between the principal direction \mathbf{e}_i and the preferred direction \mathbf{a} . Since \mathbf{a} is a unit vector, this implies $\zeta_3 = 1 - \zeta_1 - \zeta_2$. The invariant h and the spectral invariants have an experimental advantage over classical invariants presented in the literature, e.g., a simple triaxial test can vary a single invariant while keeping the remaining invariants fixed [Shariff 2008].

Note that (34) has the symmetrical property

$$\Omega(\lambda_1, \lambda_2, \lambda_3, \zeta_1, \zeta_2, \zeta_3, \mathbf{g}, h) = \Omega(\lambda_2, \lambda_1, \lambda_3, \zeta_2, \zeta_1, \zeta_3, \mathbf{g}, h) = \Omega(\lambda_3, \lambda_2, \lambda_1, \zeta_3, \zeta_2, \zeta_1, \mathbf{g}, h). \quad (35)$$

²See [Criscione 2003] for a criticism on the use of the classical invariants by Spencer and Rivlin [1962].

In view of the nonunique values of \mathbf{e}_i and \mathbf{e}_j when $\lambda_i = \lambda_j$, a unique valued Ω should be independent of ζ_i and ζ_j when $\lambda_i = \lambda_j$ and Ω should be independent of ζ_1, ζ_2 and ζ_3 when $\lambda_1 = \lambda_2 = \lambda_3$. We call this independent property together with the symmetrical property (35) the P -property [Shariff 2016]. Our total energy function proposed later in this paper is required to satisfy the P -property.

In view of (22), (23), (24), (26) and (7),

$$\mathbf{T} = 2\mathbf{F} \frac{\partial \Omega_e}{\partial \mathbf{C}} \mathbf{F}^T - p\mathbf{I}. \quad (36)$$

The total nominal stress \mathbf{S} is given by [Dorfmann and Ogden 2004b]

$$\mathbf{S} = \mathbf{F}^{-1} \mathbf{T}. \quad (37)$$

Following the results presented in [Shariff 2008], the Lagrangean spectral components of $\frac{\partial \Omega_e}{\partial \mathbf{C}}$ can be expressed as

$$\left(\frac{\partial \Omega_e}{\partial \mathbf{C}} \right)_{ii} = \frac{1}{2\lambda_i} \frac{\partial \Omega}{\partial \lambda_i} \quad (i \text{ not summed}), \quad (38)$$

and the shear components

$$\left(\frac{\partial \Omega_e}{\partial \mathbf{C}} \right)_{ij} = \frac{\mathbf{e}_i \cdot \mathbf{A} \mathbf{e}_j}{(\lambda_i^2 - \lambda_j^2)} \left(\frac{\partial \Omega}{\partial \zeta_i} - \frac{\partial \Omega}{\partial \zeta_j} \right), \quad (39)$$

where $\mathbf{A} = \mathbf{a} \otimes \mathbf{a}$. The Eulerian spectral components of T_{ij} of the total stress \mathbf{T} are [Bustamante and Shariff 2015]

$$T_{ii} = \lambda_i \frac{\partial \Omega}{\partial \lambda_i} - p, \quad (40)$$

$$T_{ij} = 2\lambda_i \lambda_j \frac{\mathbf{e}_i \cdot \mathbf{A} \mathbf{e}_j}{(\lambda_i^2 - \lambda_j^2)} \left(\frac{\partial \Omega}{\partial \zeta_i} - \frac{\partial \Omega}{\partial \zeta_j} \right), \quad i \neq j. \quad (41)$$

Expressed in terms of spectral components, the magnetic induction has the form [Bustamante and Shariff 2015]

$$\mathbf{b}_l = \sum_{k=1}^3 b_k \mathbf{e}_k, \quad (42)$$

where in view of (28)

$$b_k = -(\mathbf{a} \cdot \mathbf{e}_k) \left[\frac{\partial \Omega}{\partial h} + \frac{2}{h} \left(\frac{\partial \Omega}{\partial \zeta_k} - \sum_{i=1}^3 \frac{\partial \Omega}{\partial \zeta_i} \zeta_i \right) \right]. \quad (43)$$

The magnetic induction in the deformed configuration is obtained from (3), i.e.,

$$\mathbf{b} = \mathbf{F} \mathbf{b}_l. \quad (44)$$

The Eulerian expression of \mathbf{b} is simply

$$\mathbf{b} = \sum_{k=1}^3 \lambda_k b_k \mathbf{v}_k, \quad (45)$$

where \mathbf{v}_k is the principal direction of the left stretch tensor \mathbf{V} .

3.4. The undeformed configuration. Magnetic fields distort an MS body, so if the body is to remain in the undeformed state ($\mathbf{F} = \mathbf{I}$) when a magnetic field is applied, then it must be subject to an external traction that depends on the magnetic field. In the undeformed state, $\lambda_1 = \lambda_2 = \lambda_3 = 1$ and the principal directions of \mathbf{U} are not unique. For simplicity, let $\mathbf{a} = \mathbf{e}_3$ such that $\zeta_3 = 1, \zeta_1 = \zeta_2 = 0$. From (40) and (41), for the case of when \mathbf{h}_l is constant, it is necessary to apply an external traction such that the body remains undeformed, i.e.,

$$\mathbf{T} = \mathbf{T}_0 = \sum_{i=1}^3 \frac{\partial \Omega}{\partial \lambda_i} (1, 1, 1, 0, 0, 1, h) \mathbf{e}_i \otimes \mathbf{e}_i - p \mathbf{I}. \tag{46}$$

From (42) and (43), the magnetic induction takes the form,

$$\mathbf{b} = -\Omega'_0(h) \mathbf{e}_3, \tag{47}$$

where

$$\Omega'_0(h) = \frac{\partial \Omega}{\partial h} (1, 1, 1, 0, 0, 1, h). \tag{48}$$

3.5. A specific constitutive equation. Using the damage parameter α_i and the above set of spectral invariants and following the work of [Bustamante and Shariff 2015; Shariff 2014], a simple separable constitutive equation

$$\Omega_e = \sum_{i=1}^3 [\hat{\eta}(g(\lambda_i), g(\alpha_i)) r(\lambda_i) + \phi(\lambda_i, \alpha_i) + \zeta_i z(\lambda_i, h)] \tag{49}$$

$$= \sum_{i=1}^3 \left[\int_1^{\lambda_i} \hat{\eta}(g(y), g(\alpha_i)) r'(y) dy + \zeta_i z(\lambda_i, h) \right] \tag{50}$$

is proposed, where

$$\phi(\lambda_i, \alpha_i) = - \int_1^{\lambda_i} r(y) \frac{d\hat{\eta}}{dy}(g(y), g(\alpha_i)) dy \tag{51}$$

and

$$z(y, h) = q(y, h) - \frac{\mu_0 h^2}{2y^2}. \tag{52}$$

The first term of the total energy Ω_e (50) can be considered as the sum of energies, where each energy depends on λ_i and on the damage function $g(\alpha_i)$ of the \mathbf{e}_i line element, while the second term can be considered as the sum of energies, where each energy depends on λ_i , the magnitude of \mathbf{h} and its components in the principal directions of \mathbf{U} . The Eulerian magnetic induction then takes the form

$$\mathbf{b} = -\mathbf{F} \frac{\partial Q}{\partial \mathbf{h}_l} + \mu_0 \mathbf{h} \tag{53}$$

and the magnetization is

$$\mathbf{m} = -\frac{\mathbf{F}}{\mu_0} \frac{\partial Q}{\partial \mathbf{h}_l}, \tag{54}$$

where

$$Q = \sum_{i=1}^3 \zeta_i q(\lambda_i, h). \quad (55)$$

For simplicity of notation, let

$$\eta(y, d) = \hat{\eta}(g(y), g(d)). \quad (56)$$

The stress softening function η is introduced in (50) to soften the stress and has the properties $0 < \eta \leq 1$ and $\eta(s, s) = 1$. In view of (53), (54) and (55), it is clear that in vacuum $\mathbf{b} = \mu_0 \mathbf{h}$ and $\mathbf{m} = 0$, and our model suggests that the magnetic induction and the magnetization are independent of the stress-softening, although the stress is affected by the magnetic field and the softening function.

The free energy (50) satisfies the P -property and is direction dependent since the damage parameter α_i is direction-dependent and hence it describes anisotropic damage.

On the primary loading $\eta = 1$, the free energy function simply becomes

$$\Omega_e = \sum_{i=1}^3 [r(\lambda_i) + \phi(\lambda_i, \alpha_i) + \zeta_i z(\lambda_i, h)]. \quad (57)$$

Based on the work of Shariff [2000] on nonlinear isotropic elasticity, we let

$$r(\lambda_i) = \int_1^{\lambda_i} \frac{f(y)}{y} dy, \quad (58)$$

where $f(1) = 0$ and f is strictly monotone. It is clear that $r(1) = 0$, $r'(1) = 0$, $0 = r(1) \leq r(y)$ and $r(y)$ increases (strictly) monotonically away from $y = 1$.

The condition

$$\frac{\partial \hat{\eta}}{\partial g(\alpha_i)}(g(\lambda_i), g(\alpha_i)) < 0 \quad (59)$$

ensures that the inequality (27) is satisfied.

In this paper, we are not concerned with specific forms of the functions f , η , g and q , since there is no available experimental data in the literature about Mullins effect for MS elastomers. However, some qualitative properties of the functions f , η and g are discussed in [Shariff 2014] and specific forms for f , η and g can be found in [Shariff 2000; 2014], i.e.,

$$f(y) = \sum_{i=1}^4 a_i \phi_i(y), \quad (60)$$

where

$$\phi_1(y) = \frac{2}{3} \ln(y), \quad \phi_2(y) = e^{(1-y)} + y - 2, \quad \phi_3(y) = e^{(y-1)} - y, \quad (61)$$

$$\phi_4(y) = \frac{(y-1)^3}{y^k}, \quad (62)$$

a_1, a_2, a_3, a_4 and k are material constants,

$$\hat{\eta}(g(y), g(d)) = e^{b_1(g(y)-g(d))g(y)^{b_2}} - b_3 e^{-b_4 g(y)}(g(d) - g(y)), \quad (63)$$

where b_1 , b_2 and b_3 are material constants and

$$g(y) = \frac{(y^{c_1} - 1)^2}{y^{c_2}}, \quad (64)$$

where c_1 and c_2 are material constants and must be constrained so that $g(y)$ increases monotonically as y moves away from the point $y = 1$ [Shariff 2014]. In this paper we let

$$z(y, h) = d_1 \frac{\mu_0 h^2}{2y^2} - \frac{\mu_0 h^2}{2y^2}, \quad (65)$$

where d_1 is a material constant.

4. Homogeneous deformations

The objective of this section is to discuss the anisotropic mechanical behavior of the proposed constitutive model in simple tension and simple shear deformations, where it can be important from the experimental point of view. We note in passing, that for non-Mullins behavior, simple tension experiments have been done by Bellan and Bossis [2002] and a simple shear experiment has been done by Jolly et al. [1996]. Results for nonproportional loadings to analyze the anisotropic behavior of Mullins materials are given in this section. In the simple shear case, results on the anisotropic behavior due to the application of a magnetic field in different directions are also given.

4.1. Simple tension. Due to edge effects, the continuity conditions on the surfaces are not easily satisfied when simple tension is applied on a rectangular slab. To reduce the edge effects, a specific slab configuration is considered, where the slab thickness in the e_3 direction is very small relative to its width (which is in the e_1 direction), and its length in the e_2 direction is very large relative to its width³. This configuration is denoted as the S -configuration. A simple tension is applied in the e_2 direction.

4.1.1. Simple tension in a fixed direction. To discuss the effect of a magnetic field on stress-softening materials in fixed direction loadings, a simple tension in the Cartesian 2-direction is considered and the magnetic field $\mathbf{h}_I \equiv [0, h, 0]^T$ is applied (where h is a constant) in the undeformed configuration which automatically satisfies (4). With this particular type of deformation, the spectral variables take values $\zeta_2 = 1$, $\zeta_1 = \zeta_3 = 0$. Consider $1 \leq \lambda_2 = \lambda \leq \lambda_m$, hence $s_2^{(\max)} = \lambda_m$ and $s_3^{(\max)} = s_1^{(\max)} = 1/\sqrt{\lambda_m} = 1/\sqrt{s_2^{(\max)}}$. The total uniaxial stress simply takes the form

$$T_{22}(\lambda_2, h) = \eta(\lambda, s_2^{(\max)})f(\lambda) - \eta\left(\frac{1}{\sqrt{\lambda}}, \frac{1}{\sqrt{s_2^{(\max)}}}\right)f\left(\frac{1}{\sqrt{\lambda}}\right) + \lambda \frac{\partial z}{\partial \lambda}(\lambda, h) - \mu_0 \frac{h^2}{2\lambda^2}. \quad (66)$$

The derivation of (66) has taken into account the effect of the Maxwell stress

$$T_{M33} = -\mu_0 \frac{h^2}{2\lambda^2} \quad (67)$$

³It is assumed that the length in direction 2 is very large in comparison with the dimensions in the other two directions so that the continuity conditions (9) and (10) are satisfied only for the surface with normal e_3 .

at the exterior surfaces of the material, where it is assumed that there are no mechanical stresses at these surfaces. In the undeformed configuration,

$$T_{22}(1, h) = \frac{\partial z}{\partial \lambda}(1, h) - \mu_0 \frac{h^2}{2}. \quad (68)$$

Without the magnetic field it is expected that $T_{22}(1, 0) = 0$ in the undeformed configuration. Hence, the condition $\frac{\partial z}{\partial \lambda}(1, 0) = 0$ is imposed. It is assumed that the magnetic induction and the magnetization are given as $\mathbf{b} \equiv [0, -\lambda(\frac{\partial z}{\partial h}(\lambda, h)), 0]^T$ and $\mathbf{m} \equiv [0, m, 0]^T$, where

$$m = -\frac{1}{\mu_0} \lambda \frac{\partial q}{\partial h}(\lambda, h). \quad (69)$$

In this section, for illustrative purposes, it is assumed

$$z(y, h) = \mu_0 h^2 \left(\frac{d_1}{(y-a)^2 + y} - \frac{1}{2y^2} \right) \quad (70)$$

which satisfies the property $\frac{\partial z}{\partial \lambda}(1, 0) = 0$ mentioned previously. For simplicity, consider [Shariff 2014]

$$\eta(y, d) = e^{b_1(g(y)-g(d))g(y)^{b_2}}, \quad (71)$$

$$g(y) = \frac{(y-1)^2}{y} \quad (72)$$

and

$$f(y) = a_1 \phi_1(y) + a_2 \phi_2(y), \quad (73)$$

with the ad hoc values

$$a = 1.2, \quad a_1 = a_2 = 1.0 \text{ kPa}, \quad b_1 = 2, \quad b_2 = 0.5, \quad d_1 = -2 \text{ kPa}$$

for the material constants.

In Figure 2, the nominal stress (T_{22}/λ_2)-strain behavior is depicted for $\lambda_m = 2.5$, and from the figure it is clear that our model produces stiffer stress when a magnetic field is applied and stress softening Mullin's behavior is simulated. The behavior of the stress difference depicted in Figure 3 due to two different magnetic field values is similar to the experimental behavior found in Coquelle and Bossis [2006].

4.1.2. Anisotropy induced by a uniaxial prestretch. Here, uniaxial deformations of the nonvirgin MS material in directions different from the uniaxial prestretch direction are studied. Experiments on these types of deformations on a non-MS material have been done by Machado et al. [2012], and Shariff [2014] has developed a model to successfully describe these deformations. Consider a uniaxial prestretch deformation in the 2-direction (corresponds to 0°) of S -configuration virgin samples defined by

$$\mathbf{U}(\lambda) \equiv \text{diag}(1/\sqrt{\lambda}, \lambda, 1/\sqrt{\lambda}), \quad (74)$$

where $1 \leq \lambda \leq \lambda_m$.

Then a set of smaller S -configuration specimens is cut from each of these preconditioned large samples in different directions and each direction corresponds to an angle θ (the angle subtended, anticlockwise,

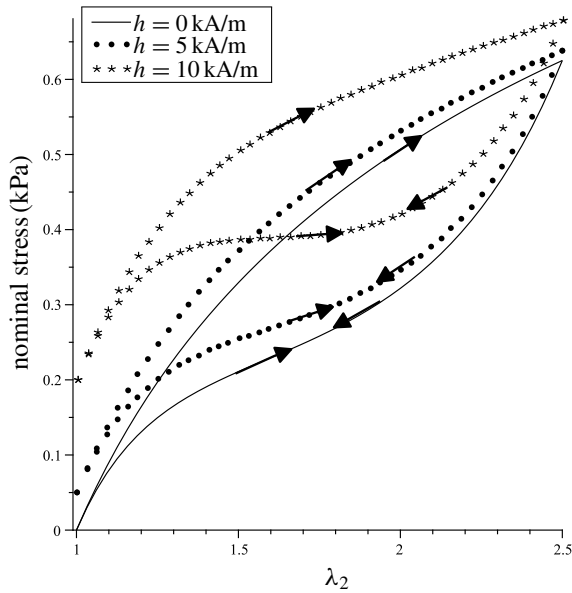


Figure 2. Simple tension in a fixed 2-direction for different magnetic field values.

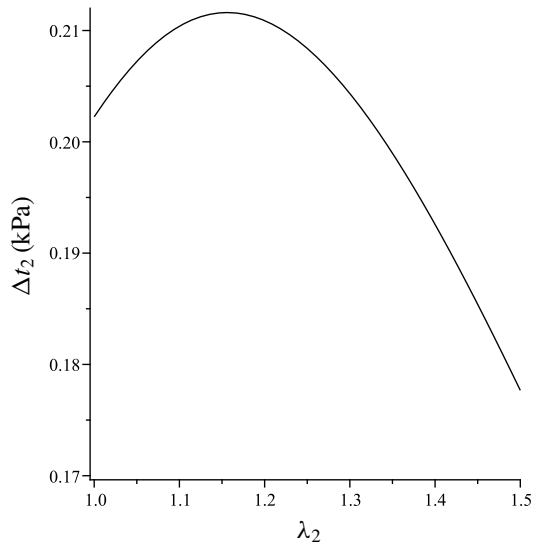


Figure 3. Simple tension in a fixed 2-direction, where $\lambda = \lambda_2$ and $\Delta t_2 = T_{22}/\lambda_2(\lambda, 10) - T_{22}/\lambda_2(\lambda, 0)$.

from the 2 direction). Each of these smaller specimens is then subjected to a uniaxial deformation in one of these directions and we let this direction to be the e_2 direction, where the Cartesian components of

the principal directions of \mathbf{U} are given by

$$\mathbf{e}_1 \equiv \begin{bmatrix} c \\ s \\ 0 \end{bmatrix}, \quad \mathbf{e}_2 \equiv \begin{bmatrix} -s \\ c \\ 0 \end{bmatrix}, \quad \mathbf{e}_3 \equiv \begin{bmatrix} 0 \\ 0 \\ 1 \end{bmatrix}, \quad (75)$$

where $c = \cos(\theta)$, $s = \sin(\theta)$ and $0 \leq \theta \leq \pi/2$. Consider the extremum values

$$\hat{s}_i^{(\max)} = \max_{1 \leq \lambda \leq \lambda_m} \sqrt{\mathbf{e}_i \cdot \mathbf{U}^2(\lambda) \mathbf{e}_i}, \quad \hat{s}_i^{(\min)} = \min_{1 \leq \lambda \leq \lambda_m} \sqrt{\mathbf{e}_i \cdot \mathbf{U}^2(\lambda) \mathbf{e}_i} \quad (76)$$

of the prestretch deformation in the \mathbf{e}_i directions. The extremum values given in (76) are [Shariff 2014]:

$$\hat{s}_1^{(\max)} = \begin{cases} 1, & 1 \geq c \geq \sqrt{\lambda_m(1 + \lambda_m)/(1 + \lambda_m + \lambda_m^2)}, \\ f_c(\lambda_m), & 0 \leq c \leq \sqrt{\lambda_m(1 + \lambda_m)/(1 + \lambda_m + \lambda_m^2)}, \end{cases} \quad (77)$$

$$\hat{s}_1^{(\min)} = \begin{cases} 1, & 0 \leq c \leq \sqrt{\frac{2}{3}}, \\ f_c(c^2/(2(1 - c^2)))^{1/3}, & \sqrt{\frac{2}{3}} \leq c \leq \sqrt{2\lambda_m^3/(1 + 2\lambda_m^3)}, \\ f_c(\lambda_m), & \sqrt{2\lambda_m^3/(1 + 2\lambda_m^3)} \leq c \leq 1, \end{cases} \quad (78)$$

$$\hat{s}_2^{(\max)} = \begin{cases} 1, & 1 \geq s \geq \sqrt{(\lambda_m(1 + \lambda_m))/(1 + \lambda_m + \lambda_m^2)}, \\ f_s(\lambda_m), & 0 \leq s \leq \sqrt{(\lambda_m(1 + \lambda_m))/(1 + \lambda_m + \lambda_m^2)}, \end{cases} \quad (79)$$

$$\hat{s}_2^{(\min)} = \begin{cases} 1, & 0 \leq s \leq \sqrt{\frac{2}{3}}, \\ f_s(s^2/(2(1 - s^2)))^{1/3}, & \sqrt{\frac{2}{3}} \leq s \leq \sqrt{2\lambda_m^3/(1 + 2\lambda_m^3)}, \\ f_s(\lambda_m), & \sqrt{2\lambda_m^3/(1 + 2\lambda_m^3)} \leq s \leq 1, \end{cases} \quad (80)$$

$$\hat{s}_3^{(\max)} = 1, \quad \hat{s}_3^{(\min)} = \frac{1}{\lambda_m}, \quad (81)$$

where

$$f_c(\lambda) = \sqrt{(1/\lambda - \lambda^2)c^2 + \lambda^2}, \quad f_s(\lambda) = \sqrt{(1/\lambda - \lambda^2)s^2 + \lambda^2}. \quad (82)$$

The maximum and minimum values for the principal-direction line elements corresponding to (75) during the deformation of the prestretch nonvirgin material are

$$s_i^{(\max)} = \begin{cases} \hat{s}_i^{(\max)}, & 1 \leq \lambda_i \leq \hat{s}_i^{(\max)}, \\ \lambda_i, & \lambda_i \geq \hat{s}_i^{(\max)}, \end{cases} \quad s_i^{(\min)} = \begin{cases} \hat{s}_i^{(\min)}, & 1 \geq \lambda_i \geq \hat{s}_i^{(\min)}, \\ \lambda_i, & \lambda_i \leq \hat{s}_i^{(\min)}. \end{cases} \quad (83)$$

Here, the magnetic field $\mathbf{h}_l = h\mathbf{e}_2$ is considered. For this type of deformation $\zeta_1 = \zeta_3 = 0$ and $\zeta_2 = 1$. For $\theta = 0^\circ$, $\lambda_1 = \lambda_3$ and the axial nominal stress

$$S_2 = \frac{\eta(\lambda_2, s_2^{(\max)})f(\lambda_2) - \eta(1/\sqrt{\lambda_2}, 1/\sqrt{s_2^{(\max)}})f(1/\sqrt{\lambda_2}) + \lambda_2 \frac{\partial z}{\partial \lambda_2}(\lambda_2, h) - \mu_o h^2/(2\lambda_2^2)}{\lambda_2}. \quad (84)$$

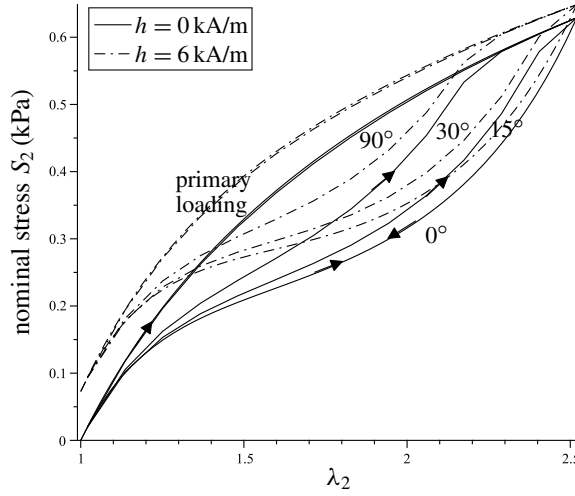


Figure 4. Induced anisotropy represented by the theoretical uniaxial stress-strain responses for the different angles between the first and second loading directions ($\mathbf{h}_l = h\mathbf{e}_2$).

In the case of when θ is nonzero, $\lambda_1 \neq \lambda_3$ in general and

$$S_2 = \frac{\eta(\lambda_2, s_2^{(\max)})f(\lambda_2) - \eta(\lambda_3, s_3^{(\min)})f(\lambda_3) + \lambda_2 \frac{\partial z}{\partial \lambda_2}(\lambda_2, h) - \mu_o h^2 / (2\lambda_2^2)}{\lambda_2}. \quad (85)$$

Note that for the non-0° deformations, the value for λ_3 in (85) is obtained from λ_2 via the equation

$$\eta(\lambda_3, s_3^{(\min)})f(\lambda_3) = \eta(1/(\lambda_2\lambda_3), s_1^{(\min)})f(1/(\lambda_2\lambda_3)), \quad (86)$$

considering the boundary stress condition $T_{33} = -\mu_o h^2 / (2\lambda_2^2)$, the incompressibility condition $\lambda_1\lambda_2\lambda_3 = 1$ and assuming $T_{11} = T_{33}$, where T_{ij} are the components of the total stress \mathbf{T} relative to a basis that coincide with the basis $\{\mathbf{e}_1, \mathbf{e}_2, \mathbf{e}_3\}$.

The anisotropic stress softening behavior for $\lambda_m = 2.5$ is clearly shown in Figure 4, where the behavior for $h = 0$ is similar to the Machado et al. [2012] experiment.

4.2. Anisotropy induced by a simple shear predeformation. The proposed model is based on direction-dependent parameters where their values depend on the principal directions of \mathbf{U} . Hence, it is important to study stress-softening behavior in a sequence of deformations when the principal directions of \mathbf{U} change continuously. An example of such deformation is the simple shear deformations where the principal directions of \mathbf{U} change continuously during the deformation. Shariff [2014] has studied anisotropic simple shear stress softening behavior for non-MS materials and the calculations in this section follow

that paper. Consider the prestretching of a material by a simple shear deformation described by

$$\mathbf{U}^2(\gamma) \equiv \begin{pmatrix} 1 & \gamma & 0 \\ \gamma & 1 + \gamma^2 & 0 \\ 0 & 0 & 1 \end{pmatrix}, \quad (87)$$

where $0 \leq \gamma \leq \gamma_m$ and γ is commonly called *the amount of shear*.

Without loss of generality, the total stress normal to the plane of shear is assumed to be zero, since incompressibility allows the superposition of an arbitrary hydrostatic stress without effecting the deformation. In view of this, the total shear stress is

$$\begin{aligned} \sigma_s &= \left[\eta(\lambda_1, \alpha_1) f(\lambda_1) - \eta(\lambda_2, \alpha_2) f(\lambda_2) + \zeta_1 \lambda_1 \frac{\partial z}{\partial \lambda_1}(\lambda_1, h) - \zeta_2 \lambda_2 \frac{\partial z}{\partial \lambda_2}(\lambda_2, h) \right] c s \\ &\quad + \frac{2}{\lambda_1^2 - \lambda_2^2} [z(\lambda_1, h) - z(\lambda_2, h)] (\mathbf{e}_1 \cdot \mathbf{a})(\mathbf{e}_2 \cdot \mathbf{a}) \gamma c s \\ &= \left[\eta(\lambda_1, \alpha_1) f(\lambda_1) - \eta(\lambda_2, \alpha_2) f(\lambda_2) \right. \\ &\quad \left. + \mu_0 h^2 \left(-d_1 \zeta_1 \lambda_1 \frac{2(\lambda_1 - a) + 1}{((\lambda_1 - a)^2 + \lambda_1)^2} + d_1 \zeta_2 \lambda_2 \frac{2(\lambda_2 - a) + 1}{((\lambda_2 - a)^2 + \lambda_2)^2} + \frac{\zeta_1}{\lambda_1^2} - \frac{\zeta_2}{\lambda_2^2} \right) \right] c s \\ &\quad + \frac{2\mu_0 h^2}{\lambda_1 + \lambda_2} \left(\frac{d_1(2a - 1 - \lambda_1 - \lambda_2)}{[(\lambda_1 - a)^2 + \lambda_1][(\lambda_2 - a)^2 + \lambda_2]} - \frac{\lambda_1 + \lambda_2}{2\lambda_1 \lambda_2} \right) (\mathbf{e}_1 \cdot \mathbf{a})(\mathbf{e}_2 \cdot \mathbf{a}) \gamma c s, \quad (88) \end{aligned}$$

where [Bustamante and Shariff 2015]

$$c = \frac{1}{\sqrt{1 + \lambda_1^2}}, \quad s = \frac{\lambda_1}{\sqrt{1 + \lambda_1^2}}, \quad c^2 - s^2 = -\gamma c s, \quad (89)$$

$$\lambda_1 = \frac{\gamma + \sqrt{\gamma^2 + 4}}{2} \geq 1, \quad \lambda_2 = \frac{1}{\lambda_1} = \frac{\sqrt{\gamma^2 + 4} - \gamma}{2} \leq 1, \quad \lambda_3 = 1. \quad (90)$$

Note that c and s in this section are different from those defined in Section 4.1.2.

4.2.1. Simple shear of the prestretch in the primary shear direction. Consider a simple shear deformation of the prestretched material in the same direction as the primary shear direction of the virgin material [Shariff 2014]. The components of the principal directions of \mathbf{U} of this nonvirgin simple shear are

$$\mathbf{e}_1 \equiv \begin{bmatrix} c \\ s \\ 0 \end{bmatrix}, \quad \mathbf{e}_2 \equiv \begin{bmatrix} -s \\ c \\ 0 \end{bmatrix}, \quad \mathbf{e}_3 \equiv \begin{bmatrix} 0 \\ 0 \\ 1 \end{bmatrix}. \quad (91)$$

For a fixed c and s ,

$$\begin{aligned} s_1^{(\max)} &= \max_{0 \leq \gamma \leq \gamma_m} \sqrt{(\gamma s + c)^2 + s^2}, & s_1^{(\min)} &= \min_{0 \leq \gamma \leq \gamma_m} \sqrt{(\gamma s + c)^2 + s^2}, \\ s_2^{(\max)} &= \max_{0 \leq \gamma \leq \gamma_m} \sqrt{(\gamma c - s)^2 + c^2}, & s_2^{(\min)} &= \min_{0 \leq \gamma \leq \gamma_m} \sqrt{(\gamma c - s)^2 + c^2}, \\ s_3^{(\max)} &= s_3^{(\min)} = 1. \end{aligned}$$

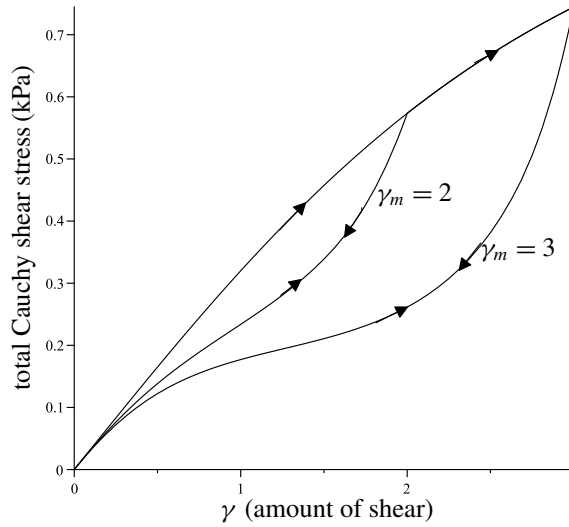


Figure 5. Simple shear loadings and unloadings in the primary shear direction.

After some manipulation, the values

$$s_1^{(\max)} = \sqrt{(\gamma_m s + c)^2 + s^2}, \quad s_1^{(\min)} = 1, \quad 0 \leq \gamma \leq \gamma_m, \quad \gamma_m \geq 0,$$

are obtained. For $0 \leq \gamma_m \leq 2$,

$$s_2^{(\max)} = 1, \quad 0 \leq \gamma \leq \gamma_m,$$

and for $\gamma_m > 2$

$$s_2^{(\max)} = \begin{cases} \sqrt{(\gamma_m c - s)^2 + c^2}, & 0 \leq \gamma \leq (\gamma_m^2 - 4)/(2\gamma_m), \\ 1, & (\gamma_m^2 - 4)/(2\gamma_m) < \gamma \leq \gamma_m. \end{cases}$$

For $\gamma_m > 1$,

$$s_2^{(\min)} = \begin{cases} c, & 0 \leq \gamma < (\gamma_m^2 - 1)/\gamma_m, \\ \sqrt{(\gamma_m c - s)^2 + c^2}, & (\gamma_m^2 - 1)/\gamma_m \leq \gamma \leq \gamma_m, \end{cases}$$

and for $0 \leq \gamma_m \leq 1$

$$s_2^{(\min)} = \sqrt{(\gamma_m c - s)^2 + c^2}, \quad 0 \leq \gamma \leq \gamma_m.$$

The shear stress σ_s for the primary loading is

$$\sigma_s = (f(\lambda_1) - f(\lambda_2))cs. \tag{92}$$

The shear stress for the unloading and reloading of the prestretched material is given by

$$\sigma_s = (\eta_1(\lambda_1, s_1^{(\max)})f(\lambda_1) - \eta_2(\lambda_2, s_2^{(\min)})f(\lambda_2))cs. \tag{93}$$

For illustration purposes the ad-hoc values

$$a = 1.2, \quad a_1 = a_2 = 1.0 \text{ kPa}, \quad b_1 = 1.5, \quad b_2 = 0.5, \quad d_1 = -2 \text{ kPa},$$

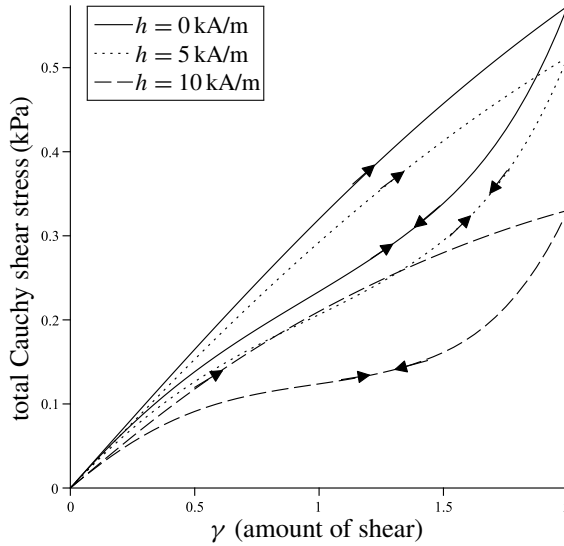


Figure 6. Simple shear loadings and unloadings in the primary shear direction in the presence of the Lagrangean magnetic field $\mathbf{h}_l \equiv [h, 0, 0]^T$.

are used.

Figure 5 depicts the loading and unloading curves for $\gamma_m = 2$ and $\gamma_m = 3$ when $h = 0$. It is clear from Figure 5 that the stress-deformation curves behave as expected.

Only results for constant magnetic fields $\mathbf{h}_l \equiv [h, 0, 0]^T$, $\mathbf{h}_l \equiv [0, h, 0]^T$ and $\mathbf{h}_l \equiv [0, 0, h]^T$ are given, taking note that the conditions in (4) are automatically satisfied. In Figure 6, the stress-strain curves for $\mathbf{h}_l \equiv [h, 0, 0]^T$ are depicted for $h = 0, 5, 10$. From the figure, it is found that the magnitude of the shear stress is reduced, when a magnetic field in the same direction as the shear direction is applied. The results for $\mathbf{h}_l \equiv [0, h, 0]^T$ are depicted in Figure 7, where in this case, a larger shear stress is required in the presence of a magnetic field. It is clear from (88), as expected, the shear stress is not affected by the magnetic field $\mathbf{h}_l \equiv [0, 0, h]^T$; hence, the corresponding graph will not be depicted.

In view of (88), in contrast to the simple tension case described in Section 4.1, no shear stress is required to maintain the undeformed deformation when the magnetic field $h \neq 0$ for the magnetic directions considered in this section.

4.2.2. Simple shear of the prestretch in the opposite direction to the primary loading direction. In this section, the prestretched material is sheared in the direction opposite to the primary direction up to $\gamma = 2$. The components of the principal eigenvectors for this opposite direction shearing are

$$\mathbf{e}_1 \equiv \begin{bmatrix} -c \\ s \\ 0 \end{bmatrix}, \quad \mathbf{e}_2 \equiv \begin{bmatrix} s \\ c \\ 0 \end{bmatrix}, \quad \mathbf{e}_3 \equiv \begin{bmatrix} 0 \\ 0 \\ 1 \end{bmatrix}. \quad (94)$$

Consider the extremum prestretch values

$$\hat{s}_i^{(\max)} = \max_{0 \leq \gamma \leq 2} \sqrt{\mathbf{e}_i \cdot \mathbf{U}^2(\gamma) \mathbf{e}_i}, \quad \hat{s}_i^{(\min)} = \min_{0 \leq \gamma \leq 2} \sqrt{\mathbf{e}_i \cdot \mathbf{U}^2(\gamma) \mathbf{e}_i}, \quad (95)$$

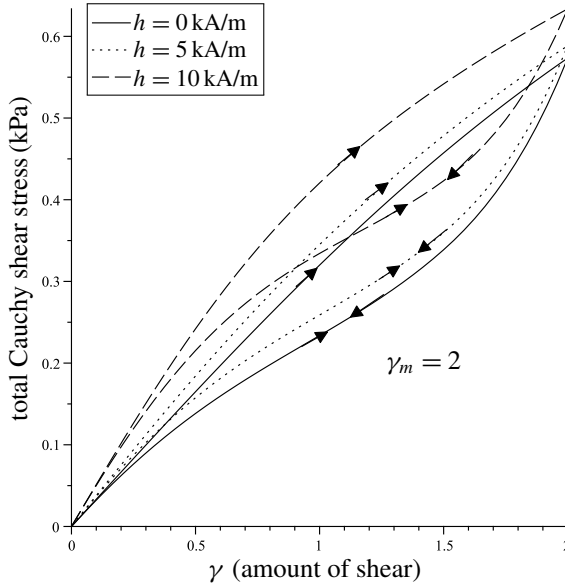


Figure 7. Simple shear loadings and unloadings in the primary shear direction in the presence of the Lagrangean magnetic field $\mathbf{h}_l \equiv [0, h, 0]^T$.

of the line elements of the presheared material in the \mathbf{e}_i directions for $\gamma_m = 2$.

$$\hat{s}_1^{(\max)} = \sqrt{(2s - c)^2 + s^2}, \quad \hat{s}_1^{(\min)} = s,$$

$$\hat{s}_2^{(\max)} = \sqrt{(2c + s)^2 + c^2}, \quad \hat{s}_2^{(\min)} = 1.$$

The maximum and minimum values for the relevant principal-stretch line elements when $0 \leq \gamma \leq 2$ are

$$s_1^{(\max)} = \begin{cases} \hat{s}_1^{(\max)}, & 1 \leq \lambda_1 \leq \hat{s}_1^{(\max)}, \\ \lambda_1, & \hat{s}_1^{(\max)} \leq \lambda_1 \leq 1 + \sqrt{2}, \end{cases}$$

$$s_2^{(\min)} = \begin{cases} \hat{s}_2^{(\min)}, & 1 \geq \lambda_2 \geq \hat{s}_2^{(\min)}, \\ \lambda_2, & \hat{s}_2^{(\min)} \geq \lambda_2 \geq \sqrt{2} - 1, \end{cases}$$

$$s_3^{(\max)} = s_3^{(\min)} = 1.$$

4.2.3. Simple shear of the prestretch in a direction perpendicular to the primary plane of shear. Here, the prestretched material is sheared in a direction perpendicular to the initial plane of shear up to $\gamma = 2$. The components of the principal eigenvectors for this shearing are

$$\mathbf{e}_1 \equiv \begin{bmatrix} 0 \\ s \\ c \end{bmatrix}, \quad \mathbf{e}_2 \equiv \begin{bmatrix} 0 \\ c \\ -s \end{bmatrix}, \quad \mathbf{e}_3 \equiv \begin{bmatrix} 1 \\ 0 \\ 0 \end{bmatrix}. \tag{96}$$

In view of (95), the extremum values of the prestretch line elements are

$$\hat{s}_1^{(\max)} = \sqrt{4s^2 + 1}, \quad \hat{s}_1^{(\min)} = 1, \quad \hat{s}_2^{(\max)} = \sqrt{4c^2 + 1}, \quad \hat{s}_2^{(\min)} = 1.$$

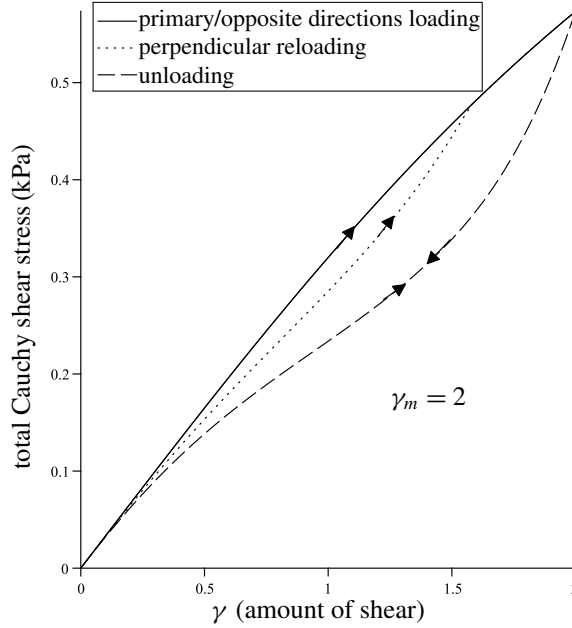


Figure 8. Simple shear in directions different from the preshear direction.

The maximum and minimum values for the relevant principal-stretch line elements for $0 \leq \gamma \leq 2$ are

$$\begin{aligned}
 s_1^{(\max)} &= \begin{cases} \hat{s}_1^{(\max)}, & 1 \leq \lambda_1 \leq \hat{s}_1^{(\max)}, \\ \lambda_1, & \hat{s}_1^{(\max)} \leq \lambda_1 \leq 1 + \sqrt{2}, \end{cases} \\
 s_2^{(\min)} &= \begin{cases} \hat{s}_2^{(\min)}, & 1 \geq \lambda_2 \geq \hat{s}_2^{(\min)}, \\ \lambda_2, & \hat{s}_2^{(\min)} \geq \lambda_2 \geq \sqrt{2} - 1, \end{cases} \\
 s_3^{(\min)} &= s_3^{(\max)} = 1.
 \end{aligned}$$

Figure 8 depicts, for $h = 0$, the results for various loadings given in Sections 4.2.2 and 4.2.3. The theory closely predicts the experimental results of Muhr et al. [1999], where they stated that “the softening is greatest for simple shear in the same direction, least for simple shear in the opposite direction and intermediate for shear at 90 degrees”. The shear stress-strain behavior in the presence of a Lagrangean magnetic field in a direction parallel to the shear direction or perpendicular to the shear direction and parallel to the shear plane or perpendicular to the shear plane is similar to that described in 4.2.1.

5. Conclusions

The motivating key for this work is to provide a phenomenological model that could describe three dimensional anisotropic stress softening behavior (Mullins effect) of MS materials in the presence of a magnetic field, which up-to-date has not been proposed in the literature. The proposed model uses a set of spectral invariants, where each invariant has a clear physical meaning, and hence have an experimental advantage over other types of invariants with no physical interpretation such as the classical invariants

by Spencer and Rivlin [1962]. Due to the absence of relevant experimental data, at the moment we are not concerned with the construction of specific forms of the functions f , η , g and q ; nevertheless, the crude specific forms proposed in this paper seem to reasonably predict the anisotropic stress softening behavior of MS elastomers in the presence of a magnetic field.

Acknowledgements

The authors would like to thank the anonymous reviewers for their contribution towards the development of this paper.

References

- [Bellan and Bossis 2002] C. Bellan and G. Bossis, “Field dependence of viscoelastic properties of MR elastomers”, *Int. J. Modern Physics* **16** (2002), 2447–2453.
- [Boczkowska and Awietjan 2012] A. Boczkowska and S. Awietjan, *Advanced elastomers: technology, properties and applications*, edited by A. Boczkowska, InTech, 2012.
- [Böse et al. 2012] H. Böse, R. Rabindranath, and J. Ehrlich, “Soft magnetorheological elastomers as new actuators for valves”, *J. Intell. Mater. Syst. Struct.* **23** (2012), 989–994.
- [Brown 1966] W. F. Brown, *Magnetoelastic interactions*, Springer Tracts in Natural Philosophy **9**, Springer, Berlin, 1966.
- [Bustamante and Shariff 2015] R. Bustamante and M. H. B. M. Shariff, “A principal axis formulation for nonlinear magnetoelastic deformations: isotropic bodies”, *Eur. J. Mech. A Solids* **50** (2015), 17–27.
- [Coquelle and Bossis 2006] E. Coquelle and G. Bossis, “Mullins effect in elastomers filled with particles aligned by a magnetic field”, *Int. J. Solids Struct.* **43**:25–26 (2006), 7659–7672.
- [Criscione 2003] J. C. Criscione, “Rivlin’s representation formula is ill-conceived for the determination of response functions via biaxial testing”, *J. Elasticity* **70**:1–3 (2003), 129–147.
- [Danas et al. 2012] K. Danas, S. V. Kankanala, and N. Triantafyllidis, “Experiments and modeling of iron-particle-filled magnetorheological elastomers”, *J. Mech. Phys. Solids* **60**:1 (2012), 120–138.
- [Dorfmann and Ogden 2003] A. Dorfmann and R. W. Ogden, “Magnetoelastic modelling of elastomers”, *Eur. J. Mech. A Solids* **22**:4 (2003), 497–507.
- [Dorfmann and Ogden 2004a] A. Dorfmann and R. W. Ogden, “Nonlinear magnetoelastic deformations”, *Q. J. Mech. Appl. Math.* **57**:4 (2004), 599–622.
- [Dorfmann and Ogden 2004b] A. Dorfmann and R. W. Ogden, “Nonlinear magnetoelastic deformations of elastomers”, *Acta Mech.* **167**:1–2 (2004), 13–28.
- [Dorfmann and Ogden 2005] A. Dorfmann and R. W. Ogden, “Some problems in nonlinear magnetoelasticity”, *Z. Angew. Math. Phys.* **56**:4 (2005), 718–745.
- [Eringen and Maugin 1990] A. C. Eringen and G. A. Maugin, *Electrodynamics of continua, I*, Springer, New York, 1990.
- [Farshad and Roux 2004] M. Farshad and M. L. Roux, “A new active noise abatement barrier system”, *Polymer Testing* **23**:7 (2004), 855–860.
- [Ghafoorianfar et al. 2013] N. Ghafoorianfar, X. Wang, and F. Gordaninejad, “On the sensing of magnetorheological elastomers”, in *Sensors and smart structures technologies for civil, mechanical, and aerospace systems*, vol. 8692, edited by J. P. Lynch et al., 2013.
- [Ginder et al. 2001] J. M. Ginder, W. F. Schlotter, and M. E. Nichols, “Magnetorheological elastomers in tunable vibration absorbers”, pp. 103–110 in *Smart structures and materials: damping and isolation*, vol. 4331, edited by D. J. Inman, 2001.
- [Govindjee and Simo 1991] S. Govindjee and J. Simo, “A micro-mechanically based continuum damage model for carbon black-filled rubbers incorporating Mullins’ effect”, *J. Mech. Phys. Solids* **39**:1 (1991), 87–112.
- [Holzapfel and Ogden 2009] G. A. Holzapfel and R. W. Ogden, “On planar biaxial tests for anisotropic nonlinearly elastic solids: a continuum mechanical framework”, *Math. Mech. Solids* **14**:5 (2009), 474–489.

- [Humphrey et al. 1990] J. D. Humphrey, R. K. Strumpf, and F. C. Yin, “Determination of a constitutive relation for passive myocardium, I: A new functional form”, *J. Biomech. Eng.* **112**:3 (1990), 333–339.
- [Hutter et al. 2006] K. Hutter, A. Ursescu, and A. A. F. van de Ven, *Electromagnetic field matter interactions in thermoelastic solids and viscous fluids*, Lecture Notes in Physics **710**, Springer, Berlin, 2006.
- [Itskov et al. 2010] M. Itskov, A. E. Ehret, R. Kazakevičiūtė-Makovska, and G. W. Weinhöhl, “A thermodynamically consistent phenomenological model of the anisotropic Mullins effect”, *Z. Angew. Math. Mech.* **90**:5 (2010), 370–386.
- [Johnson and Beatty 1993] M. A. Johnson and M. F. Beatty, “A constitutive equation for the Mullins effect in stress controlled uniaxial extension experiments”, *Contin. Mech. Thermodyn.* **5**:4 (1993), 301–318.
- [Jolly et al. 1996] M. R. Jolly, J. D. Carlson, and B. C. M. noz, “A model of the behaviour of magnetorheological materials”, *Smart Mater. and Struct.* **5**:5 (1996), 607–614.
- [Kankanala and Triantafyllidis 2004] S. V. Kankanala and N. Triantafyllidis, “On finitely strained magnetorheological elastomers”, *J. Mech. Phys. Solids* **52**:12 (2004), 2869–2908.
- [Kashima et al. 2012] S. Kashima, F. Miyasaka, and K. Hirata, “Novel soft actuator using magnetorheological elastomer”, *IEEE Transactions on Magnetics* **48**:4 (2012), 1649–1652.
- [Kovetz 2000] A. Kovetz, *Electromagnetic theory*, Oxford University Press, Oxford, England, 2000.
- [Lin and Yin 1998] D. H. Lin and F. C. Yin, “A multiaxial constitutive law for mammalian left ventricular myocardium in steady-state barium contracture or tetanus”, *J. Biomech. Eng.* **120**:4 (1998), 504–517.
- [Machado et al. 2012] G. Machado, G. Chagnon, and D. Favier, “Induced anisotropy by the Mullins effect in filled silicone rubber”, *Mech. Mater.* **50** (2012), 70–80.
- [Maugin 1988] G. A. Maugin, *Continuum mechanics of electromagnetoelastic solids*, North-Holland Series in Applied Mathematics and Mechanics **33**, North-Holland Publishing Co., Amsterdam, 1988.
- [Muhr et al. 1999] A. H. Muhr, J. Gough, and I. H. Gregory, “Experimental determination of model for liquid silicone rubber”, pp. 181–187 in *Constitutive models for rubber*, edited by A. Muhr and A. Dorfmann, A. A. Balkema, Rotterdam, Netherlands, 1999.
- [Mullins 1947] L. Mullins, “Effect of stretching on the properties of rubber”, *J. Rubber Res.* **16** (1947), 275–289.
- [Ogden and Roxburgh 1999] R. W. Ogden and D. G. Roxburgh, “A pseudo-elastic model for the Mullins effect in filled rubber”, *R. Soc. Lond. Proc. Ser. A Math. Phys. Eng. Sci.* **455**:1988 (1999), 2861–2877.
- [Ogden and Steigmann 2010] R. W. Ogden and D. J. Steigmann (editors), *Mechanics and electrostatics of magneto- and electro-elastic materials*, CISM International Centre for Mechanical Sciences **527**, Springer, Vienna, 2010.
- [Pawelski 2001] H. Pawelski, “Softening behaviour of elastomeric media after loading in changing directions”, pp. 27–36 in *Constitutive models for rubber II*, edited by D. Besdo et al., A. A. Balkema, Lisse, Netherlands, 2001.
- [Shariff 2000] M. H. B. M. Shariff, “Strain energy function for filled and unfilled rubberlike material”, *Rubber Chem. Technol.* **73**:1 (2000), 1–18.
- [Shariff 2006] M. H. B. M. Shariff, “An anisotropic model of the Mullins effect”, *J. Eng. Math.* **56**:4 (2006), 415–435.
- [Shariff 2008] M. H. B. M. Shariff, “Nonlinear transversely isotropic elastic solids: an alternative representation”, *Q. J. Mech. Appl. Math.* **61**:2 (2008), 129–149.
- [Shariff 2014] M. H. B. M. Shariff, “Direction dependent orthotropic model for Mullins materials”, *Int. J. Solids Struct.* **51**:25–26 (2014), 4357–4372.
- [Shariff 2016] M. H. B. M. Shariff, “Anisotropic separable free energy functions for elastic and non-elastic solids”, *Acta Mech.* (2016), 1–25.
- [Simo 1987] J. C. Simo, “On a fully three-dimensional finite-strain viscoelastic damage model: formulation and computational aspects”, *Comput. Method Appl. M.* **60**:2 (1987), 153–173.
- [Spencer 1971] A. J. M. Spencer, “Theory of invariants”, pp. 239–353 in *Continuum physics*, vol. 1, edited by A. C. Eringen, Academic Press, New York, 1971.
- [Spencer and Rivlin 1962] A. J. M. Spencer and R. S. Rivlin, “Isotropic integrity bases for vectors and second-order tensors I”, *Arch. Rational Mech. Anal.* **9** (1962), 45–63.

- [Steigmann 2004] D. J. Steigmann, “Equilibrium theory for magnetic elastomers and magnetoelastic membranes”, *Int. J. Non-Linear Mech.* **39**:7 (2004), 1193–1216.
- [Vu and Steinmann 2010] D. K. Vu and P. Steinmann, “Material and spatial motion problems in nonlinear electro- and magneto-elastostatics”, *Math. Mech. Solids* **15**:2 (2010), 239–257.
- [Zhu et al. 2012] J.-T. Zhu, Z.-D. Xu, and Y.-Q. Guo, “Magnetoviscoelasticity parametric model of an MR elastomer vibration mitigation device”, *Smart Mater. Struct.* **21**:7 (2012), 075034.

Received 13 Jan 2016. Revised 14 Jun 2016. Accepted 20 Jun 2016.

M. H. B. M. SHARIFF: shariff@kustar.ac.ae

Department of Applied Mathematics and Science, Khalifa University of Science, Technology and Research, Sharjah, United Arab Emirates

ROGER BUSTAMANTE: rogbusta@ing.uchile.cl

Departamento de Ingeniería Mecánica, Universidad de Chile, Beauchef 850 Santiago Centro, Chile

PREDICTIVE MODELING OF MECHANICAL PROPERTIES OF METAL FILLED ANODIC ALUMINUM OXIDE

VLADIMIR V. BARDUSHKIN, YULIA I. SHILYAEVA, SERGEY A. GAVRILOV, MAXIM V. SILIBIN,
VICTOR B. YAKOVLEV, MIKHAIL L. ZHELUDKEVICH AND NATALIA I. POPENKO

Filling dielectric porous matrices, particularly anodic aluminum oxide, with metal confers a promising solution for nanocomposite creation. In this regard, the problem of estimating and predicting the physical and mechanical properties of such materials is of prime importance. The present work focuses on the numerical modeling of the effective and ultimate stress-strain (under compression) characteristics of nanocomposites based on anodic aluminum oxide with unidirectional filamentary pores filled with different metals (In, Sn, and Zn). The dependences of the tensor components of the effective elastic moduli, coefficients of elastic anisotropy (in different directions), and compression strength (along the nanowires) on the structure parameters and the concentration of nanowires are investigated.

1. Introduction

One of the possible ways to create nanocomposites is filling dielectric ordered porous matrices with metal. In this regard, porous anodic aluminum oxide (AAO) [Yao et al. 2008] is the most widely used candidate. AAO-based nanocomposites have unique characteristics and are promising for a wide range of possible applications for optical systems and sensors, as well as functional parts of solar and thermoelectric batteries [Poddubny et al. 2013]. The high thermal stability and the possibility of precise control of geometrical parameters and consequently size-dependent properties make AAO the material of choice in many cases. Produced by a two-step anodization by the method of [Masuda and Fukuda 1995], AAO has a high degree of ordering — representing an array of hexagonal cells with cylindrical pores. It allows the creation of nanocomposites with well controllable properties and is an ideal model structure for fundamental research. Moreover, AAO-based template synthesis is an alternative to expensive lithographic techniques.

The mechanical properties of nanocomposites become very important when considering practical applications. The basis of such analysis is the calculation of performance (effective) and ultimate stress-strain properties [Shermergor 1977; Pobedrya 1984; Khoroshun et al. 1989; Mori and Tanaka 1973; Kanaun and Levin 1993; Milton 2002; Buryachenko 2007; Böhm 2013; Bardushkin and Yakovlev 2011; Sychev and Bardushkin 2013]. Thus, the task of developing predictive methods for physical and mechanical properties of matrix composites like “AAO-nanowires” is very relevant.

The problem of predicting the effective elastic properties of heterogeneous media has been considered by many authors. A detailed review of studies on this subject can be found in [Buryachenko 2007; Böhm 2013; Bardushkin and Yakovlev 2011; Sychev and Bardushkin 2013].

Keywords: nanocomposite, modeling, anodic aluminum oxide, performance elastic characteristics, compressive strength.

Predicting the distribution of local (internal) stress and deformation fields is key for a correct analysis of the ultimate strength properties of heterogeneous media. The local elastic characteristics include operators (tensors) of stress/deformation concentration and volumetric density of deformation energy [Buryachenko 2007; Böhm 2013; Bardushkin and Yakovlev 2011; Sychev and Bardushkin 2013]. The distribution analysis of the above characteristics allows correct predictions of the behavior of materials under loads (especially extreme). It can provide recommendations on the selection of components taking into account the concentration of heterogeneous elements and features of the shape structure and inclusion orientation in the material matrix.

The concept of concentration tensors connecting the average values in the phase with average values in the whole body (or in a representative volume element) was introduced by Hill [1963]. The solution to the problem of strength concentration on the surface of an ellipsoidal heterogeneity in an anisotropic medium was obtained in [Laws 1977; Kunin and Sosnina 1973; Buryachenko and Lipanov 1986; Yakovlev and Nikitin 1997; Shermergor and Yakovlev 1998; Maslov 1987]. Concentration functionals and operators expressing stress and strain in a heterogeneous body by using those in a homogeneous body with efficient features were described in [Pobedrya and Gorbachev 1984]. In [Pobedrya and Gorbachev 1984; Gorbachev 1989], explicit analytical expressions for the concentration tensors in the case of a layered composite and in the case of a cylindrical hole in an infinite homogeneous isotropic medium were obtained. The concentration tensors in an n -dimensional elastic medium with an n -dimensional spherical inclusion were suggested in [Gorbachev and Mikhailov 1993]. By assuming homogeneity of the stress and strain fields (via the generalized singular approximation used to determine the effective properties of heterogeneous media [Shermergor 1977]), the expressions for calculating these operators were obtained in [Yakovlev 2000; Kolesnikov et al. 2005; Bardushkin and Yakovlev 2005; Bardushkin et al. 2013], in which the effect of composite microstructures on their local characteristics was investigated.

2. Formulation of the problem and model

The aim of this work is to solve the two main issues of predicting the elastic-strength properties of nanocomposites based on anodic aluminum oxide with filamentary pores filled with metal (In, Sn, and Zn), namely:

- (1) predicting the operational (effective) elastic characteristics, and
- (2) predicting the ultimate stress-strain (under compression) characteristics.

The problem of predicting the mechanical properties can be solved firstly by constructing a model taking into account the structure of the nanocomposites by introducing a dimensionless structural parameter associated with the concentration of heterogeneous elements; and secondly by performing the numerical modeling of elastic-strength characteristics.

2.1. Introduction of a dimensionless structural parameter. The following points should be resolved before creating a numerical model for the performance and ultimate stress-strain properties of matrix composites like “AAO-nanowires”:

- (a) a correlation between the distance between the nanowires and structural parameters that can be measured directly, and

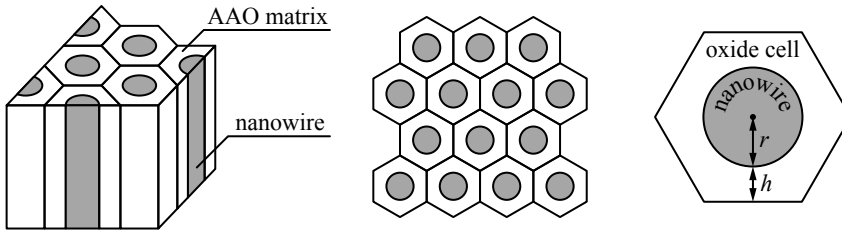


Figure 1. Schematic representation of the composite structure (left), several elementary volumes (middle), an elementary volume in the cross-sectional plane (right).

(b) the derivation of mathematical formulas convenient for numerical analysis without losing information about the structure of the composite [Bardushkin and Yakovlev 2011; 2005; Kolesnikov et al. 2005; Bardushkin et al. 2013; Shilyaeva et al. 2013b; 2013a; 2014].

The actual structure of composites must be taken into account when conducting simulations, as described earlier [Shilyaeva et al. 2014]. As it is known, AAO consists of densely packed hexagonal cells that are adjacent to each other with their sides. Therefore, we assume that in a considered uniaxially reinforced composite the components are isotropic and the position of nanowires in the template is random. However, the material is assumed to be statistically homogeneous as a whole. This assumption results in the existence of an average distance between wires that may be related to the loading of the metal in the composite matrix. An average volume element in the shape of a regular hexagonal prism with one cylindrical nanowire oriented along the z axis in the center can be considered. Some of these elementary volumes are schematically shown in Figure 1.

One can assume that each nanowire has an average radius r and the distance from the center of a regular hexagon to its side is $r + h$ (see Figure 1, right). The base area of the elementary cell is then $S = 2\sqrt{3}(r + h)^2$, and the cross sectional area of the wire is $S_w = \pi r^2$. Defining the concentration of wires as $v_w = S_w/S$, we have $v_w = \pi/(2\sqrt{3}(1 + h/r)^2)$, $v_m = 1 - v_w$.

The index “ w ” here and below denotes the values related to the metallic wires, while “ m ” indicates those related to the matrix.

The characteristic parameter h/r defining the structure of the composite can thus be represented by the concentration of nanowires as

$$\frac{h}{r} = \sqrt{\frac{\pi}{2\sqrt{3} \cdot v_w}} - 1. \quad (1)$$

It is evident that the maximum theoretical value of the concentration of nanowires is observed when $h/r \rightarrow 0$, which corresponds to $v_w \rightarrow \pi/(2\sqrt{3}) \approx 0.9$. The minimum value of the concentration of wires is observed when $h/r \rightarrow \infty$; hence, $v_w \rightarrow 0$. This range of concentrations for nanowires corresponds to the boundaries of the applicability for the suggested approach of simulating such materials.

2.2. Elastic characteristics. The effective elastic characteristics of the considered composites can be determined by the fourth-rank tensor c^* (“ $*$ ” here and below indicates that composite’s effective characteristics are considered) connecting the average values of stresses $\langle \sigma_{ij}(\mathbf{r}) \rangle$ and strains $\langle \epsilon_{kl}(\mathbf{r}) \rangle$ in the material via

$$\langle \sigma_{ij}(\mathbf{r}) \rangle = c_{ijkl}^* \langle \epsilon_{kl}(\mathbf{r}) \rangle, \quad i, j, k, l = 1, 2, 3,$$

where \mathbf{r} is the radius-vector of a random point in the medium. Angular brackets here and below define the procedure of ensemble averaging. For statistically homogeneous composites, i.e., when performing the hypothesis of ergodicity, it coincides with the averaging in volume [Shermergor 1977; Pobedrya 1984; Khoroshun et al. 1989; Mori and Tanaka 1973; Kanaun and Levin 1993; Milton 2002; Buryachenko 2007; Böhm 2013; Bardushkin and Yakovlev 2011; Sychev and Bardushkin 2013; Walter et al. 1993; Mitin et al. 2001].

The equations for the equilibrium of an elastic heterogeneous medium should be solved to conduct a correct analysis of elastic properties of composites which depend on the interaction of elements of heterogeneity, composition, shape, orientation, and concentration of components. The ratio for the numerical calculations of an effective elastic moduli tensor c^* is usually hard to obtain. Therefore, various approximations are used for its calculation. Within the framework of the generalized singular approximation of the theory of random fields [Shermergor 1977], only the singular component of Green's tensor of equations for the equilibrium is used. It depends only on the Dirac delta function. A homogeneous reference body whose material constants are included in the final expression for calculating c^* is also introduced. The physical meaning of the generalized singular approximation is the assumption of homogeneity of the stress and strain fields within the element of heterogeneity. In this case, the expression for calculating c^* is (indices omitted) [Shermergor 1977; Walter et al. 1993; Mitin et al. 2001]

$$c^* = \langle c(\mathbf{r})(I - g(\mathbf{r})c''(\mathbf{r}))^{-1} \rangle \langle (I - g(\mathbf{r})c''(\mathbf{r}))^{-1} \rangle^{-1}, \quad (2)$$

where I is the fourth-rank unit tensor; $c(\mathbf{r})$ is elastic modulus tensor; the double primes indicate the difference between the corresponding parameters of a heterogeneous medium and a homogeneous reference body, characteristics of which are denoted hereinafter by the superscript "ref": $c''(\mathbf{r}) = c(\mathbf{r}) - c^{\text{ref}}$; $g(\mathbf{r})$ is the integral of the singular component of the second derivative of Green's tensor of equations for the equilibrium, which is a fourth-rank tensor. Components g_{ijkl} of $g(\mathbf{r})$ tensor can be calculated upon knowing components a_{ijkl} of the fourth-rank tensor A as

$$a_{ijkl} = -\frac{1}{4\pi} \int n_k n_j t_{il}^{-1} d\Omega, \quad (3)$$

and then symmetrization [Shermergor 1977; Walter et al. 1993; Mitin et al. 2001] is performed using pairs of i and j and k and l indices.

In (3), $d\Omega = \sin \theta d\theta d\phi$ is an element of the solid angle in a spherical system of coordinates; t_{il}^{-1} are the elements of the reverse matrix T where elements $t_{il} = c_{ijkl}^{\text{ref}} n_k n_j$; n_k and n_j ($k, j = 1, 2, 3$) are components of a vector of an external normal to the inclusion's surface. For ellipsoidal inclusions with principal semiaxes l_1, l_2 , and l_3 , the components of the normal vector are determined by the relationship

$$n_1 = \frac{1}{l_1} \sin \theta \cos \phi, \quad n_2 = \frac{1}{l_2} \sin \theta \sin \phi, \quad n_3 = \frac{1}{l_3} \cos \theta.$$

The relation (2), as shown in [Bardushkin and Yakovlev 2011], can be used to calculate the effective characteristics of a statistically homogeneous matrix composite with ellipsoidal inclusions oriented relative to each other.

As it was mentioned, under the condition of ergodicity it is possible to use volume averaging for each component of the composite [Shermergor 1977; Pobedrya 1984; Khoroshun et al. 1989; Mori and Tanaka 1973; Kanaun and Levin 1993; Milton 2002; Buryachenko 2007; Böhm 2013; Bardushkin and Yakovlev

2011; Sychev and Bardushkin 2013]. Then, the averaging operation over the entire material volume for some random variable $a(\mathbf{r})$ is reduced to summing

$$\langle a(\mathbf{r}) \rangle = \sum_s v_s \langle a_s(\mathbf{r}) \rangle,$$

where v_s is the volumetric concentration of the s -type component and $a_s(\mathbf{r})$ is random variable $\sum_s v_s = 1$ corresponding to the specified component. In particular, for a two-component composite containing isotropic inclusions and the matrix, the procedure of averaging is reduced to summing

$$\langle a(\mathbf{r}) \rangle = v_w a_w + v_m a_m. \quad (4)$$

When considering inclusions in the form of nanowires with principal semiaxes $l_1 = l_2 = r$ and $l_3 \rightarrow \infty$ for the normal vector components, the obtained ratios are

$$n_1 = \frac{1}{r} \sin \theta \cos \phi, \quad n_2 = \frac{1}{r} \sin \theta \sin \phi, \quad n_3 \rightarrow 0.$$

The elastic characteristics of the matrix can be taken as the parameters of the reference body [Khoroshun et al. 1989]. Then in (2) $c''(\mathbf{r}) = c(\mathbf{r}) - c_m$, and $c''(\mathbf{r}) = c_w - c_m$ in calculations for the nanowires and $c''(\mathbf{r}) = 0$ for the matrix. Considering (4), (2) will take the form for calculating the effective elastic properties of composites as

$$c^* = (v_w c_w (I - g_w (c_w - c_m))^{-1} + v_m c_m) \times (v_w (I - g_w (c_w - c_m))^{-1} + v_m I)^{-1}. \quad (5)$$

In (5), c_w and c_m are the elastic moduli tensors for the wires and matrix, respectively; g_w is a tensor $g(\mathbf{r})$ (for the wires) with the components calculated by (3).

2.3. Ultimate strength characteristics. When solving the problem of predicting ultimate strength properties of composites under compression, the situation associated with the fast fracture of materials is considered. The solution is based on the method of predicting the ultimate strength properties of matrix composites under compression, which is based on the use of the stress concentration operator (fourth-rank tensor). This operator binds the local values of the stress tensor $\sigma_{ij}(\mathbf{r})$ with the average external stress of material $\langle \sigma_{kl}(\mathbf{r}) \rangle$ [Buryachenko 2007; Böhm 2013; Bardushkin and Yakovlev 2011; Sychev and Bardushkin 2013]

$$\sigma_{ij}(\mathbf{r}) = K_{ijkl}^\sigma(\mathbf{r}) \langle \sigma_{kl}(\mathbf{r}) \rangle, \quad i, j, k, l = 1, 2, 3. \quad (6)$$

The kind and magnitude of the stress $\sigma_{ij}(\mathbf{r})$ occurring inside the heterogeneous element of any type can be determined knowing the nature of the external impact $\langle \sigma_{kl}(\mathbf{r}) \rangle$ based on the definition (6) for $K^\sigma(\mathbf{r})$. It should be emphasized that the emerging local (internal) stresses either in the matrix or in the wires will differ in appearance and size from the applied impact $\langle \sigma_{kl}(\mathbf{r}) \rangle$ [Bardushkin and Yakovlev 2011].

The idea of using the relation (6), providing a means to link macroscopic stresses with microscopic stresses within the microstructure of the material, in order to predict the ultimate strength characteristics was described in [Fritsch et al. 2009; 2010; 2013; Pichler and Hellmich 2011]. The solution to the problem of predicting the strength characteristics for the matrix composites (within the framework of the generalized singular approximation of random field theory [Shermergor 1977]) is given in [Kolesnikov et al. 2014].

The matrix plays a fundamental role in the composites by making the material monolithic and redistributing the mechanical stresses between all elements of heterogeneity. The matrix breakdown leads to full failure of the material. Therefore, it is believed [Kolesnikov et al. 2014; Bardushkin et al. 2015] that stress applied to the composite (for example, compression in a certain direction) becomes destructive only when the internal stress in the matrix exceeds its ultimate strength. Here the magnitude of the internal stress in the matrix under external impact is compared to the known value of the ultimate strength of the matrix set experimentally or taken from the respective references. The value of the ultimate strength of the matrix should correspond to the external stress (for example, compression performed in the same direction as that for the considered composite) applied to a homogeneous body consisting only of the matrix material.

The equations for the equilibrium of an elastic heterogeneous medium must be solved for the correct analysis of the local stress concentration in the composite that allows the consideration of the interaction of elements of heterogeneity, composition and structure of the material, and concentration of wires. However, in general (as well as when calculating the effective elastic properties c^*), it is impossible to derive the relation for numerical calculations of the stress concentration operator $K^\sigma(\mathbf{r})$. Therefore, we use the generalized singular approximation of the theory of random fields for its evaluation (see Section 2.2). In this case, the expression for $K^\sigma(\mathbf{r})$ is (indices omitted) [Bardushkin and Yakovlev 2011; Sychev and Bardushkin 2013]

$$K^\sigma(\mathbf{r}) = c(\mathbf{r})(I - g(\mathbf{r})c''(\mathbf{r}))^{-1} \times \langle c(\mathbf{r})(I - g(\mathbf{r})c''(\mathbf{r}))^{-1} \rangle^{-1}. \quad (7)$$

The analysis of (7) shows that when evaluating the local stress-strain state of a heterogeneous medium using a stress concentration operator, the information about an external mechanical impact is excluded, because $K^\sigma(\mathbf{r})$ depends only on the material parameters of the medium and the composite structure. As before (see Section 2.2), taking the elastic characteristics of the matrix as the parameters for the reference body and considering (4), (7) will take the form

$$K_m^\sigma = c_m(v_w c_w (I - g(c_w - c_m))^{-1} + v_m c_m)^{-1}. \quad (8)$$

3. Numerical calculations

3.1. Numerical modeling of the elastic properties. For unidirectional matrix composites with isotropic components, like metal nanowires of In, Sn, and Zn in the AAO matrix, the model calculations for the effective elastic moduli c^* were carried out. Information about elastic characteristics of the composite components is known from the literature [Grigor'ev and Meilikhov 1991; Xia et al. 2004; Gu et al. 2004], and is given in Table 1.

Material	Young's modulus E (GPa)	Poisson's ratio ν
Indium	10.5	0.46
Tin	48	0.33
Zinc	115	0.325
Aluminum oxide	140	0.32

Table 1. Elastic characteristics of the composite components.

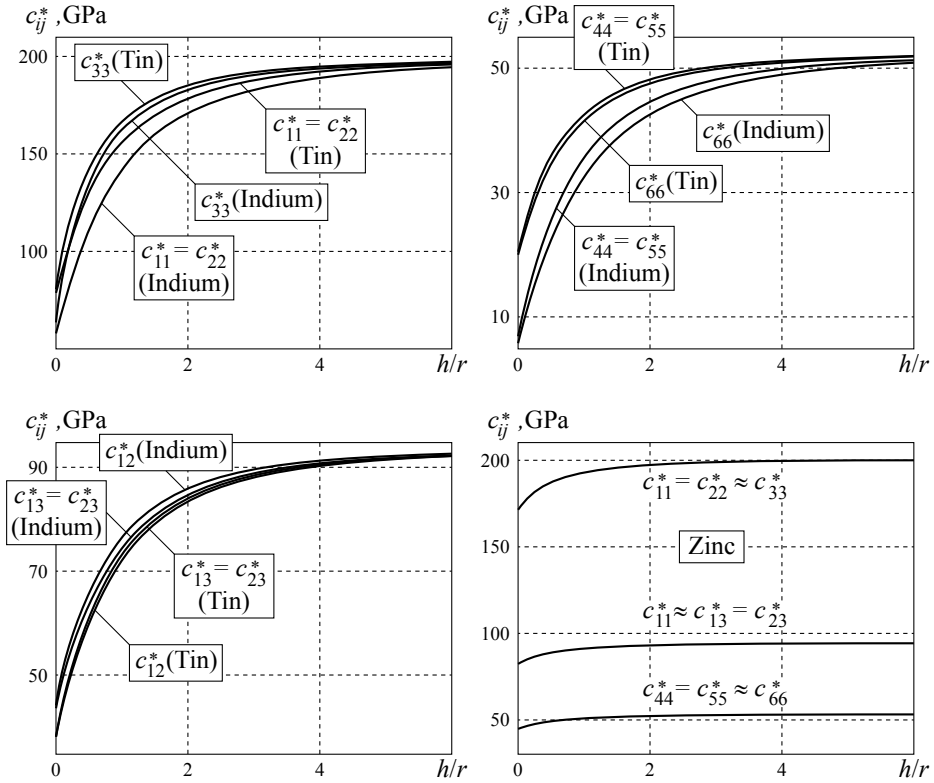


Figure 2. Effective elastic moduli as a function of h/r for model composites.

Considering wires as ellipsoids of rotation with semiaxes $l_1 = l_2 = r = 1$ and $l_3 \rightarrow \infty$, calculations of the tensor components c^* depending on the structural parameter h/r were carried out using (5).

In the calculations, we used tensors written in the matrix form. The nonzero elements c_{ij} ($i, j = 1, \dots, 6$) of the symmetrical matrix of the elastic moduli tensor c for an isotropic material can be expressed through its Young's modulus E and Poisson's ratio ν [Shermergor 1977]:

$$c_{11} = c_{22} = c_{33} = \frac{E(1-\nu)}{(1+\nu)(1-2\nu)};$$

$$c_{44} = c_{55} = c_{66} = \frac{E}{2(1+\nu)};$$

$$c_{12} = c_{13} = c_{23} = \frac{E\nu}{(1+\nu)(1-2\nu)}.$$

The results of the numerical modeling of the nonzero elements c_{ij}^* of the matrix of the effective elastic moduli tensor c^* depending on the structural parameter h/r are given in Figure 2.

The model calculations of the elastic anisotropy coefficients A_x and A_z (along x and z axes respectively) were also carried out: $A_x = (c_{11}^* - c_{12}^*)/(2c_{44}^*)$, $A_z = (c_{33}^* - c_{23}^*)/(2c_{66}^*)$. The values of the anisotropy coefficient A_y (along the y axis) are similar to the values of the anisotropy coefficient A_x .

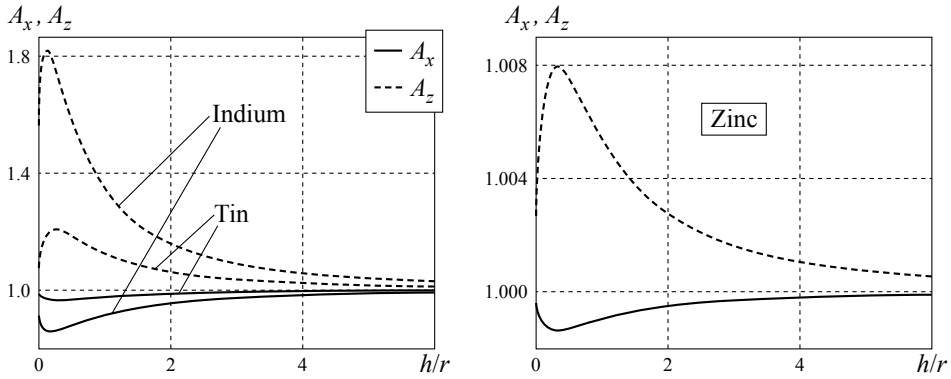


Figure 3. Anisotropy coefficients as a function of h/r for model composites.

Figure 3 shows the results of the numerical modeling of the anisotropy coefficients A_x and A_z depending on the structural parameter h/r .

Note that in Figures 2 and 3, the resulting curves for the composite with Zn nanowires are shown separately. This is because the symmetry of the effective elastic properties of the material is close to isotropic (see the elastic moduli of the components presented in Table 1). Thus, for the effective elastic moduli the relations can be expressed as $c_{11}^* = c_{22}^* \approx c_{33}^*$, $c_{44}^* = c_{55}^* \approx c_{66}^*$, $c_{12}^* \approx c_{13}^* = c_{23}^*$, $c_{66}^* = (c_{11}^* - c_{12}^*)/2$, and are applied [Shermergor 1977], and the anisotropy coefficients A_x and A_z for this composite are slightly different from 1.

3.2. Numerical modeling of the ultimate stress properties. This subsection discusses failure of composites when exposed to compressive stress directed along the z axis (i.e., along the wires). This situation is most frequently encountered in practice.

The analysis of the dependence of compressive strength limits on the composition and concentration of components was carried out for model composites.

The computational procedure used to determine the ultimate compressive characteristics for model composites was arranged in the work as follows. It was assumed that the external action $\langle \sigma_{kl}(\mathbf{r}) \rangle$ (MPa) was given in the laboratory coordinate system $Oxyz$ by a (3×3) matrix with the only nonzero element $\sigma_{33} = B$. First, any value of the structural parameter h/r was recorded for the model composite. Then the operator K_m^σ was calculated by formula (8). Then a certain positive value B was assumed. Then, elements σ_{ij} ($i, j = 1, 2, 3$) of the matrix of the stress tensor (in AAO) were calculated based on the definition (6) of the stress concentration operator. After that the comparison of the values of the computed element σ_{33} with the value of the limit of compressive stress for aluminum oxide equal to $\sigma_m = 4000$ MPa [Grigor'ev and Meilikhov 1991, p. 63] was made. If $\sigma_{33} < \sigma_m$, then value B was increased by 1 MPa and the calculation of the stress tensor matrix elements σ_{ij} in AAO was repeated again. The computational procedure in each case was stopped as soon as the condition $\sigma_{33} \geq \sigma_m$ was met, and the last value of B was taken as the compressive strength limit of the whole composite in the direction parallel to the wires. Then a new value of the structural parameter h/r was recorded and the calculation of the compressive strength limit for the model composite was repeated again.

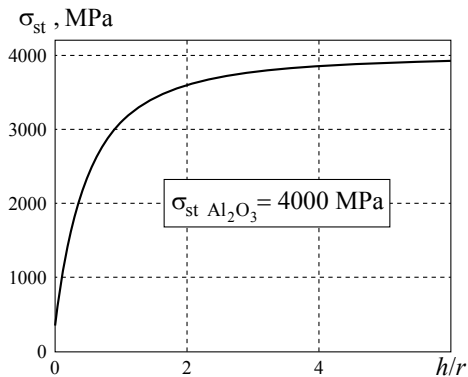


Figure 4. Compressive strength as a function of h/r for model composites.

Figure 4 shows the results of the numerical modeling of compressive strength limits σ_{st} for the above described load mode of model composites depending on the structural parameter.

4. Conclusions

The performed model studies allow us to draw the following conclusions.

The considered composites possess hexagonal symmetry for the effective elastic properties [Shermergor 1977], since for nonzero elements c_{ij}^* in the symmetric matrix tensor c^* the following relations were performed: $c_{11}^* = c_{22}^*, c_{44}^* = c_{55}^*, c_{13}^* = c_{23}^*, c_{66}^* = (c_{11}^* - c_{12}^*)/2$ (Figure 2).

When $0 < h/r < 6$, the dependence of the nonzero c_{ij}^* values on the average distance between the wires is essentially nonlinear. When $h/r > 6$ (i.e., when $\nu_w \rightarrow 0$), c_{ij}^* stabilizes around values equal to the isotropic elastic moduli of AAO, for the elements c_{ij} of the matrix elastic moduli tensor of which the following relations are valid: $c_{11} = 200.34; c_{44} = 53.03; c_{12} = 94.28$. Indeed, when $h/r > 6$, the following equations for c_{ij}^* start executing: $c_{11}^* = c_{22}^* = c_{33}^*, c_{44}^* = c_{55}^* = c_{66}^*, c_{12}^* = c_{13}^* = c_{23}^*$ (Figure 2). Moreover, $A_x \rightarrow 1, A_z \rightarrow 1$ (Figure 3). The strongest variation of anisotropy occurs along z axis. The values of anisotropy parameters in the composites show the strongest deviations from 1 when changing the structural parameter h/r in the range of 0 to 2.

In the considered composites, the dependence of σ_{st} on the parameter h/r has a steady and nonlinear character; moreover at $0.3 < h/r < 3$ this nonlinearity manifests itself most significantly.

Numerical modeling showed that the values σ_{st} are the same for composites with In, Sn, and Zn wires. This result is explained by the known stress properties of the aluminum oxide and the direction of the applied compression load. This follows from the simulation results of changing the values of the stress concentration tensor components K_m^σ (in matrix), described in [Bardushkin et al. 2013], since these values were similar for composites with In, Sn, and Zn wires.

At average distances between the wires $h/r > 6$ there occurs a stabilization of σ_{st} values. With the increase of h/r there is an increase in σ_{st} values of the ultimate stress limit for the composites up to the values $\sigma_m = 4000$ MPa for ultimate strength of the AAO matrix.

At average distances between the wires $h/r < 1$, the ultimate stress limit value σ_{st} is most sensitive to changes in its volume fraction.

Acknowledgement

This work was financially supported by the Ministry of Education and Science of the Russian Federation: reference number 2014/101.

References

- [Bardushkin and Yakovlev 2005] V. V. Bardushkin and V. B. Yakovlev, “Characteristics of the local stress-strain state in a statistically homogeneous matrix composites”, *Deformatsiya i Razrushenie Materialov* **2005**:9 (2005), 38–42. In Russian.
- [Bardushkin and Yakovlev 2011] V. Bardushkin and V. Yakovlev, Механика микроструктур: эффективные и локальные свойства текстурированных поликристаллов и композитов, Lambert Academic, Saarbrücken, Germany, 2011.
- [Bardushkin et al. 2013] V. V. Bardushkin, Y. I. Shilyaeva, and V. B. Yakovlev, “Stress and strain concentration in anodic aluminum oxide having pores filled with metallic nanowires”, *Deformatsiya i Razrushenie Materialov* **2013**:10 (2013), 24–29. In Russian.
- [Bardushkin et al. 2015] V. V. Bardushkin, V. B. Yakovlev, A. P. Sychev, A. A. Sychev, D. A. Kirillov, and A. I. Sorokin, “Predicting the limiting strength of nontextured matrix composites”, *Russ. Eng. Res.* **35**:1 (2015), 14–18.
- [Böhm 2013] H. J. Böhm, “A short introduction to basic aspects of continuum micromechanics”, Report 206, Institute of Lightweight Design and Structural Biomechanics (ILSB), University of Technology, Vienna, 2013, <https://www.ilsb.tuwien.ac.at/links/downloads/ilsbrep206.pdf>.
- [Buryachenko 2007] V. A. Buryachenko, *Micromechanics of heterogeneous materials*, Springer, Berlin, 2007.
- [Buryachenko and Lipanov 1986] V. A. Buryachenko and A. M. Lipanov, “Stress concentration at ellipsoidal inclusions and effective thermoelastic properties of composite materials”, *Soviet Applied Mechanics* **22**:11 (1986), 1103–1109.
- [Fritsch et al. 2009] A. Fritsch, L. Dormieux, C. Hellmich, and J. Sanahuja, “Mechanical behavior of hydroxyapatite biomaterials: an experimentally validated micromechanical model for elasticity and strength”, *J. Biomed. Mater. Res. A* **88A**:1 (2009), 149–161.
- [Fritsch et al. 2010] A. Fritsch, C. Hellmich, and L. Dormieux, “The role of disc-type crystal shape for micromechanical predictions of elasticity and strength of hydroxyapatite biomaterials”, *Phil. Trans. R. Soc. A* **368**:1917 (2010), 1913–1935.
- [Fritsch et al. 2013] A. Fritsch, C. Hellmich, and P. Young, “Micromechanics-derived scaling relations for poroelasticity and strength of brittle porous polycrystals”, *J. Appl. Mech.* **80**:2 (02/04 2013), 020905.
- [Gorbachev 1989] V. I. Gorbachev, “Operators of stress and strain concentration in elastic bodies”, *Raschety na prochnost* **30** (1989), 124–130. In Russian.
- [Gorbachev and Mikhailov 1993] V. I. Gorbachev and A. L. Mikhailov, “The stress concentration tensor in the case of an n -dimensional elastic space with spherical inclusions”, *Vesn. Mosk. Univ. (1)* **48**:2 (1993), 78–83. In Russian; translated in *Moscow Univ. Mech. Bull.* **48**:2 (1993), 27–33.
- [Grigor’ev and Meilikhov 1991] I. S. Grigor’ev and E. Z. Meilikhov (editors), Физические величины: справочник, Energoatomizdat, Moscow, 1991.
- [Gu et al. 2004] P. Gu, H. Miao, Z. T. Liu, X. P. Wu, and J. H. Zhao, “Investigation of elastic modulus of nanoporous alumina membrane”, *J. Mater. Sci.* **39**:10 (2004), 3369–3373.
- [Hill 1963] R. Hill, “Elastic properties of reinforced solids: some theoretical principles”, *J. Mech. Phys. Solid.* **11**:5 (1963), 357–372.
- [Kanaun and Levin 1993] S. K. Kanaun and V. M. Levin, Метод эффективного поля в механике композитных материалов, Izd. Petrozavodsk. Univ., Petrozavodsk, 1993.
- [Khoroshun et al. 1989] L. P. Khoroshun, B. P. Maslov, and P. V. Leshchenko, Прогнозирование эффективных свойств пьезоактивных композитных материалов, Naukova Dumka, Kiev, 1989.
- [Kolesnikov et al. 2005] V. I. Kolesnikov, V. V. Bardushkin, V. B. Yakovlev, and A. P. Sychev, “Influence of the microstructure on local values of stresses and strains in fibrous composite”, *Russ. Eng. Res.* **25**:8 (2005), 19–25.

- [Kolesnikov et al. 2014] V. I. Kolesnikov, V. V. Bardushkin, V. B. Yakovlev, A. P. Sychev, D. A. Kirillov, and A. I. Sorokin, “On the method of predicting extreme strength characteristics of matrix composites using operator of stress concentration”, *Ekolog. Vestn. Nauchn. Tsentrov ChES* **1** (2014), 45–51. In Russian.
- [Kunin and Sosnina 1973] I. A. Kunin and E. G. Sosnina, “Stress concentration on an ellipsoidal inhomogeneity in an anisotropic elastic medium”, *J. Appl. Math. Mech.* **37**:2 (1973), 287–296.
- [Laws 1977] N. Laws, “The determination of stress and strain concentrations at an ellipsoidal inclusion in an anisotropic material”, *J. Elasticity* **7**:1 (1977), 91–97.
- [Maslov 1987] B. P. Maslov, “Stress concentration in an isotropic matrix bonded by anisotropic fibers”, *Prikl. Mekh.* **23**:10 (1987), 73–79. In Russian; translated in *Sov. Appl. Mech.* **23**:10 (1987), 963–969.
- [Masuda and Fukuda 1995] H. Masuda and K. Fukuda, “Ordered metal nanohole arrays made by a two-step replication of honeycomb structures of anodic alumina”, *Science* **268**:5216 (1995), 1466–1468.
- [Milton 2002] G. W. Milton, *The theory of composites*, Cambridge Monographs on Applied and Computational Mathematics **6**, Cambridge University Press, 2002.
- [Mitin et al. 2001] B. S. Mitin, M. M. Serov, and V. B. Yakovlev, “The crystallographic texture and properties of metal materials, received by the PDME-method”, *Mat. Sci. Eng., A* **304–306**:1–2 (2001), 637–640.
- [Mori and Tanaka 1973] T. Mori and K. Tanaka, “Average stress in matrix and average elastic energy of materials with misfitting inclusions”, *Acta Metall.* **21**:5 (1973), 571–574.
- [Pichler and Hellmich 2011] B. Pichler and C. Hellmich, “Upscaling quasi-brittle strength of cement paste and mortar: a multi-scale engineering mechanics model”, *Cement Concrete Res.* **41**:5 (2011), 467–476.
- [Pobedrya 1984] B. E. Pobedrya, Механика композиционных материалов, Izd. MGU, Moscow, 1984.
- [Pobedrya and Gorbachev 1984] B. E. Pobedrya and V. I. Gorbachev, “Stress and strain concentration in composite materials”, *Mekh. Kompoz. Mater. (Riga)* **20**:2 (1984), 141–148. In Russian; translated in *Mech. Compos. Mater.* **20**:2 (1984), 207–214.
- [Poddubny et al. 2013] A. Poddubny, I. Iorsh, P. Belov, and Y. Kivshar, “Hyperbolic metamaterials”, *Nat. Photon* **7**:12 (2013), 948–957.
- [Shermergor 1977] T. D. Shermergor, Теория упругости микронеоднородных сред, Nauka, Moscow, 1977.
- [Shermergor and Yakovlev 1998] T. D. Shermergor and V. B. Yakovlev, “Stress concentration at the cavity surface inhomogeneity in the textured geophysical medium”, *Izv. RAN Fizika Zemli* **1** (1998), 81–89. In Russian.
- [Shilyaeva et al. 2013a] Y. I. Shilyaeva, V. V. Bardushkin, S. A. Gavrilov, M. V. Silibin, V. B. Yakovlev, and O. V. Pyatilova, “Bulk density of the energy of deformation in an anodic aluminum oxide with pores filled by threadlike metal nanocrystals”, *Russ. J. Phys. Chem. A* **87**:11 (2013), 1870–1874.
- [Shilyaeva et al. 2013b] Y. I. Shilyaeva, V. V. Bardushkin, M. V. Silibin, S. A. Gavrilov, V. B. Yakovlev, and O. V. Pyatilova, “Effect of the structure and thermoelastic properties of components on the average stress in anodic aluminum oxide having pores filled with metallic nanowires”, *Inorg. Mater.* **49**:7 (2013), 676–680.
- [Shilyaeva et al. 2014] Y. I. Shilyaeva, V. V. Bardushkin, S. A. Gavrilov, M. V. Silibin, V. B. Yakovlev, N. I. Borgardt, R. L. Volkov, D. I. Smirnov, and M. L. Zheludkevich, “Melting temperature of metal polycrystalline nanowires electrochemically deposited into the pores of anodic aluminum oxide”, *Phys. Chem. Chem. Phys.* **16**:36 (2014), 19394–19401.
- [Sychev and Bardushkin 2013] A. P. Sychev and V. V. Bardushkin, Микромеханика трибокомполитов: напряженно-деформированное состояние, износ и разрушение, Lambert Academic, Saarbrücken, Germany, 2013.
- [Walter et al. 1993] K. Walter, T. I. Ivankina, A. N. Nikitin, V. Voytus, T. D. Shermergor, and V. B. Yakovlev, “Determination of the effective physical properties of anisotropic geological materials from texture analysis”, *Doklady Earth Sciences* **319A**:6 (1993), 12–17.
- [Xia et al. 2004] Z. Xia, L. Riester, B. W. Sheldon, W. A. Curtin, J. Liang, A. Yin, and J. M. Xu, “Mechanical properties of highly ordered nanoporous anodic alumina membranes”, *Rev. Adv. Mater. Sci.* **6** (2004), 131–139.
- [Yakovlev 2000] V. B. Yakovlev, “Local stress-strain conditions of textured polycrystals under high pressure”, *High Pressure Res.* **17**:3–6 (2000), 375–383.
- [Yakovlev and Nikitin 1997] V. B. Yakovlev and A. N. Nikitin, “Influence of the orientation of an isolated quartz granule inside textured mountain rock on the distribution of local stress near its surface”, *J. Earth Pred. Res.* **6**:2 (1997), 235–243.

[Yao et al. 2008] J. Yao, Z. Liu, Y. Liu, Y. Wang, C. Sun, G. Bartal, A. M. Stacy, and X. Zhang, “Optical negative refraction in bulk metamaterials of nanowires”, *Science* **321**:5891 (2008), 930.

Received 2 Feb 2016. Revised 18 May 2016. Accepted 13 Jun 2016.

VLADIMIR V. BARDUSHKIN: bardushkin@mail.ru

*Department of Intellectual Technical Systems, National Research University of Electronic Technology,
Bld. 1, Shokin Square, Zelenograd, Moscow, 124498, Russia*

YULIA I. SHILYAEVA: shylyaeva@gmail.com

*Department of Intellectual Technical Systems, National Research University of Electronic Technology,
Bld. 1, Shokin Square, Zelenograd, Moscow, 124498, Russia*

SERGEY A. GAVRILOV: pcfme@mieee.ru

*Department of Intellectual Technical Systems, National Research University of Electronic Technology,
Bld. 1, Shokin Square, Zelenograd, Moscow, 124498, Russia*

MAXIM V. SILIBIN: sil_m@mail.ru

*Department of Intellectual Technical Systems, National Research University of Electronic Technology,
Bld. 1, Shokin Square, Zelenograd, Moscow, 124498, Russia*

VICTOR B. YAKOVLEV: yakovlev@mieee.ru

*Department of Intellectual Technical Systems, National Research University of Electronic Technology,
Bld. 1, Shokin Square, Zelenograd, Moscow, 124498, Russia*

MIKHAIL L. ZHELUDKEVICH: mzheludkevich@ua.pt

*Institute of Materials Research, Helmholtz-Zentrum Geesthacht, Zentrum für Material- und Küstenforschung,
Max-Planck-Straße 1, D-21502 Geesthacht, Germany*

and

Department of Materials and Ceramic Engineering/CICECO, University of Aveiro, Portugal

NATALIA I. POPENKO: n.popenko@mail.ru

*Department of Intellectual Technical Systems, National Research University of Electronic Technology,
Bld. 1, Shokin Square, Zelenograd, Moscow, 124498, Russia*

THE HEMISPHERICAL NANOPIT AT THE PLANE BOUNDARY OF AN ELASTIC HALF-SPACE SUBJECTED TO STATICALLY EQUIVALENT SHEAR TRACTIONS

CHANGWEN MI, ZHONGWEI SUN AND DEMITRIS KOURIS

The elastic deformation of a semi-infinite substrate containing a nanosized hemispherical pit on its plane boundary crucially relies on the mechanical response of the pit surface. In this paper, we develop a micromechanical model that couples Gurtin and Murdoch's model of surface mechanics with the classical theory of elasticity, and we explicitly evaluate the stress concentration, displacement and stress distribution resulting from a family of statically equivalent shear tractions applied on the pit surface. We found that two intrinsic dimensionless parameters, both constructed from the characteristic length and material properties, govern the highly localized elastic field. Both the magnitude and sign of these parameters are of great importance. Negative values tend to increase stress concentrations, whereas positive ones have the opposite effect. We further highlight the consequences of our analysis by comparing a number of shear tractions that correspond to the same torque. The comparison provides the means of evaluating the degree of difference in elastic fields in the immediate vicinity of statically equivalent force distributions.

1. Introduction

The discontinuities in geometry and load distribution are primary causes of stress concentrations that affect the otherwise smooth stress variations in elastic solids. The presence of geometric defects and concentrated loads typically results in high stresses that are multiple times greater than their nominal values in small and localized regions [Barber 2010]. Experimental methods and advanced theoretical and numerical analysis are means of determining stress concentrations. Many results of practical engineering importance can be found in the literature [Young and Budynas 2002].

Nevertheless, recent advancements in surface/interface mechanics call for a reevaluation of stress concentrations near geometric defects at the nanoscale [Wang et al. 2011]. It is a fact that the area-to-volume ratio of an elastic element is inversely proportional to its characteristic length [Sharma et al. 2003; Mi and Kouris 2014b]. The order of magnitude of this ratio can be as large as nine as the relevant characteristic length goes from the macroscopic level down to the nanoscale. At such a small length scale, the contribution of surface strain energy becomes comparable or even dominant to that of its bulk counterpart in the total strain energy stored in the system [Streitz et al. 1994; Wang et al. 2011]. The linearly elastic model specifically tailored for a coherent surface/interface proposed by Gurtin and Murdoch [1975; 1978] has gained major popularity in a continuous effort to couple surface effects with the classical theory of elasticity [Sharma et al. 2003; Mi and Kouris 2006; 2014a; 2014b; He and Li 2006; Kushch et al. 2013; Steigmann and Ogden 1999]. Closed-form, semianalytical and numerical solutions have all been developed to investigate the consequences of material surface/interface on both

Keywords: surface mechanics, nanopit, half-space, torsional loading, stress concentration.

the overall effective modulus and the localized elastic field [Wang et al. 2011]. Among these works, stress concentration near geometric defects at the nanoscale is one of the most important foci [He and Li 2006; Mi and Kouris 2013].

Theoretical analysis performed within the context of Gurtin–Murdoch’s surface mechanics model and the classical theory of elasticity shows that the introduction of surface effects inevitably calls for a modification to the solution predicted by the classical theory of elasticity alone. The net effect is dependent on the type of surface model and the material properties describing the mechanical behavior of a solid surface. For example, for a spherical nanocavity embedded in an infinite or semi-infinite elastic, substrate positive surface material parameters tend to alleviate the stress concentration effect, in the case of a metal surface [He and Li 2006; Mi and Kouris 2013; 2015]. This argument is supported by molecular dynamics simulations of a spherical cavity inside an aluminum substrate axially loaded at a high strain rate [Mi et al. 2011]. It can also be expected that the inclusion of a surface mechanics model worsens the stress concentration, provided that the sign of surface materials properties is reversed.

While previous studies focus on the stress concentration behavior near a nanoscale geometric defect subjected merely to nontorsional loads, the present work is directed towards the investigation of stress concentrations under torsional deformation modes. When a twisting moment is transmitted through a rigid-sphere embedded in an elastic medium, shear tractions develop on the surface of the rigid inclusion [Hill 1966; Miyao et al. 1975]. In geotechnical engineering, both the static and dynamic behaviors of rigid inclusions provide practical means of exploring the response of infrastructure foundations resting in soil environments [Kausel 2010; Osman and Rouainia 2012]. Rigid inclusions also find applications in offshore engineering, where vessels and floating structures are supported by anchors of different shapes. In large scale systems, attention is typically paid to the dynamic propagation of elastic waves generated by programming the motion of a distant rigid sphere or by applying dynamic loads on the surface of a distant void. Stress distributions in the vicinity of the rigid sphere or cavity are another concern [Eringen 1957]. Torsion is one of the most important loading conditions considered in the literature [Reissner and Sagoci 1944; Williams 1971; Chadwick and Johnson 1971; Zakout et al. 1999].

The behavior of these solutions due to a rigid sphere or void at the nanoscale is intricate and requires further consideration. These problems naturally arise in nanoelectromechanical systems, particularly in those systems involving structural elements made from soft materials. Since both the bulk and surface material properties of soft materials are several orders of magnitude lower than those of metals [Gere and Goodno 2009; Markidou et al. 2005; Białopiotrowicz and Jańczuk 2002; Weijs et al. 2014], particles of secondary phases easily serve as rigid inclusions. In this case, torsional loading naturally kicks in, due to the strong resistance of rigid particles to both volume and shape changes. As an early attempt to reach this goal, here we consider a nanosized hemispherical pit at the plane boundary of an elastic half-space subjected to a family of statically equivalent shear tractions.

The static equivalence means that the first moment of any traction mode with respect to the z -axis reduces to the same torque. The effects of the pit surface were modeled by the coherent surface model of Gurtin and Murdoch. This model consists of three components: a definition of surface strain, a surface constitutive relation, and a force-balance law, as detailed in the original article [Gurtin and Murdoch 1978] as well as in the main body of the present paper. The method of displacement potential renders us an efficient solution strategy for a three-dimensional torsional problem like the one we are examining [Barber 2010]. A single Boussinesq displacement potential function represented by an infinite series is sufficient

to yield the required solution that satisfies a given shear traction boundary condition. The obtained solution converges rapidly as a function of the number of terms included in the series and is available in closed-form for certain forms of shear tractions. This approach is capable of generating displacements and stresses at any point in the pitted half-space, including the stress concentration conditions at the pit surface.

We show that the resultant elastic field is extremely localized and is dependent upon two key intrinsic dimensionless parameters that are constructed from the pit radius, shear modulus of the half-space, and the residual surface tension and shear modulus of the pit surface. The surface material parameter that represents the dilatational deformation of an area element turns out to be irrelevant to twisting deformation. Depending on both the magnitude and sign of the two intrinsic dimensionless parameters, the pit surface model could alleviate or aggravate the stress concentration and distribution to a certain extent. Dimension analysis suggests that the pit surface effects are much more significant for a soft solid than for a metal material. In addition, by comparing different modes of shear tractions resulting in the exact same torque, the developed solution provided us a means of examining the degree of difference in elastic stresses near statically equivalent force distributions.

In Section 2, we derive a micromechanical model to determine the displacements and stresses in the half-space, which we use to derive both closed-form and semianalytical solutions in Section 3. The causes and consequences of these solutions will also be discussed in detail in this section. Finally, in Section 4, we discuss a number of conclusions drawn from the theoretical and numerical analysis.

2. Method of solution

We consider a hemispherical pit of radius a , centered at the free surface of a semi-infinite elastic solid, as shown in Figure 1. The center of the pit was chosen as the common origin for the cylindrical (r, θ, z) and spherical (R, φ, θ) coordinates. The elastic half-space is modeled as an isotropic and linearly elastic material with shear modulus G and Poisson's ratio ν . The external loading is modeled by a family of statically equivalent shear tractions applied on the hemispherical pit surface. The net moment of these shear tractions with respect to the symmetry axis z corresponds to the exact same torque T . The mechanical property of the pit surface is characterized by the residual surface stress τ_0 and two surface Lamé constants λ_0 and μ_0 .

The method of displacement potentials was adopted to tackle the present problem. For the case of axial symmetric torsion in the absence of body forces, a single harmonic function (e.g., λ_3) is sufficient to represent the solution. This harmonic function is part of the well known Boussinesq displacement potentials that was first proposed by Boussinesq in his memoirs in 1888, and later quoted by Todhunter and Pearson [2010]. The harmonic function λ_3 automatically satisfies the elastostatic Navier's equation

$$\nabla^2 \mathbf{u} + \frac{1}{1-2\nu} \nabla(\nabla \cdot \mathbf{u}) = \mathbf{0}, \quad (1)$$

via the representation $2G\mathbf{u} = \nabla \times (\mathbf{k}\lambda_3)$, where \mathbf{u} is the displacement vector and \mathbf{k} denotes a unit vector oriented in the z -direction. The displacement potential λ_3 could be related to the more familiar Papkovitch–Neuber solution to the equilibrium equation of displacements (1) via [Barber 2010]

$$\phi = -\frac{1}{4(1-\nu)} \nabla \times (\mathbf{k}\lambda_3). \quad (2)$$

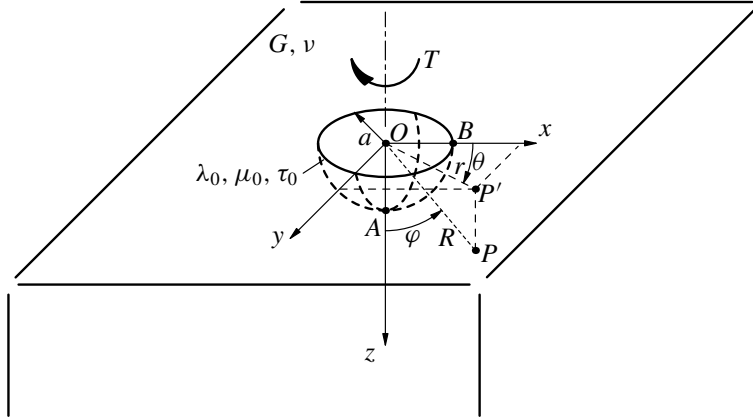


Figure 1. Geometry of the problem.

In terms of spherical coordinates, the displacements resulting from the single torsional potential λ_3 read

$$2Gu_R = \frac{1}{R} \frac{\partial \lambda_3}{\partial \theta}, \quad 2Gu_\varphi = \frac{\cot \varphi}{R} \frac{\partial \lambda_3}{\partial \theta}, \quad 2Gu_\theta = -\frac{\cos \varphi}{R} \frac{\partial \lambda_3}{\partial \varphi} - \sin \varphi \frac{\partial \lambda_3}{\partial R}. \quad (3)$$

The change of variable $\mu = \cos[\varphi]$ transforms the displacement components into

$$2Gu_R = \frac{1}{R} \frac{\partial \lambda_3}{\partial \theta}, \quad 2Gu_\varphi = \frac{\mu}{R\sqrt{1-\mu^2}} \frac{\partial \lambda_3}{\partial \theta}, \quad 2Gu_\theta = \sqrt{1-\mu^2} \left(\frac{\mu}{R} \frac{\partial \lambda_3}{\partial \mu} - \frac{\partial \lambda_3}{\partial R} \right). \quad (4)$$

Recall that under the condition of axial symmetry, all derivatives with respect to θ vanish and hence

$$u_R = u_\varphi = 0, \quad 2Gu_\theta = \sqrt{1-\mu^2} \left(\frac{\mu}{R} \frac{\partial \lambda_3}{\partial \mu} - \frac{\partial \lambda_3}{\partial R} \right). \quad (5)$$

The corresponding stress components are then given by

$$\begin{aligned} \sigma_{RR} = \sigma_{\varphi\varphi} = \sigma_{\theta\theta} = \sigma_{R\varphi} &= 0, \\ \frac{\sigma_{R\theta}}{\sqrt{1-\mu^2}} &= \frac{1}{2R} \frac{\partial \lambda_3}{\partial R} - \frac{1}{2} \frac{\partial^2 \lambda_3}{\partial R^2} + \frac{1}{2R^2(1-\mu^2)} \frac{\partial^2 \lambda_3}{\partial \theta^2} - \frac{\mu}{R^2} \frac{\partial \lambda_3}{\partial \mu} + \frac{\mu}{2R} \frac{\partial^2 \lambda_3}{\partial R \partial \mu}, \\ \sigma_{\varphi\theta} &= \frac{\mu}{R} \frac{\partial \lambda_3}{\partial R} + \frac{\mu}{2} \frac{\partial^2 \lambda_3}{\partial R^2} - \frac{(1+\mu^2)}{2R^2} \frac{\partial \lambda_3}{\partial \mu} + \frac{(1-\mu^2)}{2R} \frac{\partial^2 \lambda_3}{\partial R \partial \mu}. \end{aligned} \quad (6)$$

Since $P_n[\cos \varphi]/R^{n+1}$, where P_n is the Legendre polynomial with the argument $\mu = \cos[\varphi]$, is a spherical harmonic function for an arbitrary integer n [Arfken and Weber 2013], a more general representation can be written in the form

$$\lambda_3 = G \sum_{n=0}^{\infty} A_n \frac{a^{2n+3}}{R^{2n+1}} P_{2n}[\mu], \quad (7)$$

where A_n stands for the unknown coefficients to be determined from the boundary conditions. The shear modulus and power function of the pit radius were introduced to make the unknown coefficients dimensionless. It should also be noted that in this representation only even orders of Legendre polynomials were incorporated in order to clear tractions at the straight boundary of the pitted half-space.

Upon substituting the potential function (7) into (5) and (6), the nonzero displacement and stress components become

$$2Gu_\theta = G\sqrt{1-\mu^2} \sum_{n=0}^{\infty} \left\{ A_n \frac{a^{2n+3}}{R^{2n+2}} ((2n+1)P_{2n}[\mu] + \mu P'_{2n}[\mu]) \right\}, \tag{8}$$

$$\sigma_{R\theta} = -\frac{1}{2}G\sqrt{1-\mu^2} \sum_{n=0}^{\infty} \left\{ A_n \frac{a^{2n+3}}{R^{2n+3}} (2n+3)((2n+1)P_{2n}[\mu] + \mu P'_{2n}[\mu]) \right\}, \tag{9}$$

$$\sigma_{\varphi\theta} = -\frac{(1-\mu^2)}{2}G \sum_{n=1}^{\infty} A_n \frac{a^{2n+3}}{R^{2n+3}} \{ (2n+2)P'_{2n}[\mu] + \mu P''_{2n}[\mu] \}.$$

The above expressions can be simplified to

$$2Gu_\theta = -G \sum_{n=0}^{\infty} \left\{ A_n \frac{a^{2n+3}}{R^{2n+2}} P^1_{2n+1}[\mu] \right\}, \tag{10}$$

$$\sigma_{R\theta} = \frac{1}{2}G \sum_{n=0}^{\infty} \left\{ A_n \frac{a^{2n+3}}{R^{2n+3}} (2n+3)P^1_{2n+1}[\mu] \right\}, \quad \sigma_{\varphi\theta} = -\frac{1}{2}G \sum_{n=1}^{\infty} \left\{ A_n \frac{a^{2n+3}}{R^{2n+3}} P^2_{2n+1}[\mu] \right\}. \tag{11}$$

by the introduction of the recurrence relation of Legendre polynomials [Arfken and Weber 2013]

$$P'_{2n+1}[\mu] = (2n+1)P_{2n}[\mu] + \mu P'_{2n}[\mu], \tag{12}$$

and the associated Legendre function of the first kind [loc. cit.]

$$P^m_n[\mu] = (-1)^m (1-\mu^2)^{m/2} \frac{d^m}{d\mu^m} P_n[\mu]. \tag{13}$$

At the straight boundary of the half-space, as illustrated by (6) and (11),

$$\sigma_{\varphi R} = \sigma_{\varphi\varphi} = 0, \quad \sigma_{\varphi\theta} = -\frac{1}{2} \sum_{n=1}^{\infty} \left\{ A_n \frac{a^{2n+3}}{R^{2n+3}} P^2_{2n+1}[0] \right\}. \tag{14}$$

The parity relation satisfied by the associated Legendre functions exemplifies that $P^m_n[\mu]$ is an odd function provided that $n+m$ is an odd number [Arfken and Weber 2013]. As a result, the only nonzero stress component $\sigma_{\varphi\theta}$ also disappears on the straight boundary of the half-space $\mu = 0$.

As one of the most adopted models of surface mechanics, Gurtin and Murdoch [1975] chose to treat a solid surface as an elastic layer of material boundary whose thickness is vanishingly small. Within the context of their theory, the fundamental equations that govern the mechanical behavior of the pit surface (i.e., the surface version of the displacement-strain relation, surface constitutive law and force

equilibrium condition) can be formulated as [Gurtin and Murdoch 1978]

$$E_{\alpha\beta} = \frac{1}{2}((\nabla_S \mathbf{u})_{\alpha\beta} + (\nabla_S \mathbf{u})_{\beta\alpha}), \tag{15}$$

$$\Sigma_{\alpha\beta} = \tau_0 \delta_{\alpha\beta} + 2(\mu_0 - \tau_0)E_{\alpha\beta} + (\lambda_0 + \tau_0)E_{\gamma\gamma} \delta_{\alpha\beta} + \tau_0 (\nabla_S \mathbf{u})_{\alpha\beta}, \quad \Sigma_{3\alpha} = \tau_0 (\nabla_S \mathbf{u})_{3\alpha}, \tag{16}$$

$$\sigma_{ij} n_j = (\nabla_S \cdot \Sigma)_i + T_i^{(\mathbf{n})}, \tag{17}$$

where E stands for the 2×2 surface strain tensor defined on the hemispherical pit surface with unit normal vector $\mathbf{n} = -\mathbf{e}_R$. Its four components are the same as the corresponding ones in the bulk strain tensor when confined to the pit surface. In contrast, the surface stress tensor Σ is defined as a 3×2 superficial tensor, i.e., only those three of its nine components applied perpendicular to the pit surface were not taken into account [Mogilevskaya et al. 2010]. As a result, the surface stress tensor is not a symmetric one, a well known property possessed by its bulk counterpart. To completely describe the mechanical response of the pit surface, three surface moduli (τ_0 , λ_0 and μ_0) are required.

Particularly, the first term in the right hand side of the first equation of (16) states that the two normal components Σ_{11} and Σ_{22} do not vanish in the absence of external loads. Namely, this term is deformation-independent. Nonetheless, if we decompose the work done by the surface stress tensor against the surface strain field, the contribution due to this term will only enter into the resultant area component but not the distortional one. Consequently, this deformation-independent term is not compatible with the torsional deformation considered in the present work. Its effects should be studied in terms of loading conditions that result in area/volume changes [He and Li 2006; Mogilevskaya et al. 2008; Mi and Kouris 2013].

It is also worth mentioning that the net traction at the pit surface does not vanish—in contrast, it must be balanced by the surface divergence of the surface stress. Equation (17) directly bridges the gap between surface mechanics and the classical bulk elasticity.

The above unique properties of a solid material surface serve as a fundamental tool for understanding the various counter-classical phenomena that have been observed in nanoscale materials and structures. The finite curvature of radius a of the hemispherical pit surface suggests that its surface mechanics effects are of primary importance when compared to those of the half-space straight boundary. As a result, we have chosen not to account for the latter in the present work.

In (15) and (16), the explicit expressions of the surface gradient of displacements should be self-explanatory in Cartesian coordinates. In spherical coordinates, however, unit coordinate vectors (\mathbf{e}_R , \mathbf{e}_φ , \mathbf{e}_θ) are themselves functions of the angular coordinates (φ , θ). Consequently, the rate of change of unit vectors with respect to spherical coordinate variables must be also considered. Based on the definition of surface strain, the surface gradient of displacements can simply be extracted from the bulk displacement gradient projected onto the pit surface

$$\begin{aligned} (\nabla_S \mathbf{u})_{\varphi\varphi} &= \frac{1}{R} \left(u_R + \frac{\partial u_\varphi}{\partial \varphi} \right), & (\nabla_S \mathbf{u})_{\varphi\theta} &= \frac{1}{R} \left(\frac{1}{\sin \varphi} \frac{\partial u_\varphi}{\partial \theta} - \frac{\cos \varphi}{\sin \varphi} u_\theta \right), \\ (\nabla_S \mathbf{u})_{\theta\varphi} &= \frac{1}{R} \frac{\partial u_\theta}{\partial \varphi}, & (\nabla_S \mathbf{u})_{\theta\theta} &= \frac{1}{R \sin \varphi} \left(\frac{\partial u_\theta}{\partial \theta} + \cos \varphi u_\varphi + \sin \varphi u_R \right), \\ (\nabla_S \mathbf{u})_{R\varphi} &= \frac{1}{R} \left(\frac{\partial u_R}{\partial \varphi} - u_\varphi \right), & (\nabla_S \mathbf{u})_{R\theta} &= \frac{1}{R} \left(\frac{1}{\sin \varphi} \frac{\partial u_R}{\partial \theta} - u_\theta \right). \end{aligned} \tag{18}$$

Plugging the above expressions into (15) produces the surface strain components

$$\begin{aligned}
 E_{\varphi\varphi} &= \frac{u_R}{R} + \frac{1}{R} \frac{\partial u_\varphi}{\partial \varphi}, & E_{\theta\theta} &= \frac{u_R}{R} + \frac{1}{R \sin \varphi} \frac{\partial u_\theta}{\partial \theta} + \frac{\cot \varphi u_\varphi}{R}, \\
 E_{\varphi\theta} &= \frac{1}{2} \left(\frac{1}{R} \frac{\partial u_\theta}{\partial \varphi} - \frac{\cot \varphi u_\theta}{R} + \frac{1}{R \sin \varphi} \frac{\partial u_\varphi}{\partial \theta} \right).
 \end{aligned}
 \tag{19}$$

By the use of (18) and (19) the surface constitutive law (16) can be reformulated directly in terms of surface displacements

$$\begin{aligned}
 \Sigma_{\varphi\varphi} &= \frac{1}{R} \left\{ (\lambda_0 + 2\mu_0) \left(u_R + \frac{\partial u_\varphi}{\partial \varphi} \right) + (\lambda_0 + \tau_0) \left(u_R + \frac{\cos \varphi}{\sin \varphi} u_\varphi + \frac{1}{\sin \varphi} \frac{\partial u_\theta}{\partial \theta} \right) \right\}, \\
 \Sigma_{\varphi\theta} &= \frac{1}{R} \left\{ \mu_0 \left(\frac{1}{\sin \varphi} \frac{\partial u_\varphi}{\partial \theta} - \frac{\cos \varphi}{\sin \varphi} u_\theta \right) + (\mu_0 - \tau_0) \frac{\partial u_\theta}{\partial \varphi} \right\}, \\
 \Sigma_{\theta\varphi} &= \frac{1}{R} \left\{ \mu_0 \frac{\partial u_\theta}{\partial \varphi} + (\mu_0 - \tau_0) \left(\frac{1}{\sin \varphi} \frac{\partial u_\varphi}{\partial \theta} - \frac{\cos \varphi}{\sin \varphi} u_\theta \right) \right\}, \\
 \Sigma_{\theta\theta} &= \frac{1}{R} \left\{ (\lambda_0 + 2\mu_0) \left(u_R + \frac{\cos \varphi}{\sin \varphi} u_\varphi + \frac{1}{\sin \varphi} \frac{\partial u_\theta}{\partial \theta} \right) + (\lambda_0 + \tau_0) \left(u_R + \frac{\partial u_\varphi}{\partial \varphi} \right) \right\}, \\
 \Sigma_{R\varphi} &= \frac{\tau_0}{R} \left\{ \frac{\partial u_R}{\partial \varphi} - u_\varphi \right\}, \\
 \Sigma_{R\theta} &= \frac{\tau_0}{R} \left\{ \frac{1}{\sin \varphi} \frac{\partial u_R}{\partial \theta} - u_\theta \right\}.
 \end{aligned}
 \tag{20}$$

The transform of the force balance condition (17) is less straightforward. Following Gurtin et al. [1998], explicit expressions of its three component equations can be developed with the help of a constant vector. In the present analysis, we have derived these expressions by first evaluating the surface gradient of the superficial surface stress tensor and subsequently contracting the second and third base vectors of the resultant third-order tensor. It should be noted that the surface gradient operator should be applied on the surface stress tensor from right to left [Malvern 1969], based on the argument in [Gurtin and Murdoch 1978]. Thus,

$$\begin{aligned}
 \sigma_{RR}n_R &= \frac{1}{R} \left\{ \frac{1}{\sin \varphi} \frac{\partial \Sigma_{R\theta}}{\partial \theta} + \frac{\partial \Sigma_{R\varphi}}{\partial \varphi} + \cot \varphi \Sigma_{R\varphi} - (\Sigma_{\theta\theta} + \Sigma_{\varphi\varphi}) \right\} + T_R, \\
 \sigma_{R\varphi}n_R &= \frac{1}{R} \left\{ \frac{1}{\sin \varphi} \frac{\partial \Sigma_{\varphi\theta}}{\partial \theta} + \frac{\partial \Sigma_{\varphi\varphi}}{\partial \varphi} + \cot \varphi (\Sigma_{\varphi\varphi} - \Sigma_{\theta\theta}) + \Sigma_{R\varphi} \right\} + T_\varphi, \\
 \sigma_{R\theta}n_R &= \frac{1}{R} \left\{ \frac{1}{\sin \varphi} \frac{\partial \Sigma_{\theta\theta}}{\partial \theta} + \frac{\partial \Sigma_{\theta\varphi}}{\partial \varphi} + \cot \varphi (\Sigma_{\theta\varphi} + \Sigma_{\varphi\theta}) + \Sigma_{R\theta} \right\} + T_\theta,
 \end{aligned}
 \tag{21}$$

where $\{T_R, T_\varphi, T_\theta\}$ denote the surface traction vector due to external loads. The above boundary conditions are valid for a general spherical free surface with unit normal vector $\mathbf{n} = \pm \mathbf{e}_R$. To proceed further, we could substitute (20) into (21) in order to develop general expressions of the surface divergence of the surface stresses in terms of displacements. It is these three boundary equations that couple the mechanics of a spherical free surface into the classical theory of elasticity for the abutting bulk solid. The development of their explicit expressions are straightforward yet quite tedious. Instead, we provide

a simplified version that is particularly tailored for the present axial torsion condition ($T_R = T_\varphi = 0$). In view of (5), it becomes obvious that only the last equation of (21) is nontrivial,

$$-\sigma_{R\theta} = (\nabla_S \cdot \Sigma)_\theta + T_\theta. \quad (22)$$

In this condition, T_θ now represents the distributed shear traction due to the external torque. The combination of equations (20) and (21) results in

$$(\nabla_S \cdot \Sigma)_\theta = -\frac{2\tau_0}{R^2}u_\theta + \frac{\mu_0}{R^2} \left(\frac{\partial^2 u_\theta}{\partial \varphi^2} + \frac{\cos \varphi}{\sin \varphi} \frac{\partial u_\theta}{\partial \varphi} - \frac{\cos^2 \varphi}{\sin^2 \varphi} u_\theta + u_\theta \right). \quad (23)$$

Furthermore, the change of the polar angular variable φ to $\mu = \cos[\varphi]$ transforms the above equation to

$$(\nabla_S \cdot \Sigma)_\theta = -\frac{2\tau_0}{R^2}u_\theta + \frac{\mu_0}{R^2} \left((1 - \mu^2) \frac{\partial^2 u_\theta}{\partial \mu^2} - 2\mu \frac{\partial u_\theta}{\partial \mu} + \frac{1 - 2\mu^2}{1 - \mu^2} u_\theta \right). \quad (24)$$

Substituting the hoop displacement u_θ from (5) into the above relation and noting the harmonic property of the displacement potential λ_3 ,

$$\nabla^2 \lambda_3 = \frac{\partial^2 \lambda_3}{\partial R^2} + \frac{2}{R} \frac{\partial \lambda_3}{\partial R} + \frac{(1 - \mu^2)}{R^2} \frac{\partial^2 \lambda_3}{\partial \mu^2} - \frac{2\mu}{R^2} \frac{\partial \lambda_3}{\partial \mu}. \quad (25)$$

We may recast (24) in the form

$$\begin{aligned} (\nabla_S \cdot \Sigma)_\theta = & \frac{\tau_0}{2GR} \frac{2\sqrt{1 - \mu^2}}{R^2} \left\{ R \frac{\partial \lambda_3}{\partial R} - \mu \frac{\partial \lambda_3}{\partial \mu} \right\} \\ & - \frac{\mu_0}{2GR} \frac{\sqrt{1 - \mu^2}}{R^2} \left\{ 2R \frac{\partial \lambda_3}{\partial R} - 2R^2 \frac{\partial^2 \lambda_3}{\partial R^2} - R^3 \frac{\partial^3 \lambda_3}{\partial R^3} - \mu \left(2 \frac{\partial \lambda_3}{\partial \mu} - R^2 \frac{\partial^3 \lambda_3}{\partial R^2 \partial \mu} \right) \right\}. \end{aligned} \quad (26)$$

In view of the proposed form of λ_3 from (7) we arrive at

$$(\nabla_S \cdot \Sigma)_\theta = -G\sqrt{1 - \mu^2} \sum_{n=0}^{\infty} \left\{ A_n \frac{(2n(2n+3)\mu_0 + 2\tau_0)}{2aG} ((2n+1)P_{2n}[\mu] + \mu P'_{2n}[\mu]) \right\}. \quad (27)$$

Eventually, by the use of (12) and (13) the surface divergence of the surface stress tensor is given by

$$(\nabla_S \cdot \Sigma)_\theta = \frac{G}{2} \sum_{n=0}^{\infty} \left\{ A_n (2n(2n+3)\mu'_0 + 2\tau'_0) P_{2n+1}^1[\mu] \right\}, \quad (28)$$

where $\mu'_0 = \mu_0/aG$ and $\tau'_0 = \tau_0/aG$ are two intrinsic dimensionless parameters that characterize the strength of the hemispherical pit surface. It is worth noting that the other surface Lamé constant, λ_0 , turns out to be irrelevant to the present axial-symmetric torsion problem.

Next, we substitute the shear stress $\sigma_{R\theta}$ from (11) and the surface divergence component $(\nabla_S \cdot \Sigma)_\theta$ from (28) into the nonclassical boundary condition (22)

$$\frac{1}{2}G \sum_{n=0}^{\infty} A_n ((2n+3)(2n\mu'_0 + 1) + 2\tau'_0) P_{2n+1}^1[\mu] = -T_\theta[\mu]. \quad (29)$$

Since for each m , the associated Legendre functions P_n^m of different n are orthogonal and form a complete basis, thus it is possible to perform the series expansion

$$T_\theta[\mu] = \sum_{n=0}^{\infty} f_n P_{2n+1}^1[\mu], \tag{30}$$

where the coefficients f_n are found by multiplying the series by $P_{2m+1}^1[\mu]$ and integrating term by term in the interval $\mu \in [0, 1]$. Using the orthogonality property of the associated Legendre functions

$$\int_{-1}^1 P_{2n+1}^1[\mu] P_{2m+1}^1[\mu] d\mu = \frac{2(2n+1)(2n+2)}{4n+3} \delta_{nm}, \tag{31}$$

and the parity relation

$$P_{2n+1}^1[-\mu] = P_{2n+1}^1[\mu], \tag{32}$$

we obtain

$$\int_0^1 P_{2n+1}^1[\mu] P_{2m+1}^1[\mu] d\mu = \frac{(2n+1)(2n+2)}{4n+3} \delta_{nm}. \tag{33}$$

As a result, it is derived that

$$f_n = \frac{4n+3}{(2n+1)(2n+2)} \int_0^1 T_\theta[\mu] P_{2n+1}^1[\mu] d\mu. \tag{34}$$

A simple comparison of (29) and (30) implies that the unknown coefficients A_n can be connected to the expansion coefficients f_n via

$$A_n = -\frac{2f_n}{G\{(2n+3)(2n\mu'_0+1)+2\tau'_0\}}. \tag{35}$$

Upon successful derivation of the unknown dimensionless coefficients A_n , the azimuthal displacement (10) and two shear stress components (11) can be evaluated as a function of the shear traction distribution T_θ and material parameters (G , ν , μ'_0 and τ'_0).

3. Results and discussion

Clearly, the determination of the shear traction distribution T_θ from the applied net torque T is an indeterminate problem. Different distributions might result in the same torque. Nevertheless, force equilibrium requires that

$$T = 2\pi a^3 \int_0^1 T_\theta[\mu] \sqrt{1-\mu^2} d\mu. \tag{36}$$

For a perfect elastic half-space without surface pits, a concentrated torque applied at the origin produces a shear stress distribution that is proportional to the $\sin \varphi$ [Hill 1966; Miyao et al. 1975]. Thus, we may assume

$$T_\theta[\mu] = T_0 \sqrt{1-\mu^2}, \tag{37}$$

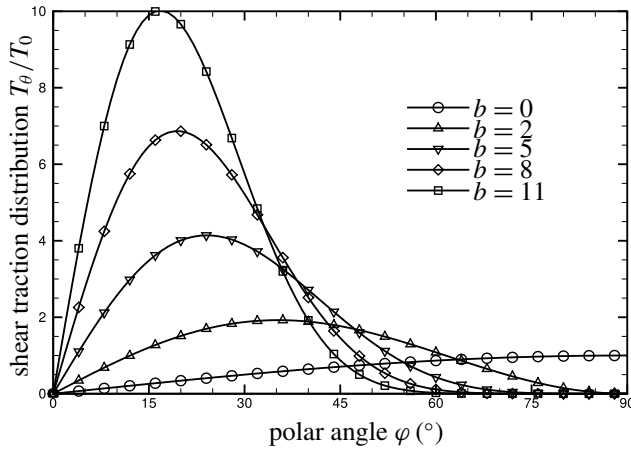


Figure 2. Distributions of five example shear tractions that result in the same torque load at the hemispherical pit surface ($\mu = \cos \varphi$).

where T_0 is the maximum shear traction evaluated at $\mu = \cos[\pi/2] = 0$. For the shear traction distribution (37), an expression that relates the maximum shear traction and the applied torque can be determined as

$$T_0 = \frac{3T}{4\pi a^3}. \tag{38}$$

For the general case of a pitted elastic half-space, the shear traction at the pit surface is treated as a distribution of the applied load and thus may have a different form. It was found that for an arbitrary nonnegative integer b , the shear traction distribution

$$T_\theta[\mu] = (T_0/3)(3 + 4b + b^2)\mu^b \sqrt{1 - \mu^2}, \tag{39}$$

will result in the exact same torque as that of the fundamental distribution form (37). A few example distributions are

$$T_\theta[\mu] = \begin{cases} T_0\sqrt{1 - \mu^2}, & b = 0, \\ 5T_0\mu^2\sqrt{1 - \mu^2}, & b = 2, \\ 16T_0\mu^5\sqrt{1 - \mu^2}, & b = 5, \\ 33T_0\mu^8\sqrt{1 - \mu^2}, & b = 8, \\ 56T_0\mu^{11}\sqrt{1 - \mu^2}, & b = 11. \end{cases} \tag{40}$$

For comparison purposes, the distributions of these five shear tractions are shown in Figure 2. It can be seen that the maximum value of the traction function transfers from the pit rim toward the hemispherical pit pole as b increases.

Replacing $T_\theta[\mu]$ under the integral sign in (34) with the proposed shear traction distribution (39) and noticing the definite integral [Gradshteyn and Ryzhik 2014]

$$\int_0^1 \mu^b (1 - \mu^2)^{m/2} P_\nu^m[\mu] d\mu = \frac{(-1)^m 2^{-m-1} \Gamma[\frac{1}{2} + \frac{1}{2}b] \Gamma[1 + \frac{1}{2}b] \Gamma[1 + m + \nu]}{\Gamma[1 - m + \nu] \Gamma[1 + \frac{1}{2}b + \frac{1}{2}m - \frac{1}{2}\nu] \Gamma[\frac{3}{2} + \frac{1}{2}b + \frac{1}{2}m + \frac{1}{2}\nu]}, \tag{41}$$

it can be derived that

$$f_n = -\frac{T_0 (3 + 4b + b^2)(4n + 3)}{12 (2n + 1)(2n + 2)} \frac{\Gamma[\frac{1}{2} + \frac{1}{2}b]\Gamma[1 + \frac{1}{2}b]\Gamma[2n + 3]}{\Gamma[2n + 1]\Gamma[1 + \frac{1}{2}b - n]\Gamma[\frac{5}{2} + \frac{1}{2}b + n]}, \tag{42}$$

where $\Gamma[z] = (z - 1)\Gamma[z - 1]$ is referred to as the Gamma-factorial function [Arfken and Weber 2013]. The interesting result $\Gamma[1/2] = \sqrt{\pi}$ becomes very useful in the subsequent evaluation of the expansion coefficients f_n in the Legendre series (30).

In view of (10), (11), (35) and (42), the semianalytical series representations of the solution have been successfully developed for the present problem. Prior to exploring solutions that must be represented by the Legendre series, let us examine a few simplified cases for which closed-form solutions are available. We first consider the fundamental distribution of shear tractions (37). We observe that for this case $T_\theta[\mu] = -T_0 P_1^1[\mu]$ and thus only the zeroth mode $f_0 = -T_0$ contributes to the series expansion. Evidently, (35) becomes

$$A_0 = -\frac{2f_0}{G(2\tau'_0 + 3)} = \frac{2T_0}{G(2\tau'_0 + 3)}. \tag{43}$$

A closed-form solution is now developed for the fundamental distribution of shear tractions

$$2Gu_\theta = -\frac{2T_0}{(2\tau'_0 + 3)} \frac{a^3}{R^2} P_1^1[\mu], \quad \sigma_{R\theta} = \frac{3T_0}{(2\tau'_0 + 3)} \frac{a^3}{R^3} P_1^1[\mu], \quad \sigma_{\varphi\theta} = 0. \tag{44}$$

Note that in this special case the stress component $\sigma_{\varphi\theta}$ vanishes.

The next case we examine is for $b = 2$ in (40). It is not hard to find that only two terms in the series expansion (30) are required since

$$T_\theta[\mu] = 5T_0\mu^2\sqrt{1 - \mu^2} = f_0 P_1^1[\mu] + f_1 P_3^1[\mu], \tag{45}$$

where the two coefficients required in the expansion are given by $f_0 = -T_0$ and $f_1 = -2T_0/3$. As a result, (35) results in

$$A_0 = \frac{2T_0}{G(2\tau'_0 + 3)}, \quad A_1 = \frac{4T_0}{3G(10\mu'_0 + 2\tau'_0 + 5)}. \tag{46}$$

Similar to the case of fundamental traction distribution, closed-form displacements and stresses can now be identified as

$$\begin{aligned} 2Gu_\theta &= -\frac{2T_0}{(2\tau'_0 + 3)} \frac{a^3}{R^2} P_1^1[\mu] - \frac{4T_0}{3(10\mu'_0 + 2\tau'_0 + 5)} \frac{a^5}{R^4} P_3^1[\mu], \\ \sigma_{R\theta} &= \frac{3T_0}{(2\tau'_0 + 3)} \frac{a^3}{R^3} P_1^1[\mu] + \frac{10T_0}{3(10\mu'_0 + 2\tau'_0 + 5)} \frac{a^5}{R^5} P_3^1[\mu], \\ \sigma_{\varphi\theta} &= -\frac{2T_0}{3(10\mu'_0 + 2\tau'_0 + 5)} \frac{a^5}{R^5} P_3^2[\mu]. \end{aligned} \tag{47}$$

The availability of closed-form solutions is not an accident. As a matter of fact, the expansion coefficients f_n are truncated by $n < 1 + b/2$ for a nonnegative even integer b since $\Gamma[z]$ has simple poles at $z = 0, -1, -2, -3, -4, \dots$. Such behavior is solely due to $\Gamma[1 + b/2 - n]$ in the denominator of (42). Thus, for a b even and equal to $2s$, where s is a positive integer, the shear traction distribution can be

represented by a truncated Legendre series expansion. Only the first $s + 1$ terms are required in (30), e.g., $s = 4$ for the fourth case ($b = 8$) in (40). In this case, the closed-form displacements and stresses are given by

$$\begin{aligned}
 2G_{u\theta} &= -\frac{2T_0}{(2\tau'_0 + 3)} \frac{a^3}{R^2} P_1^1[\mu] - \frac{112T_0}{39(10\mu'_0 + 2\tau'_0 + 5)} \frac{a^5}{R^4} P_3^1[\mu] \\
 &\quad - \frac{352T_0}{195(28\mu'_0 + 2\tau'_0 + 7)} \frac{a^7}{R^6} P_5^1[\mu] - \frac{128T_0}{221(54\mu'_0 + 2\tau'_0 + 9)} \frac{a^9}{R^8} P_7^1[\mu] \\
 &\quad - \frac{256T_0}{3315(88\mu'_0 + 2\tau'_0 + 11)} \frac{a^{11}}{R^{10}} P_9^1[\mu], \\
 \sigma_{R\theta} &= \frac{3T_0}{(2\tau'_0 + 3)} \frac{a^3}{R^3} P_1^1[\mu] + \frac{280T_0}{39(10\mu'_0 + 2\tau'_0 + 5)} \frac{a^5}{R^5} P_3^1[\mu] \\
 &\quad + \frac{1232T_0}{195(28\mu'_0 + 2\tau'_0 + 7)} \frac{a^7}{R^7} P_5^1[\mu] + \frac{576T_0}{221(54\mu'_0 + 2\tau'_0 + 9)} \frac{a^9}{R^9} P_7^1[\mu] \\
 &\quad + \frac{1408T_0}{3315(88\mu'_0 + 2\tau'_0 + 11)} \frac{a^{11}}{R^{11}} P_9^1[\mu], \\
 \sigma_{\varphi\theta} &= -\frac{56T_0}{39(10\mu'_0 + 2\tau'_0 + 5)} \frac{a^5}{R^5} P_3^2[\mu] - \frac{176T_0}{195(28\mu'_0 + 2\tau'_0 + 7)} \frac{a^7}{R^7} P_5^2[\mu] \\
 &\quad - \frac{64T_0}{221(54\mu'_0 + 2\tau'_0 + 9)} \frac{a^9}{R^9} P_7^2[\mu] - \frac{128T_0}{3315(88\mu'_0 + 2\tau'_0 + 11)} \frac{a^{11}}{R^{11}} P_9^2[\mu],
 \end{aligned} \tag{48}$$

It is worth noting that if b is odd, the coefficients of the Legendre series expansion f_n are well defined for every n . Fortunately, the coefficient of expansion f_n behaves as a strong decaying function of n and thus it is possible to truncate the series with a desired accuracy.

In the remainder of this section, parametric study was employed to facilitate the investigation of surface effects. In view of (35), (44), (47) and (48) it can be seen that the influence of surface mechanics becomes important when τ'_0 and μ'_0 approach the order of magnitudes of unity and one tenth, respectively. For smaller magnitudes of τ'_0 and μ'_0 , the incorporation of surface mechanics introduces inappreciable modifications to the classical solution. The magnitude of both the residual surface stress τ_0 and the surface shear modulus μ_0 of typical crystalline metal materials is 1 N/m [Mi et al. 2008] whereas that of their bulk modulus is $\sim 10^{10}$ Pa [Gere and Goodno 2009]. As a result, the order of magnitude of the pit radius a must be nearly as large as the subnanoscale to cause noticeable surface effects. This is because only the deformation-dependent component of the surface constitutive law (17) can be accommodated in a torsion problem. This scenario is in sharp contrast with that of the dilatational deformation mode in which significant surface influence can still be observed at much larger characteristic length scales [He and Li 2006; Mi and Kouris 2014b].

Nevertheless, the story could be quite different for soft materials in which the relative magnitude between surface elastic parameters and bulk shear modulus increases remarkably. As intuition could expect, soft materials possess much smaller bulk shear modulus in magnitude. For example, the shear modulus of rubber falls in the interval of 0.2 – 1 MPa [Gere and Goodno 2009]. More strikingly, the shear modulus of gelatin is in the order of tens of kPa ($\sim 10^4$ N/m²). Specimens made by these soft materials

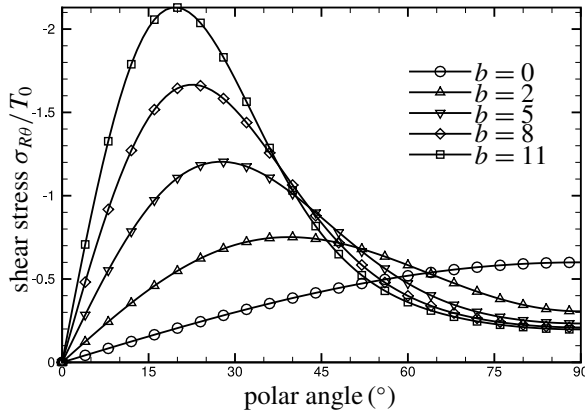


Figure 3. The distribution of normalized shear stress ($\sigma_{R\theta}/T_0$) as a function of the polar angle (φ) at the hemispherical pit surface ($R = a$). Numerical values of the two intrinsic dimensionless parameters are taken as $\mu'_0 = \tau'_0 = 1$.

stay fairly linearly elastic for strains below 10% of such a level of shear modulus, while the Young's modulus ranges from a few kPa to a few hundred kPa [Markidou et al. 2005]. The shear modulus of gelatin gels fluctuates with a few factors including concentration, preparation procedure of testing samples and temperatures at which the measurement was performed.

Little work has been done on the estimation of the surface mechanical properties for soft materials compared to that of crystalline systems. Bialopiotrowicz and Janczuk [2002] managed to employ the method of contact angle measurement to investigate the wetting characteristics of gelatin films and a number of liquids. For those probe liquids with known energy components, the surface free energy of a gelatin film is able to be determined. Experimental measurements demonstrate that the surface free energy of gelatin films with concentrations ranging 0.005 – 100 mg/mL is in the magnitude of a few tens of mJ/m². Based on the force equilibrium, Weijjs et al. [2014] developed a microscopic model that correlates the interface stress and interface energy for an interface separating a liquid and an amorphous soft solid. Although the quantitative behavior of their model is governed by the Poisson's ratio of the interfacial region, the interface stress and interface energy share the same order of magnitude. Furthermore, the definition of elastic modulus [Gumbusch and Daw 1991; Mi et al. 2008] explains that interface energy, interface stress and interface elastic moduli are all about the same order of magnitude ($\sim 10^{-2}$ N/m).

To summarize the dimension analysis up to this point, for soft materials such as gelatin gels the effects of surface mechanics become noticeable and even significant when the characteristic length goes down to the microscale ($a \leq 10^{-6}$ m). At such a length scale, those two intrinsic dimensionless parameters are both comparable to unity ($\mu'_0 = \mu_0/aG \sim 1$ and $\tau'_0 = \tau_0/aG \sim 1$) and thus the model of surface mechanics starts to participate in the mechanics and physics of the concerned material systems. Of course, for rubber-like soft materials, a smaller length scale is preferred for highlighting the surface effects.

Figure 3 shows the distributions of the normalized shear stress $\sigma_{R\theta}/T_0$ at the hemispherical pit surface resulting from the five example shear tractions emphasized in Figure 2. Undoubtedly, these shear stress

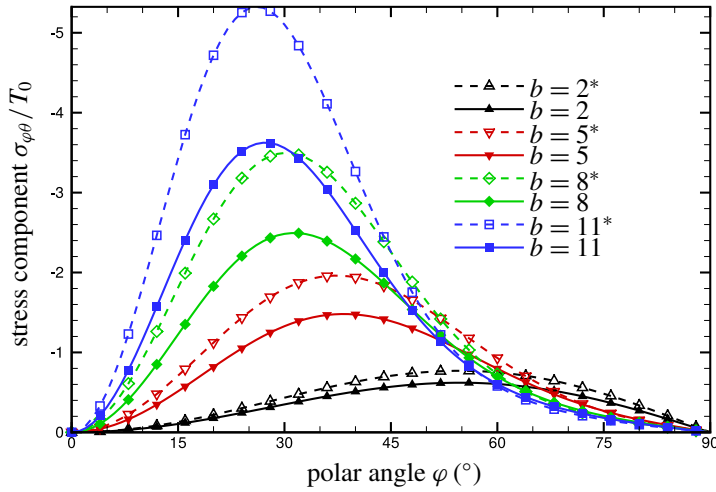


Figure 4. The distribution of normalized stress component ($\sigma_{\varphi\theta}/T_0$) as a function of the polar angle (φ) at the hemispherical pit surface ($R = a$). Numerical values of the two intrinsic dimensionless parameters are taken as $\mu'_0 = \tau'_0 = 0.1$. For comparison, the corresponding classical solutions ($\mu'_0 = \tau'_0 = 0$) are also shown, indicated by *.

distributions would exactly recover to the shear tractions within the framework of the classical theory of elasticity. Nonetheless, the model of surface mechanics ($\mu'_0 = \tau'_0 = 1$) has reduced the maximum shear stress by more than 40% for all cases. The strength of surface mechanics increases monotonically with b . For $b = 11$, the maximum shear stress becomes less than one fourth of its classical counterpart. Close examination reveals that the value of the polar angle coordinate φ at which the maximum shear stress takes place is now closer to the vertex A of the hemispherical pit. Furthermore, the stress level at the pit perimeter ($\varphi = 90^\circ$) seems to converge to a limit value ($\sigma_{R\varphi} \sim -0.2T_0$) as the parameter b increases. This behavior is clearly not observed in the classical solutions, cf. Figure 2.

The comparison of Figures 2 and 3 makes it clear that the parameter combination $\mu'_0 = \tau'_0 = 1$ represents a fairly strong effect of surface mechanics. To better illustrate the effects of surface mechanics, we now adjust these parameters to $\mu'_0 = \tau'_0 = 0.1$. The curves in Figure 4 show the distributions of the normalized stress component $\sigma_{\varphi\theta}/T_0$ at the pit surface for four traction distributions ($b = 2, 5, 8$ and 11). Note that this stress component vanishes for the case of $b = 0$, see (44). Both the curves with and without the model of surface mechanics are plotted for the purpose of comparison. For both groups, $\sigma_{\varphi\theta}$ becomes zero at the pit vertex A and the pit perimeter B , defined in Figure 1. For a given value of b , the maximum stress occurs at the same place for both the classical and corrected solution. These places are $\varphi = 55, 38, 31$ and 27 degrees for $b = 2, 5, 8$ and 11 , respectively. We expect that the value of φ at which the stress extremities take place will converge to a specific value as b continues to increase. The strength of surface mechanics depends on how the shear tractions distribute — the larger the value of b , the stronger the surface effects become.

Figure 5 shows the distributions of the dimensionless displacement $2Gu_\theta/T_0/a$ at the pit surface for the five example traction loads. These curves share similar distribution characteristics as those of

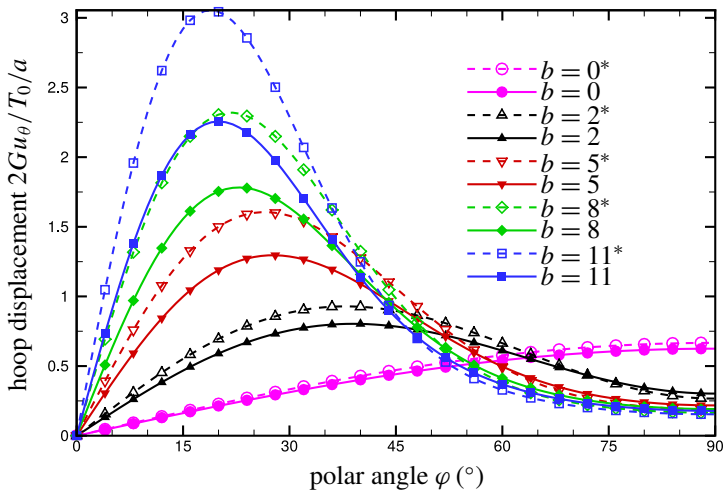


Figure 5. The distribution of normalized hoop component ($2Gu_{\theta}/T_0/a$) as a function of the polar angle (φ) at the hemispherical pit surface ($R = a$). Numerical values of the two intrinsic dimensionless parameters are taken as $\mu'_0 = \tau'_0 = 0.1$. For comparison, the corresponding classical solutions ($\mu'_0 = \tau'_0 = 0$) are also shown, indicated by *.

the shear stress $\sigma_{R\theta}$. Displacement extremities roughly occur at the same locations. Once again, the significance of surface mechanics depends on loading mode of surface tractions. For $b = 2, 5, 8$ and 11 , crossovers are observed between the classical and perturbed curves belonging to the same traction mode. The coordinates of these intersections behave as functions of the loading mode — the larger the parameter b , the farther the crossover deviates from the pit perimeter.

To investigate the range of the elastic field resulting from the surface tractions applied at the pit surface, we further performed numerical experiments to evaluate the displacements and stresses on a couple of concentric hemispherical coordinate surfaces. Shown in Figure 6 is the distribution of the normalized shear stress $\sigma_{R\theta}/T_0$ for three surface traction loads ($b = 0, 5$ and 11) at two radial distances ($R = 1.5a$ and $R = 2a$). The classical solutions for which $\mu'_0 = \tau'_0 = 0$ are also plotted for each of the six cases. Although the variation characteristics for an individual curve is quite similar to its corresponding counterpart at the pit surface, see Figures 2 and 3, the stress magnitude decays drastically as the radial coordinate increases. For example, the maximum stress for the case of $b = 11$ reduced more than nine tenths as the radial coordinate changes from $R = a$ to $R = 1.5a$. The rate of decay is slightly slower for the solution accounting for surface effects as the maximum stress decreased approximately two thirds. For both the classical and modified solutions, the traction loads applied at the pit surface on the plane boundary of an elastic half-space is a short-range force field since the resulting elastic field is completely localized and confined within a distance that is just a couple of multiples of the pit radius.

Numerical results shown in Figure 7 and Figure 8 further support the argument of a localized elastic field made above in which the normalized stress $\sigma_{\varphi\theta}/T_0$ and displacement component $2Gu_{\theta}/T_0/a$ are now plotted for the radial coordinates $R = 1.25a$ and $R = 1.5a$. It should be noted that Figure 7 only shows two modes of traction loads ($b = 5$ and 11) since $\sigma_{\varphi\theta}$ is identically zero for the fundamental

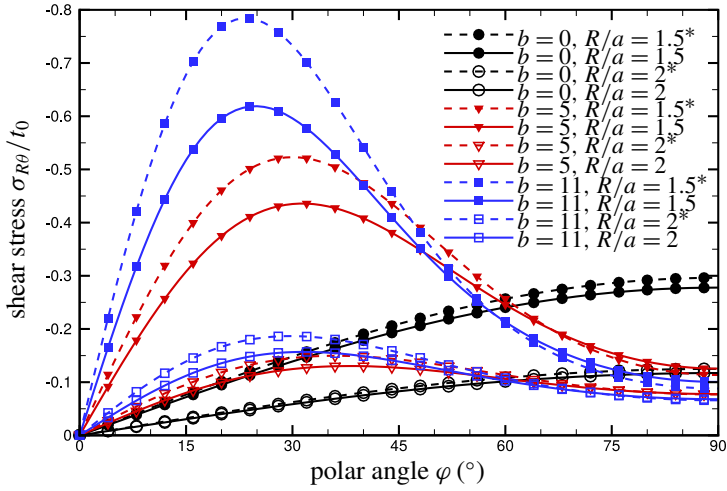


Figure 6. The distribution of normalized shear stress ($\sigma_{R\theta}/T_0$) as a function of the polar angle (φ) for two constant radial coordinates ($R = 1.5a$ and $2a$). Numerical values of the two intrinsic dimensionless parameters are taken as $\mu'_0 = \tau'_0 = 0.1$. For comparison, results due to three traction distributions ($b = 0, 5$ and 11) are plotted with the classical solutions indicated by $*$.

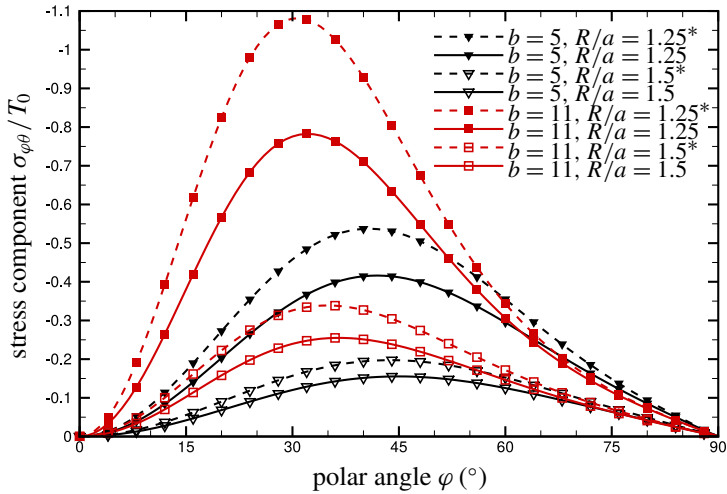


Figure 7. The distribution of normalized stress component ($\sigma_{\varphi\theta}/T_0$) as a function of the polar angle (φ) for two constant radial coordinates ($R = 1.25a$ and $1.5a$). Numerical values of the two intrinsic dimensionless parameters are taken as $\mu'_0 = \tau'_0 = 0.1$. For comparison, results due to two traction distributions ($b = 5$ and 11) are plotted with the classical solutions indicated by $*$.

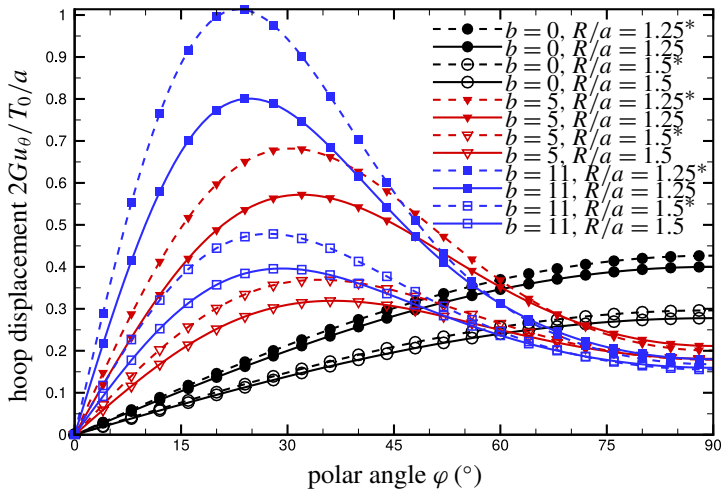


Figure 8. The distribution of normalized hoop displacement ($2Gu_\theta/T_0/a$) as a function of the polar angle (φ) for two constant radial coordinates ($R = 1.25a$ and $1.5a$). Numerical values of the two intrinsic dimensionless parameters are taken as $\mu'_0 = \tau'_0 = 0.1$. For comparison, results due to three traction distributions ($b = 0, 5$ and 11) are plotted with the classical solutions indicated by $*$.

traction distribution ($b = 0$). The trend of decay as a function of the radial coordinate is obvious for the stress $\sigma_{\varphi\theta}$ (Figure 7) and the displacement component u_θ (Figure 8). These elastic components become numerically negligible at a distance only a few radii away from the pit center.

4. Concluding remarks

In this paper, we analyzed in detail the axial-symmetric torsion problem of a nanoscale hemispherical pit on the plane boundary of a semi-infinite elastic solid. We considered a number of traction loads, see (39), that are proportional to the shear stress distribution on a hemispherical coordinate surface due to a concentrated torque applied on an intact half-space. Although all considered traction loads resulted in the exact same torque, displacement and stress distributions differ from one case to another, reflecting the indeterminate nature of the problem. Semianalytical solutions in the form of infinite series were successfully developed. Within the framework of Gurtin and Murdoch’s theory of surface elasticity [1978], two intrinsic dimensionless parameters, $\mu'_0 = \mu_0/Ga$ and $\tau'_0 = \tau_0/Ga$, were formulated to account for the significance of the pit surface. The other surface Lamé parameter λ_0 , which is indispensable to a torsionless problem, turns out to be irrelevant in the present analysis.

Dimension analysis carried out in the previous section suggests that the assumed model of a pit surface can reasonably be neglected for a metal substrate. The drastic difference between metals’ surface and bulk elastic constants make the two dimensionless parameters comparable to unity only for picoscale pits. Nonetheless, for soft substrates, such as gelatin gels, the pit surface effects became a dominant factor that affected the resulting stress levels. To bring the model of surface mechanics into effect, we inferred that μ'_0 and τ'_0 should be at the order of magnitude of unity and one tenth, respectively — which is fairly

practical for a soft substrate [Białopiotrowicz and Jańczuk 2002; Weijs et al. 2014]. It can be further argued that the surface shear modulus μ_0 is more important than the residual surface stress τ'_0 in a torsion problem. This interpretation is in opposition to a dilatational problem in which the residual surface stress proves to be much more important than surface Lamé constants [Mi and Kouris 2014b]. The reason is due to the fact that the deformation-dependent component of the surface constitutive relation is not applicable in the torsion analysis. Numerical results prove that the parameter combination of $\mu'_0 = \tau'_0 = 0.1$ is strong enough to change both the magnitude and distribution of the classical solution when the model of surface mechanics is excluded.

We have based our calculations merely on nominal values of the two dimensionless parameters, μ'_0 and τ'_0 . For a practical soft material, it is a challenge to determine accurate values of surface and bulk elastic parameters. Considering what has been done for metal systems [Gumbsch and Daw 1991; Shenoy 2005; Mi et al. 2008], this could be one future line of research. Another possibility is to extend the static problem to investigate the coupling effects of surface mechanics and dynamic loading.

Acknowledgements

This work was supported by the Natural Science Foundation of Jiangsu Province (Grant no. BK20130597), the National Natural Science Foundation of China (Grant no. 11472079), and the Project Sponsored by the Scientific Research Foundation for the Returned Overseas Chinese Scholars, State Education Ministry.

References

- [Arfken and Weber 2013] G. B. Arfken and H. J. Weber, *Mathematical methods for physicists*, 7th ed., Harcourt/Academic Press, Burlington, Massachusetts, 2013.
- [Barber 2010] J. Barber, *Elasticity*, 3rd ed., Solid Mechanics and Its Applications, Springer, New York, 2010.
- [Białopiotrowicz and Jańczuk 2002] T. Białopiotrowicz and B. Jańczuk, “Surface properties of gelatin films”, *Langmuir* **18**:24 (2002), 9462–9468.
- [Chadwick and Johnson 1971] P. Chadwick and A. F. Johnson, “High-frequency torsional oscillations of a rigid inclusion embedded in an elastic solid”, *Q. J. Mech. Appl. Math.* **24**:1 (1971), 105–114.
- [Eringen 1957] A. C. Eringen, “Elasto-dynamic problem concerning the spherical cavity”, *Q. J. Mech. Appl. Math.* **10** (1957), 257–270.
- [Gere and Goodno 2009] J. M. Gere and B. J. Goodno, *Mechanics of materials*, 7th ed., Cengage Learning, Toronto, 2009.
- [Gradshteyn and Ryzhik 2014] I. S. Gradshteyn and I. M. Ryzhik, *Table of integrals, series, and products*, 8th ed., edited by D. Zwillinger and V. Moll, Elsevier Academic Press, Boston, 2014.
- [Gumbsch and Daw 1991] P. Gumbsch and M. S. Daw, “Interface stresses and their effects on the elastic moduli of metallic multilayers”, *Phys. Rev. B* **44** (1991), 3934–3938.
- [Gurtin 1998] M. E. Gurtin, “A general theory of curved deformable interfaces in solids at equilibrium”, *Philos. Mag. A* **78**:5 (1998), 1093–1109.
- [Gurtin and Murdoch 1975] M. E. Gurtin and A. I. Murdoch, “A continuum theory of elastic material surfaces”, *Arch. Rational Mech. Anal.* **57** (1975), 291–323.
- [Gurtin and Murdoch 1978] M. E. Gurtin and A. I. Murdoch, “Surface stress in solids”, *Int. J. Solids Struct.* **14**:6 (1978), 431–440.
- [He and Li 2006] L. H. He and Z. R. Li, “Impact of surface stress on stress concentration”, *Int. J. Solids Struct.* **43**:20 (2006), 6208–6219.

- [Hill 1966] J. L. Hill, “Torsional-wave propagation from a rigid sphere semiembedded in an elastic half-space”, *J. Acoust. Soc. Am.* **40**:2 (1966), 376–379.
- [Kausel 2010] E. Kausel, “Early history of soil-structure interaction”, *Soil Dyn. Earthq. Eng.* **30**:9 (2010), 822–832.
- [Kushch et al. 2013] V. I. Kushch, S. G. Mogilevskaya, H. K. Stolarski, and S. L. Crouch, “Elastic fields and effective moduli of particulate nanocomposites with the Gurtin–Murdoch model of interfaces”, *Int. J. Solids Struct.* **50**:7–8 (2013), 1141–1153.
- [Malvern 1969] L. E. Malvern, *Introduction to the mechanics of a continuous medium*, Prentice-Hall, 1969.
- [Markidou et al. 2005] A. Markidou, W. Y. Shih, and W.-H. Shih, “Soft-materials elastic and shear moduli measurement using piezoelectric cantilevers”, *Rev. Sci. Instrum.* **76**:6 (2005).
- [Mi and Kouris 2006] C. Mi and D. Kouris, “Nanoparticles under the influence of surface/interface elasticity”, *J. Mech. Mater. Struct.* **1**:4 (2006), 763–791.
- [Mi and Kouris 2013] C. Mi and D. Kouris, “Stress concentration around a nanovoid near the surface of an elastic half-space”, *Int. J. Solids Struct.* **50**:18 (2013), 2737–2748.
- [Mi and Kouris 2014a] C. Mi and D. Kouris, “Elastic disturbance due to a nanoparticle near a free surface”, *Math. Mech. Solids* **19**:7 (2014), 868–881.
- [Mi and Kouris 2014b] C. Mi and D. Kouris, “On the significance of coherent interface effects for embedded nanoparticles”, *Math. Mech. Solids* **19**:4 (2014), 350–368.
- [Mi and Kouris 2015] C. Mi and D. Kouris, “Surface mechanics implications for a nanovoided metallic thin-plate under uniform boundary loading”, *Math. Mech. Solids* (2015).
- [Mi et al. 2008] C. Mi, S. Jun, D. A. Kouris, and S. Y. Kim, “Atomistic calculations of interface elastic properties in noncoherent metallic bilayers”, *Phys. Rev. B* **77** (2008), 075425.
- [Mi et al. 2011] C. Mi, D. A. Buttry, P. Sharma, and D. A. Kouris, “Atomistic insights into dislocation-based mechanisms of void growth and coalescence”, *J. Mech. Phys. Solids* **59**:9 (2011), 1858–1871.
- [Miyao et al. 1975] S. Miyao, E. Tsuchida, H. Matsumoto, and I. Nakahara, “A semi-infinite body subjected to an impulsive torque on a hemispherical pit of a free surface”, *B. JSME* **18**:123 (1975), 959–964.
- [Mogilevskaya et al. 2008] S. G. Mogilevskaya, S. L. Crouch, and H. K. Stolarski, “Multiple interacting circular nanoinhomogeneities with surface/interface effects”, *J. Mech. Phys. Solids* **56**:6 (2008), 2298–2327.
- [Mogilevskaya et al. 2010] S. G. Mogilevskaya, S. L. Crouch, A. L. Grotta, and H. K. Stolarski, “The effects of surface elasticity and surface tension on the transverse overall elastic behavior of unidirectional nano-composites”, *Compos. Sci. Technol.* **70**:3 (2010), 427–434.
- [Osman and Rouainia 2012] A. S. Osman and M. Rouainia, “Dynamic response of an axially loaded rigid sphere embedded in a saturated poroelastic medium”, *Arch. Appl. Mech.* **82**:3 (2012), 407–421.
- [Reissner and Sagoci 1944] E. Reissner and H. F. Sagoci, “Forced torsional oscillations of an elastic half-space, I”, *J. Appl. Phys.* **15** (1944), 652–654.
- [Sharma et al. 2003] P. Sharma, S. Ganti, and N. Bhate, “Effect of surfaces on the size-dependent elastic state of nanoinhomogeneities”, *Appl. Phys. Lett.* **82**:4 (2003), 535–537.
- [Shenoy 2005] V. B. Shenoy, “Atomistic calculations of elastic properties of metallic fcc crystal surfaces”, *Phys. Rev. B* **71** (2005), 094104.
- [Steigmann and Ogden 1999] D. J. Steigmann and R. W. Ogden, “Elastic surface-substrate interactions”, *R. Soc. Lond. Proc. Ser. A Math. Phys. Eng. Sci.* **455**:1982 (1999), 437–474.
- [Streitz et al. 1994] F. H. Streitz, R. C. Cammarata, and K. Sieradzki, “Surface-stress effects on elastic properties, I: Thin metal films”, *Phys. Rev. B* **49** (1994), 10699–10706.
- [Todhunter and Pearson 2010] I. Todhunter and K. Pearson, *A history of the theory of elasticity and of the strength of materials: from Galilei to the present time*, vol. 2, Kessinger, 2010.
- [Wang et al. 2011] J. Wang, Z. Huang, H. Duan, S. Yu, X. Feng, G. Wang, W. Zhang, and T. Wang, “Surface stress effect in mechanics of nanostructured materials”, *Acta Mech. Solida Sin.* **24**:1 (2011), 52–82.
- [Weijs et al. 2014] J. H. Weijs, J. H. Snoeijer, and B. Andreotti, “Capillarity of soft amorphous solids: a microscopic model for surface stress”, *Phys. Rev. E* **89** (2014), 042408.

- [Williams 1971] W. E. Williams, “Slow torsional oscillations of a rigid inclusion in an elastic medium”, *Q. J. Mech. Appl. Math.* **24**:1 (1971), 99–104.
- [Young and Budynas 2002] W. C. Young and R. G. Budynas, *Roark’s formulas for stress and strain*, 7th ed., McGraw–Hill, New York, 2002.
- [Zakout et al. 1999] U. Zakout, Z. Akkas, and G. E. Tupholme, “Transient response of an infinite elastic medium containing a spherical cavity subjected to torsion”, *J. Appl. Mech.* **67**:2 (1999), 282–287.

Received 31 Mar 2016. Revised 12 Aug 2016. Accepted 13 Aug 2016.

CHANGWEN MI: mi@seu.edu.cn

Jiangsu Key Laboratory of Engineering Mechanics, School of Civil Engineering, Southeast University, 2 Sipailou Street, Nanjing, 210096, China

ZHONGWEI SUN: 2318125756@qq.com

Jiangsu Key Laboratory of Engineering Mechanics, School of Civil Engineering, Southeast University, 2 Sipailou Street, Nanjing, 210096, China

DEMITRIS KOURIS: Dimitris.Kouris@sdsmt.edu

Office of the Provost, South Dakota School of Mines & Technology, 501 East St. Joseph Street, Rapid City, SD 57701, United States

**BOOK REVIEW: SHORR'S
*THERMAL INTEGRITY IN MECHANICS AND ENGINEERING***

FEODOR M. BORODICH

Boris F. Shorr

Springer-Verlag, 2015

Series: Foundations of Engineering Mechanics

hard cover: ISBN 978-3-662-46967-5 US\$179.00

electronic: ISBN 978-3-662-46968-2 US\$139.00

A number of books and papers reporting theoretical and experimental research in mechanics of structures and materials functioning at high temperatures were published during the last fifty years. The range of thermostrength applications widens all the time due to the generation of thermal stresses and inhomogeneous thermal fields in many modern technologies.

The reviewed monograph starts from analytical generalization of research done by a multidisciplinary academic community, including a substantial contribution from the author. Professor B. F. Shorr is a leading Russian scholar in the area of material and structure thermostrength. He has been affiliated with the Baranov Central Institute of Aviation Motors (CIAM) in Moscow for many years and participated in the design of a number of high temperature gas turbines.

This book has several peculiarities which distinguish it from other publications on the subject. It brings the general ideas of modern approaches to basic thermostrength problems and appeals to both academic and engineering communities. The phenomenological treatment of thermostrength phenomena in solids adopted in the book is based on the thorough analysis of data from numerous experiments, revealing most typical and verified models of material behavior. Preference is given to models characterized by a minimal number of experimentally evaluated parameters. An obvious advantage of the book is that it combines rigorous formulations and solution methods with a user friendly presentation style. This makes it attractive for audiences with various levels of theoretical background.

The first and second chapters deal with the basics of thermoelasticity, which are necessary for strength analyses of machine parts. The content of these chapters is crucial for understanding the rest of the book. Here, the conventional energy principles and variational equations underlying the finite element method (FEM) are introduced.

The problems of thermoplasticity and nonisothermal creep, including cyclic loading, are central to the book. They are considered in six of the twelve chapters based on the detailed analysis of experimental

Keywords: thermal fields, thermostrength, thermoplasticity, thermocreep.

results. In particular, data from the author's colleagues from CIAM are incorporated in the chapters. The importance of a material property's adaptivity is emphasized. This results in the stabilization of material response in case of long-term or cyclic mechanical and thermal loading.

The author shows that well known theories of plastic flow, plastic deformation and isotropic and anisotropic hardening have certain restrictions when applied to modeling nonstationary processes. The novel theory of stabilizing anisotropic ray hardening is suggested for implementation in thermoplasticity and nonisothermal creep. It takes into account the history of loading trajectories and operates only with measured material parameters.

Chapter nine is devoted to evaluating the strength and life span of machine parts and structures under nonisothermal loading. This distinguishes the book from numerous publications analyzing stress and strain calculation only. Along with local strength, load carrying capacity of the whole mechanical system is also studied. The design of uniform strength structures is also discussed. The weak link approach used for avoiding global catastrophes is also mentioned. A robust methodology for a statistical analysis of thermostrength using a limited amount of experimental data under the conditions simulating the operational environment is proposed.

The next two chapters deal with the loss of elastic and nonelastic stability of isotropic mechanical systems and the strength of anisotropic structures, respectively. Basic methods are addressed, and the peculiarities of the side buckling of compressed rods are also discussed, taking into account the effects of plasticity and creep. The von Mises frame example clearly demonstrates a jump of a mechanical system to a new equilibrium due to the variation of its temperature field.

A monocrystal nickel alloy used in high temperature gas turbine blades is considered as a typical anisotropic material. Theoretical arguments and experimental evidence are presented to show that the maximal value of the Schmid factor characterizing shear stress levels along monocrystal yield surfaces cannot be generally chosen as a reliable strength characteristic. Better results are achieved by making use of the maximal shear stress as a characteristic.

Researchers in solid mechanics and academics interested in a better understanding of material and structure behavior in the presence of high temperatures will benefit from reading the last chapter treating special issues in thermostrength, which is mainly ignored in other publications. In particular, it is shown that variations of contact conditions as well as thermal stresses may change the overall stiffness of the system. This is especially true for thin walled structures. For the latter, the associated frequency spectra may be strongly affected. The author also clarifies without referencing hard-core mathematics that the decay of elastic vibration may be caused by the thermodynamic coupling of mechanical and thermal phenomena and an infinite heat propagation speed in the classical theory of heat transfer.

The author pays tribute to the theoretical and experimental considerations of his predecessors without avoiding the criticism of some established statements. In particular, he argues that the modeling of elastic-plastic flow without its separation into elastic and plastic parts is justified only for special types of loading. He also demonstrates that the Odqvist parameter in the case of cyclic loading varies over broad limits and is hardly an adequate measure of damage and fracture.

Limited attention in the book is given to purely computational aspects because of the relatively easy access to modern commercial FEM software. A detailed numerical procedure is only described for nonstationary thermoplasticity and thermocreep problems within the framework of the aforementioned theory of stabilizing anisotropic ray hardening.

The monograph might be criticized for not covering several interesting topics: low temperature strength is not considered, and the range of analyzed materials is often restricted to those used in aviation. At the same time, the content of the book is dictated by its size and originates from the author's research interests.

This book will be of obvious interest to researchers, engineers, university lecturers and postgraduate students specializing in the design and modeling of the thermostrength of materials, machine parts and structures, as well as those dealing with various applications related to thermal stress analysis. The solid mechanics academic community will also benefit from this book.

Received 7 Mar 2016. Accepted 18 Mar 2016.

FEODOR M. BORODICH: [BorodichFM@Cardiff.ac.uk](mailto:borodichFM@Cardiff.ac.uk)

School of Engineering, Cardiff University, The Parade, Queen's Buildings, Cardiff, CF24 3AA, United Kingdom

SUBMISSION GUIDELINES

ORIGINALITY

Authors may submit manuscripts in PDF format online at the Submissions page. Submission of a manuscript acknowledges that the manuscript is original and has neither previously, nor simultaneously, in whole or in part, been submitted elsewhere. Information regarding the preparation of manuscripts is provided below. Correspondence by email is requested for convenience and speed. For further information, write to contact@msp.org.

LANGUAGE

Manuscripts must be in English. A brief abstract of about 150 words or less must be included. The abstract should be self-contained and not make any reference to the bibliography. Also required are keywords and subject classification for the article, and, for each author, postal address, affiliation (if appropriate), and email address if available. A home-page URL is optional.

FORMAT

Authors can use their preferred manuscript-preparation software, including for example Microsoft Word or any variant of $\text{T}_{\text{E}}\text{X}$. The journal itself is produced in $\text{L}^{\text{A}}\text{T}_{\text{E}}\text{X}$, so accepted articles prepared using other software will be converted to $\text{L}^{\text{A}}\text{T}_{\text{E}}\text{X}$ at production time. Authors wishing to prepare their document in $\text{L}^{\text{A}}\text{T}_{\text{E}}\text{X}$ can follow the example file at www.jomms.net (but the use of other class files is acceptable). At submission time only a PDF file is required. After acceptance, authors must submit all source material (see especially Figures below).

REFERENCES

Bibliographical references should be complete, including article titles and page ranges. All references in the bibliography should be cited in the text. The use of $\text{BibT}_{\text{E}}\text{X}$ is preferred but not required. Tags will be converted to the house format (see a current issue for examples); however, for submission you may use the format of your choice. Links will be provided to all literature with known web locations; authors can supply their own links in addition to those provided by the editorial process.

FIGURES

Figures must be of publication quality. After acceptance, you will need to submit the original source files in vector format for all diagrams and graphs in your manuscript: vector EPS or vector PDF files are the most useful. (EPS stands for Encapsulated PostScript.)

Most drawing and graphing packages—Mathematica, Adobe Illustrator, Corel Draw, MATLAB, etc.—allow the user to save files in one of these formats. Make sure that what you're saving is vector graphics and not a bitmap. If you need help, please write to graphics@msp.org with as many details as you can about how your graphics were generated.

Please also include the original data for any plots. This is particularly important if you are unable to save Excel-generated plots in vector format. Saving them as bitmaps is not useful; please send the Excel (.xls) spreadsheets instead. Bundle your figure files into a single archive (using zip, tar, rar or other format of your choice) and upload on the link you been given at acceptance time.

Each figure should be captioned and numbered so that it can float. Small figures occupying no more than three lines of vertical space can be kept in the text (“the curve looks like this:”). It is acceptable to submit a manuscript with all figures at the end, if their placement is specified in the text by means of comments such as “Place Figure 1 here”. The same considerations apply to tables.

WHITE SPACE

Forced line breaks or page breaks should not be inserted in the document. There is no point in your trying to optimize line and page breaks in the original manuscript. The manuscript will be reformatted to use the journal's preferred fonts and layout.

PROOFS

Page proofs will be made available to authors (or to the designated corresponding author) at a Web site in PDF format. Failure to acknowledge the receipt of proofs or to return corrections within the requested deadline may cause publication to be postponed.

- Interface stress of orthotropic materials with a nanodefekt under antiplane shear loading**
JUNHUA XIAO, CHUANFU SHI, YAOLING XU and FUCHENG ZHANG 491
- Propagation of waves in masonry-like solids**
MARIA GIRARDI, CRISTINA PADOVANI and DANIELE PELLEGRINI 505
- Two-dimensional fretting contact of piezoelectric materials under a rigid conducting cylindrical punch**
JIE SU, LIAO-LIANG KE and YUE-SHENG WANG 535
- An anisotropic model for the Mullins effect in magnetoactive rubber-like materials**
M. H. B. M. SHARIFF and ROGER BUSTAMANTE 559
- Predictive modeling of mechanical properties of metal filled anodic aluminum oxide**
VLADIMIR V. BARDUSHKIN, YULIA I. SHILYAEVA,
SERGEY A. GAVRILOV, MAXIM V. SILIBIN, VICTOR B. YAKOVLEV,
MIKHAIL L. ZHELUDKEVICH and NATALIA I. POPENKO 583
- The hemispherical nanopit at the plane boundary of an elastic half-space subjected to statically equivalent shear tractions**
CHANGWEN MI, ZHONGWEI SUN and DEMITRIS KOURIS 595
- Book review: Shorr's *Thermal integrity in mechanics and engineering***
FEODOR M. BORODICH 615